N-Heterocyclic Carbene Stabilisation of Low Valent Metal Centres for the Activation of E-H Bonds

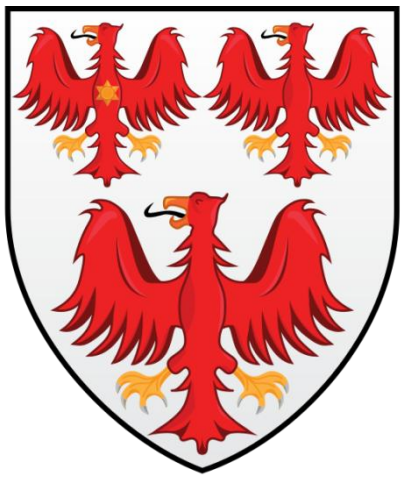

Nicholas Phillips
The Queen's College, Oxford
January 2014

A thesis submitted in partial fulfilment of the requirements for the degree of Doctor of Philosophy

Acknowledgements

First and foremost, I would like to thank my supervisor Prof. Simon Aldridge for the countless hours he has dedicated to mentoring and supporting my research. He has always provided enthusiasm, advice and encouragement throughout the entire process and for that I am eternally grateful.

I extend my thanks to all the members of the Aldridge group past and present for making these past few years ones to remember and supporting me through the results droughts. In particular I would like to acknowledge the work of Dr. Christina Tang, Dr. David Addy, Dr. Ian Riddlestone, Mr. Mike Kelly, Dr. Josh Bates, Mr. Remi Tirfoin and Mr. Joe Abdalla for their contributions of various analytical techniques and hours of helpful discussion. Valuable contributions to the discussion were made by past Part IIs from the group; Mr. Johnny Rowles, Mr. Tristan Dodson and Miss Lucinda Treasure.

Many thanks go out to Dr. Christina Tang, Mr. Remi Tirfoin, Mr. Mike Kelly, Dr. Ian Riddlestone and Dr. Amber Thompson for both help with running and processing X-ray crystal structures. The collection and processing of neutron data was very kindly performed by Dr. Matthias Guttmann at ISIS.

Detailed analyses of the complexes in this thesis were only performed as a result of the help from Dr. Nick Rees, who spent many hours analysing and processing variable temperature NMR data. Prof. John McGrady provided much useful discussion as well as supervising Miss. Lucinda Treasure performing mechanistic DFT studies of my complexes.

I would like to thank the EPSRC (Doctoral Training Account) for my funding over the past three years.

My fiancée, Ellie, has constantly supported me throughout the process. I thank her for putting up with the moaning when things go wrong and celebrating with me when they went right. She always kept my enthusiasm levels up! I can't imagine going through this process without the love and support she gave.

In addition, I would like to thank my family, Mum, Dad and Jon, for all their support and advice. As well as many home-cooked and restaurant meals that were integral to my thesis! Also, Ellie's parents Tess and Paul constantly provided me with help and support for which I am hugely appreciative.

Abstract

This thesis examines the effects of coordinating highly sterically demanding and strongly electron donating saturated *N*-heterocyclic carbenes (NHCs) at late transition metal centres.

Chapter III details the synthesis of a range of iridium complexes of the type $(NHC)_2IrH_xCl_y$ [x = 1, 2; y = 0, 1], bearing the saturated NHCs 5-Mes, 6-Mes and 7-Mes. Unusually facile activation chemistry is observed in the reaction of $[Ir(COE)_2Cl]_2$ with 6-Mes and 7-Mes to form the doubly cyclometallated species $(6\text{-Mes}')_2IrH$ and $(7\text{-Mes}')_2IrH$, which were fully characterised. The responses of these complexes to the addition of dihydrogen and HCl were studied, leading to the controlled synthesis of range of precursors to 14-electron iridium cations.

In Chapter IV the formation of low valent iridium cations with weakly coordinating anions is targeted. Isolation of the cationic complexes $[(NHC)(NHC')IrH][BAr^f_4]$ and $[(NHC)_2IrH_2][BAr^f_4]$ (NHC = 6-Mes, 7-Mes) showcases the stabilising power offered by these expanded ring systems. This allowed the study the interaction of these low valent species with a range of amine-borane substrates which are known to be readily dehydrogenated. Thermodynamic data on the C-H bond activation processes occurring at these iridium centres were able to be obtained due to facile, reversible oxidative addition of C-H bonds across the 14-electron iridium.

Chapter V focuses on the effects of increasing the steric bulk of these NHCs to limit the coordination of multiple ligands at the metal centre. Use of 2,6-diisopropyl-phenyl (Dipp) groups on the expanded ring NHCs, instead of mesityl groups, leads to an unprecedented mode of reactivity with $[Ir(COE)_2Cl]_2$. Activation and cleavage of C-N bonds in the carbene ring is observed, resulting in an open chain ligand chelating to the metal centre. Activation of the backbone in this manner has allowed the synthesis of saturated NHCs bearing a weakly coordinating anion on the ring. Here the first example of an anionic, saturated NHC is reported.

In Chapter VI these highly sterically demanding NHCs are exploited to stabilise active species in low valent gold chemistry. The extreme steric bulk of the 6-Dipp ligand disfavours reduction of Au(I) to Au(0), however the resulting cation is observed to interact strongly with the weakly coordinating anion, $[BAr^f_4]^-$. Thus, attempts were made to optimise the anion and conditions to isolate a catalytically relevant intermediate. The strong donating power of these expanded ring NHCs is also exploited to activate gold hydride complexes of the type (NHC)AuH (NHC = 6-Dipp, 7-Dipp). Analogues of $[H_3]^+$ containing gold atoms ($[\{LAu\}_2H]^+$ and $[LAuH_2]^+$) supported by expanded ring NHCs were also targeted.

Abbreviations

The following abbreviations will be used throughout this report:

Ar – aryl

Ar^f – 3,5-bis(trifluoromethyl)phenyl

Ar^F – pentafluorophenyl

br – broad

calc. – calculated

COE – cyclooctene

Cy – cyclohexyl

d – doublet

DCM – dichloromethane

DFT – density functional theory

Dipp – 2,6-diisopropylphenyl

EI – electron impact

ESI – electrospray ionisation

h – hours

^{i}Pr – isopropyl

J – coupling constant

m – multiplet

Me – methyl

meas. – measured

Mes – 2,4,6-trimethylphenyl

NHC – *N*-heterocyclic carbene

NMR – nuclear magnetic resonance

obs. – observed

Ph – phenyl

ppm – parts per million

pftb – perfluoro-*tert*-butoxide

q – quartet

qn – quintet

s – singlet

sept – septet

THF – tetrahydrofuran

THT – tetrahydrothiophene

tr – triplet

VT-NMR – variable temperature NMR

Xyl – 2,6-dimethylphenyl

δ – NMR chemical shift

λ – wavelength

IMes (Ar = Mes)

IPr (Ar = Dipp)

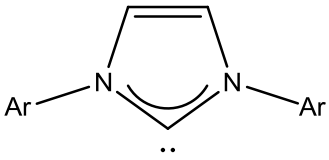

5-Mes (Ar = Mes)

5-Dipp (Ar = Dipp)

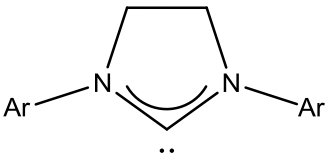

6-Mes (Ar = Mes)

6-Dipp (Ar = Dipp)

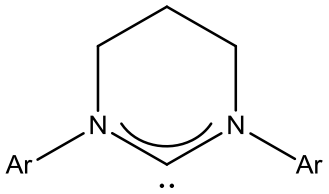

7-Mes (Ar = Mes)

7-Dipp (Ar = Dipp)

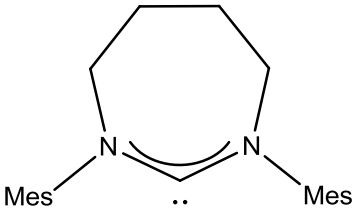

7'-Mes

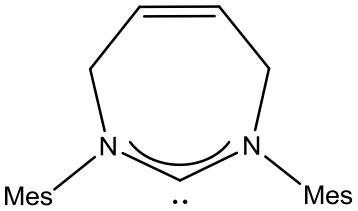

Xyl7-Mes

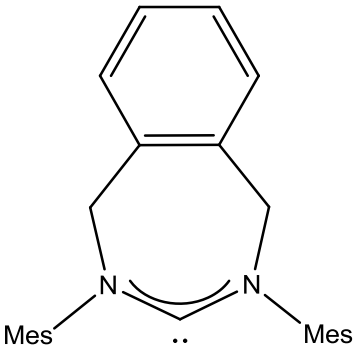

5-Mes' (n = 0)

6-Mes' (n = 1)

7-Mes' (n = 2)

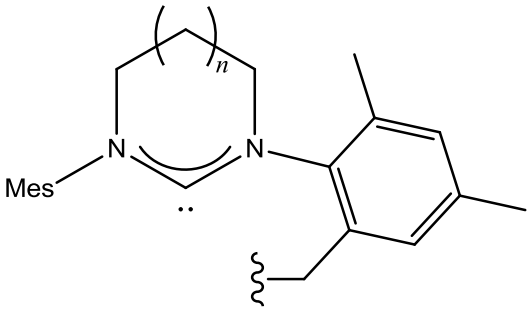

6'-Dipp

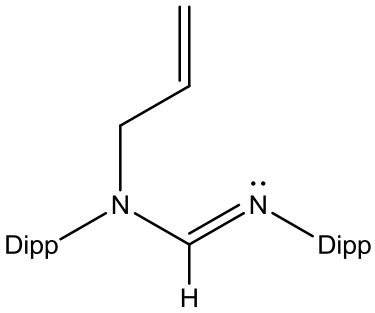

6[a]-Dipp

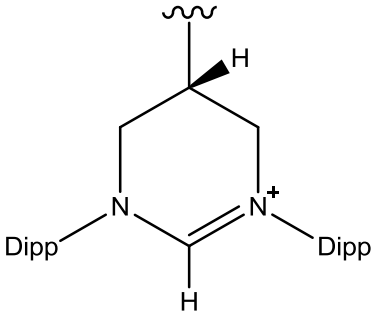

Contents

Chapter I

Introduction

1.1 Carbenes

Carbenes are classified as species containing a divalent carbon centre with a non-bonding pair of electrons, and hence possessing six valence electrons.[1] These non-bonding electrons can either be paired in the same orbital to give a singlet spin-state, or parallel in orthogonal orbitals leading to a triplet state. The geometry at the carbene centre will affect the ground spin-state; thus a linear carbene system has sp-hybridisation resulting in a degenerate pair of orthogonal p-orbitals leading to a triplet ground state. As the angle at the carbenic centre decreases, the hybridisation tends to a more sp^2-like arrangement leading to a stabilisation of what is now the σ-orbital. At a certain energy gap, the singlet state becomes more favourable (Fig 1.1).[2]

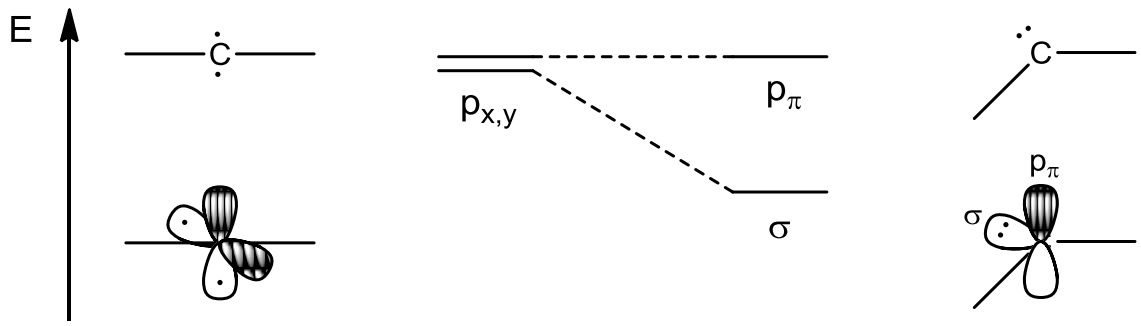

Figure 1.1: Stabilisation of the sp^2 (σ) orbital on decreasing the angle at the carbene.

Most carbenes possess a bent geometry and, as a result, can exist in one of two spin states: the singlet state has two paired electrons found in the sp^2 framework, with a formally vacant p-orbital, whereas the triplet state has parallel spins singly occupying both the sp^2

and p-orbitals (Fig 1.2). Hoffmann determined that an energy gap of 2 eV is required to overcome the repulsive energy from pairing the electrons resulting in a singlet ground state.[3]

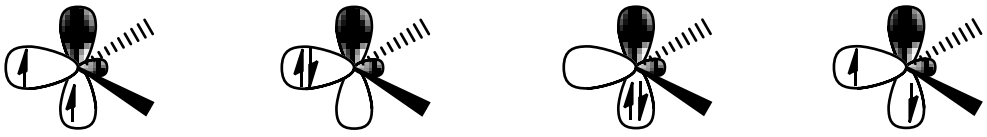

Figure 1.2: Orbital occupancy of ground state singlet ($^1A_1$) and triplet ($^3B_1$) bent carbenes; potentially excited singlet states ($^1A_1$ and $^1B_1$).

The spin state of a generic carbene CX_2 is dependent upon the σ-donating or σ-withdrawing effects of the X substituents. σ-Withdrawing substituents stabilise the sp^2 orbitals increasing the energy gap with the carbon-based p-orbital, while σ-donating groups decrease the energy gap thereby favouring the triplet state. Orbital diagrams by Bertrand *et al*. display the effects of the nature of X on the spin state of the carbene (Fig 1.3).[2]

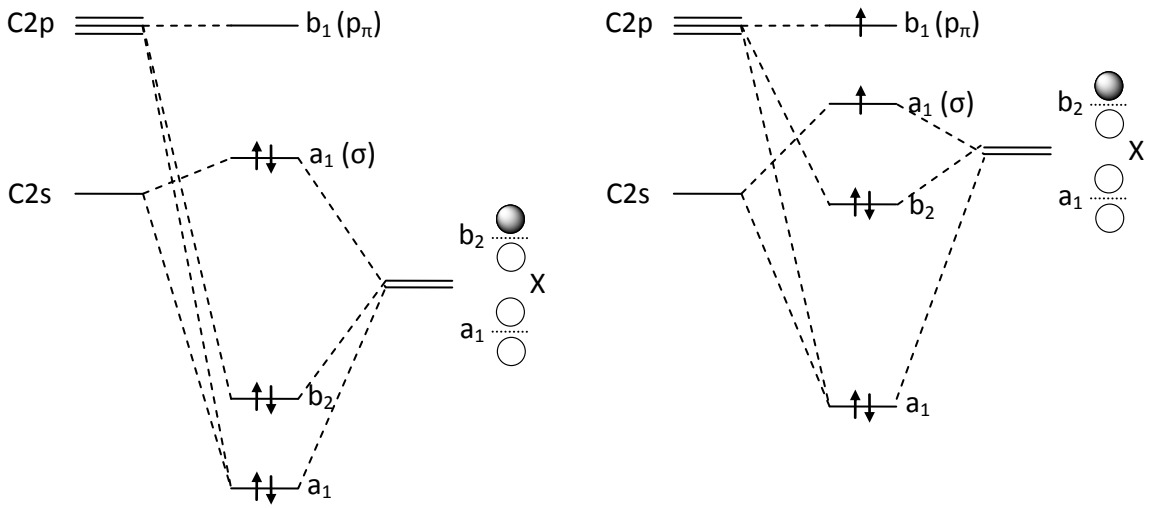

a) σ-electron withdrawing substituents *b) σ-electron donating substituents*

Figure 1.3: Orbital diagrams for a carbene, CX_2, when X = σ-withdrawing (*left*) or X = σ-donating substituent (*right*).

As a consequence of spin conservation rules, the singlet and triplet carbenes have different modes of reactivity. Singlet carbenes have a donor and an acceptor site, and so can insert into polar bonds such as C–H, N–H, O–H and C=C; triplet carbenes, considered as diradicals, can add across C–H and C=C bonds but with reduced stereoselectivity as the addition is not concerted. Due to the inherent kinetic and thermodynamic instability of the free carbene species, both spin states will readily undergo dimerisation in order to complete the octet at carbon. Hence, carbenes are rarely observed as free species.

As well as the reactions detailed above (dimerisation, bond insertion, etc.), carbenes form complexes with a wide variety of metal fragments, including main group metals,[4-10] transition metals,[11-22] as well as the lanthanides and actinides.[23-26]

1.1.2 Metal-Carbene Complexes

In 1964, the first stable Transition-metal carbene complex was reported by Fischer and Maasböl. Treating $W(CO)_6$ with $LiCH_3$ in diethyl ether under N_2 resulted in nucleophilic addition to the carbon of a CO ligand, with no elimination of CO. Formation of the tetramethylammonium salt, $[NMe_4][W(CO)_5COMe]$, led to precipitation of yellow, diamagnetic crystals from aqueous solution. Protonation followed by methylation with CH_2N_2 then yielded $W(CO)_5[C(OMe)Me]$ (**I**), (Scheme 1.4).[27]

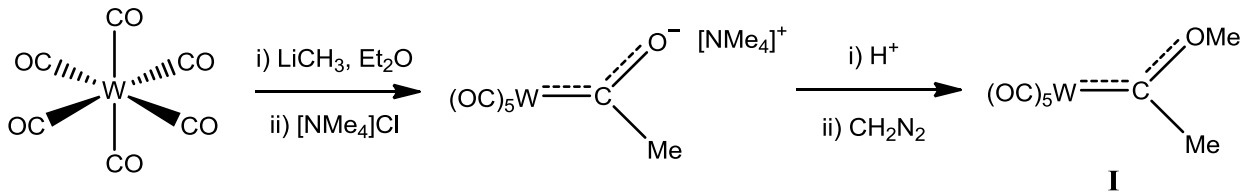

Scheme 1.4: Synthesis of the first Fischer carbene complex.

These Fischer-type carbenes are singlet carbenes. Hence, they are σ-donating, π-acceptor ligands and tend to form with low oxidation state, mid- to late-transition metal centres. A π-donor substituent, such as an alkoxy or amino group, is also required on the carbene atom to stabilise the species.

In 1974, a second class of metal-bound carbene species was identified by Schrock upon treatment of $Ta[CH_2C(CH_3)_3]_3Cl_2$ with 2 equivalents of neopentyllithium.[28] The resulting complex, often described as an alkylidene complex (**II**), bears a carbene featuring an alkyl substituent (Scheme 1.5).

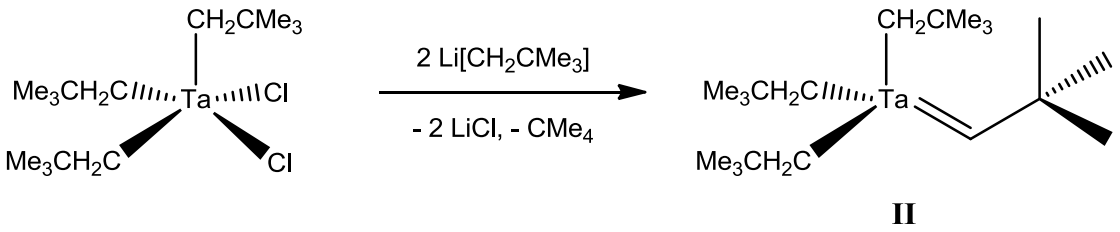

II

Scheme 1.5: Synthesis of the first Schrock alkylidene complex.

These alkylidene ligands possess a formal -2 charge whereas the Fischer carbene ligand is formally charge neutral. The lack of π-donation from the alkyl chains to the carbenic centre results in a higher energy sp^2-orbital, and hence, a triplet state carbene. This in turn means that the p_π-orbital lies lower in energy than the metal d-orbitals so, upon complexation, the filled π-backbonding orbitals are more C-based. This leads to a more nucleophilic carbene centre in the complex. Conversely, the π-donor substituents associated with Fischer carbenes raise the energy of the p_π-orbital forcing a singlet state. Hence, when complexed to a metal, the vacant antibonding component of the π-backbond is C-based, so the carbene in these complexes are electrophilic in nature.

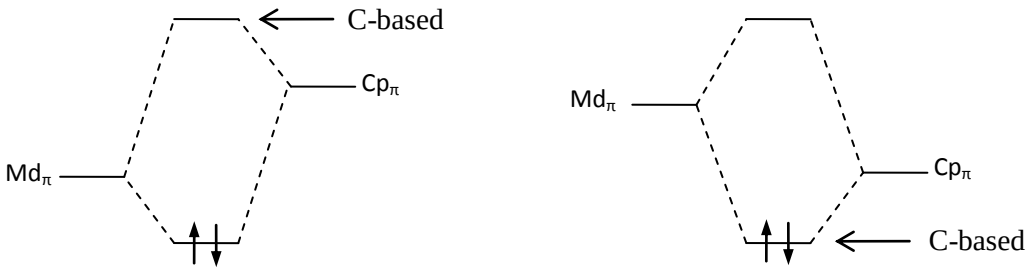

Figure 1.6: Simplified molecular orbital scheme for the π-orbitals for Fischer (*left*) and Schrock (*right*) carbene complexes.

1.2 *N*-Heterocyclic Carbenes

It was identified by Wanzlick, in 1962, that in order to make inherently electrophilic carbenes into nucleophilic species, strongly electron donating substituents were required about the carbene centre.[29] More specifically, strong π-donation was needed to stabilise the electron deficient carbon. This was achieved by placing two nitrogen atoms next to the carbenic centre linked by an ethylene backbone to yield a heterocyclic precursor (Scheme 1.7). Thermolysis of this compound resulted in a species characterised by a Raman band at 1640 cm^{-1} due to the formation of a C=C bond. The small steric hindrance in this system allows dimerisation of the carbene centres at room temperature (**IV**), but 50% dissociation was observed at 170 °C.

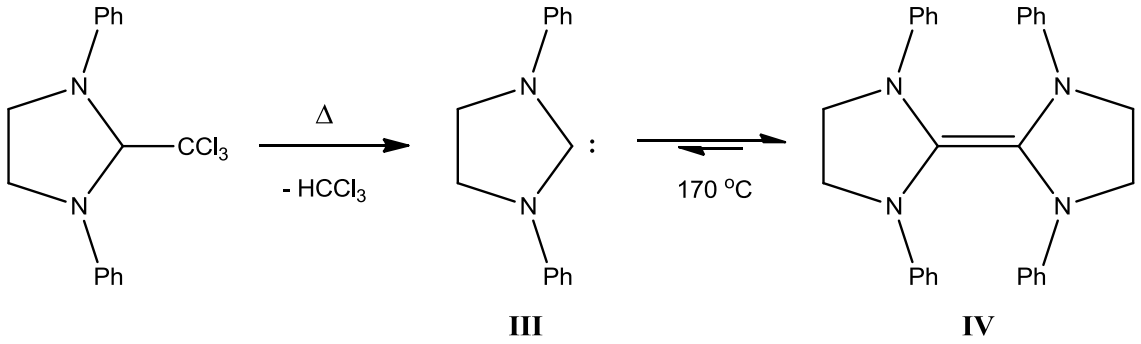

Scheme 1.7: First synthesis of an *N*-heterocyclic carbene.

Evidence for the dissociation of this dimeric species at room temperature was derived from the reaction of **III** with methanol. A purple colour developed which disappeared on warming. The observations are attributed to the reaction shown in Scheme 1.8 involving net addition of MeOH to the carbenic carbon.

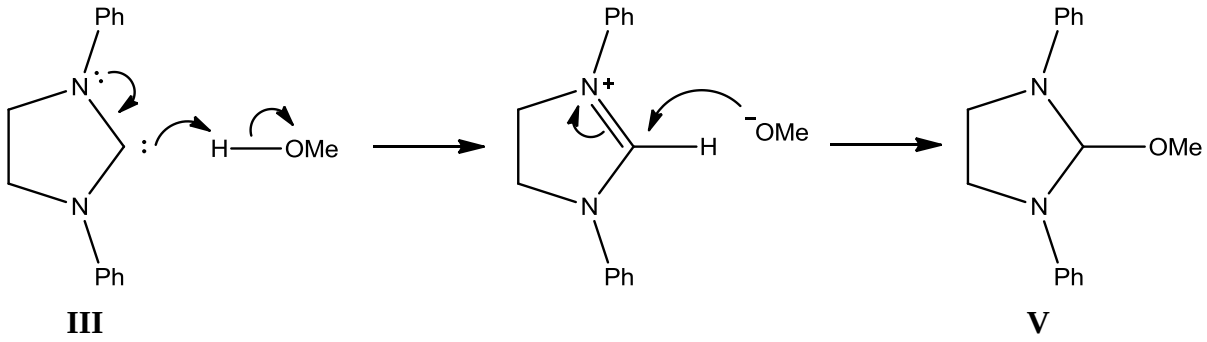

III **V**

Scheme 1.8: Proposed mechanism for the reaction of **III** with methanol.

The fact that this process could be reversed on heating led to a synthesis of NHC systems that is still used today.[30] Heating the dianilinoethane with orthoformic esters is reported to give yields of ring closed products of >90 % (Scheme 1.9).

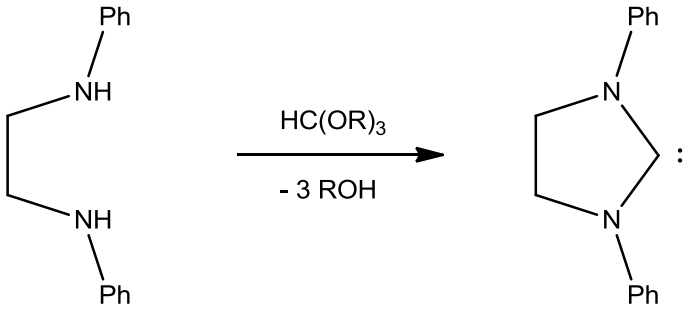

Scheme 1.9: Ring closing with orthoformic ester to form an NHC.

Wanzlick's theory that NHC species existed in an equilibrium involving mono- and dimeric forms was subsequently cast into doubt by work from Lemal *et al.*[31] and supporting work from Winberg *et al.*[32] These experiments probed the potential for cross-reactions of

NHC dimers, on the basis that if the equilibrium did indeed exist, unsymmetrical products would be observed. However, the equilibrium outlined in Scheme 1.10 was not observed.

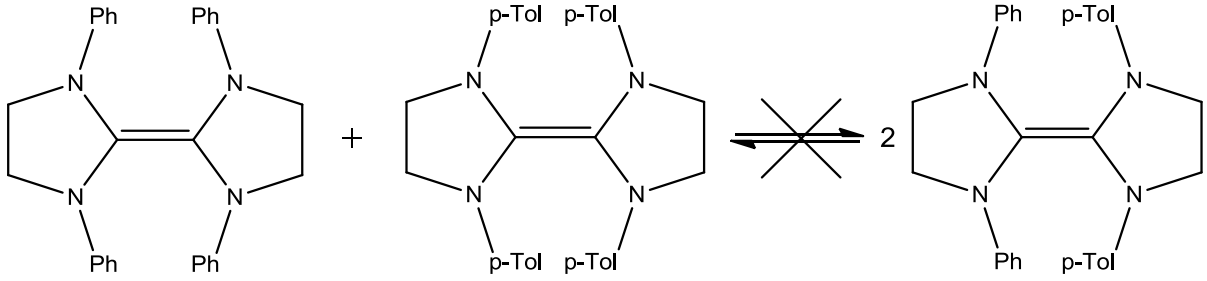

Scheme 1.10: Lemal's experiment to test the dissociation of NHC dimers.

A new mechanism to explain the observation by Wanzlick was now required. One suggestion by Lemal included the possibility of initial electrophilic attack across the C=C bond, i.e. protonation by MeOH.

This problem was resurrected over 30 years later by Denk *et al.*,[33] who showed that this equilibrium could, in fact, exist. Taking a mixture of dimeric species with a variety of *N*-substituents (Me, Et, ^{i}Pr, Ph, *p*-Tol) at 150 °C in several experiments, led to the observation of statistical mixtures of the possible homo- and hetero-coupled products. These findings do not, however, necessarily prove Wanzlick's equilibrium postulate, with several mechanisms being consistent with the observed transformations (Fig 1.11).

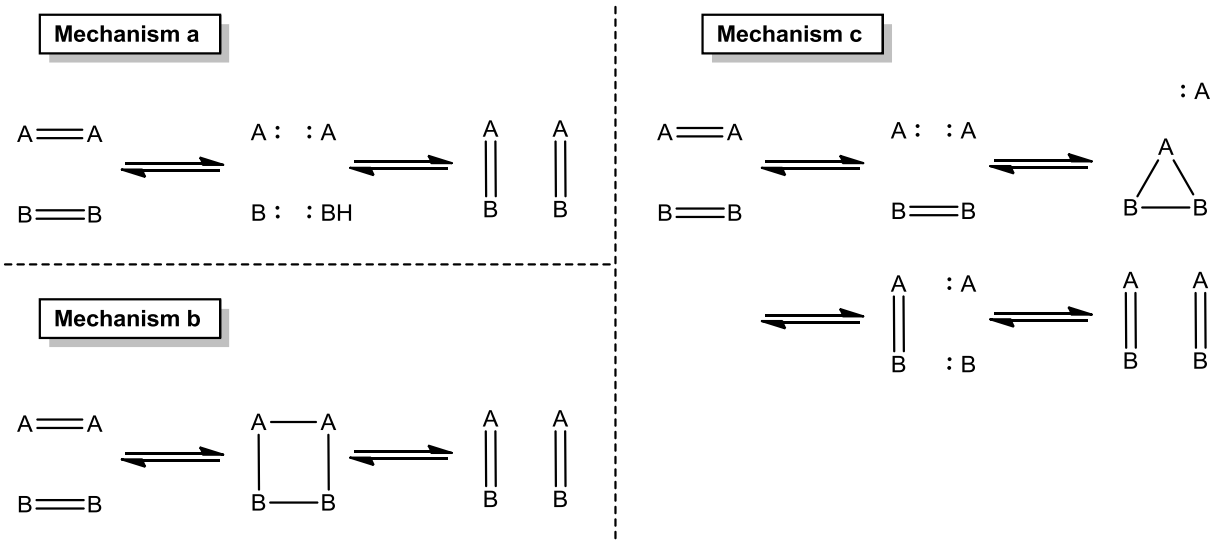

Figure 1.11: Denk's possible mechanisms for dimer scrambling. (a) and (c) require a Wanzlick equilibrium for at least one of the species.

1.2.1 The First NHC-Metal Complexes

Due to the inherent instability of the free species, the first NHC-metal complexes where not formed until the late 1960s, and generation of the free NHC had to be performed *in situ*. In 1968, Wanzlick took the approach of deprotonating an imidazolium salt with basic $Hg(OAc)_2$,[34] resulting in a *bis*-coordinated Hg(II) salt (**VI**) which could be reverted to the original NHC salt on addition of H_2S (Scheme 1.12).

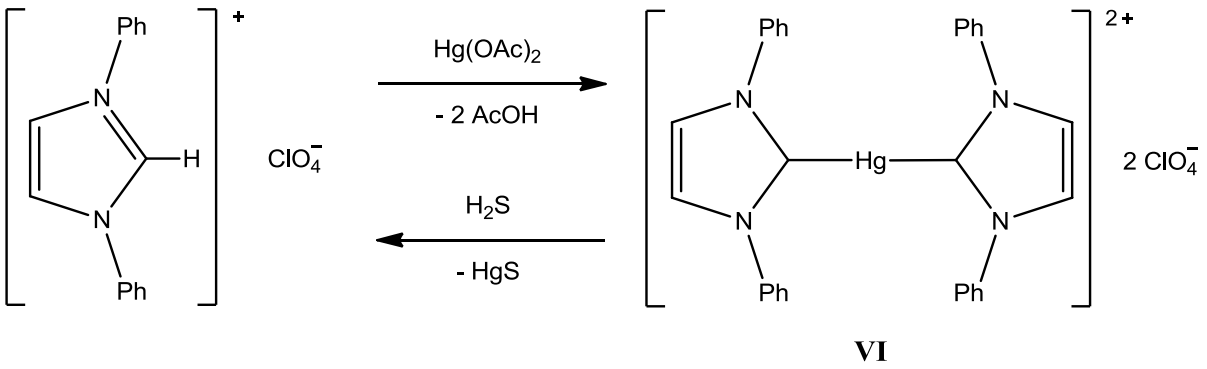

VI

Scheme 1.12: Formation of the first cationic NHC-metal complex.

Also in 1968, Öfele synthesised a chromium-NHC complex (**VII**) by thermolysis of an imidazolium salt containing a metal hydride counter-ion acting as an *in situ* base (Scheme 1.13).[11]

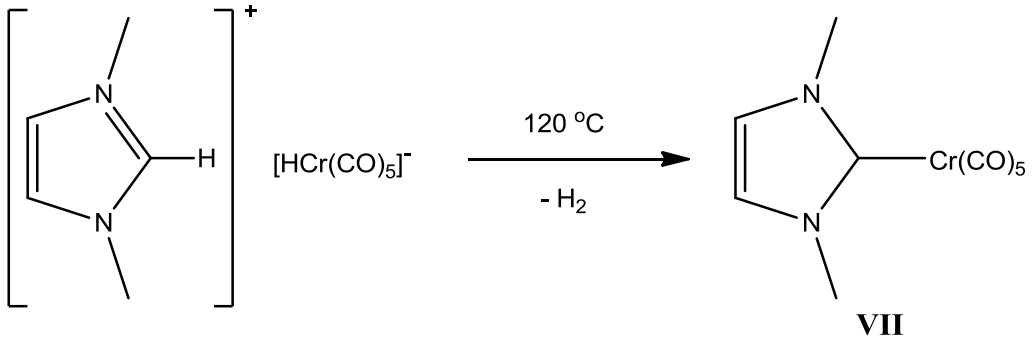

VII

Scheme 1.13: Synthesis of the first neutral NHC-metal complex.

Both these complexes are thermally robust and were synthesised in good yield. These complexes showcased the stability offered by using NHCs as ligands, and paved the way for a new area of coordination chemistry.

1.2.2 Free *N*-Heterocyclic Carbenes

The first successful attempt at creating a free NHC in solution was achieved by Wanzlick *et al.* in 1970.[13, 35] Extending the π-system of the imidizole ring with phenyl groups was thought to increase the electronic stabilisation available to the electron deficient carbon centre, as well as offering increased steric shielding. Reactions carried out with electrophilic species proceeded as expected leading to nucleophilic addition of the NHC or deprotonation of an acidic proton (Scheme 1.14). In additional support, analogous imidazolylidene species were also observed to exhibit the characteristics of a free NHC in solution.

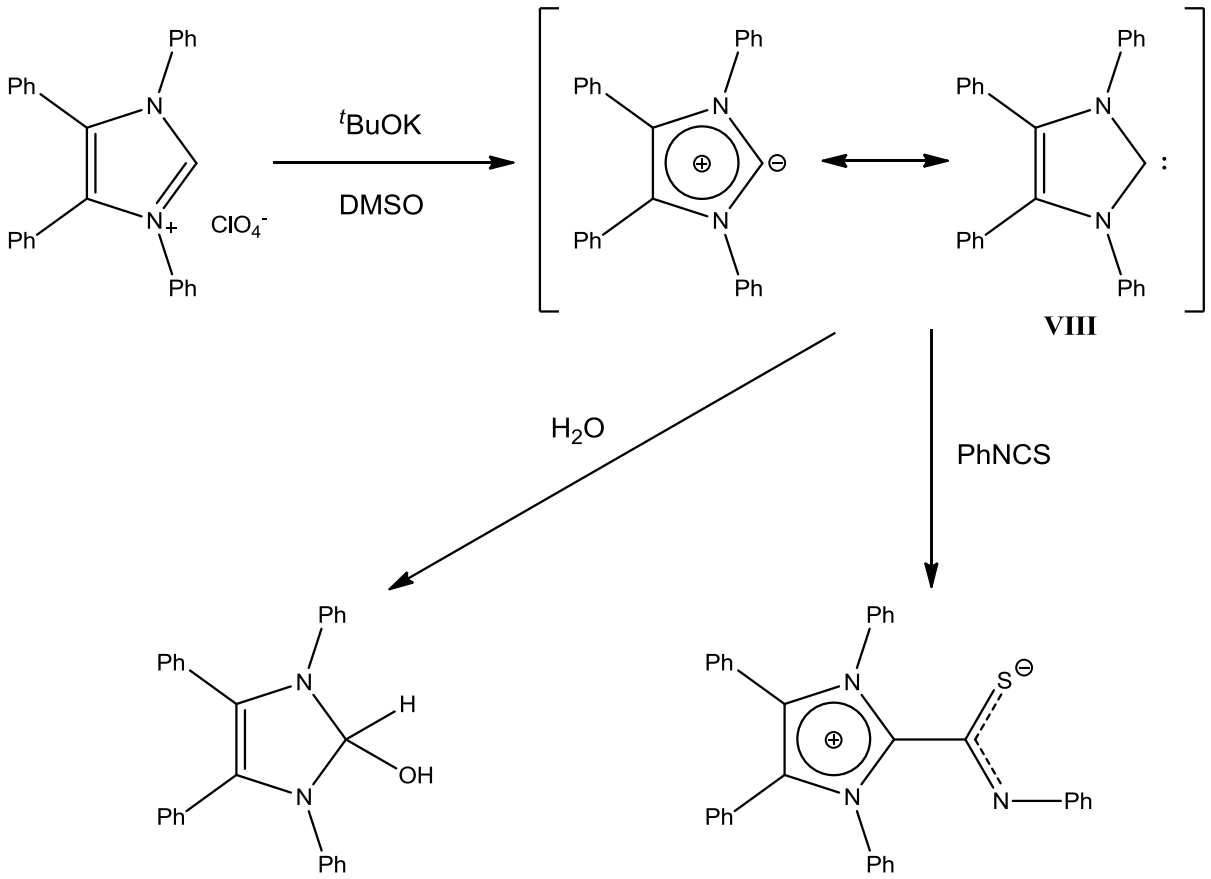

Scheme 1.14: Products observed by Wanzlick supporting the existence of a free nucleophilic carbene in solution.

However, the free NHC was never isolated or characterised, although subsequent reactions were indicative of a basic/nucleophilic species. In this case, the sterics of the system were sufficient that no dimerisation was observed as a side product in any of these processes.

In 1988, Bertrand *et al.* reported a heteroatom stabilised carbene.[36] This λ^3-phosphinocarbene species (**IX**) exhibited surprising stability in solution, an observation attributed to the potential for a λ^5-phosphaactylene resonance form. Studies of the reactivity of these systems generally favoured the phosphaacetylene form, although there were some examples of carbene-like behaviour.

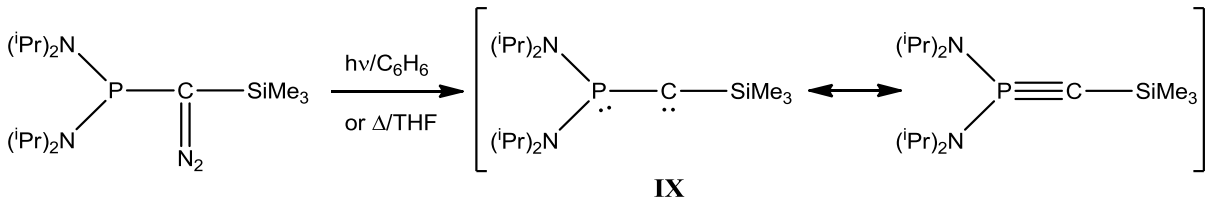

IX

Scheme 1.15: Synthesis of a stable phosphinocarbene/phosphaacetylene

In a review of these systems, some years later, their synthesis and reactivity had been optimised and a crystal structure was obtained to support these initial findings.[37] It was not until 1991 however that a free, crystalline NHC was isolated in efforts by Arduengo *et al*.[38] Highly sterically demanding adamantyl groups were exploited as the *N*-substituents; this extra bulk around the carbene centre prevented dimerisation and allowed the isolation and analysis by X-ray crystallography of a stable, crystalline NHC (**X**).

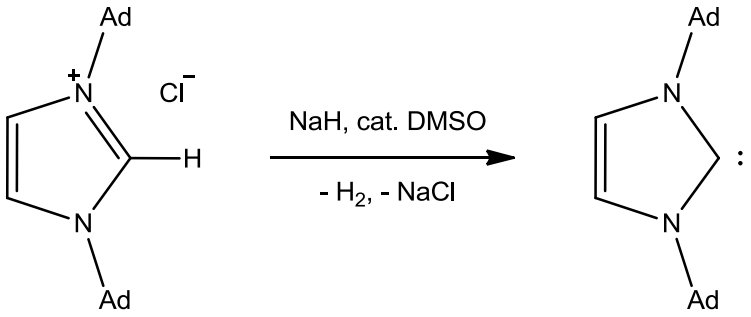

X

Scheme 1.16: Synthesis of the first crystalline *N*-heterocyclic carbene.

X was isolated in high yield (96%), and was found to be thermally stable, as it could be melted and reformed without change at its melting point (240 °C). Subsequently, this work has paved the way for development of a range of crystalline NHCs which can be stored as solids under dry atmospheres (Fig 1.17).[2, 15, 39-41]

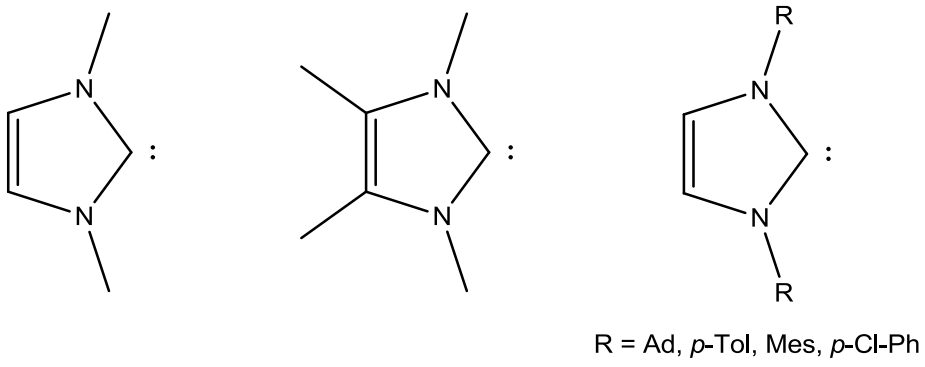

XI **XII** **XIII - XVI**

Figure 1.17: Novel crystalline (except **XI**) NHCs synthesised by Arduengo and Herrmann.

Due to the poor solubility of the NHC salts themselves and the bases used for their deprotonation in more inert solvents (e.g. THF, acetonitrile), Herrmann *et al.* reported a modified method of producing free NHCs.[40] By using a mixture of liquid NH_3 and THF, the solubility of the imidazolium salt and base (NaH or KNH_2) could be dramatically improved, and deprotonation was reported to occur within minutes at -30 °C. After evaporation of the NH_3 and addition of ether or hexane, the pure NHC could then be isolated by filtration.

1.2.3 Electronic Properties of NHCs

In 1993, Öfele came to the conclusion that "heterocyclic mono- and (chelating) dicarbenes of the aza-type are congeners of phosphines and diphosphines, with regard to their metal-coordination chemistry".[42] A series of spectroscopic studies was employed to determine the donor properties of NHC ligands, and it was found that, like phosphines, NHCs are strong σ-donors and exhibit almost no π-backbonding.[7, 14, 43] It is now widely accepted that, in general, NHC species are better σ-donors than even the most potent phosphine ligands.[44]

The inductively electron withdrawing amino substituents in NHCs stabilise the σ-orbital of the carbene, whereas the π-donating properties of the nitrogens raise the energy of the p_π-orbital. This results in singlet-triplet gaps of 65-85 kcal/mol across the NHC class.[45] As a result, it would be expected the NHCs would bind in a Fischer-type mode to Transition metals. Conversely, photoelectron spectroscopy and density functional theory (DFT) calculations have shown that, for the group 10 metals, binding occurs almost entirely through the σ-framework.[46] There is found to be some interaction of the high energy NHC p_π-orbital with the metal d_π orbital, however this is a weak interaction and coordination of NHC complexes can be generally thought of as being bonded via a single bond. In the 1990s, a wide range of NHC complexes with group 13 and 14,[4, 6, 8, 9] lanthanides,[23, 47, 48] alkaline earth,[5, 43, 49] and even some alkali metals[50, 51] was reported which do not offer π-back donation, thereby serving as circumstantial evidence of strong σ-donation and a lack of back-bonding.

In order to create a library of NHCs, the donor strengths of the ligands have been analysed used a variety of techniques. NHC→M donor strength has classically been measured by observing the CO stretching frequencies in carbonyl-containing carbene complexes.[52-54] Increased σ-donor strength should result in a reduced CO vibrational frequency due to a more electron-rich metal centre being able to back-bond more strongly to the CO π*-orbital and reduce the C≡O bond order. This analysis is also influenced by the small metal to NHC π-interaction which is not always a negligible contribution to the bonding (e.g. 15-30% in group 11 complexes).[55]

A more recent method employed to determine the σ-donor strength of carbenes is that of measuring the ^{13}C-NMR shift of the carbenic centre in the free ligand.[56, 57] These shifts generally appear in the region δ_C 200-260 ppm, with a higher chemical shift denoting

a more strongly donating carbene. This increase in the chemical shift can be rationalised by the increased p-character of the σ orbital, meaning that the lone pair is further extended from the carbon leading to a more deshielded carbon and stronger donating carbene. Increasing the angle at the carbene centre (section 1.1) leads to an increased p-character and a reduced s-p_π energy gap. As the energy gap reduces, the triplet contribution to the electronic structure will increase and this will also deshield the carbene centre.[58]

A series of saturated, expanded ring and acyclic *N*,*N*-substituted carbenes have been synthesised which display a wide range of donor strengths (Fig 1.18).

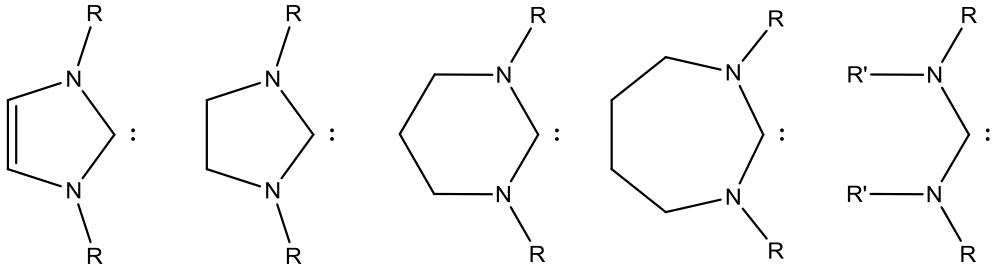

R = ^{i}Pr (δ_C/ppm)	210.5	236.8	236.1	251.2 (Cy)	255.5 (R' = ^{i}Pr)
R = Mes (δ_C/ppm)	219.7	243.8	244.9	257.3	-
R = Dipp (δ_C/ppm)	220.6	244.0	245.1	260.2	248.9 (R' = Me)

Figure 1.18: Effect of ring size/strain on ^{13}C NMR shift of carbene.

It is worth noting that changing the *N*-substituent, in cyclic carbenes, from alkyl to aryl increases the donor strength, but changing the type of aryl group has little effect. It is also advantageous that the sterics of the NHC can be altered without significantly affecting the donor properties. A few acyclic "NHC"-type systems have been synthesised which exhibit donor strengths similar to that of the 7-membered NHCs,[59, 60] suggesting that the conformational flexibility of the 7-membered rings can allow optimal geometry across the NCN framework.

As discussed above, the size of the backbone has a marked effect on the basicity of the NHC. Equally, functional groups and hydrocarbon chains can affect the electronics at the carbene centre. Glorius *et al.* investigated the effects of placing a variety of electron donating and withdrawing substituents at the 4 and 5 positions of 5-membered NHCs (Fig 1.19) by measuring the two ν(CO) stretches of the corresponding (NHC)Ir(CO)$_2$Cl complexes.[61]

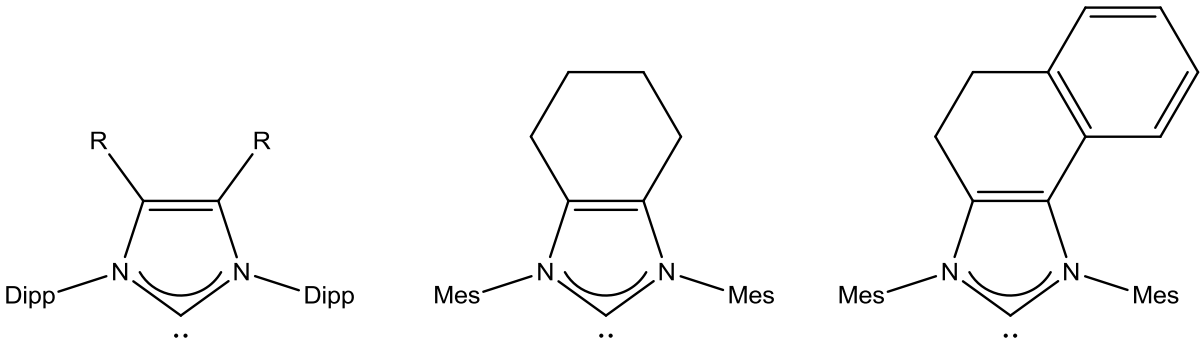

R = H, H (**XVII**); Cl, Cl (**XVIII**)
R = fused Cy (**XIX**)

XX **XXI**

Figure 1.19: Some of the NHCs analysed in the (NHC)Ir(CO)$_2$Cl complex.

For IPr (**XVII**), the average ν(CO) measured was reported as 2024 cm^{-1}. Nolan *et al.* reported that with Cl substituted on the backbone (**XVIII**) the average ν(CO) value increases to 2028 cm^{-1} implying a large reduction in the donor power of the NHC.[54] This is as expected, due to the electron withdrawing nature of the chlorine atoms. In contrast, σ-donating alkyl substituents as in **XX**, results in a reduction of ν(CO) to 2022 cm^{-1}.

Comparison of **XX** and **XXI** shows a small reduction in the σ-donating ability of the NHC when incorporating an additional aromatic substituent (average ν(CO) of 2020 cm^{-1} and 2021 cm^{-1} respectively). This is due to the aromatic π-system being orthogonal to the σ-framework through which the donation occurs. Nevertheless, the increased delocalisation

will alter the length of the backbone C–C bonds which in turn affects the NCN angle. Narrowing of the NCN angle will reduce the p-character of the σ-donor orbital, thus reducing the donor strength of the NHC.

1.2.3.1 Other Cyclic Carbenes

The first examples of cyclic carbenes featuring non-N heteroatoms appeared in 1985 as metal complexes of N,O-heterocyclic carbenes.[62] Free systems containing more than two heteroatoms were not isolated until 1995, with the synthesis of **XXII** (Fig 1.20) by Enders *et al.*[41] Surprisingly, the addition of this extra nitrogen into the backbone has little effect on the ^{13}C-NMR shift of the carbenic centre. In 1997, this was followed by the formal substitution of nitrogen with sulphur by Arduengo to form the first example of a free X,Y-type carbene.[63]

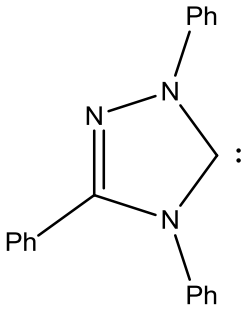

XXII

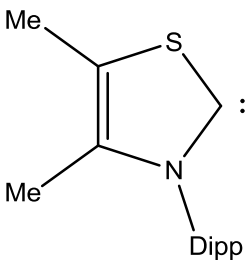

XXIII

Figure 1.20: Enders' triazolylidene (*left*) and Arduengo's thiazolylidene (*right*).

Perhaps unsurprisingly, replacing nitrogen with sulphur has a large effect on the electronic properties at the carbenic centre. The ^{13}C-NMR shift of the NCS fragment moves more than 34 ppm downfield compared to the NCN of the "parent" carbene. Relatively recently there have been more examples of these cyclic carbenes, including a P-heterocyclic carbene reported by Bertrand *et al.*[64] So called PHCs have poorer π-orbital overlap across the carbene centre and, as a result, these systems are not planar. This in turn affects the electronics of the carbene and the ^{13}C NMR shifts for PHCs fall around δ_C 185

ppm, i.e. significantly lower than NHCs. However, this is a case of failure of the correlation of σ-basicity and ^{13}C shift. When taken with the "$Rh(CO)_2Cl$" fragment, PHCs were found to be of comparable donor strength to some of the more basic NHCs, giving low values for ν(CO).

In 2001, Bertrand *et al.* showed that it is not necessary to have two electron donating atoms about the carbenic centre in order to isolate a stable, free carbene.[65] They prepared a range of (amino)(aryl)carbenes which could be crystallised and handled under inert conditions. These carbenes could not be synthesised with *tert*-butyl substituents on the aryl ring due to CH oxidative addition by the highly reactive carbene, resulting in the cyclic species **XXIV** (Scheme 1.21).

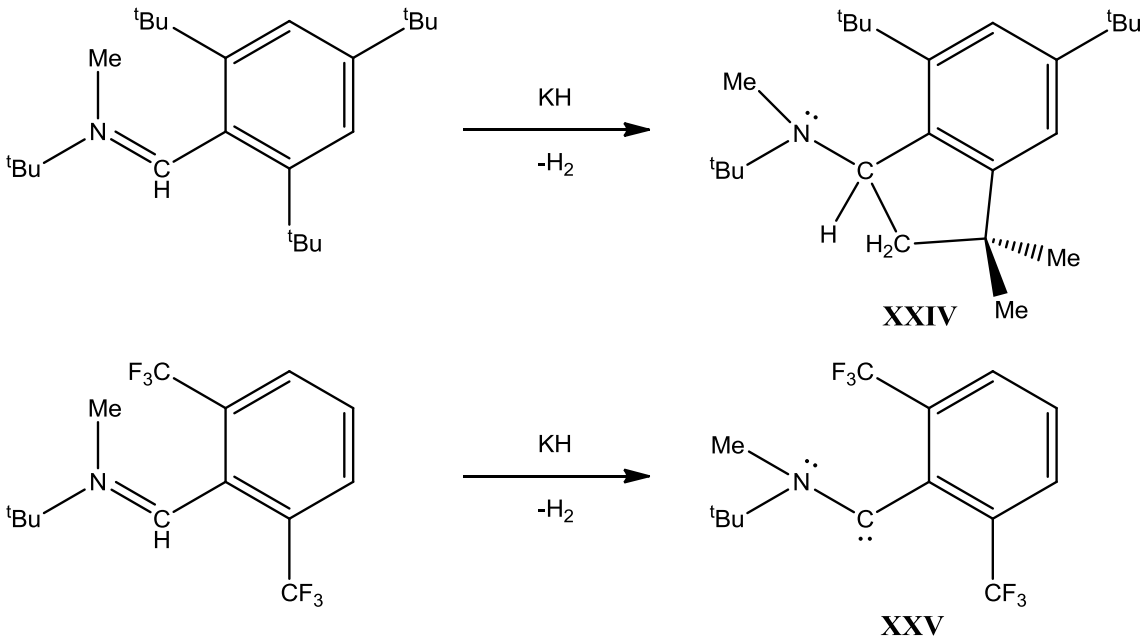

Scheme 1.21: Synthesis of a stable, crystalline (amino)(aryl)carbene.

Subsequently, in 2005, Bertrand *et al.* developed a series of cyclic analogues of these carbenes, cyclic(alkyl)(amino)carbenes, or CAACs (Fig 1.22).[66] These systems are reported to be relatively strong donors by the ν(CO) measurements, but the ^{13}C-NMR shifts

of δ_C 304-323 would imply an extremely powerful σ-donor. This shift can perhaps be explained by the reduced π-donation, due to the lack of a second heteroatom. As a result, this class of cyclic carbene also has greater potential for π-back bonding.

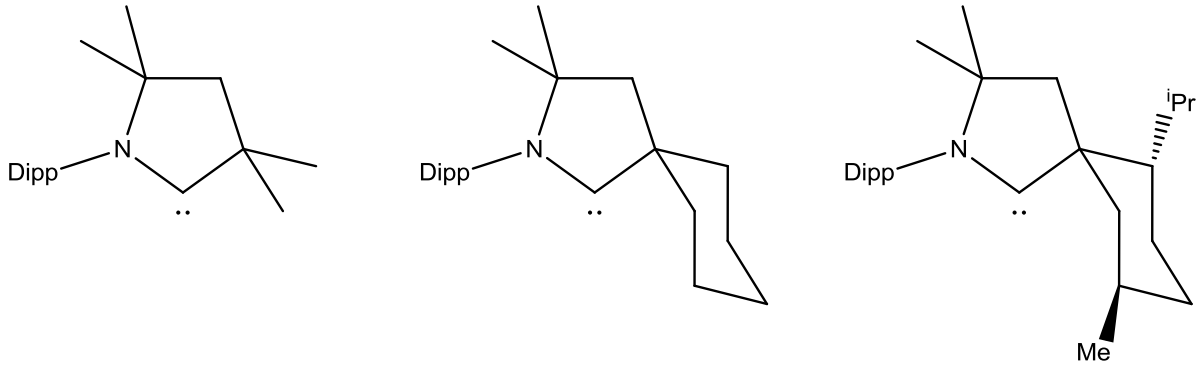

XXVI **XXVII** **XXVIII**

Figure 1.22: Range of first CAACs, **XXVIII** exhibits a locked Cy-group.

1.2.3.2 Abnormal Carbenes

First reported by Crabtree,[67, 68] Lebel,[69] and Lassaletta,[70] abnormal carbenes (aNHC) resemble Bertand's CAAC ligands as they are bound through the C4 position as opposed to the normal C2 coordination. As a result, they are considered to be much stronger donors than their normal NHC counter-parts and have received a lot of interest recently.[20, 71] It was not until 2009 that a free aNHC was isolated by Bertand *et al.*[72]

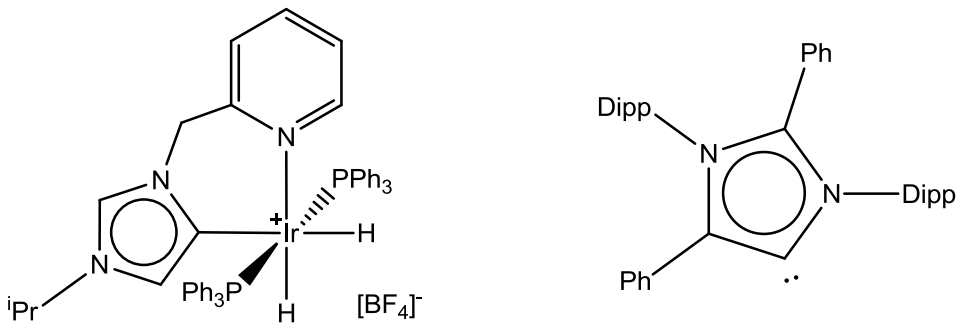

XXIV **XXX**

Figure 1.23: Crabtree's first aNHC complex (*left*); Bertrand's first crystalline aNHC (*right*).

In general, the C2 proton is much more acidic than the C4 position due to the increased stabilisation from the two nitrogen donors. Bertrand's method to isolate a free aNHC required blocking of the C2 position by, in this case, a phenyl group. In Crabtree's complex, binding through the C4 site was attributed to the increased steric congestion at the metal if bound via the C2 position. C2 coordination could be observed in an analogous system if the *N*-bound ^{i}Pr group was replaced with a methyl group.

1.2.4 Steric Properties of NHCs

N-heterocyclic carbenes are a highly customisable ligand set, being able to support a wide variety of aliphatic and aromatic N-based substituents. The steric shielding around the carbenic centre can be tuned by increasing or decreasing the size of the flanking groups on the ring. For the analogous phosphine ligands, a steric parameter referred to as the "Tolman cone angle" is used to quantity the steric demand of a given donor (Fig 1.24).[73]

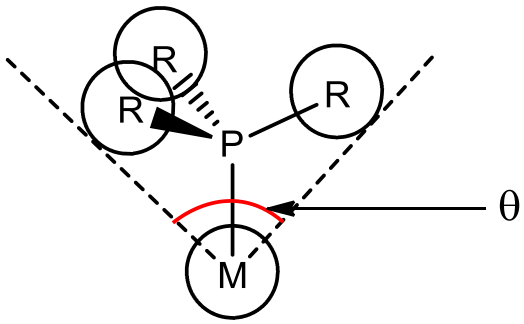

Figure 1.24: Tolman cone angle (θ) for phosphines.

This type of measurement does not apply so well to NHCs as they occupy a hemispherical space, and only contain a single angle between the *N*-substituents. As a result, a parameter known as the "Percent Buried Volume" (%V_{bur}) was developed by Nolan, Cavallo *et al.*[74-76] This method calculates the percentage volume occupied by the NHC within a sphere (of radius 3.0 Å for most metals) surrounding the metal centre by

utilizing the X-ray data of a metal complex (Fig 1.25). The values so calculated give an indication of the accessibility of the metal centre, which is useful when designing catalysts and low valent species.

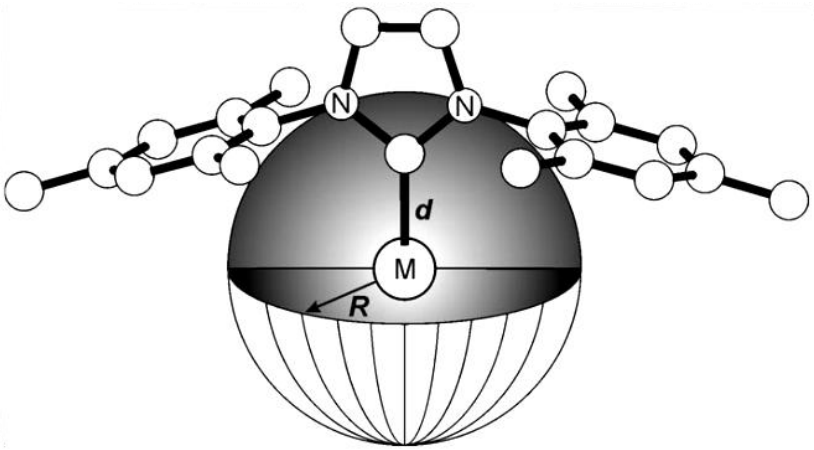

Figure 1.25: $\%V_{bur}$ for NHCs bound to a metal.[74]

In a review by Nolan *et al.*, it was shown that the Tolman parameter and $\%V_{bur}$ value for a wide range of phosphines showed a good correlation and hence, $\%V_{bur}$ could be used as a useful comparison of the steric properties of phosphines and NHCs.[77] This work reports the $\%V_{bur}$ values for some of the most common NHC ligands, ranging from 26-52% assuming a M–NHC bond length of 2.0 Å.

As one would expect, steric bulk closer the carbene centre has the greatest effect on $\%V_{bur}$ (e.g. *ortho*-substituents on aromatic groups). Hence, for the complex type (NHC)AuCl we see the trend IMes < IPr < I^{t}Bu is observed. The limitations of this model are exemplified when square-planar systems are analysed, such as (NHC)IrCl(CO)$_2$. Due to the various conformations adopted and ligand flexibility, the $\%V_{bur}$ values are affected and IPr replaces I^{t}Bu as the largest ligand in this series.[78] Ligand flexibility has now been incorporated into the $\%V_{bur}$ model by dynamic DFT calculations carried out by Cavallo *et al.*[79]

In Cavallo's original study, for systems of the type $Cp^*Ru(NHC)Cl$, there appeared to be good correlation between the percentage buried volume and the experimental bond dissociation enthalpy (BDE).[76] This data highlights the importance of sterics in affecting the bond enthalpies for NHC–M complexes.

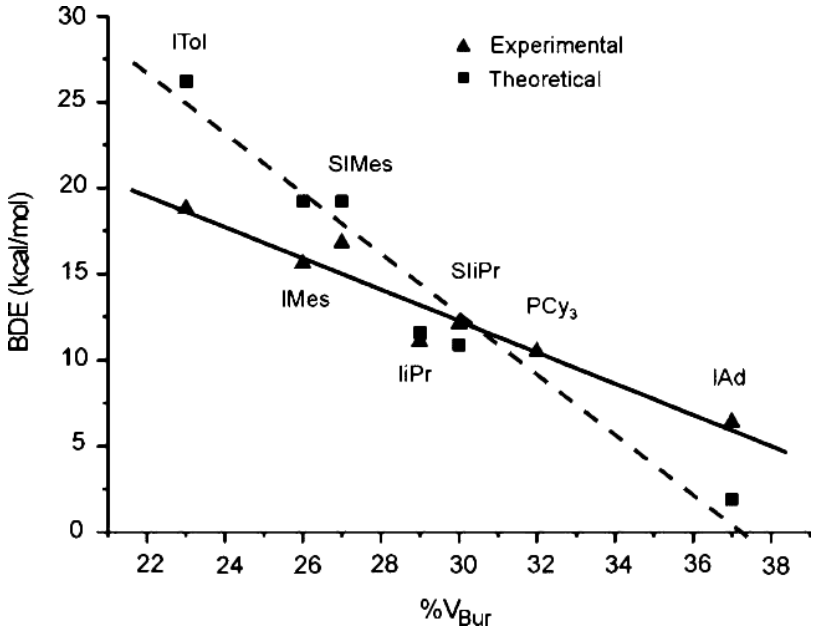

Figure 1.26: Cavallo's plot showing the association of $\%V_{bur}$ with BDE, reproduced from the paper by Cavallo *et al.*[76]

Percent buried volume is also now regarded as a useful tool to analyse the flexibility of extremely bulky ligands to accommodate a variety of metal fragments. For example, IPr* (Fig 1.27) which is widely accepted to be an extremely hindered NHC ligand, exhibits a $\%V_{bur}$ of 53.6% on AgCl but only 41.2% on Rh(acac)(CO).[80] It appears that the steric protection offered by this ligand is not as rigid as expected. More recently, the ligand IPr** has emerged, boasting a record $\%V_{bur}$ of 56.7% on AgCl.[81] Unfortunately, its $\%V_{bur}$ has not been measured on Rh(acac)(CO) for comparison with IPr*.

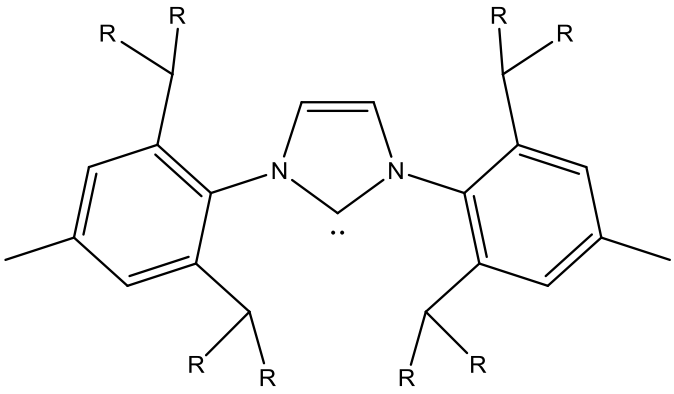

R = Ph (IPr*), 4-^{t}BuC$_6$H$_4$ (IPr**)

Figure 1.27: Two of the most sterically demanding NHCs reported to date.

While the steric properties of NHCs are constantly being tuned and altered for uses in different applications, only relatively recently has the idea of lengthening the backbone chain been thoroughly investigated.

1.3 Expanded Ring NHCs

Increasing the ring size of an NHC is thought to have two effects; (i) increased steric demands by increasing the angle across the NCN framework, and (ii) increasing the σ-donor strength through inductive effects as well as by increasing the lone pair p-character resulting from an increased NCN angle. In addition, the lack of aromaticity in these saturated systems leads to an increased π-donation contribution from the nitrogens.[82, 83] This then raises the antibonding p_π-orbital at the carbene centre, hence increasing the potential for back-bonding. Saturated NHCs have been reported as both stronger σ-donors and better π-acceptors than their unsaturated counter-parts, resulting in stronger M-C bonds and more electron rich metal centres.[84]

In 1999, Alder *et al.* reported the first example of an NHC based on a 6-membered ring.[51] The method employed is analogous to that used for the synthesis of the first saturated, 5-membered NHCs (Scheme 1.28). In contrast to its 5-membered analogue, on

formation of the carbene, the 6-membered NHC was resistant to dimerisation, presumably due to the increased steric shielding of the carbenic centre.

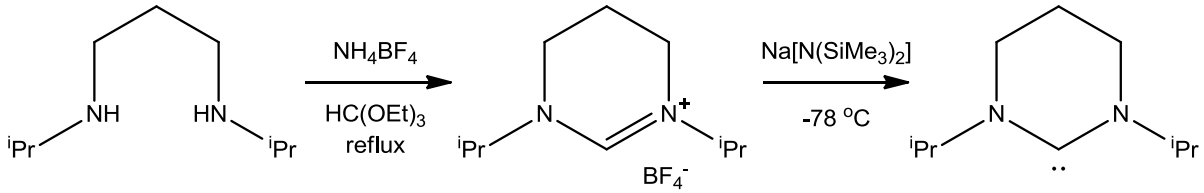

Scheme 1.28: Synthesis of the first 6-membered NHC (6-^{i}Pr).

In the presence of an extra equivalent of base, in this case K[N(SiMe$_3$)$_2$], coordination of 6-^{i}Pr to K$^+$ is observed. This is also observed with Na$^+$, and these systems were the first examples of non-lithium, Group I complexes of NHCs.

Four years later, an unsaturated analogue of this system was reported by Richeson *et al.*, bearing a naphthyl moiety across the back-bone (Fig 1.29).[85] This leads to a planar ring suggesting delocalisation of the π-electrons to stabilise the free carbene. However, the authors commented that the N–C$_{naphth}$ bond lengths are long enough to suggest that the nitrogen lone pairs are predominantly involved with interaction to the C$_{carbene}$, and do not delocalise effectively into the naphthyl system. Hence, this is not a true comparison with the imidazole-based NHCs.

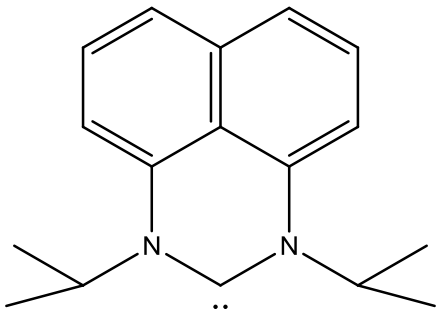

XXXI

Figure 1.29: Unsaturated, 6-membered NHC.

A study of expanded ring NHCs with rhodium carbonyls was performed by Buchmeiser *et al.* in an attempt to compare the donor strength of these new ligands with existing NHCs.[86] Also reported in this study was the synthesis of the first 6-membered NHC bearing aromatic *N*-substituents, 6-Mes (Scheme 1.31). Based on the measured ν(CO) values for these (NHC)Rh(CO)$_2$Cl complexes, 6-^{i}Pr and 6-Mes appear to be stronger donors than their 5-membered counterparts (as quantified by increased back-donation from the metal to the CO ligand) yet not as strong as the acyclic systems (Table 1.30).

NHC in (NHC)Rh(CO)$_2$Cl	**ν(CO) /cm^{-1}**
6-^{i}Pr	2063, 1982
6-Mes	2062, 1976
5-Mes	2081, 1996
IMes	2076, 2006
(^{i}Pr)$_2$NCN(^{i}Pr)$_2$	2057, 1984

Table 1.30: Comparison of ν(CO) as a measure of donor strength for expanded ring NHCs with 5-membered and acyclic systems.

An interesting example of steric pressure is highlighted here also; the coordination of two equivalents of 6-Mes at "PdCl$_2$" leads to auto-ionisation, which is not observed with the smaller 6-^{i}Pr which gives (6-^{i}Pr)$_2$PdCl$_2$ instead (Scheme 1.31). A related approach exploiting this phenomenon has led to the synthesis of a 2-coordinate Ni(I) cation by displacement of the phosphine and bromide ion from (6-Mes)(PPh$_3$)NiBr with a second 6-Mes ligand.[87]

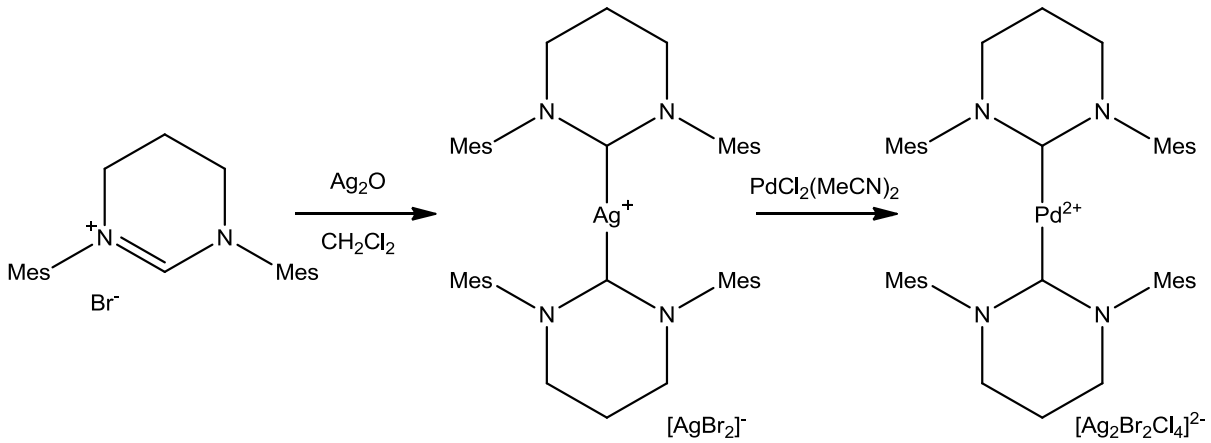

XXXII

Scheme 1.31: Coordination of 6-Mes appears to favour low valent systems by ejection of the halides.

These palladium systems were the some of the first expanded ring NHC complexes that were studied as analogues of previously reported NHC-based catalysts. The Heck catalysts, (6-^{i}Pr)$_2$PdCl$_2$ and **XXXII**, were trialled with a range of substrates. In general, they both produced excellent conversion even at low catalyst loadings. **XXXII** coupled butyl acrylate with 4-bromoacetophenone in >99% conversion after 190 h at 0.00005 mol%, equating to a TON of ~ 2 x 10^6. These successes were further supported by the synthesis of active copper catalysts supported by the 6-Mes ligand.[88]

7-membered NHCs appeared 6 years later in 2005, with the first example reported by Stahl *et al.* being based upon a diaminobiphenyl, **XXXIII** (Scheme 1.32).[89] As a result, this NHC also had the advantage of chirality, and hence, of potential use in asymmetric synthesis. Unfortunately, due to the synthetic route used, the NHC could not be formed in enantiomerically pure form. This issue was overcome by using a single enantiomer of diamino-BINAP.[90]

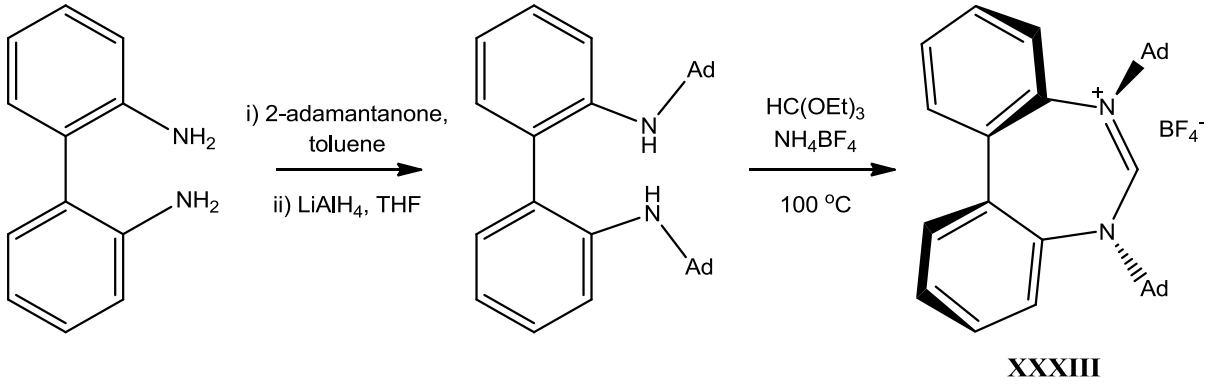

XXXIII

Scheme 1.32: Synthesis of the first 7-membered NHC salt.

These 7-membered NHCs are the first class of NHC to exhibit a non-zero torsion angle (α) between the *N*-based substituents (Fig 1.33), as defined by Fallis *et al*.[91] This distortion is due to the greater degrees of freedom in the backbone as well as the deviation from the ideal value of 120° for the CNC angles. Hence, the backbone can twist to reduce the strain energy at the sp^2 nitrogens. In an analysis by Fallis, the average angles around the nitrogens in a range of 7-membered NHC complexes and salts were calculated. These average values sum to 359.3° showing how planarity in maintained.

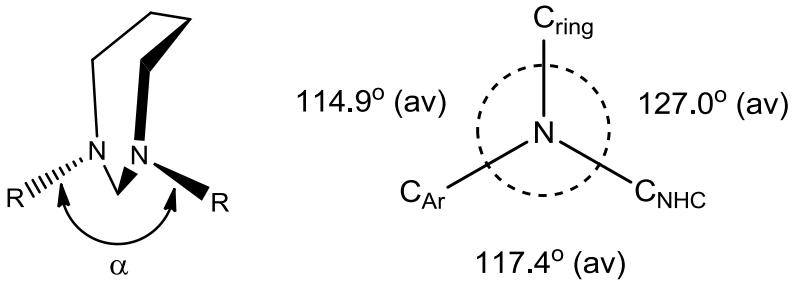

Figure 1.33: Torsion angle (α) between the two N-R bonds (*left*), and depiction by Fallis showing the average angles around the nitrogens in 7-membered NHC salts and complexes (*right*).

Subsequently, a wide variety of expanded ring NHCs have been reported,[92-94] including a series of 6-membered CAACs.[95] By far the most complete report of the

syntheses of *N*-aryl expanded ring NHCs was published by Fallis *et al.* in 2008.[91] Crystal data reported for the free NHCs and AgBr adducts give a good basis for comparison between analogous 6- and 7-membered systems. For example, one would expect the NCN angle to be affected by the ring size, and hence an increase in donor ability. Free 6-Mes and 7-Mes show NCN angles of 114.7(1)° and 116.6(4)° respectively, thus showing the expected, albeit small, difference. When coordinated to AgBr, the NCN unit widens as the non-bonding electrons interact with the metal, resulting in angles of 118.3(3)° and 118.8(6)° respectively. These angles are now identical due to the conformational flexibility of the 7-membered ring allowing optimum geometry across the NCN framework. Hence, the steric profiles of these two ligands become very similar when complexed to a metal.

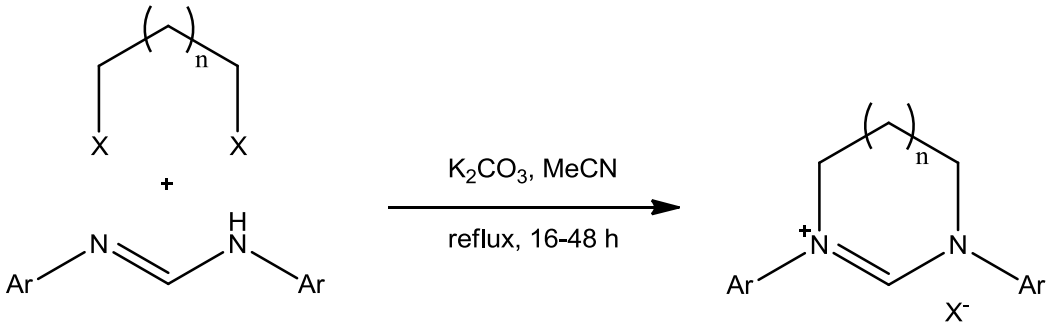

Scheme 1.34: General synthetic route to expanded ring NHC salts.

The majority of the species reported are simple to synthesise by the route depicted above (Scheme 1.34) and are highly robust when stored in a dry atmosphere. However, degradation has been observed in a subset of these expanded NHC ligands. 7'-Dipp (Scheme 1.35) has never been isolated as a free species due to cleavage of one of the N–C bonds by a suitable base, or equivalent of NHC.[96]

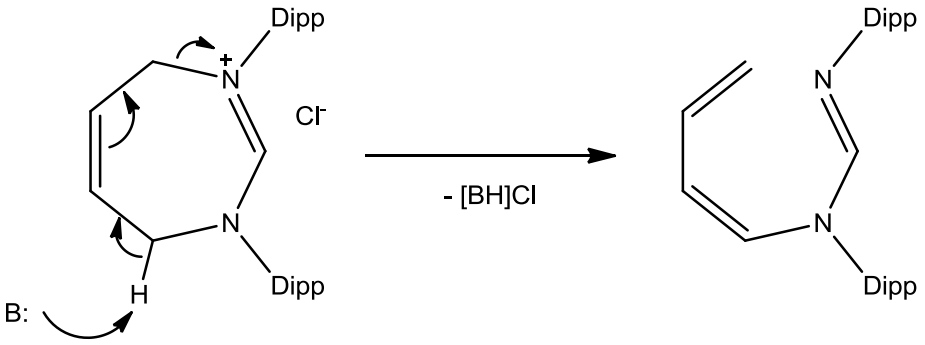

Scheme 1.35: Deprotonation of 7'-Dipp at C4 by a general base, B.

Degradation of this type has served as the explanation for the lack of existence of the NHC with a fused benzene ring on the back (Xyl7-Mes, Fig 1.36) despite its salt being well documented.[91, 95]

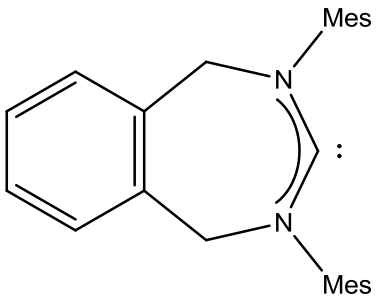

Figure 1.36: Xyl7-Mes has never been isolated in its free state due to the acidic nature of the benzylic methylene protons.

More recently, a series of 8-membered NHCs has been reported by Cavell *et al.* which now to appear to open up significantly the NCN angle (e.g. 120.1(2)° for 8-Xyl).[97] Consequently, the $\%V_{bur}$ for these systems is dramatically increased even for the smaller *N*-aryl groups (Table 1.37).

NHC complex	$\%V_{bur}$
(6-Mes)AgCl	44.0
(7-Mes)AgBr	44.7
(8-Mes)AgBr	48.7

Table 1.37: $\%V_{bur}$ for a series of expanded ring NHC silver complexes.

Understandably, the reaction times required to form these 8-membered heterocycle are long (10-14 days), yet yields are reported to be greater than 75%. Due to the time intensive procedure, there are few examples of 8-membered NHC complexes used in the literature.

1.4 NHCs in Catalysis

In recent years, NHCs have featured heavily as supporting ligands in a vast range of catalytic processes. This is attributed to the highly controllable electronic and steric properties of this ligand class, as well as the longevity of M–NHC bonds under catalytic conditions.

The first examples of NHCs replacing phosphines in catalysis were reported in 1995 when Herrmann and co-workers sought to solve the issue of phosphine-based catalyst degradation by P-C cleavage.[98] They noted that often 100 equivalents of phosphine was required to achieve suitable propagation, and systems were additionally required to be devoid of air and moisture. The solution offered was the application of NHC ligands, as exemplified in Heck coupling (Fig 1.38). Reactions were reported with turnovers of >99%, with relatively low catalyst loadings and reaction times of 10-36 h. This high activity was accompanied by high thermal stability, $(IMe)_2PdI_2$ (**XXXIV**) melts at 299 °C and resists

boiling in THF (in air) for several days, $(I_2Me)PdI_2$ (**XXXV**) melts at 280 °C but decomposes in solution above 70 °C.

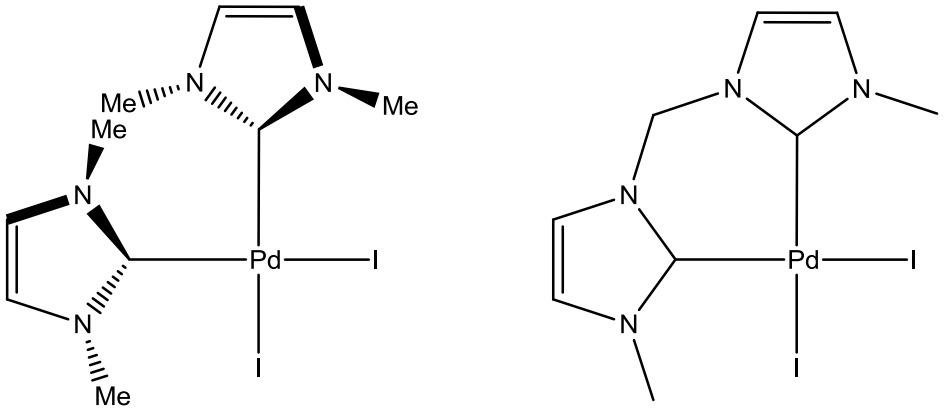

XXXIV **XXXV**

Figure 1.38: Herrmann's NHC-based Heck catalysts.

It is also of note that NHCs can arrange in a *cis*-conformation as opposed to the *trans*- arrangement required by bulky phosphines used in the analogous system. This is attributed to the planar NHCs (in contrast to conical phosphines) being able to rotate to reduce steric crowding at the *cis* position. This allows more rapid reductive elimination to Pd(0) and hence a shortened initiation time and increased rate.

This study offered an early showcase for the advantages of NHCs over phosphine ligands, and many other processes were subsequently examined.[99] Other coupling reactions, such as Suzuki,[100] Sonogashira,[101] Negishi,[102] and Buchwald-Hartwig reactions,[103] exploited the robust catalysts formed using NHCs. Perhaps one of the most famous examples of substituting a phosphine for an NHC is the development of Grubbs 2nd generation catalyst, **XXXVII** (Fig 1.39).[104] The advantages of this system over the 1st generation catalyst are a higher activity, whilst maintaining air and moisture stability. This sparked much interest in the effect of NHCs on olefin polymerisation and hydrogenation catalysts.[105-108]

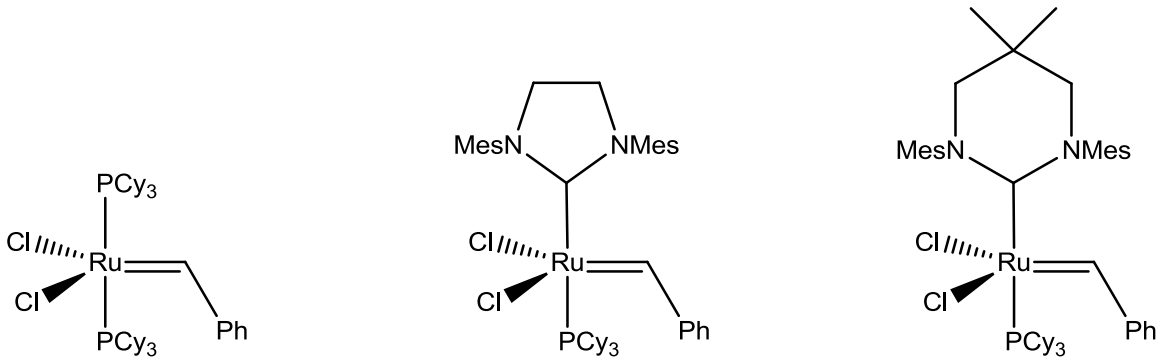

XXXVI **XXXVII** **XXXVIII**

Figure 1.39: Grubbs' 1st and 2nd generation catalysts (*left*) and a third based on a 6-membered NHC (*right*).

In 2004, Grubbs *et al.* replaced the 5-membered NHC with a 6-membered analogue to assess the effect on the activity of the system by increasing donor strength as well as sterics.[109] Despite the increased σ-donor strength of the 6-membered NHC increasing lability of the *trans*-phosphine, the activity of ring closing metathesis (RCM) was significantly reduced and ring opening metathesis polymerisation (ROMP) was slightly decreased. This was postulated to be due to the steric demand of the 6-membered NHC hindering initial coordination of the olefin, or disfavouring the formation of the metallacyclobutane intermediate. In the same year, Buchmeiser *et al.* utilised 6-Mes to modify the Hoveyda-Grubbs catalyst.[110] It was found to catalyse a narrower range of substrates and to generally give lower turnover frequencies; however the turnover numbers on suitable substrates were higher which is indicative of a more robust system.

The success of NHC-based catalysts for hydrogenation, hydrosilylation and dehydrogenation processes,[22] has led to the investigation of analogous systems bearing expanded ring NHCs. Fallis *et al.* developed rhodium and iridium systems supported by a donor-functionalised expanded ring NHC which displayed good activity for the hydrogenation of ketones (Fig 1.40).[111] Due to the size of the ring, the donor functionality

can interact strongly with the catalytic intermediate leading to prolonged life. This was followed by the synthesis of highly active and regioselective hydrosilylation catalysts by Cavell *at el.* using a Pt(0) centre supported by expanded ring NHCs (Fig 1.40).[112] More recently, Whittlesey *et al.* reported expanded ring NHC nickel catalysts which show good activity when catalysing Kumada cross-coupling reactions, in particular (6-Mes)Ni(PPh_3)Br.[113]

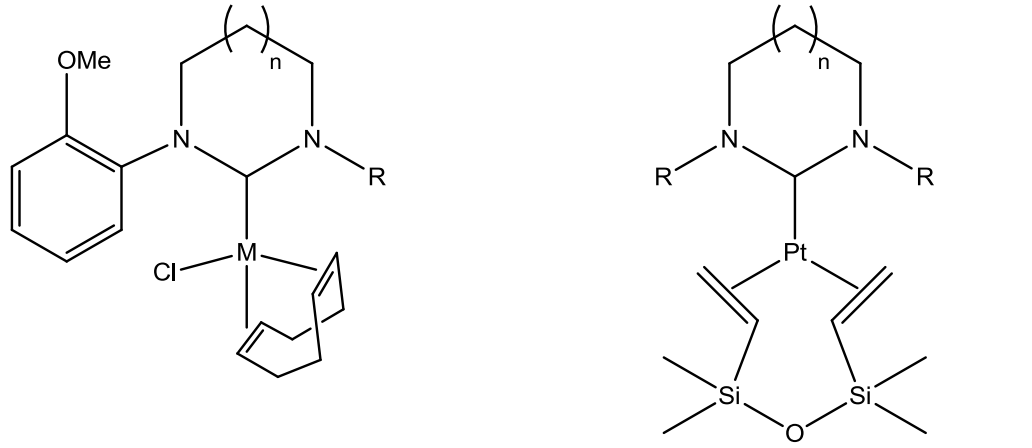

M = Rh, Ir; R = Mes, Dipp; n = 1, 2

R = Mes, Dipp, Tol, Xyl; n = 1, 2 (for Mes)

Fig 1.40: Fallis' transfer hydrogenation catalyst (*left*) and Cavell's hydrosilylation catalyst (*right*) based on expanded ring NHCs.

1.5 σ-Complexes of E-H Bonds

A σ-complex occurs when an E–H bond (E = non-metal) acts as a two electron donor towards a suitably electrophilic centre, such as an electron-poor metal (Fig 1.41).[114] These complexes contain 3 atoms and 2 electrons, and the bonding is hence described as a 3-centre-2-electron (3c-2e) bond. Depending on the electronic structure of the metal, filled d_π-orbitals can also back-donate into the σ*(EH) further weakening the E–H bond.

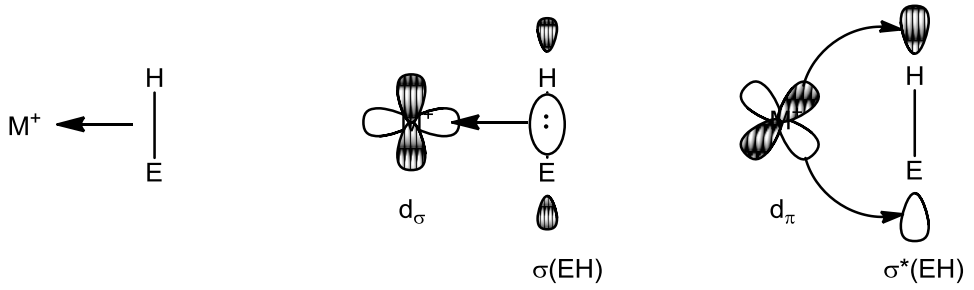

Figure 1.41: σ-bond to M^+, σ-donation component and π-back donation to σ*(EH).

In a σ-complex, coordination of the E–H bond features a σ-donation component and typically a π-back bonding component. The angle at which the E–H bond coordinates to the metal depends on the polarity of the bond and the degree of back bonding. In contrast, coordination observed in hydrogen bonding is end-on. As the bond is donating electrons from its bonding orbital, the bond is weakened and the polarity is enhanced also. The hydrogen becomes more hydridic, thus the E atom is more prone to attack by a nucleophile.

In 1960, Nöth and Hartwimmer postulated that their $Cp_2Ti(BH_4)$ complex contained σ-type interactions based upon IR data.[115] It has, however, been postulated that the electrostatic attraction due to the anionic nature of BH_4^- plays a significant role in the binding, therefore this and related complexes are not true σ-complexes. In 1965, Dahl *et al.* reported the species $Mn_3(CO)_{10}(H)(B_2H_6)$, which was crystallographically characterised as having B–H–Mn linkages (Fig 1.42).[116] However, the ligand here is formally $[B_2H_6]^{2-}$ due to there being 4-coordinate boron atoms. Then in 1969, Graham *et al.* reported what appeared to be Si-H bonds coordinating to a rhenium carbonyl species (Fig 1.42).[117] Unfortunately, complexes of this type were generally over-looked in this era, and it appears their importance had not been realised. Schubert *et al.* later examined a potential Si-H-Mn σ-interaction by neutron diffraction, yet the precise nature of the interaction could not be definitively established.[118]

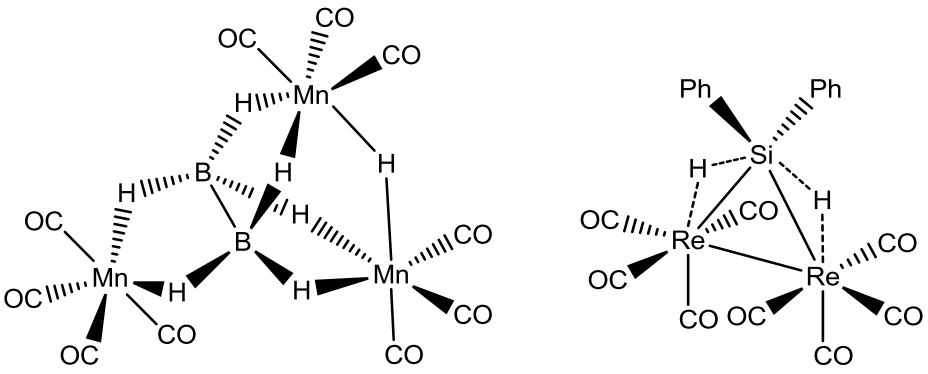

Figure 1.42: First characterised bridge B-H-M and Si-H-M complexes.

Interest in σ-complexes was sparked in earnest by the seminal paper by Kubas *et al.* in 1984 reporting the first example of a dihydrogen molecule bound to a neutral metal centre. $W(CO)_3(P^iPr_3)_2(\eta^2\text{-}H_2)$ was characterised fully by X-ray and neutron diffraction (Fig 1.43),[119] and from these experiments, it was possible to determine the location of the dihydrogen ligand as well as the H–H bond length. Given that the H–H distance was determined to be 0.84 Å (from neutron data, *cf.* 0.74 Å in free H_2), it supported the notion that the σ-bond was donating its electrons to the metal centre and thereby reducing the bond order. This partial activation had wide implications for catalytic hydrogenation chemistry, as well as a variety of other processes involving E–H cleavage.

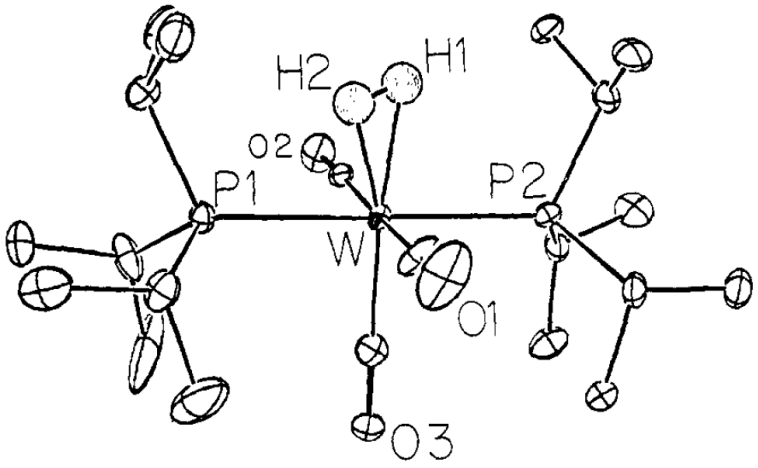

Figure 1.43: Original ellipsoid plot of Kubas' neutron diffraction data.[119]

The characterisation as a σ-complex of a non-polar bond supported the observations of Turner *et al.* based on the IR spectra of σ-complexes of CH_4 at metal-carbonyl fragments isolated in low temperature matrices.[120-122] Since then, interest has expanded in σ-complexes of alkane substrates to metals due to their potential importance in C-H activation and functionalisation. One of the biggest breakthroughs in this area was in 2009 by Brookhart *et al.*, who were able to protonate a Rh-CH_3 unit at -110 °C to form a CH_4 σ-complex at a Rh(I) centre (**XXXIX**, Scheme 1.44).[123] This species persisted at -110 °C and the authors were able to characterise the alkane complex in solution, including a ^{1}H coupled ^{13}C-NMR displaying a quintet for the rapidly interconverting methane hydrogens.

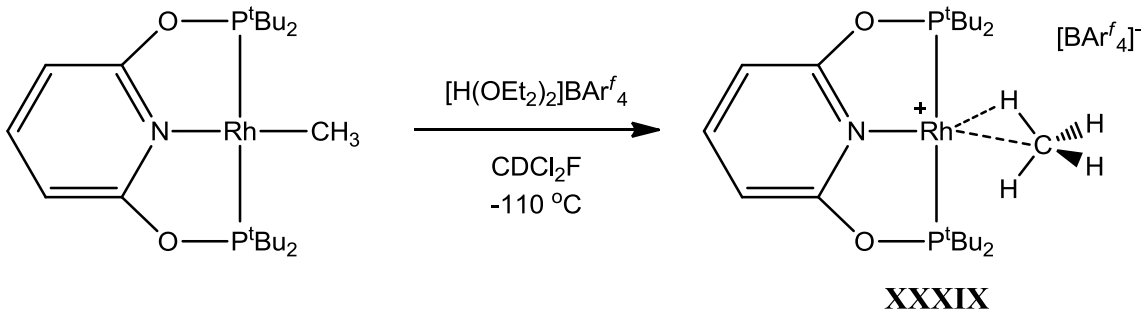

XXXIX

Scheme 1.44: Formation of the first solution stable σ-alkane complex.

Since this example there have been a couple of instances of "long-lived" σ-alkane complexes in solution that have been characterised by NMR and IR.[124-126] The first reliable solid-state structure (previous examples had featured high levels of disorder) of one of these rare Transition-metal complexes was reported by Weller *et al.* by hydrogenation of the corresponding alkene complex in the crystal phase.[127]

In 2012, Green *et al.* produced a review discussing the possible modes of σ-bonding in transition metals and beyond.[128] It was highlighted that there is a range of main group

elements that appear to accept agostic interactions (e.g. B, P, Si), hence some σ-complexes could be viewed in alternative ways (Fig 1.45).

Figure 1.45: Two representations of a B-H-M bridge: i) donation from the borane with back donation from the metal, ii) a metal-boryl complex with a bridging hydride.

1.5.1 Agostic Interactions

Intramolecular σ-complexes of C–H bonds were described and termed "agostic" interactions by Brookhart and Green in 1983.[129] Early identified examples of agostic stabilisation were observed in complexes with aryl phosphines ligands, such as $Ru(PPh_3)_3Cl_2$,[130] *trans*-$Pd(PPhMe_2)I_2$,[131] and $[Rh(PPh_3)_3]^+$,[132] in which *ortho*-hydrogens had orientated themselves to be close to the metal centre (2.5-2.8 Å). Hydrogens involved in agostic interactions were also found to be accompanied by an upfield shift in the ^{1}H-NMR spectra;[133] and in an early report by Maitlis, coupling to other ^{31}P nuclei in other metal bound phosphine ligands was observed via NMR spectroscopy.[134] The first neutron diffraction study of a system containing an agostic interaction, $[(Fe(P(OCH_3)_3)_3(\eta^3\text{-}C_8H_{13})]^+$, was reported by Williams *et al.* in 1980.[135] Here the hydrogen could be accurately located and the distance to the metal was measured as 1.874(3) Å; the corresponding C–H distance was found to be 1.164(3) Å which was the longest separation reported in a crystalline structure at that time. It was subsequently found that Kubas' dihydrogen complex, perhaps unsurprisingly, exhibited an agostic interaction when the hydrogen was removed.[136]

In 1990, Lippard *et al.* introduced the idea that C–H bonds with close proximity to metal centres may not interact, and in fact be "anagostic".[137] This was thought to be due to steric constraints forcing the C–H bond towards the metal, but with a predominantly electrostatic interaction presiding. This then brings into debate whether some of the earlier identified agostic complexes were in fact agostic. Brookhart *et al.* surmise that agostic interactions generally have a M–H separation of 1.8-2.3 Å and an upfield shift is observed in the ^{1}H NMR, whereas anagostic interactions have separations of 2.3-2.8 Å and a relatively downfield ^{1}H NMR resonance.[138]

It was observed by Shaw *et al*. that the coordination of bulky phosphines of the type $PR^{t}Bu_2$ (R = aryl) to unsaturated Ir(III) centres disfavoured dimerisation or coordination of solvent molecules.[139] Crystallographic characterisation of low valent 14-electron iridium cations bearing these ligands by Caulton *et al.* (Scheme 1.46) emphasised the importance of agostic interactions.[140] It was also highlighted that these interactions are labile and can easily be replaced by weak ligands or substrates, such as H_2, as exemplified by the interconversion of **XL** and **XLI**. This emphasised the significance of designing catalytic complexes with potential for agostic interactions.

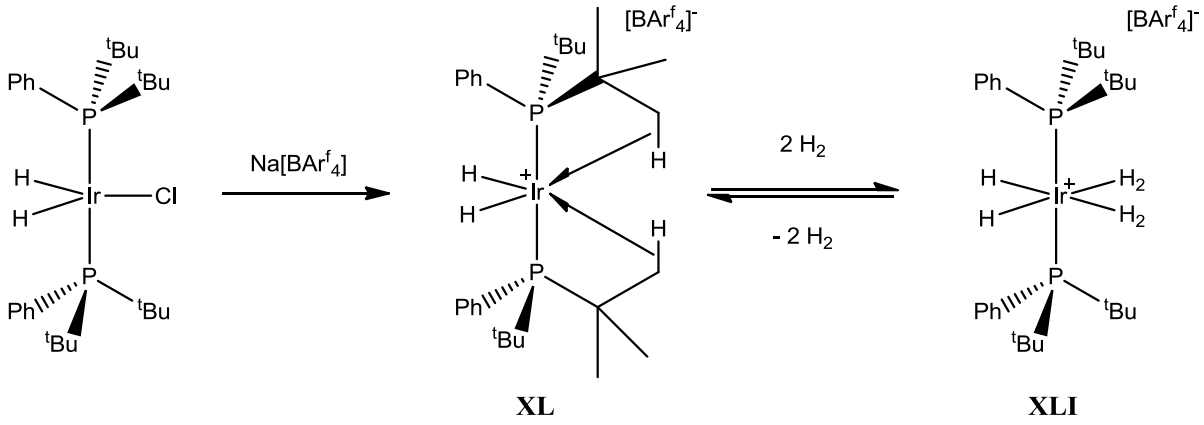

Scheme 1.46: Agostic stabilisation of a 14-electron Ir(III) cation.

Interestingly, it was reported that the analogous complexes featuring PCy_2Ph and P^iPr_2Ph behaved in a different manner.[141] The reduction in sterics allowed for *tris*-coordination of the phosphines to give $[Ir(PR_2Ph)_3(H)_2]^+$ (R = Cy, ^{i}Pr) as the cation. Furthermore, the P^iPr_2Ph ligand appeared to offer no agostic stabilisation of the 16-electron metal centre in the crystal structure, whereas an agostic interaction was clearly identifiable for PCy_2Ph. Given that the donor strength of these phosphines is near identical, it appears the increased steric demands of Cy over ^{i}Pr results in an agostic interaction caused by close proximity.

The effect of *trans*-ligands on agostic interactions has been exemplified by comparison of the crystal structures of the ruthenium complex $(P^tBu_2Me)Ru(Ph)Cl(CO)$, **XLII**, before and after chloride abstraction (Fig 1.47).[142]

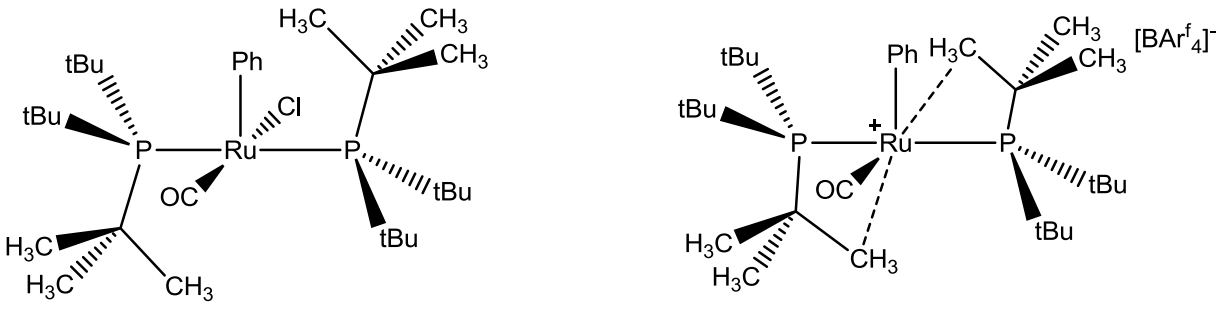

XLII **XLIII**

Figure 1.47: Formation of agostic interactions on formation of a more electron deficient, charged metal centre.

There is no interaction of the ^{t}Bu groups with the ruthenium centre in **XLII** to stabilise the 16-electron species [$d(Ru–C_{tBu})$ = 3.24 and 3.76 Å] despite its electron deficient nature. However, two agostic interactions form on halide abstraction to **XLIII**, due to the existence of 14-electron cation [$d(Ru–C_{tBu})$ = 2.87 and 2.88 Å]. The lack of agostic

interactions in **XLII** suggests that the substituents *trans*- to the vacant sites have little effect on the formation and the strength of the interaction. This is implied by **XLIII** having no variation in the agostic distance despite being *trans*- to very different ligands.

1.5.2 Activation of E–H Bonds

σ-Complexation at a relatively electron rich metal centre can lead to scission of the E–H bond if back-donation into the σ^*-orbital is appreciable. Oxidative addition has been observed before, but only recently been rationalised with the σ-complex being a potential intermediate. Oxidative addition studies of various substrates at Vaska's complex,[143] from polar HCl to non-polar H_2 (Scheme 1.48),[144] have helped to pave the way to understanding homogeneous catalysis. Four years later, Wilkinson *et al.* reported a highly actively hydrogenation catalyst, $(PPh_3)_3RhCl$, exploiting the knowledge imparted by Vaska concerning the oxidative addition of hydrogen.[145]

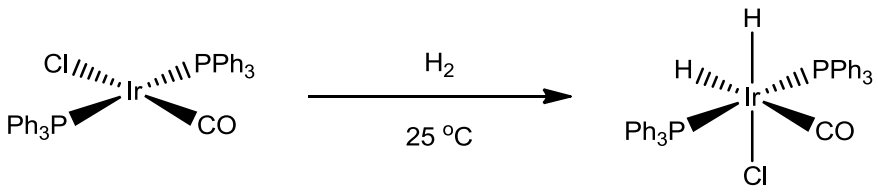

Scheme 1.48: Oxidative addition of H_2 to Vaska's complex.

Lapinte *et al.* reported the ability to trap out the dihydrogen complex at a $Cp^*Fe(dppe)$ fragment before oxidative addition to the dihydride (Scheme 1.49).[146] In this case synthesis was achieved by protonation of a metal hydride, and was confirmed by analysis of ^1H T_1 relaxation measurements.

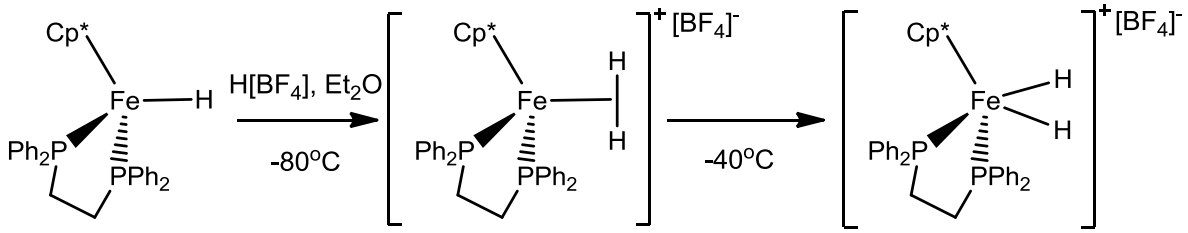

Scheme 1.49: Stabilisation of the η^2-H_2 intermediate complex before oxidative addition to the dihydride.

The first example of the activation of a C–H bond by this route was attributed to Chatt *et al.* in 1965 when they reported the oxidative addition of a naphthalene C-H bond across a $Ru(dmpe)_2$ fragment.[147] This was a breakthrough in the functionalisation of hydrocarbons and was followed up in 1972 by Shilov *et al.*, who were able to demonstrate the oxidation of CH_4 to CH_3OH and CH_3Cl using H_2O and K_2PtCl_4 with catalytic K_2PtCl_6.[148, 149]

Early evidence of intramolecular C-H activation was repoted by Whitesides *et al.* when thermolysis of $[(CH_3)_3CCH_2]_2Pt[P(C_2D_5)_3]_2$ and quenching with DCl produced a range of products (Scheme 1.50).[150]

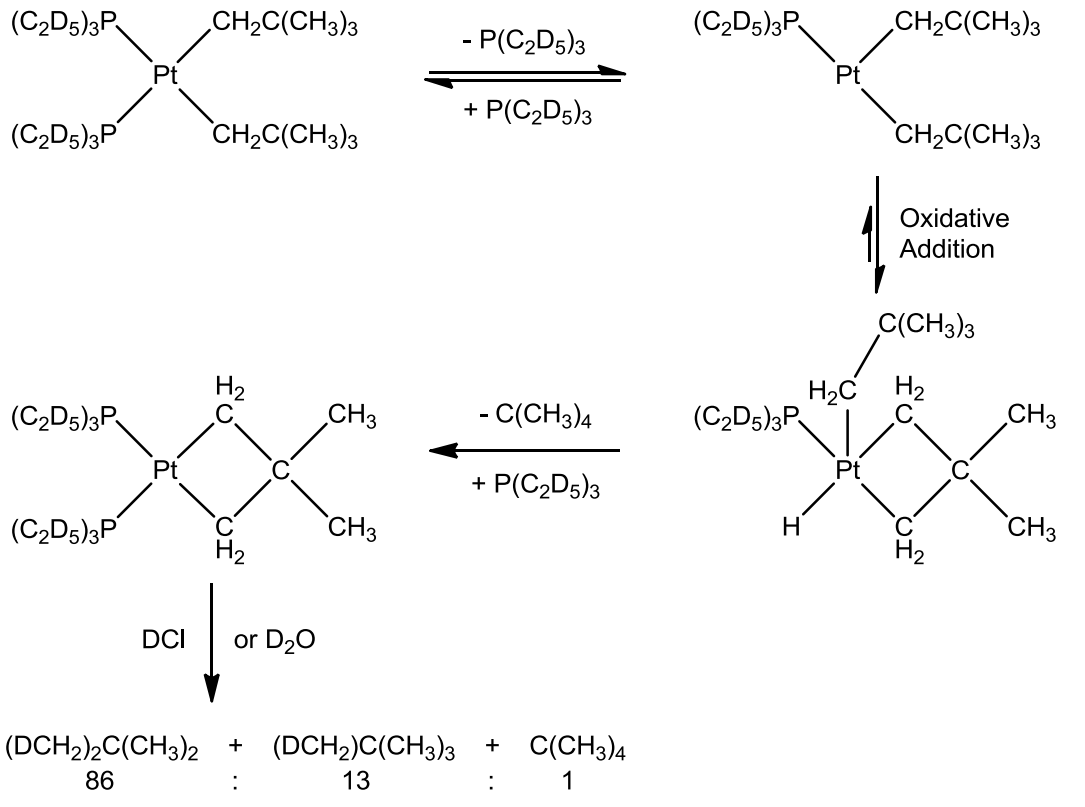

Scheme 1.50: Mechanism proposed by Whiteside *et al.* to explain the product distribution observed.

In 1982, Bergman *et al.* observed photolytically promoted activation of benzene, cyclohexane and neopentane across $Cp^*Ir(PMe_3)(H)_2$ resulting in the expulsion of dihydrogen.[151]

With this new understanding, reactions thought previously to be impossible had now been given a route via novel E–H activation pathways. In 1997, Waltz and Hartwig demonstrated the borylation of alkanes under thermal conditions by exploiting the activation of C–H and B–H bonds.[152] Since then, there have been many examples of alkane functionalisation using C–H and C–C activation methods.[153-155]

Generally, metathesis processes occurring across late Transition-metal centres tend to be considered as step-wise oxidative addition and reductive elimination. In 2007, Perutz

et al. posed a new concerted mechanism in which oxidative addition and reductive elimination cannot necessarily be distinguished.[156] The only intermediates are σ-complexes, so this allows the metal to remain in a constant oxidation state when the metathesis occurs (Scheme 1.51). Given oxidative addition requires electrons to be donated into the σ^*-orbital of the bond, this mechanism offers explanation of metathesis reactions that occur at d^0-metals; e.g. $[Cp_2ZrMe]^+$ with $PhSiH_3$,[157] and Cp^*_2ScMe with $MesSiH_3$.[158] This so called "σ-CAM", or σ-Complex Assisted Metathesis, was a completely new way to consider metal mediated transformations.

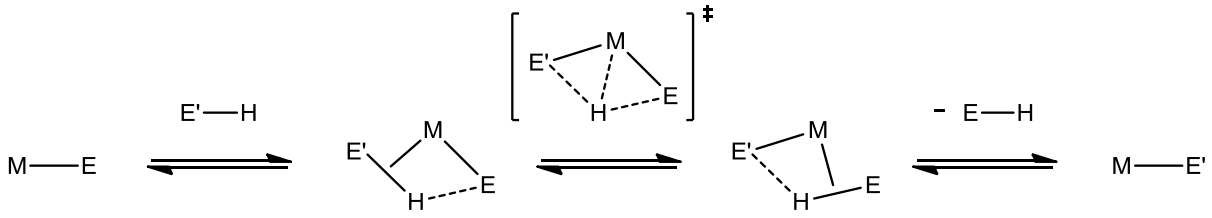

Scheme 1.51: General σ-CAM mechanism for E-H metathesis reactions.

1.5.2.1 C–H Activation in NHCs

Given the extensive use of phosphines in low valent rhodium catalysts, Nolan *et al.* probed the behaviour of analogous rhodium NHC complexes. By coordinating two IMes ligands to a Rh(I), they observed oxidative addition of one the C-H bonds from an *ortho*-methyl group on the mesityl rings (Scheme 1.52).[159] This was found to be reversible by addition of either H_2 or CO gas.

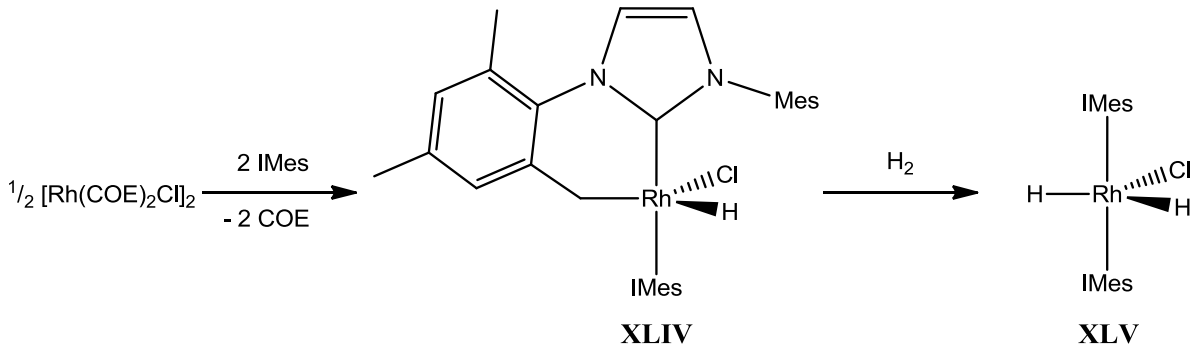

XLIV **XLV**

Scheme 1.52: Spontaneous oxidative addition of C-H at a Rh(I) centre.

In subsequent work, Nolan *et al.* reported the formation of *bis*(NHC) complexes of Rh(III) and Ir(III) in which the *tert*-butyl groups of I^{t}Bu were found to spontaneously C–H activate at the metal centre.[160] If left for long enough, both I^{t}Bu ligands would C–H activate to generate a relatively hindered metal centre (**XLVI**, Fig 1.53). Introduction of a hydride to the metal or a protic source can eliminate these metal-alkyls, hence this has been heralded as important for potential dehydrogenation chemistry.

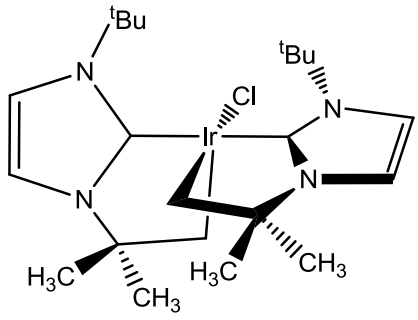

XLVI

Figure 1.53: Nolan's doubly cyclometallated Ir(III) complex.

XLVI could also be treated with Ag[PF_6] as a halide abstraction agent to give a 14-electron cation.[161] Subsequent hydrogenation of this complex leads to a low valent dihydride (Scheme 1.54). The X-ray structure of this complex shows that the iridium centre is stabilised by agostic interactions from the *tert*-butyl methyl groups. When subjected to

carbon monoxide, these agostic C–H bonds oxidatively add and H_2 is eliminated. This is an early example of reversible C–H activation at a metal centre acting as a latent source of hydrogen.

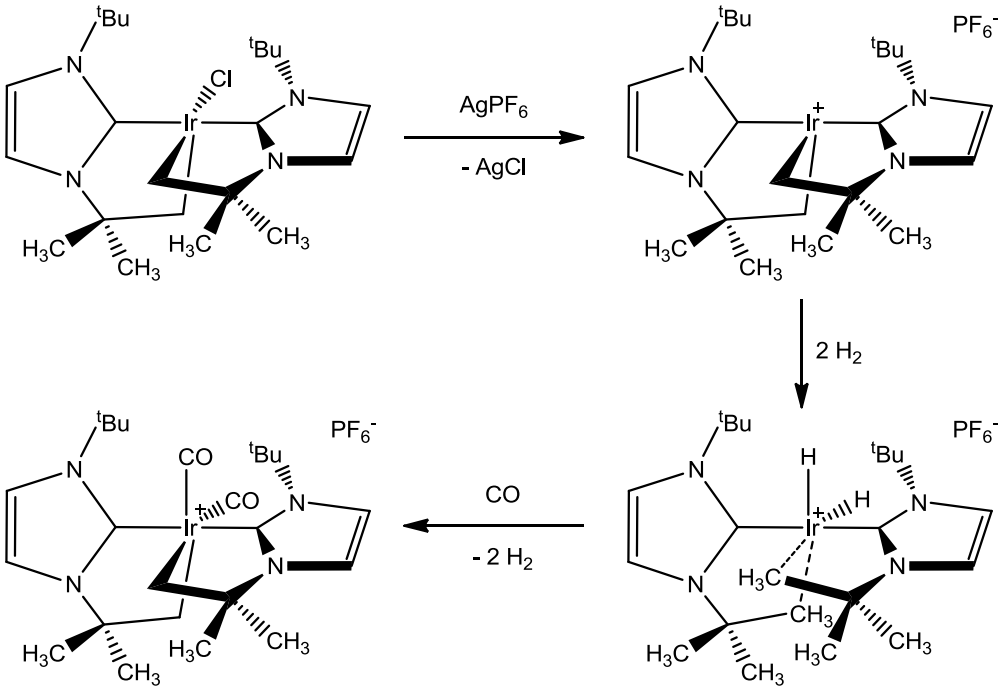

Scheme 1.54: Reversible C–H oxidative addition at a 14-electron metal centre.

Given these previous observations one might expect facile oxidative addition to be observed with the IMes ligand at iridium. Interestingly however, our group reported the synthesis of the *bis*(IMes)-iridium system still containing a cyclooctene molecule despite expecting Ir(III) to be favoured over Ir(I) (Scheme 1.55).[162] The C-H activation seen with rhodium (from Scheme 1.52) can be observed but only by heating to 65 °C overnight. Subsequent hydrogenation and halide abstraction using Na[BAr^f_4] leads to a class of compound that has been shown to extensively coordinate and dehydrocouple boranes and amine-boranes.[163-166]

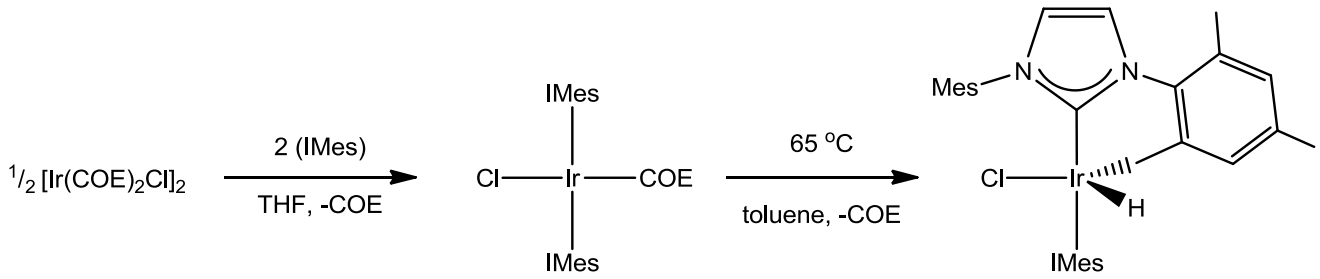

Scheme 1.55: Unexpected kinetic barrier to C-H activation of IMes at iridium(I).

It has been found possible to stimulate the activation of two C–H bonds in the IMes system to give a doubly cyclometallated complex, **XLVII** (Scheme 1.56).[167] This was achieved by carrying out a halide abstraction from the dihydride species $(IMes)_2IrH_2Cl$ in a sufficiently polar solvent (THF, but not fluorobenzene). In this case, the two C–H bonds that oxidatively add come from the same ligand and the other NHC provides an agostic interaction to stabilise the low valent metal centre. Subsequent addition of a tertiary amine-borane substrate allowed retention of the strained *bis*-tethered NHC, as in **XLVIII**.

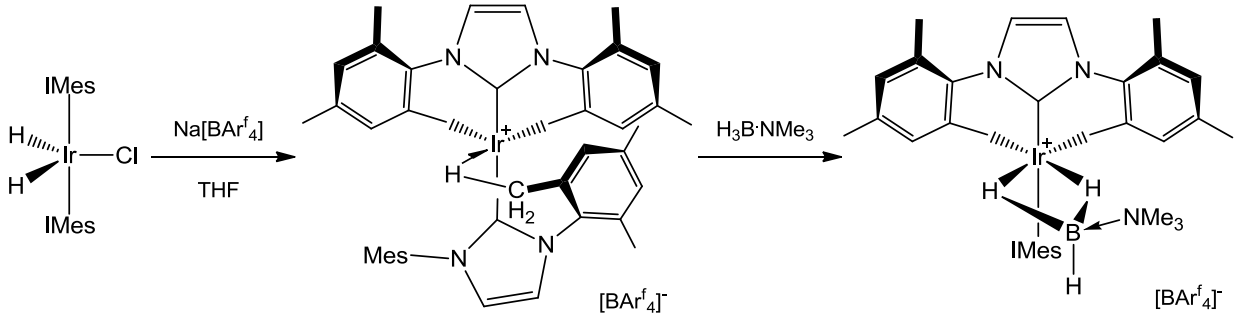

XLVII **XLVIII**

Scheme 1.56: Response of $(IMes)_2IrH_2Cl$ to halide abstraction in the polar solvent THF.

Expanded ring NHC complexes of low valent metals reported by Whittlesey *et al*. have also shown evidence for the facile C–H activation of mesityl substituents. In 2010, they reported the complex of 6-Mes with $Ni(COD)_2$ which was found to result in the ejection of one equivalent of COD and spontaneous C-H activation of an *ortho*-CH_3 group

(Fig 1.56).[168] Furthermore, abstraction of a fluoride from a 16-electron ruthenium complex also leads to a C–H activation to give **XLV** (Scheme 1.57).[169]

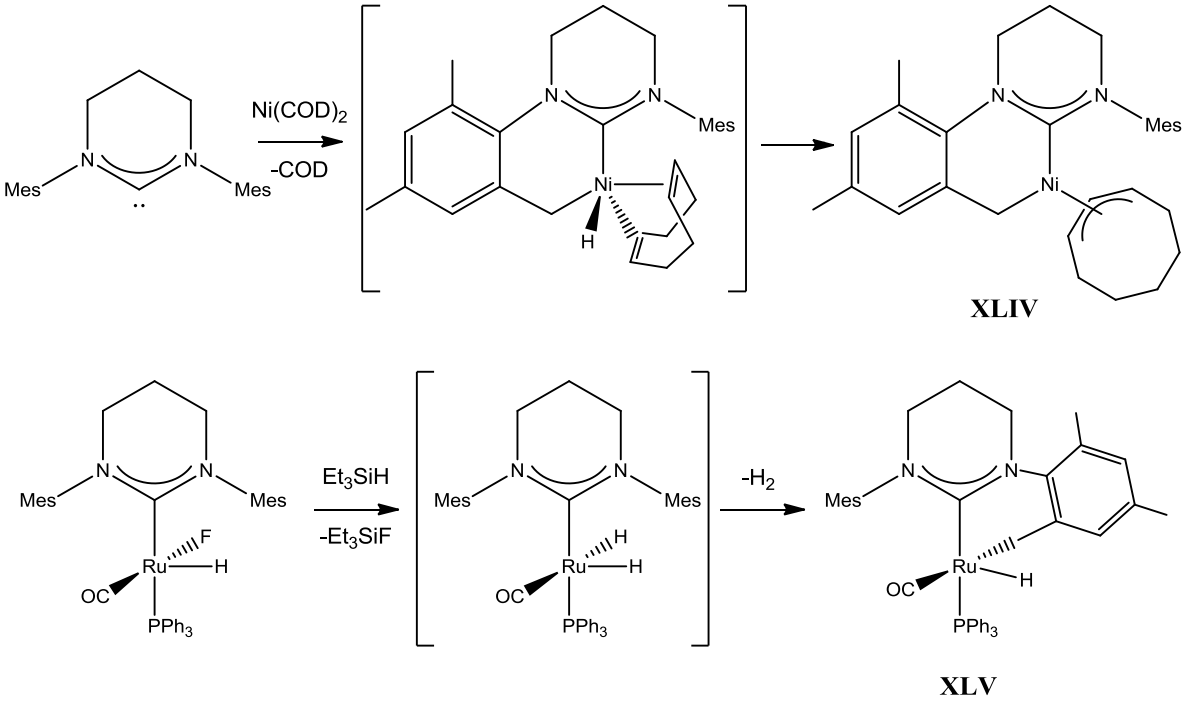

Scheme 1.57: Spontaneous C-H activation in the 6-Mes NHC ligand at Ni and Ru.

When the aryl substituents possess alkyl groups with a β-hydrogen, for example Dipp, a second mode of activation can be observed. Due to the increased proximity of the alkyl substituents to the metal centre, oxidative addition is now facile with iridium, and further activation via β-hydride elimination can yield a coordinated alkene, as in **XLVI** (Scheme 1.58).[170] Subsequent halide abstraction promotes oxidative addition of a second C–H bond to give **XLVII**.

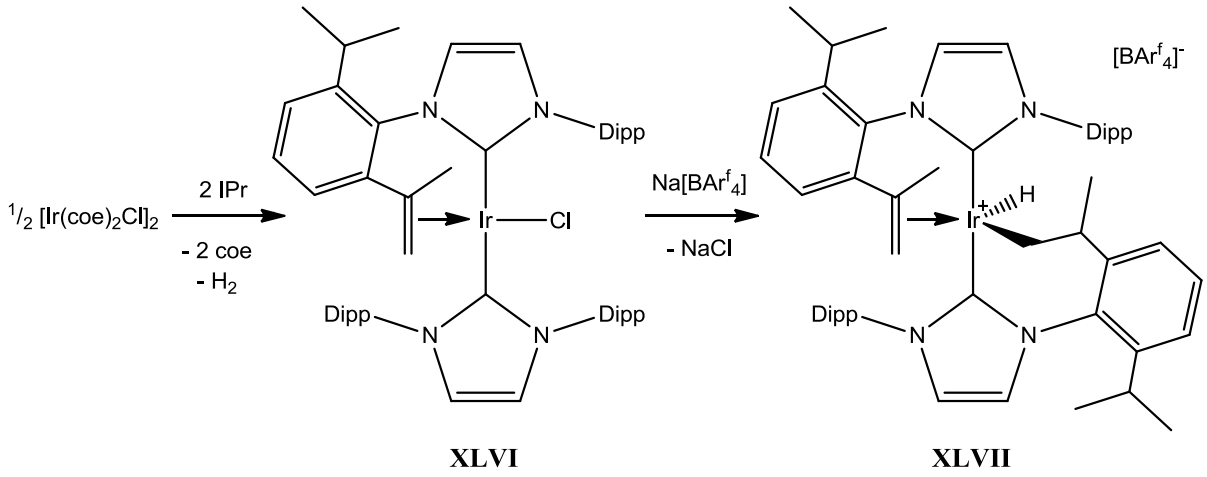

Scheme 1.58: Interaction of the IPr ligand with the low valent iridium centre.

Addition of NHC ligands can be limited to the coordination of a single equivalent by employing a chelating alkene in the metal precursor, e.g. cyclooctadiene (COD). Removal of the chloride from this system resulted in similar dehydrogenation of the ^{i}Pr group (Scheme 1.59).[171] Hydrogenation of complex **XLVIII** results in the loss of the COD ligand and rehydrogenation of the ^{i}Pr function. As a low valent species, **XLIX** is electronically stabilised by coordination of the π-system of a fluorobenzene solvent molecule. This can be removed by warming in dichloromethane, and stabilisation is then provided by the aryl ring of another NHC, resulting in the dimeric complex **L**. Analogous behaviour has been observed in low valent systems containing aryl phosphines.[172]

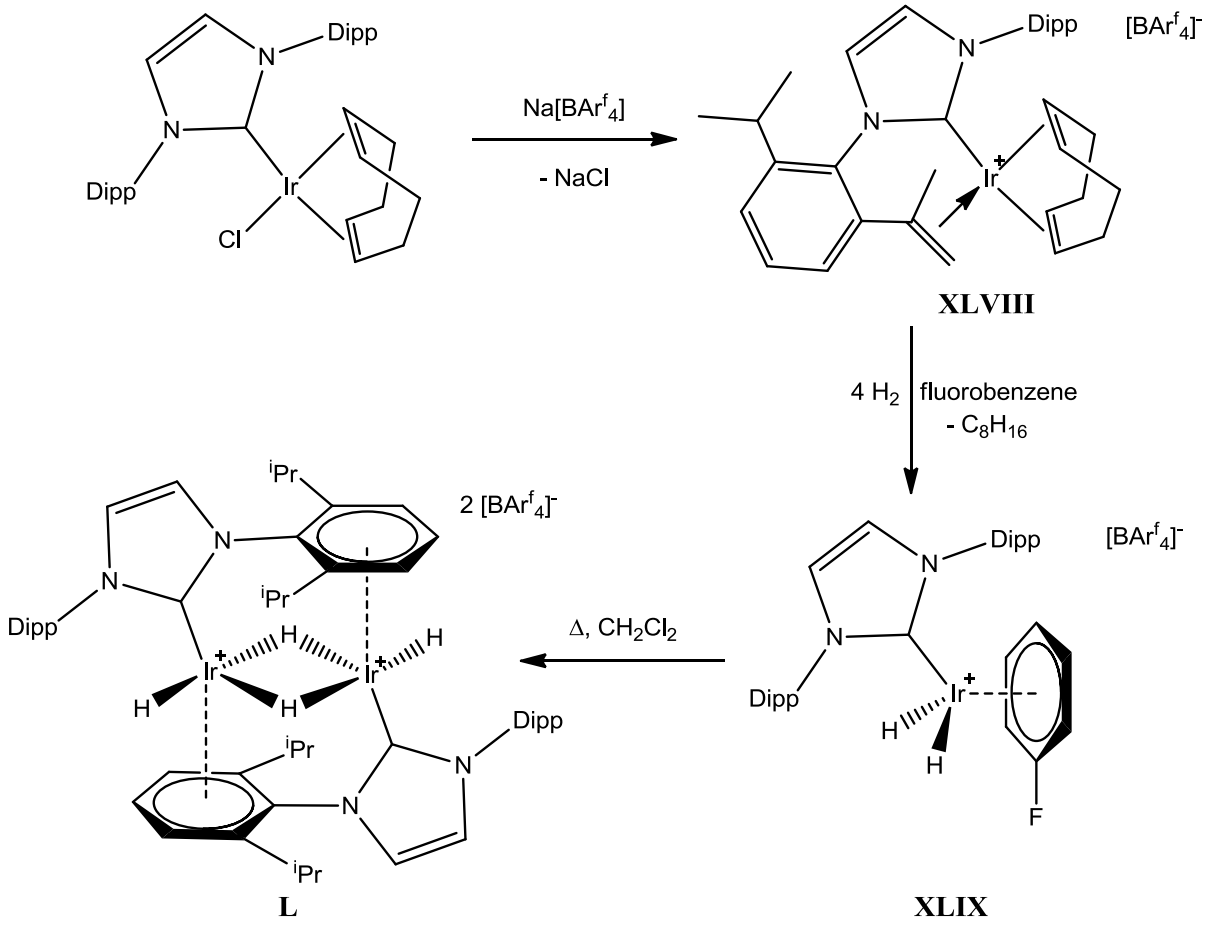

Scheme 1.59: Arene stabilisation of a low valent iridium cation.

1.5.3 Arene Interactions

Electrostatic attraction between cations and the electron π-cloud of aromatic rings has been extensively investigated.[173] Interactions of neutral aromatic π-systems with open shell metal centres started with the formation of bis(benzene)chromium in 1955.[174] This synthesis demonstrated the possibility for reducing metal complexes in the presence of neutral arenes which can increase the electron count at the metal. This is particularly advantageous for the use of *N*-aryl based NHCs as ligands in catalysis as they have the potential to stabilise the low valent catalytic intermediates and help prolong the life of the system.

However, the ideal scenario is to have a potential donor incorporated into the ligand set. Intramolecular stabilisation by arene moieties is somewhat of a recent development, Mirkin *et al.* designed a phosphine ligand with an arene appendage that was able was act as a hemi-labile ligand to a cationic Rh(I) centre.[175] This type of ligand was improved upon by Faller *et al.* in 2003, with a biphenyl based system which could be tuned to allow for chiral synthesis.[176] Work by Goldberg *et al.* then highlighted the versatility of these interactions, as they were observed to be able to switch between η^2 and η^6 coordination modes to suit the electron count at the metal (Scheme 1.60).[177]

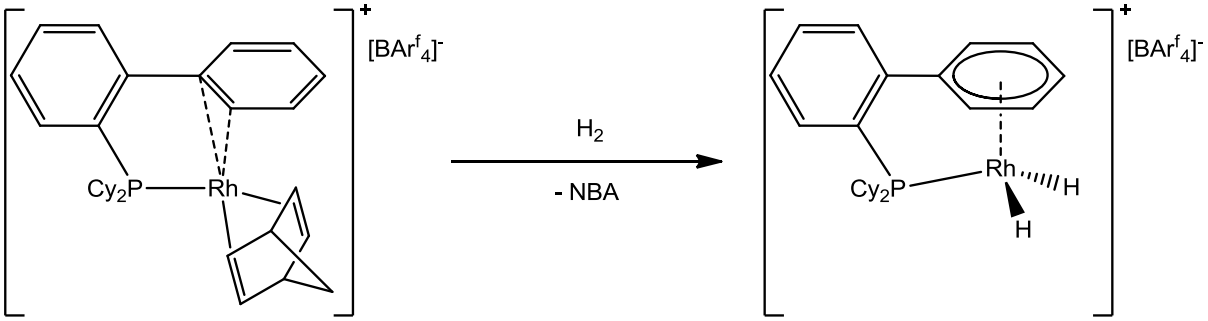

LI **LII**

Scheme 1.60: Change in hapicity of the arene interaction.

In 2005, Buchmeiser *et al.* reported a (6-Mes)Rh-based catalyst (**LIII**) for hydrosilylation and carbonyl arylation reactions with good activity and turnover number.[178] The active species in this case is a 14-electron Rh cation which exhibits close approach of a mesityl ring in the crystal structure (Fig 1.61). This results in the rhodium centre being offset from the ideal geometry when coordinated to an NHC.

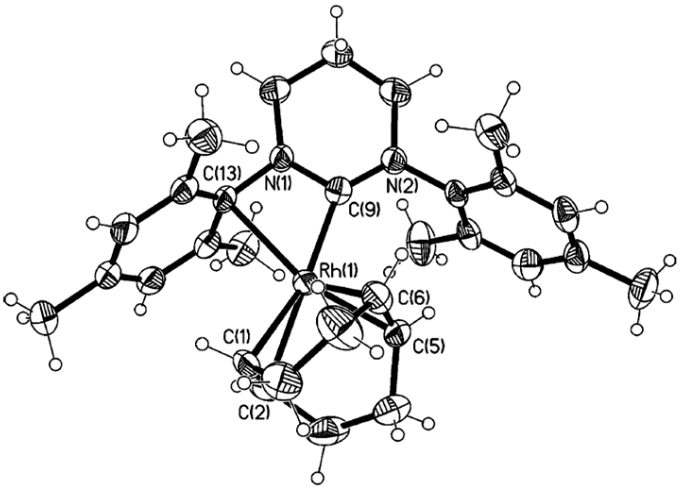

LIII

Figure 1.61: $[(6\text{-Mes})Rh(COD)]^+$ cation with close approach of the aryl ring [Rh(1)-C(13) 2.377(4) Å]. Reproduced from Buchmeiser *et al.*, 2005.[178]

In 2012, Conejero *et al.* reported a 14-electron, T-shaped platinum cation which is stabilised by the interaction of the π-cloud of a mesityl ring.[179] This complex exhibits a propensity to reversibly activate the C–H bonds of aromatic hydrocarbons at elevated temperatures, thereby demonstrating how potentially reactive metals can be stabilised by such interactions. This activation was not observed with I^{t}Bu and IPr carbenes as the supporting ligands; the larger $\%V_{bur}$ of these two ligands disfavours the activation kinetically (due to strong agostic interactions with the metal) and thermodynamically (due to the steric pressure around the metal centre).

1.6 Linear Metal Complexes

The stabilisation of the late transition metals discussed in this chapter so far has occurred by agostic or arene interactions to a vacant site located *cis*- to a suitable ligand. Metal-ions with a d^{10} configuration (Cu^+, Ag^+, Au^+, Zn^{2+}, Cd^{2+} and Hg^{2+}) often form linear, 2-coordinate complexes and have no available *cis*-geometry. Good ligands for these species tend to rely on σ-donor strength and steric crowding to stabilise the catalytic intermediates of d^{10} metals, of which Au(I) has received the most interest recently.

It wasn't until the second half of the 20th century that gold had even been considered as an active species in catalysis. In early studies, gold had been demonstrated in many heterogeneous applications to activate formic acid to release hydrogen,[180] as well as activation of molecular hydrogen.[181, 182] The first examples of homogeneous catalysis with Au(I) did not come until 1986, when Ito and Hayashi reported aldol reactions could be catalysed by a chiral phosphine ligated Au^{+}.[183] However, the majority of the early focus on organic catalysis with gold tended to be with Au(III).[184] Despite the first diaminocarbene-gold complexes being identified in 1973,[185, 186] it was not until 2003 that the first NHC-gold catalyst (**LIV**) was utilised (Scheme 1.62).[187, 188]

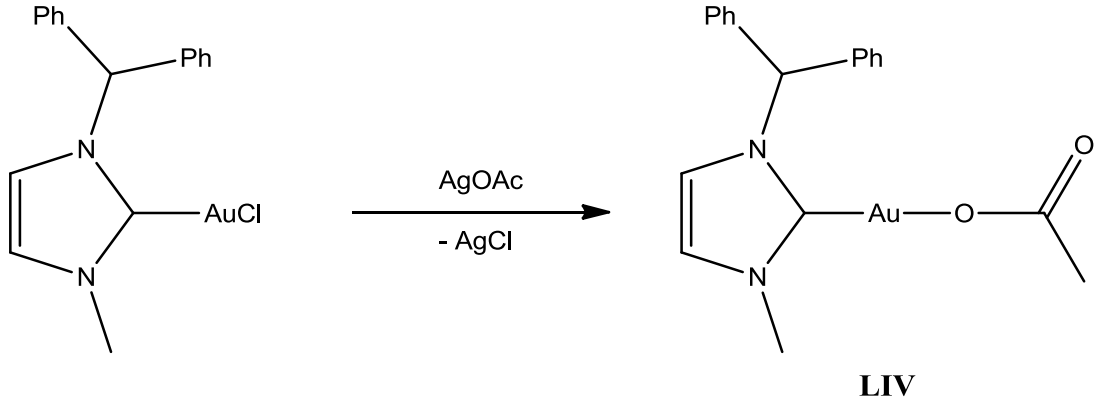

LIV

Scheme 1.62: First NHC-Au(I) catalyst.

The active fragment $[LAu]^{+}$ has long been thought of as a "soft" proton due to its isolobility with H^{+}.[189] Hence, it behaves very much like a proton in the reactions it catalyses.[190-193] Due to the soft nature of $[LAu]^{+}$, it has a good affinity for alkenes, alkynes and R^{-}.[194] As a result, the Au^{+} can help to activate less reactive substrates by pre-coordination (Scheme 1.63). However, due to the extreme electrophilicity of the one-coordinate $[LAu]^{+}$ fragment, it has never been isolated and studied. There have been many syntheses of the species with a coordinating solvent or anion,[195-197] but few promising attempts to isolate the cation itself.[81, 198]

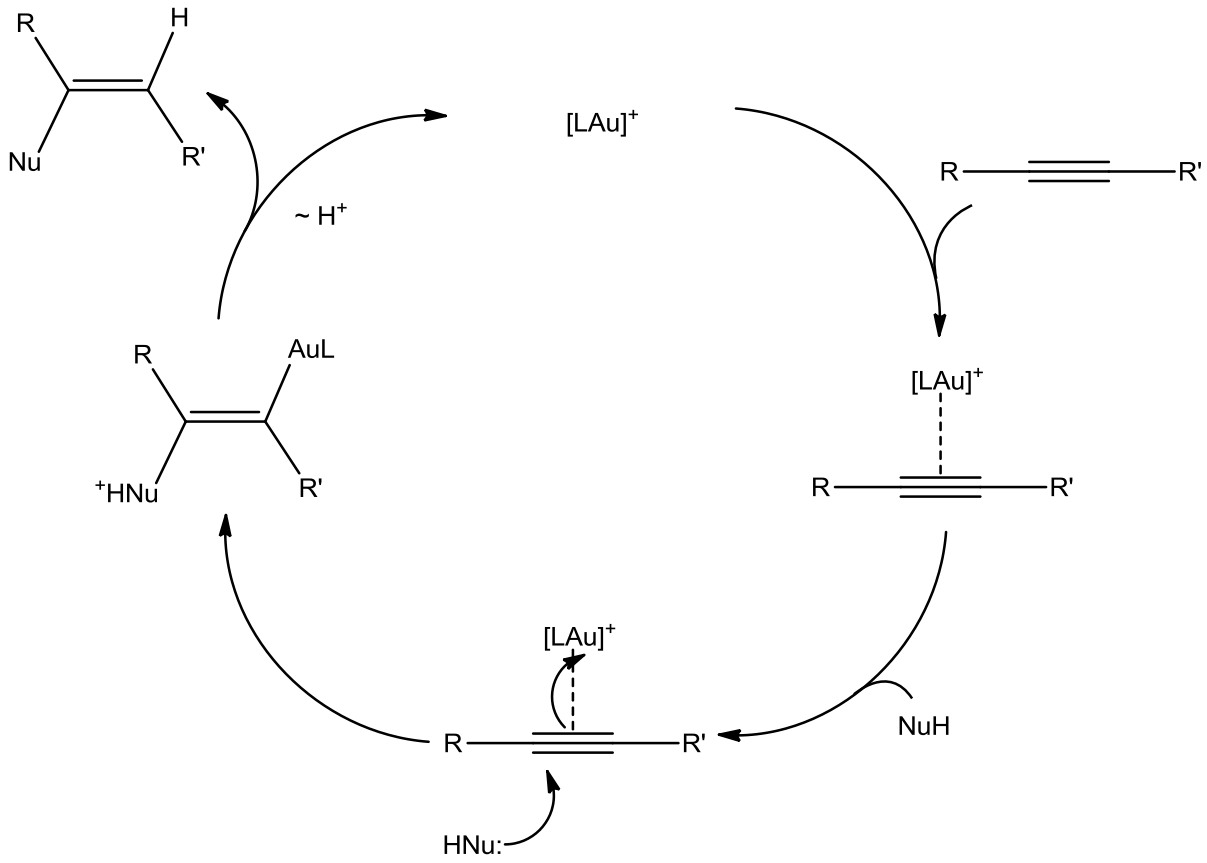

Scheme 1.63: Gold-catalysed nucleophilic addition to an alkyne.

Another intermediate postulated in a series of gold-mediated organic transformations, particularly in hydrosilylations, is a gold hydride.[190, 199, 200] Given the isolobility of $[LAu]^+$ with H^+, LAuH can be thought of as analogous to H_2. The parent species AuH and extended AuH_n systems have been studied theoretically,[201, 202] as well as in the gas phase,[203] and by matrix isolation.[204-206] However, this is a highly reactive species and reported examples of complexes containing AuH are most often supported with a phosphine or NHC.

In 1982, stable complexes of gold hydrides involving bridging interactions to other transition metals (Ir and Pt) were isolated.[207] The exact nature of the interaction is not known, as the hydride could not be located by X-ray diffraction. A study of the catalytic

activity of this class of compound showed that, in general, no catalytic activity was observed for the isomerisation of *cis*-2-hexene to *trans*-2-hexene. However, one complex, $[(PPh_3)_3(CO)Ru(\mu\text{-}H)_2\{Au(PPh_3)\}][PF_6]$, showed an increase in activity and a change in selectivity over the parent $[LAu]^+$.[208]

The first stable, monomeric (NHC)AuH species was reported by Sadighi *et al.* and, perhaps not unsurprisingly, displayed a downfield hydride ^{1}H-NMR shift (δ_H 5.11 ppm in C_6D_6).[196] These monomeric gold hydrides have been shown as reactive species,[209] as have the corresponding Au(III) hydrides.[210] Interaction of the gold hydride with "$[LAu]^+$" led to a homonuclear bridged hydride complex, also reported by Sadighi (Scheme 1.64). This sparked interest in the potential for the synthesis of analogues of H_3^+.

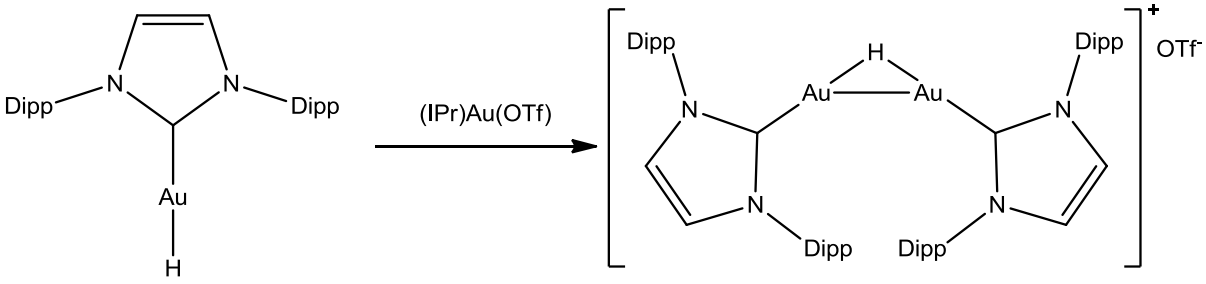

LV **LVI**

Scheme 1.64: First monomeric and homonuclear-bridge gold hydride species.

This discovery was later followed by a second analogue of H_3^+, also synthesised by Sadighi *et al.*, of the form $[(LAu)_3]^+$.[211] Reduction of $[\{(IPr)Au\}_3CO_3][OTf]$ with CO led to the trigold mono-cation $[\{(IPr)Au\}_3][OTf]$. The charge associated with this system suggests a mixed valence Au(0/I) complex; generally systems attempting to isolate a Au(0) complex result in the precipitation of colloidal gold.

In 2013, Bertrand *et al.* exploited the π-acidity of their CAAC ligands to isolate, what were reported to be, mono- and bi-nuclear Au(0) complexes (Scheme 1.65).[212] These are interesting as small molecule analogues of gold cluster and nanoparticle surfaces.

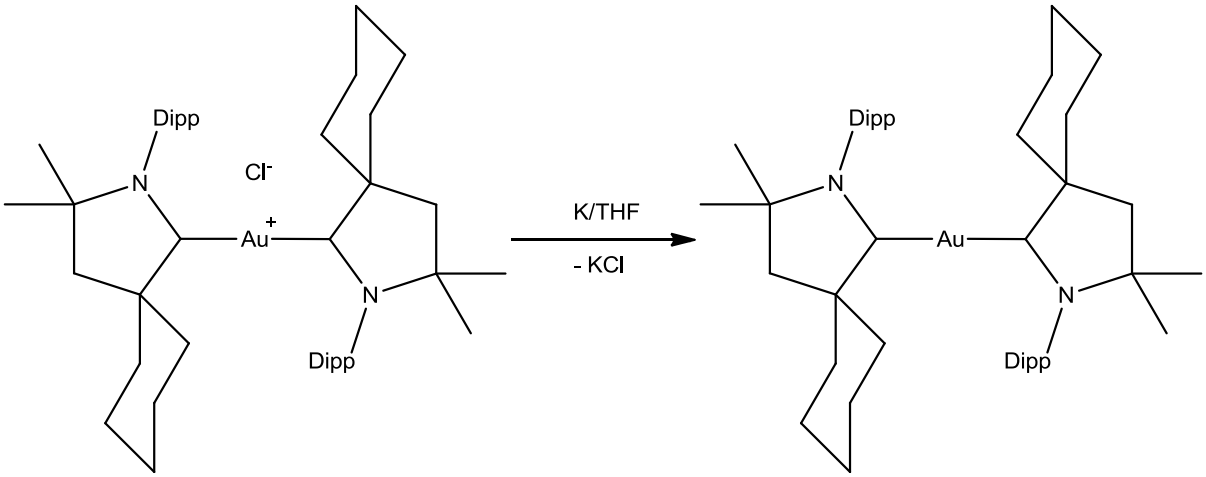

LVII

Scheme 1.65: Bertrand's mono-nuclear Au(0) CAAC complex.

In reality, it is open to question whether the complexes reported are strictly Au(0) as the majority of the spin density is to be found on the CAAC ligands. This is due to the relatively low lying LUMO on the CAAC ligand allowing for significant back-bonding from the gold. Even so, these are a great showcase of the electronic customisability of these heterocyclic carbene ligands.

1.7 References

1. W. Kirmse, *Carbene Chemistry, 2nd Ed.*, 1971.
2. D. Bourissou, O. Guerret, F. P. Gabbai and G. Bertrand, *Chem. Rev.*, 2000, **100**, 39-91.
3. R. Gleiter and R. Hoffmann, *J. Am. Chem. Soc.*, 1968, **90**, 5457-5460.
4. A. J. Arduengo, H. V. R. Dias, J. C. Calabrese and F. Davidson, *J. Am. Chem. Soc.*, 1992, **114**, 9724-9725.
5. A. J. Arduengo, H. V. R. Dias, F. Davidson and R. L. Harlow, *J. Organomet. Chem.*, 1993, **462**, 13-18.

6. N. Kuhn, G. Henkel, T. Kratz, J. Kreutzberg, R. Boese and A. H. Maulitz, *Chem. Ber. R.*, 1993, **126**, 2041-2045.
7. W. A. Herrmann, K. Ofele, M. Elison, F. E. Kuhn and P. W. Roesky, *J. Organomet. Chem.*, 1994, **480**, C7-C9.
8. A. Schafer, M. Weidenbruch, W. Saak and S. Pohl, *J. Chem. Soc.-Chem. Comm.*, 1995, 1157-1158.
9. X. W. Li, J. R. Su and G. H. Robinson, *Chem. Comm.*, 1996, 2683-2684.
10. H. Schumann, J. Gottfriedsen, M. Glanz, S. Dechert and J. Demtschuk, *J. Organomet. Chem.*, 2001, **617**, 588-600.
11. K. Ofele, *J. Organomet. Chem.*, 1968, **12**, P42-P43.
12. K. Ofele, *Angew. Chem. Int. Ed.*, 1968, **7**, 950.
13. H. J. Schonher and H. W. Wanzlick, *Chem. Ber. R.*, 1970, **103**, 1037-1046.
14. K. Ofele, W. A. Herrmann, D. Mihalios, M. Elison, E. Herdtweck, T. Priermeier and P. Kiprof, *J. Organomet. Chem.*, 1995, **498**, 1-14.
15. W. A. Herrmann, M. Elison, J. Fischer, C. Kocher and G. R. J. Artus, *Chem. Eur. J.*, 1996, **2**, 772-780.
16. W. A. Herrmann and C. Kocher, *Angew. Chem. Int. Ed.*, 1997, **36**, 2162-2187.
17. D. J. Cardin, Cetinkay.B, M. F. Lappert, Manojlov.L and K. W. Muir, *J. Chem. Soc. D-Chem. Comm.*, 1971, 400-401.
18. D. J. Cardin, Cetinkay.B and M. F. Lappert, *Chem. Rev.*, 1972, **72**, 545-574.
19. C. M. Crudden and D. P. Allen, *Coord. Chem. Rev.*, 2004, **248**, 2247-2273.
20. P. L. Arnold and S. Pearson, *Coord. Chem. Rev.*, 2007, **251**, 596-609.
21. P. de Fremont, N. Marion and S. P. Nolan, *Coord. Chem. Rev.*, 2009, **253**, 862-892.
22. S. Diez-Gonzalez, N. Marion and S. P. Nolan, *Chem. Rev.*, 2009, **109**, 3612-3676.
23. A. J. Arduengo, M. Tamm, S. J. McLain, J. C. Calabrese, F. Davidson and W. J. Marshall, *J. Am. Chem. Soc.*, 1994, **116**, 7927-7928.
24. W. J. Oldham, S. M. Oldham, B. L. Scott, K. D. Abney, W. H. Smith and D. A. Costa, *Chem. Comm.*, 2001, 1348-1349.
25. P. L. Arnold and I. J. Casely, *Chem. Rev.*, 2009, **109**, 3599-3611.
26. P. L. Arnold, Z. R. Turner, N. Kaltsoyannis, P. Pelekanaki, R. M. Bellabarba and R. P. Tooze, *Chem. Eur. J.*, 2010, **16**, 9623-9629.
27. E. O. Fischer and A. Maasbol, *Angew. Chem. Int. Ed.*, 1964, **3**, 580-581.
28. R. R. Schrock, *J. Am. Chem. Soc.*, 1974, **96**, 6796-6797.
29. H. W. Wanzlick, *Angew. Chem. Int. Ed.*, 1962, **1**, 75-80.
30. A. J. Arduengo, R. Krafczyk, R. Schmutzler, H. A. Craig, J. R. Goerlich, W. J. Marshall and M. Unverzagt, *Tetrahedron*, 1999, **55**, 14523-14534.
31. D. M. Lemal, R. A. Lovald and K. I. Kawano, *J. Am. Chem. Soc.*, 1964, **86**, 2518-2519.
32. H. E. Winberg, J. E. Carnahan, D. D. Coffman and M. Brown, *J. Am. Chem. Soc.*, 1965, **87**, 2055-2056.
33. M. K. Denk, K. Hatano and M. Ma, *Tetrahedron Lett.*, 1999, **40**, 2057-2060.
34. H. W. Wanzlick and H. J. Schonher, *Angew. Chem. Int. Ed.*, 1968, **7**, 141-142.
35. H. J. Schonher and H. W. Wanzlick, *Liebig Ann. Chem.*, 1970, **731**, 176-179.

36. A. Igau, H. Grutzmacher, A. Baceiredo and G. Bertrand, *J. Am. Chem. Soc.*, 1988, **110**, 6463-6466.
37. G. Bertrand and R. Reed, *Coord. Chem. Rev.*, 1994, **137**, 323-355.
38. A. J. Arduengo, R. L. Harlow and M. Kline, *J. Am. Chem. Soc.*, 1991, **113**, 361-363.
39. A. J. Arduengo, H. V. R. Dias, R. L. Harlow and M. Kline, *J. Am. Chem. Soc.*, 1992, **114**, 5530-5534.
40. W. A. Herrmann, C. Kocher, L. J. Goossen and G. R. J. Artus, *Chem. Eur. J.*, 1996, **2**, 1627-1636.
41. D. Enders, K. Breuer, G. Raabe, J. Runsink, J. H. Teles, J. P. Melder, K. Ebel and S. Brode, *Angew. Chem. Int. Ed.*, 1995, **34**, 1021-1023.
42. K. Ofele, W. A. Herrmann, D. Mihalios, M. Elison, E. Herdtweck, W. Scherer and J. Mink, *J. Organomet. Chem.*, 1993, **459**, 177-184.
43. W. A. Herrmann, O. Runte and G. Artus, *J. Organomet. Chem.*, 1995, **501**, C1-C4.
44. J. K. Huang, H. J. Schanz, E. D. Stevens and S. P. Nolan, *Organometallics*, 1999, **18**, 2370-2375.
45. C. Heinemann and W. Thiel, *Chem. Phys. Lett.*, 1994, **217**, 11-16.
46. J. C. Green, R. G. Scurr, P. L. Arnold and F. G. N. Cloke, *Chem. Comm.*, 1997, 1963-1964.
47. R. D. Fischer, *Angew. Chem. Int. Ed.*, 1994, **33**, 2165-2168.
48. H. Schumann, M. Glanz, J. Winterfeld, H. Hemling, N. Kuhn and T. Kratz, *Angew. Chem. Int. Ed.*, 1994, **33**, 1733-1734.
49. A. J. Arduengo, F. Davidson, R. Krafczyk, W. J. Marshall and M. Tamm, *Organometallics*, 1998, **17**, 3375-3382.
50. G. Boche, C. Hilf, K. Harms, M. Marsch and J. C. W. Lohrenz, *Angew. Chem. Int. Ed.*, 1995, **34**, 487-489.
51. R. W. Alder, M. E. Blake, C. Bortolotti, S. Bufali, C. P. Butts, E. Linehan, J. M. Oliva, A. G. Orpen and M. J. Quayle, *Chem. Comm.*, 1999, 241-242.
52. A. R. Chianese, X. W. Li, M. C. Janzen, J. W. Faller and R. H. Crabtree, *Organometallics*, 2003, **22**, 1663-1667.
53. R. Dorta, E. D. Stevens, N. M. Scott, C. Costabile, L. Cavallo, C. D. Hoff and S. P. Nolan, *J. Am. Chem. Soc.*, 2005, **127**, 2485-2495.
54. R. A. Kelly, H. Clavier, S. Giudice, N. M. Scott, E. D. Stevens, J. Bordner, I. Samardjiev, C. D. Hoff, L. Cavallo and S. P. Nolan, *Organometallics*, 2008, **27**, 202-210.
55. X. L. Hu, I. Castro-Rodriguez, K. Olsen and K. Meyer, *Organometallics*, 2004, **23**, 755-764.
56. D. Tapu, D. A. Dixon and C. Roe, *Chem. Rev.*, 2009, **109**, 3385-3407.
57. H. V. Huynh, Y. Han, R. Jothibasu and J. A. Yang, *Organometallics*, 2009, **28**, 5395-5404.
58. R. W. Alder, M. E. Blake and J. M. Oliva, *J. Phys. Chem. A*, 1999, **103**, 11200-11211.
59. R. W. Alder, P. R. Allen, M. Murray and A. G. Orpen, *Angew. Chem. Int. Ed.*, 1996, **35**, 1121-1123.
60. R. W. Alder and M. E. Blake, *Chem. Comm.*, 1997, 1513-1514.

61. S. Urban, M. Tursky, R. Frohlich and F. Glorius, *Dalton Trans.*, 2009, 6934-6940.
62. U. Plaia, H. Stolzenberg and W. P. Fehlhammer, *J. Am. Chem. Soc.*, 1985, **107**, 2171-2172.
63. A. J. Arduengo, J. R. Goerlich and W. J. Marshall, *Liebigs Ann. Rec.*, 1997, 365-374.
64. D. Martin, A. Baceiredo, H. Gornitzka, W. W. Schoeller and G. Bertrand, *Angew. Chem. Int. Ed.*, 2005, **44**, 1700-1703.
65. S. Sole, H. Gornitzka, W. W. Schoeller, D. Bourissou and G. Bertrand, *Science*, 2001, **292**, 1901-1903.
66. V. Lavallo, Y. Canac, C. Prasang, B. Donnadieu and G. Bertrand, *Angew. Chem. Int. Ed.*, 2005, **44**, 5705-5709.
67. S. Grundemann, A. Kovacevic, M. Albrecht, J. W. Faller and R. H. Crabtree, *Chem. Comm.*, 2001, 2274-2275.
68. S. Grundemann, A. Kovacevic, M. Albrecht, J. W. Faller and R. H. Crabtree, *J. Am. Chem. Soc.*, 2002, **124**, 10473-10481.
69. H. Lebel, M. K. Janes, A. B. Charette and S. P. Nolan, *J. Am. Chem. Soc.*, 2004, **126**, 5046-5047.
70. M. Alcarazo, S. J. Roseblade, A. R. Cowley, R. Fernandez, J. M. Brown and J. M. Lassaletta, *J. Am. Chem. Soc.*, 2005, **127**, 3290-3291.
71. O. Schuster, L. R. Yang, H. G. Raubenheimer and M. Albrecht, *Chem. Rev.*, 2009, **109**, 3445-3478.
72. E. Aldeco-Perez, A. J. Rosenthal, B. Donnadieu, P. Parameswaran, G. Frenking and G. Bertrand, *Science*, 2009, **326**, 556-559.
73. C. A. Tolman, *Chem. Rev.*, 1977, **77**, 313-348.
74. A. C. Hillier, W. J. Sommer, B. S. Yong, J. L. Petersen, L. Cavallo and S. P. Nolan, *Organometallics*, 2003, **22**, 4322-4326.
75. A. Poater, B. Cosenza, A. Correa, S. Giudice, F. Ragone, V. Scarano and L. Cavallo, *Eur. J. Inorg. Chem.*, 2009, 1759-1766.
76. L. Cavallo, A. Correa, C. Costabile and H. Jacobsen, *J. Organomet. Chem.*, 2005, **690**, 5407-5413.
77. H. Clavier and S. P. Nolan, *Chem. Comm.*, 2010, **46**, 841-861.
78. S. Wurtz and F. Glorius, *Acc. Chem. Res.*, 2008, **41**, 1523-1533.
79. F. Ragone, A. Poater and L. Cavallo, *J. Am. Chem. Soc.*, 2010, **132**, 4249-4258.
80. G. Berthon-Gelloz, M. A. Siegler, A. L. Spek, B. Tinant, J. N. H. Reek and I. E. Marko, *Dalton Trans.*, 2010, **39**, 1444-1446.
81. S. G. Weber, F. Rominger and B. F. Straub, *Eur. J. Inorg. Chem.*, 2012, 2863-2867.
82. C. Heinemann, T. Muller, Y. Apeloig and H. Schwarz, *J. Am. Chem. Soc.*, 1996, **118**, 2023-2038.
83. C. Boehme and G. Frenking, *J. Am. Chem. Soc.*, 1996, **118**, 2039-2046.
84. S. Fantasia, J. L. Petersen, H. Jacobsen, L. Cavallo and S. P. Nolan, *Organometallics*, 2007, **26**, 5880-5889.
85. P. Bazinet, G. P. A. Yap and D. S. Richeson, *J. Am. Chem. Soc.*, 2003, **125**, 13314-13315.

86. M. Mayr, K. Wurst, K. H. Ongania and M. R. Buchmeiser, *Chem. Eur. J.*, 2004, **10**, 1256-1266.
87. R. C. Poulten, M. J. Page, A. G. Algarra, J. J. Le Roy, I. Lopez, E. Carter, A. Llobet, S. A. Macgregor, M. F. Mahon, D. M. Murphy, M. Murugesu and M. K. Whittlesey, *J. Am. Chem. Soc.*, 2013, **135**, 13640-13643.
88. B. Bantu, D. R. Wang, K. Wurst and M. R. Buchmeiser, *Tetrahedron*, 2005, **61**, 12145-12152.
89. C. C. Scarborough, M. J. W. Grady, I. A. Guzei, B. A. Gandhi, E. E. Bunel and S. S. Stahl, *Angew. Chem. Int. Ed.*, 2005, **44**, 5269-5272.
90. C. C. Scarborough, B. V. Popp, I. A. Guzei and S. S. Stahl, *J. Organomet. Chem.*, 2005, **690**, 6143-6155.
91. M. Iglesias, D. J. Beetstra, J. C. Knight, L. L. Ooi, A. Stasch, S. Coles, L. Male, M. B. Hursthouse, K. J. Cavell, A. Dervisi and I. A. Fallis, *Organometallics*, 2008, **27**, 3279-3289.
92. M. Iglesias, D. J. Beetstra, A. Stasch, P. N. Horton, M. B. Hursthouse, S. J. Coles, K. J. Cavell, A. Dervisi and I. A. Fallis, *Organometallics*, 2007, **26**, 4800-4809.
93. D. M. Khramov, E. L. Rosen, V. M. Lynch and C. W. Bielawski, *Angew. Chem. Int. Ed.*, 2008, **47**, 2267-2270.
94. V. Cesar, N. Lugan and G. Lavigne, *J. Am. Chem. Soc.*, 2008, **130**, 11286-11287.
95. R. Jazzar, H. Z. Liang, B. Donnadieu and G. Bertrand, *J. Organomet. Chem.*, 2006, **691**, 3201-3205.
96. E. L. Kolychev, I. A. Portnyagin, V. V. Shuntikov, V. N. Khrustalev and M. S. Nechaev, *J. Organomet. Chem.*, 2009, **694**, 2454-2462.
97. W. Y. Lu, K. J. Cavell, J. S. Wixey and B. Kariuki, *Organometallics*, 2011, **30**, 5649-5655.
98. W. A. Herrmann, M. Elison, J. Fischer, C. Kocher and G. R. J. Artus, *Angew. Chem. Int. Ed.*, 1995, **34**, 2371-2374.
99. W. A. Herrmann, *Angew. Chem. Int. Ed.*, 2002, **41**, 1290-1309.
100. W. A. Herrmann, C. P. Reisinger and M. Spiegler, *J. Organomet. Chem.*, 1998, **557**, 93-96.
101. S. Caddick, F. G. N. Cloke, G. K. B. Clentsmith, P. B. Hitchcock, D. McKerrecher, L. R. Titcomb and M. R. V. Williams, *J. Organomet. Chem.*, 2001, **617**, 635-639.
102. N. Hadei, E. A. B. Kantchev, C. J. O'Brien and M. G. Organ, *Org. Lett.*, 2005, **7**, 3805-3807.
103. J. Huang, G. Grasa and S. P. Nolan, *Organic Letters*, 1999, **1**, 1307-1309.
104. M. Scholl, S. Ding, C. W. Lee and R. H. Grubbs, *Organic Letters*, 1999, **1**, 953-956.
105. U. L. Dharmasena, H. M. Foucault, E. N. dos Santos, D. E. Fogg and S. P. Nolan, *Organometallics*, 2005, **24**, 1056-1058.
106. W. J. Sommer and M. Weck, *Coord. Chem. Rev.*, 2007, **251**, 860-873.
107. A. T. Normand, K. J. Hawkest, N. D. Clernentt, K. J. Cavell and B. F. Yates, *Organometallics*, 2007, **26**, 5352-5363.
108. C. L. Lund, M. J. Sgro and D. W. Stephan, *Organometallics*, 2012, **31**, 580-587.
109. J. Yun, E. R. Marinez and R. H. Grubbs, *Organometallics*, 2004, **23**, 4172-4173.

110. L. R. Yang, M. Mayr, K. Wurst and M. R. Buchmeiser, *Chem. Eur. J.*, 2004, **10**, 5761-5770.
111. A. Binobaid, M. Iglesias, D. Beetstra, A. Dervisi, I. Fallis and K. J. Cavell, *Eur. J. Inorg. Chem.*, 2010, 5426-5431.
112. J. J. Dunsford, K. J. Cavell and B. Kariuki, *J. Organomet. Chem.*, 2011, **696**, 188-194.
113. M. J. Page, W. Y. Lu, R. C. Poulten, E. Carter, A. G. Algarra, B. M. Kariuki, S. A. Macgregor, M. F. Mahon, K. J. Cavell, D. M. Murphy and M. K. Whittlesey, *Chem. Eur. J.*, 2013, **19**, 2158-2167.
114. R. H. Crabtree, *Angew. Chem. Int. Ed.*, 1993, **32**, 789-805.
115. H. Noth and R. Hartwimmer, *Chem. Ber. R.*, 1960, **93**, 2238-2245.
116. H. D. Kaesz, W. Fellmann, G. R. Wilkes and L. F. Dahl, *J. Am. Chem. Soc.*, 1965, **87**, 2753-2755.
117. J. K. Hoyano, M. Elder and W. A. G. Graham, *J. Am. Chem. Soc.*, 1969, **91**, 4568-4569.
118. U. Schubert, K. Ackermann and B. Worle, *J. Am. Chem. Soc.*, 1982, **104**, 7378-7380.
119. G. J. Kubas, R. R. Ryan, B. I. Swanson, P. J. Vergamini and H. J. Wasserman, *J. Am. Chem. Soc.*, 1984, **106**, 451-452.
120. M. A. Graham, J. J. Turner, M. Poliakof and R. N. Perutz, *J. Organomet. Chem.*, 1972, **34**, C34-C36.
121. M. Poliakof and J. J. Turner, *J. Chem. Soc.-Dalton Trans.*, 1974, 2276-2285.
122. R. N. Perutz and J. J. Turner, *J. Am. Chem. Soc.*, 1975, **97**, 4791-4800.
123. W. H. Bernskoetter, C. K. Schauer, K. I. Goldberg and M. Brookhart, *Science*, 2009, **326**, 553-556.
124. R. D. Young, A. F. Hill, W. Hillier and G. E. Ball, *J. Am. Chem. Soc.*, 2011, **133**, 13806-13809.
125. J. A. Calladine, S. B. Duckett, M. W. George, S. L. Matthews, R. N. Perutz, O. Torres and Q. V. Khuong, *J. Am. Chem. Soc.*, 2011, **133**, 2303-2310.
126. I. Castro-Rodriguez, H. Nakai, P. Gantzel, L. N. Zakharov, A. L. Rheingold and K. Meyer, *J. Am. Chem. Soc.*, 2003, **125**, 15734-15735.
127. S. D. Pike, A. L. Thompson, A. G. Algarra, D. C. Apperley, S. A. Macgregor and A. S. Weller, *Science*, 2012, **337**, 1648-1651.
128. J. C. Green, M. L. H. Green and G. Parkin, *Chem. Comm.*, 2012, **48**, 11481-11503.
129. M. Brookhart and M. L. H. Green, *J. Organomet. Chem.*, 1983, **250**, 395-408.
130. S. J. Laplaca and J. A. Ibers, *Inorg. Chem.*, 1965, **4**, 778-783.
131. N. A. Bailey, J. M. Jenkins, R. Mason and B. L. Shaw, *Chem. Comm.*, 1965, 237-238.
132. Y. W. Yared, S. L. Miles, R. Bau and C. A. Reed, *J. Am. Chem. Soc.*, 1977, **99**, 7076-7078.
133. S. Trofimen, *J. Am. Chem. Soc.*, 1967, **89**, 6288-6294.
134. D. M. Roe, P. M. Bailey, P. P. M. Maitlis and K. Moseley, *J. Chem. Soc.-Chem. Comm.*, 1972, 1273-1274.

135. R. K. Brown, J. M. Williams, A. J. Schultz, G. D. Stucky, S. D. Ittel and R. L. Harlow, *J. Am. Chem. Soc.*, 1980, **102**, 981-987.
136. H. J. Wasserman, G. J. Kubas and R. R. Ryan, *J. Am. Chem. Soc.*, 1986, **108**, 2294-2301.
137. W. I. Sundquist, D. P. Bancroft and S. J. Lippard, *J. Am. Chem. Soc.*, 1990, **112**, 1590-1596.
138. M. Brookhart, M. L. H. Green and G. Parkin, *PNAS*, 2007, **104**, 6908-6914.
139. H. D. Empsall, E. M. Hyde, E. Mentzer, B. L. Shaw and M. F. Uttley, *J. Chem. Soc.-Dalton Trans.*, 1976, 2069-2074.
140. A. C. Cooper, W. E. Streib, O. Eisenstein and K. G. Caulton, *J. Am. Chem. Soc.*, 1997, **119**, 9069-9070.
141. A. C. Cooper, E. Clot, J. C. Huffman, W. E. Streib, F. Maseras, O. Eisenstein and K. G. Caulton, *J. Am. Chem. Soc.*, 1999, **121**, 97-106.
142. D. J. Huang, W. E. Streib, J. C. Bollinger, K. G. Caulton, R. F. Winter and T. Scheiring, *J. Am. Chem. Soc.*, 1999, **121**, 8087-8097.
143. L. Vaska and J. W. Diluzio, *J. Am. Chem. Soc.*, 1961, **83**, 2784-2785.
144. L. Vaska and J. W. Diluzio, *J. Am. Chem. Soc.*, 1962, **84**, 679-680.
145. J. A. Osborn, F. H. Jardine, J. F. Young and G. Wilkinson, *J. Chem. Soc. a -Inorg. Phys. Theor.*, 1966, 1711-1732.
146. P. Hamon, L. Toupet, J. R. Hamon and C. Lapinte, *Organometallics*, 1992, **11**, 1429-1431.
147. J. Chatt and J. M. Davidson, *J. Chem. Soc.*, 1965, 843-855.
148. N. F. Goldshleger, A. A. Shteinman, A. E. Shilov and V. V. Eskova, *Zh. Fiz. Khim.*, 1972, **46**, 1353.
149. A. E. Shilov and G. B. Shul'pin, *Chem. Rev.*, 1997, **97**, 2879-2932.
150. P. Foley and G. M. Whitesides, *J. Am. Chem. Soc.*, 1979, **101**, 2732-2733.
151. A. H. Janowicz and R. G. Bergman, *J. Am. Chem. Soc.*, 1982, **104**, 352-354.
152. K. M. Waltz and J. F. Hartwig, *Science*, 1997, **277**, 211-213.
153. R. H. Crabtree, *J. Organomet. Chem.*, 2004, **689**, 4083-4091.
154. T. Bolano, M. L. Buil, M. A. Esteruelas, S. Izquierdo, R. Lalrempuia, M. Olivan and E. Onate, *Organometallics*, 2010, **29**, 4517-4523.
155. A. R. Chianese, A. Mo, N. L. Lampland, R. L. Swartz and P. T. Bremer, *Organometallics*, 2010, **29**, 3019-3026.
156. R. N. Perutz and S. Sabo-Etienne, *Angew. Chem. Int. Ed.*, 2007, **46**, 2578-2592.
157. F. Wu and R. F. Jordan, *Organometallics*, 2005, **24**, 2688-2697.
158. A. D. Sadow and T. D. Tilley, *J. Am. Chem. Soc.*, 2005, **127**, 643-656.
159. J. K. Huang, E. D. Stevens and S. P. Nolan, *Organometallics*, 2000, **19**, 1194-1197.
160. N. M. Scott, R. Dorta, E. D. Stevens, A. Correa, L. Cavallo and S. P. Nolan, *J. Am. Chem. Soc.*, 2005, **127**, 3516-3526.
161. N. M. Scott, V. Pons, E. D. Stevens, D. M. Heinekey and S. P. Nolan, *Angew. Chem. Int. Ed.*, 2005, **44**, 2512-2515.
162. C. Y. Tang, W. Smith, A. L. Thompson, D. Vidovic and S. Aldridge, *Angew. Chem. Int. Ed.*, 2011, **50**, 1359-1362.

163. C. Y. Tang, A. L. Thompson and S. Aldridge, *J. Am. Chem. Soc.*, 2010, **132**, 10578-10591.
164. C. Y. Tang, A. L. Thompson and S. Aldridge, *Angew. Chem. Int. Ed.*, 2010, **49**, 921-925.
165. C. Y. Tang, N. Phillips, J. I. Bates, A. L. Thompson, M. J. Gutmann and S. Aldridge, *Chem. Comm.*, 2012, **48**, 8096-8098.
166. G. C. Fortman, A. M. Z. Slawin and S. P. Nolan, *Organometallics*, 2011, **30**, 5487-5492.
167. C. Y. Tang, N. Phillips, M. J. Kelly and S. Aldridge, *Chem. Comm.*, 2012, **48**, 11999-12001.
168. C. J. E. Davies, M. J. Page, C. E. Ellul, M. F. Mahon and M. K. Whittlesey, *Chem. Comm.*, 2010, **46**, 5151-5153.
169. R. Armstrong, C. Ecott, E. Mas-Marza, M. J. Page, M. F. Mahon and M. K. Whittlesey, *Organometallics*, 2010, **29**, 991-997.
170. C. Y. Tang, W. Smith, D. Vidovic, A. L. Thompson, A. B. Chaplin and S. Aldridge, *Organometallics*, 2009, **28**, 3059-3066.
171. C. Y. Tang, J. Lednik, D. Vidovic, A. L. Thompson and S. Aldridge, *Chem. Comm.*, 2011, **47**, 2523-2525.
172. J. Halpern, D. P. Riley, A. S. C. Chan and J. J. Pluth, *J. Am. Chem. Soc.*, 1977, **99**, 8055-8057.
173. J. C. Ma and D. A. Dougherty, *Chem. Rev.*, 1997, **97**, 1303-1324.
174. E. O. Fischer and W. Hafner, *Z. Naturforsch. B*, 1955, **10**, 665-668.
175. E. T. Singewald, C. A. Mirkin, A. D. Levy and C. L. Stern, *Angew. Chem. Int. Ed.*, 1994, **33**, 2473-2475.
176. J. W. Faller and D. G. D'Alliessi, *Organometallics*, 2003, **22**, 2749-2757.
177. A. R. O'Connor, W. Kaminsky, D. M. Heinekey and K. I. Goldberg, *Organometallics*, 2011, **30**, 2105-2116.
178. N. Imlinger, K. Wurst and M. R. Buchmeiser, *J. Organomet. Chem.*, 2005, **690**, 4433-4440.
179. O. Rivada-Wheelaghan, M. A. Ortuno, J. Diez, A. Lledos and S. Conejero, *Angew. Chem. Int. Ed.*, 2012, **51**, 3936-3939.
180. G. M. Schwab, *Trans. Faraday Soc.*, 1946, **42**, 689-697.
181. R. J. Mikovksy, M. Boudart and H. S. Taylor, *J. Am. Chem. Soc.*, 1954, **76**, 3814-3819.
182. G. C. Bond, P. A. Sermon, G. Webb, D. A. Buchanan and P. B. Wells, *J. Chem. Soc.-Chem. Comm.*, 1973, 444-445.
183. Y. Ito, M. Sawamura and T. Hayashi, *J. Am. Chem. Soc.*, 1986, **108**, 6405-6406.
184. G. Dyker, *Angew. Chem. Int. Ed.*, 2000, **39**, 4237-4239.
185. F. Bonati and G. Minghett, *J. Organomet. Chem.*, 1973, **59**, 403-410.
186. J. E. Parks and A. L. Balch, *J. Organomet. Chem.*, 1973, **57**, C103-C106.
187. S. K. Schneider, W. A. Herrmann and E. Herdtweck, *Z. Anorg. Allg. Chem.*, 2003, **629**, 2363-2370.
188. I. J. B. Lin and C. S. Vasam, *Can. J. Chem.-Rev. Can. Chim.*, 2005, **83**, 812-825.
189. R. Hoffmann, *Angew. Chem. Int. Ed.*, 1982, **21**, 711-724.

190. A. S. K. Hashmi and G. J. Hutchings, *Angew. Chem. Int. Ed.*, 2006, **45**, 7896-7936.
191. A. S. K. Hashmi, *Chem. Rev.*, 2007, **107**, 3180-3211.
192. Z. G. Li, C. Brouwer and C. He, *Chem. Rev.*, 2008, **108**, 3239-3265.
193. N. Marion and S. P. Nolan, *Chem. Soc. Rev.*, 2008, **37**, 1776-1782.
194. R. G. Pearson, *J. Chem. Educ.*, 1968, **45**, 581.
195. M. V. Baker, P. J. Barnard, S. K. Brayshaw, J. L. Hickey, B. W. Skelton and A. H. White, *Dalton Trans.*, 2005, 37-43.
196. E. Y. Tsui, P. Muller and J. R. Sadighi, *Angew. Chem. Int. Ed.*, 2008, **47**, 8937-8940.
197. B. W. Gung, L. N. Bailey, D. T. Craft, C. L. Barnes and K. Kirschbaum, *Organometallics*, 2010, **29**, 3450-3456.
198. S. G. Weber, D. Zahner, F. Rominger and B. F. Straub, *Chem. Comm.*, 2012, **48**, 11325-11327.
199. H. Ito, K. Takagi, T. Miyahara and M. Sawamura, *Org. Lett.*, 2005, **7**, 3001-3004.
200. H. Ito, T. Saito, T. Miyahara, C. M. Zhong and M. Sawamura, *Organometallics*, 2009, **28**, 4829-4840.
201. P. Pyykko, *Angew. Chem. Int. Ed.*, 2004, **43**, 4412-4456.
202. H. T. Liu, Y. L. Wang, X. G. Xiong, P. D. Dau, Z. A. Piazza, D. L. Huang, C. Q. Xu, J. Li and L. S. Wang, *Chem. Sci.*, 2012, **3**, 3286-3295.
203. U. Ringstrom, *Nature*, 1963, **198**, 981.
204. X. F. Wang and L. Andrews, *J. Am. Chem. Soc.*, 2001, **123**, 12899-12900.
205. L. Andrews and X. F. Wang, *J. Am. Chem. Soc.*, 2003, **125**, 11751-11760.
206. X. F. Wang and L. Andrews, *Angew. Chem. Int. Ed.*, 2003, **42**, 5201-5206.
207. H. Lehner, D. Matt, P. S. Pregosin, L. M. Venanzi and A. Albinati, *J. Am. Chem. Soc.*, 1982, **104**, 6825-6827.
208. B. D. Alexander, M. P. Gomezsal, P. R. Gannon, C. A. Blaine, P. D. Boyle, A. M. Mueting and L. H. Pignolet, *Inorg. Chem.*, 1988, **27**, 3301-3308.
209. H. B. Lv, J. H. Zhan, Y. B. Cai, Y. Yu, B. W. Wang and J. L. Zhang, *J. Am. Chem. Soc.*, 2012, **134**, 16216-16227.
210. D. A. Rosca, D. A. Smith, D. L. Hughes and M. Bochmann, *Angew. Chem. Int. Ed.*, 2012, **51**, 10643-10646.
211. T. J. Robilotto, J. Bacsa, T. G. Gray and J. P. Sadighi, *Angew. Chem. Int. Ed.*, 2012, **51**, 12077-12080.
212. D. S. Weinberger, M. Melaimi, C. E. Moore, A. L. Rheingold, G. Frenking, P. Jerabek and G. Bertrand, *Angew. Chem. Int. Ed.*, 2013, **52**, 8964-8967.

Chapter II

Experimental Methods

2.1 Manipulation of Air-Sensitive Compounds

Much of the work detailed in this thesis involved compounds which are highly sensitive to air and moisture. As a result, it was necessary to carry out transformations in inert environments as opposed to traditional bench-top methods.

2.1.1 Inert Atmosphere Techniques

Two common techniques were employed for the handling of air- and moisture-sensitive species: a Schlenk line for solution-phase manipulation, and a glove box for the manipulation of solids. Both offer an inert atmosphere (of argon or nitrogen gas, respectively) in which to store and handle sensitive compounds.[1, 2]

Schlenk line techniques have been shown to be an effective and efficient method of carrying out solution-phase reactions of air- and moisture-sensitive compounds, with low risk of oxidation or hydrolysis.[3] The line consists of a dual Pyrex glass manifold connected to a high vacuum pump and also to a source of purified inert gas, in this case, argon (Fig 2.1). This allows access to a positive pressure of argon gas, as well as evacuation of glassware down to ca. 10^{-2} Torr. Several two-way taps allows connection of reaction vessels to both environments.

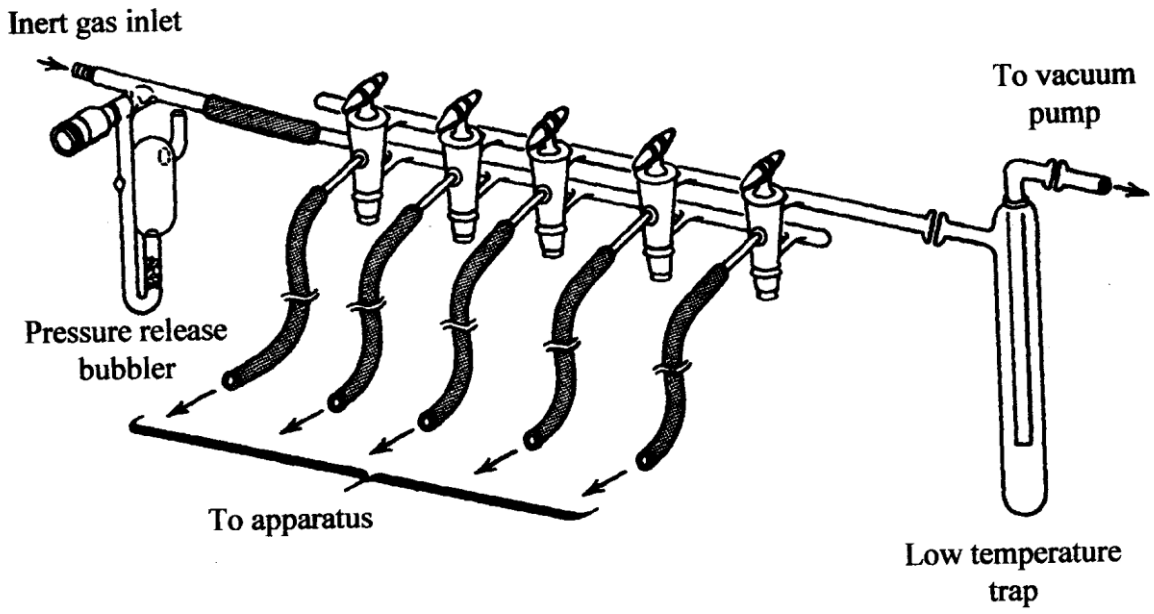

Figure 2.1: A Schlenk Line

A ‘pump and purge’ cycle, of alternating vacuum and gas, was employed three times to create an environment near-free from oxygen and moisture. The vacuum manifold was fitted with a liquid nitrogen cold trap to prevent volatile solvents and reactants from contaminating the pump, and excess pressure in the argon manifold was vented through a mercury bubbler. To ensure an air-tight seal, all ground glass joints and taps were lubricated with high vacuum grease. Transferring of liquids and solutions between reaction vessels was achieved by the use of cannulae and syringes to avoid exposure to air.

Air-sensitive solids were handled and stored in a nitrogen atmosphere glove box. The atmosphere was purified by passing through activated copper metal and molecular sieves to remove oxygen and water, respectively. Neoprene gloves were built in to the side of the box to allow access to the sealed system. Materials and apparatus entered the box via a side port to which the standard ‘pump and purge’ method was applied.

2.2 Spectroscopic Techniques

2.2.1 NMR Spectroscopy

NMR spectra were measured on a Varian 'Mercury' 300 MHz, 500 MHz or a Bruker 400 MHz spectrometer. For ^{1}H and ^{13}C NMR spectra, deuterated solvents were used for referencing; ^{11}B and ^{19}F NMR spectra were referenced against $BF_3{\cdot}OEt_2$ and $CFCl_3$ respectively. Air-sensitive solutions were prepared in Young's NMR tubes. Detailed line shape analysis experiments were kindly carried out by Dr Nick Rees, University of Oxford.

2.2.2 Infrared Spectroscopy

Infrared spectra were measured on a Nicolet 500 FT-IR spectrometer. Solution phase samples were prepared in a sealed KBr cell.

2.2.3 Mass Spectrometry

Neutral samples were submitted to the EPSRC National Mass Spectrometry Service Centre, Swansea University and to Colin Sparrow, University of Oxford for EI measurements. Charged compounds were analysed using a Bruker MicroTOF ESI mass spectrometer connected to a glove box via PEEK tubing.[4] These ESI mass spectrometry measurements were carried out by Dr Ian Riddlestone or Mr Joe Abdalla of the Aldridge research group.

2.2.4 Elemental Analysis

Elemental analyses were carried out by Stephen Boyer of London Metropolitan University. Analyses were collected on all novel compounds; however, in some cases, multiple attempts were made but accurate results could not be obtained.

2.2.5 X-Ray Crystallography

X-Ray data were collected on Bruker-Nonius KappaCCD and Oxford Diffraction (Agilent) SuperNova diffractometers. Data were reduced using DENZO/SCALEPACK[5] or CrysAlisPro. Structure determinations were carried out by the author, or by Dr Christina Tang, Mr Michael Kelly, Dr Ian Riddlestone or Mr Remi Tirfoin of the Aldridge research group using SIR92[6] or SuperFlip,[7] and refined with full-matrix least-squares within CRYSTALS[8, 9] or SHELX.[10]

2.2.6 Neutron Diffraction

Neutron diffraction data were collected on the time-of-flight Laue diffractometer SXD at the ISIS spallation neutron source. Data processing and structural determination were performed by Dr Amber Thompson (Oxford) and Dr Matthias Guttman (ISIS).

2.2.7 Theoretical Calculations

DFT calculations were performed by Dr Joshua Bates of the Aldridge group and by Miss Lucinda Treasure of the McGrady/Aldridge group. Calculations of the dihydrogen complexes **5a**, **16** and $[(NHC)Au(H_2)]^+$ were carried out by Dr Bates using the Amsterdam Density Functional (ADF 2012) Software Package.[11, 12] Calculations were performed using the Vosko-Wilk-Nusair local density approximation with exchange from Becke[13] and correlation corrections from Perdew (BP).[14] Slater-type orbitals (STOs)[15] were used for the triple zeta basis set with an additional set of polarization functions (TZP). The large frozen core basis set approximation was applied with no molecular symmetry. The general numerical integration was 6.

Mechanistic calculations on **14a** and **14b** were carried out by Miss Treasure using the Gaussian ’09 program to model the truncated structure with PBE0, as B3LYP fails to

accurately model agostic interactions.[16] An SDD basis set was used for iridium, with SVP on all atoms in the immediate coordination sphere and SV on all other atoms.

2.3 Preparation and Purification of Starting Materials

Reagents and solvents were bought from suppliers and, in most cases, purified before use. Details of the purification and supplier for all commercially available chemicals are provided in the CD Appendix.

2.3.1 Synthesis of Starting Materials

Previously reported chemicals which are not readily available from commercial sources needed to be synthesised using literature procedures. These are briefly outlined here.

General procedure for synthesis of N,N'-diaryl-formamidines (Ar = Mes, Xyl, Dipp).

The method employed followed that reported by Nechaev *et al*.[17] A round-bottomed flask containing $ArNH_2$ (0.130 mol), $HC(OEt)_3$ (0.065 mol) and AcOH (0.007 mol) was fitted with a short path distillation head. The mixture was stirred and heated to 180 °C over a period of 2 h resulting in the distillation of EtOH. On cooling to room temperature, a colourless crystalline mass formed which is subsequently washed with hexanes (200 cm^3) and dried under vacuum. ^1H NMR spectroscopy data agrees with that reported in the literature.[17]

General procedure for synthesis of expanded-ring N-heterocyclic carbene salts ([(6-Mes)H][BF_4], [(6-Xyl)H][BF_4], [(6-Dipp)H][BF_4], [(7-Mes)H][BF_4], [(7-Dipp)H][BF_4]).

The method employed followed that reported by Fallis *et al*.[18] The respective *N,N'*-diaryl-formamidine (0.036 mol), dibromoalkane (1,3-dibromo-propane or 1,4-dibromo-

butane) (0.040 mol) and K_2CO_3 (0.019 mol) were combined in acetonitrile (200 cm^3) and heated to reflux for 16 h (Xyl and Mes) or 96 h (Dipp). After cooling, the solvent was removed *in vacuo* and the residue dissolved in dichloromethane (50 cm^3). This solution was filtered through 0.5 cm of silica and solvent was removed to give an off-white solid. Acetone (40 cm^3) was used to dissolve the solid, then an aqueous solution of $Na[BF_4]$ (0.043 mol, 100 cm^3) added and the mixture stirred for 10 min. Volatiles were removed under vacuum and the product was extracted with dichloromethane (3 x 50 cm^3). This solution was then dried with $MgSO_4$ and filtered. Concentration to a minimum (*ca*. 10 cm^3) and addition of diethyl ether (300 cm^3) yielded a white powder than can be collected by filtration. After drying under vacuum, ^{1}H NMR data were found to be identical to those reported.[18]

General procedure for the deprotonation of N-heterocyclic carbene salts

The method employed followed that reported by Fallis *et al.*[18] A flame dried Schlenk tube was charged with the $[(NHC)H][BF_4]$ salt (0.01 mol) and was further dried using three 'pump and purge' cycles followed by continuous vacuum for 30 min. The salt was then suspended in THF (20 cm^3) and a solution of $K[N(SiMe_3)_2]$ (0.011 mol) in THF (30 cm^3) was added via cannula. After stirring for 30 min, the salt dissolved; filtration and removal of the volatiles under vacuum gave a yellow residue. The free NHC was extracted with diethyl ether (3 x 30 cm^3) and the solution concentrated until cloudy. Storage overnight at -30 °C yielded white crystalline NHC. ^{1}H NMR spectroscopy confirmed formation of pure product.[18]

Preparation of $Na[B(3,5\text{-}CF_3\text{-}C_6H_3)_4]$ ($Na[BAr^f_4]$)

The procedure for the synthesis of $Na[BAr^f_4]$ reported by Reger *et al.* was modified slightly.[19] Mg (3.0 g, 0.123 mol) was added to a flame dried 3-necked round-bottomed flask

and dried under vacuum. Vigorous heating with a heat gun was used to activate the Mg before suspending in diethyl ether (400 cm^3) under argon. A reflux condenser was attached and 1-bromo-3,5-trifluoromethyl-benzene (14.2 cm^3, 0.082 mol) was added dropwise over 30 min to avoid excessive heating. The solution turned dark brown and was stirred for a further 1.5 h. $BF_3 \cdot OEt_2$ (2.4 cm^3, 0.02 mol) was added slowly to the stirred mixture which was then refluxed for 6 h. After reflux, the reaction was opened to air and a saturated aqueous solution of Na_2CO_3 (50 g, 0.47 mol) added, accompanied by effervescence. The solution was filtered and the ethereal layer separated and combined with diethyl ether washings (5 x 30 cm^3). Volatiles were removed *in vacuo*, heating to 60 °C to remove residual H_2O. A mixture of Et_2O:THF:CH_2Cl_2 (15:15:15 cm^3) was used to dissolve the orange/brown solid, and this solution was layered with hexane. Storage at 5 °C for several days yielded large, colourless crystals of the desired product. Characterisation by ^1H and ^{11}B NMR deemed the product to have been formed in high purity.[19] Grinding the crystals to a white powder and drying overnight under vacuum at 60 °C yielded a product ready for use with sensitive substrates.

Preparation of $[H(OEt_2)_2][BAr^f_4]$ (Brookhart's acid)

The synthesis used the procedure reported by Brookhart *et al.*[20] In a flame dried round-bottomed flask, $Na[BAr^f_4]$ (1.0 g, 1.13 mmol) was dissolved in Et_2O (40 cm^3) and cooled to -30 °C. HCl in Et_2O (3 cm^3, 2.0 M, 6 mmol) was added, and the mixture stirred while warming to 0 °C. The reaction mixture was left to settle at 0 °C, allowing precipitation of NaCl. The solution was then filtered and the residue washed with Et_2O (2 x 20 cm^3). Concentration of the combined ether fractions at 0 °C to *ca.* 5 cm^3, and subsequent cooling to -78 °C led to the formation of colourless crystals. After standing for 1 h, hexanes (50 cm^3) were added slowly to promote precipitation of further product. The supernatant was decanted and the white solid was dried under vacuum and stored at -30 °C. Due to the

reactive nature of this species, it was used for further reactions without characterisation by NMR spectroscopy.

Preparation of $[Ph_3C][BAr^f_4]$

A modified version of the synthesis reported by Boudjouk *et al.* was used.[21] In a flame dried Schlenk tube, Ph_3CCl (94 mg, 0.34 mmol) was dissolved in dichloromethane (30 cm^3) and $Na[BAr^f_4]$ (300 mg, 0.34 mmol) was added. Stirring for 6 h gave a yellow solution which was then filtered and concentrated to 5 cm^3. Addition of hexanes (40 cm^3) caused the precipitation of the yellow product. The solid was isolated and dried under vacuum. ^{1}H NMR spectroscopy confirmed synthesis of the product in high purity. [21]

Preparation of $B(C_6F_5)_3$

A minor modification of the procedure reported by Wang *et al*. was employed.[22] A 1.6 M hexane solution of ^{n}BuLi (31.0 cm^3, 50.0 mmol) was added dropwise to a stirred solution of BrC_6F_5 (12.35 g, 50.0 mmol) in pentane at -78 °C. The reaction mixture was stirred at -78 °C for 1 h being careful to keep the temperature low as LiC_6F_5 is explosive above -50 °C. A 1.0 M heptane solution of BCl_3 (16.7 cm^3, 16.7 mmol) was then added rapidly and the mixture was stirred at -78 °C for a further 3 h. The mixture was allowed to warm to room temperature over a period of 12 h. After filtration and concentration, the solution was cooled to -30 °C to a yield a white precipitate of $B(C_6F_5)_3$. Characterisation by ^{11}B and ^{19}F NMR confirmed the formation of pure product.[22]

Preparation of $Li[Al(OC\{CF_3\}_3)_4]$

The method reported by Krossing was followed.[23] $LiAlH_4$ (0.265 g, 7 mmol) was suspended in toluene (50 cm^3) and cooled to 0 °C. $(CF_3)_3COH$ (4 cm^3, 28 mmol) was then added dropwise over 5 min and the reaction mixture allowed to stir for a further 1 h. The

mixture was then heated to reflux over 16 h during which time the solid dissolved. Cooling the toluene solution to -30 °C for 1 h caused the precipitation of the white product. After decanting the supernatant and drying *in vacuo*, the crude product appeared off-white. This was further purified by sublimation at 130 °C and 5 x 10^{-2} Torr. ^{27}Al NMR confirmed the production of the pure product.[23]

Preparation of $Cs[HCB_{11}Me_{11}]$

A small sample of $Cs[HCB_{11}Me_{11}]$ was obtained from the Weller research group, Oxford University. The synthesis employed was that of Michl *et al.*[24]

Preparation of $[Ir(COE)_2Cl]_2$

This procedure was first reported by Herde *et al.*[25] A round-bottomed Schenk flask under argon was charged with $IrCl_3 \cdot 3H_2O$ (3.0 g, 10.1 mmol), isopropanol (33 cm^3), H_2O (12 cm^3) and cyclooctene (6 cm^3, 46.2 mmol). The mixture was refluxed for 3 h during which time an orange precipitate formed. After cooling, the supernatant was decanted and the resulting solid washed with ice cold ethanol (2 x 30 cm^3). The orange product was dried under vacuum for 3 h. Analysis by ^{1}H NMR confirmed the product purity.[25]

Preparation of (THT)AuCl

The reported procedure by Puddephatt *et al.* was modified slightly for this synthesis.[26] Gold powder (1 g, 5.1 mmol) was dissolved in boiling *aqua regia* (40 cm^3). The initial volume was reduced to 10 cm^3, then more *conc.* HCl added (40 cm^3) and the mixture concentrated down again. This was repeated until no more brown fumes of NO_2 were produced. The resulting solution (*ca.* 10 cm^3) was cooled to 20 °C and then ethanol (40 cm^3) added. With minimum light exposure, THT (1.2 cm^3, 14 mmol) was then added dropwise. After 15 min, the resulting white precipitate was collected by filtration and

washed with Et_2O (10 cm^3) and pentane (10 cm^3). The product was briefly dried under vacuum and used without further analysis.

General preparation of (NHC)AuCl (NHC = 6-Xyl, 6-Mes, 6-Dipp, 7-Mes, 7-Dipp)

Syntheses were based on the procedure reported by Cavell *et al*.[27] [(NHC)H][BF_4] (0.3 mmol) was loaded into a flame dried Schlenk tube and placed under vacuum for 20 min. Addition of THF (30 cm^3) to dissolve the salt was followed by K[$N(SiMe_3)_2$] (0.35 mmol). The solution stirred for a further 30 min. In a second, dry Schlenk tube, (THT)AuCl (0.3 mmol) was dried briefly under vacuum and suspended in THF (10 cm^3). In the absence of light, the solution of the NHC was filtered onto the suspension and the resulting reaction mixture stirred for 1 h. During this time a blue colour developed. Now open to air, activated charcoal was added and the mixture stirred for a further 30 min. The solution was then filtered through a pad of Celite and concentrated to *ca.* 5 cm^3. Addition of pentane (40 cm^3) afforded the product as a white solid which was isolated and dried *in vacuo*. ^{1}H NMR spectroscopy confirmed the synthesis of a pure sample.[27]

2.4 References

1. R. E. Dodd and P. L. Robinson, *Experimental Inorganic Chemistry. A Guide to Laboratory Practice*, pp. xii. 424, Elsevier Publishing Co., Amsterdam, 1954.
2. R. J. Errington, *Advanced Practical Inorganic and Metalorganic Chemistry*, Blackie Academic & Professional, London, 1997.
3. D. Shriver and M. Drezdon, *The Manipulation of Air-Sensitive Compounds*, Wiley-Interscience, 1986.
4. A. T. Lubben, J. S. McIndoe and A. S. Weller, *Organometallics*, 2008, **27**, 3303-3306.
5. Z. Otwinowski and W. Minor, *Processing of X-Ray Diffraction Data Collected in Oscillation Mode, Methods Enzymol.*, Sweet, Academic Press, 1997.
6. A. Altomare, G. Cascarano, C. Giacovazzo and A. Guagliardi, *J. Appl. Crystallogr.*, 1993, **26**, 343-350.
7. L. Palatinus and G. Chapuis, *J. Appl. Crystallogr.*, 2007, **40**, 786-790.
8. R. I. Cooper, A. L. Thompson and D. J. Watkin, *J. Appl. Crystallogr.*, 2010, **43**, 1100-1107.

9. A. L. Thompson and D. J. Watkin, *J. Appl. Crystallogr.*, 2011, **44**, 1017-1022.
10. G. M. Sheldrick, *Acta Crystallogr. Sect. A*, 2008, **64**, 112-122.
11. C. F. Guerra, J. G. Snijders, G. te Velde and E. J. Baerends, *Theor. Chem. Acc.*, 1998, **99**, 391-403.
12. G. te Velde, F. M. Bickelhaupt, E. J. Baerends, C. F. Guerra, S. J. A. Van Gisbergen, J. G. Snijders and T. Ziegler, *J. Comput. Chem.*, 2001, **22**, 931-967.
13. A. D. Becke, *Phys. Rev. A*, 1988, **38**, 3098-3100.
14. J. P. Perdew, *Phys. Rev. B*, 1986, **33**, 8822-8824.
15. J. G. Snijders, P. Vernooijs and E. J. Baerends, *At. Data Nucl. Data Tables*, 1982, **26**, 483-509.
16. D. A. Pantazis, J. E. McGrady, F. Maseras and M. Etienne, *J. Chem. Theor. Comput.*, 2007, **3**, 1329-1336.
17. E. L. Kolychev, I. A. Portnyagin, V. V. Shuntikov, V. N. Khrustalev and M. S. Nechaev, *J. Organomet. Chem.*, 2009, **694**, 2454-2462.
18. M. Iglesias, D. J. Beetstra, J. C. Knight, L. L. Ooi, A. Stasch, S. Coles, L. Male, M. B. Hursthouse, K. J. Cavell, A. Dervisi and I. A. Fallis, *Organometallics*, 2008, **27**, 3279-3289.
19. D. L. Reger, T. D. Wright, C. A. Little, J. J. S. Lamba and M. D. Smith, *Inorg. Chem.*, 2001, **40**, 3810-3814.
20. M. Brookhart, B. Grant and A. F. Volpe, *Organometallics*, 1992, **11**, 3920-3922.
21. S. R. Bahr and P. Boudjouk, *J. Org. Chem.*, 1992, **57**, 5545-5547.
22. C. Wang, G. Erker, G. Kehr, K. Wedeking and R. Frohlich, *Organometallics*, 2005, **24**, 4760-4773.
23. I. Krossing, *Chem. Eur. J.*, 2001, **7**, 490-502.
24. B. T. King, B. C. Noll and J. Michl, *Collect. Czech. Chem. Comm.*, 1999, **64**, 1001-1012.
25. J. L. Herde, J. C. Lambert, C. V. Senoff and M. A. Cushing, *Inorg. Synth.*, 1974, **15**, 18-20.
26. M. C. Brandys, M. C. Jennings and R. J. Puddephatt, *J. Chem. Soc.-Dalton Trans.*, 2000, 4601-4606.
27. J. J. Dunsford, K. J. Cavell and B. M. Kariuki, *Organometallics*, 2012, **31**, 4118-4121.

Chapter III

Saturated Ring NHC Complexes: Electronic and Steric Stabilisation of Group 9 Metals

3.1 Introduction

Imidazolium-based *N*-heterocyclic carbene complexes have received significant attention in recent years in part due to the electronic and steric stabilisation offered by the NHC ligand to low valent systems.[1-10] Ease of synthesis and high stability of unsaturated NHCs have made them an attractive prospect for the replacement of more sensitive phosphine ligands. By contrast, the saturated analogues of these NHCs have received much less attention despite being the target of some of the earliest work on NHCs.[11] This is most likely due to saturated NHCs requiring bulky *N*-based substituents to prevent dimerisation.[12] Hence this structural variety is more limited than unsaturated systems. Additionally, they require bases such as potassium hydride rather than potassium *tert*-butoxide due to reaction with the resulting alcohol; as a result the syntheses tend to be more air and moisture sensitive. The saturated backbone increases σ-donor properties (i.e. increased basicity[13-15] and more highly shielded C_{NHC} centres[16]) due to the slight elongation of the backbone C–C bond resulting in a wider N–C–N angle. Widening this angle results in increased p-character of the donor orbital, and hence a more extended and available lone pair. In the case of 5-Mes (Fig 3.1; also referred to as SIMes), the steric profile does not vary much from the unsaturated NHC IMes yet it offers enhanced donor capabilities. This scenario allows for useful comparison of electronic properties, while keeping the steric demands essentially invariant.

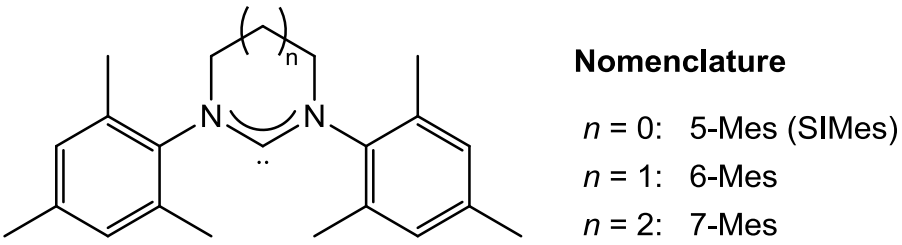

Figure 3.1: Expanded ring NHC nomenclature.

Recent interest has focused on the utilisation of more sterically demanding expanded ring NHC systems to stabilise more reactive species (nomenclature in Fig 3.1).[17-39] Increasing the ring size of the heterocycle from 5 to 6- and 7-membered rings increases the N-C_{NHC}-N angle (IMes, 101.4°;[40] 6-Mes, 114.6°; 7-Mes, 116.6°[16]) and has a marked impact on the $\%V_{bur}$ of the NHC (36.1, 44.0 and 44.7% respectively).[14, 41, 42] This has implications for their use in the stabilisation of low valent, electron-deficient metal centres as catalytic intermediates.[19, 22, 35, 37, 43] The increased σ-donor capacity of this ligand set should also help to produce a more robust species which can exist longer as an intermediate. Catalyst life could also be prolonged by the greater steric shielding offered in the expanded ring NHC ligands, potentially reducing decomposition by M–C bond cleavage.

The aim of the research reported in this chapter is the synthesis of a range of saturated-NHC stabilized late transition metal complexes. These will act as precursors to species analogous to previously reported 14-electron complexes of the type $[(L)_2M(H)_2]^+$ (L = phosphine, NHC; M = Rh, Ir). Low valent, cationic complexes of rhodium and iridium have been widely reported for a range of substrate activation processes, including alkane dehydrogenation and alkene hydrogenation.[44, 45] Species of this type are often accessed by halide abstraction from the metal using salt metathesis,[46-48] so the design of these precursor complexes will aim to incorporate halide atoms.

3.2 Experimental

*Preparation of (5-Mes)$_2$Ir(COE)Cl (**1**)*

A solution of 5-Mes (274 mg, 2.6 mmol) in THF (30 cm^3) was added to a stirred solution of [Ir(COE)$_2$Cl]$_2$ (200 mg, 0.65 mmol) in THF (20 cm^3). The orange solution was stirred overnight and darkened to an orange/brown colour. Removal of the volatiles *in vacuo* yields an orange solid. The product was subsequently extracted into diethyl ether (3 x 30 cm^3). Concentration and storage at -30 °C produced orange crystals in 82% yield (350 mg). Crystals for X-ray crystallography were obtained by slow evaporation of a diethyl ether solution at room temperature.

*Spectroscopic data for **1***

^{1}H NMR (C_6D_6, 300 MHz, 298 K): δ_H 6.96 (2H, s, *meta*-CH Mes), 6.84 (6H, s, *meta*-CH Mes), 3.16 (4H, m, NCH_2), 3.08 (4H, m, NCH_2), 2.55 (6H, s, *para*-CH_3), 2.47 (6H, s, *para*-CH_3), 2.32 (6H, s, *ortho*-CH_3), 2.29 (6H, s, *ortho*-CH_3), 2.24 (6H, s, *ortho*-CH_3), 2.20 (6H, s, *ortho*-CH_3), 2.06 (2H, d, $^3J_{HH}$ = 9.6 Hz, CH COE), 1.73, 1.38, 1.23 (4H, m, CH_2 COE). ^{13}C NMR (C_6D_6, 75 MHz, 298 K): δ_C 207.9, 204.0 (NCN), 138.7, 137.7 (NC Mes), 137.4, 137.3 (*para*-C Mes), 134.8, 134.3, 134.1, 133.7 (*ortho*-C Mes), 128.9, 128.5, 128.2, 127.6 (*meta*-CH Mes), 51.1, 49.6 (NCH_2), 36.5 (CH COE), 30.1, 27.1, 26.3 (CH_2 COE), 20.8, 19.8 (*para*-CH_3), 19.4, 18.7, 18.0, 17.3 (*ortho*-CH_3). MS (EI +ve): *m/z* 950.5 (M^+, 4%). Accurate mass ([$C_{50}H_{66}N_4{}^{191}IrCl]^+$): 948.4574 (meas.), 948.45819 (calc.).

*Crystallographic data for **1***

$C_{54}H_{76}IrN_4ClO$, M_r = 1024.90, monoclinic, $P2_1/a$, a = 15.12070(10), b = 18.8464(2), c = 17.3193(2) Å, β = 96.0023(4)°, V = 4908.44(8) Å^3, Z = 4, ρ_c = 1.387 Mg/m^3, T = 150 K, λ = 0.71073 Å, 69693 reflections collected, 11168 independent [R(int) = 0.077], which were

used in all calculations. R_1 = 0.0350, wR_2 = 0.0641 for observed reflections [I > 2σ(I)] and R_1 = 0.0647, wR_2 = 0.0883 for all unique reflections. Max. and min. residual electron densities 3.21 and -1.55 eÅ^{-3}.

*Preparation of (5-Mes)(5-Mes')IrHCl (**2**)*

A solution of (5-Mes)$_2$Ir(COE)Cl (450 mg, 0.47 mmol) in toluene (40 cm^3) was heated to 70 °C for 48 h. The volatiles were removed *in vacuo* and the red residue was extracted with diethyl ether (3 x 20 cm^3). Concentration and storage at -30 °C yielded bright red, X-ray quality crystals in 79% yield (320 mg).

*Spectroscopic data for **2***

^{1}H NMR (C_6D_6, 300 MHz, 298 K): δ_H 6.79 (4H, s, *meta*-CH Mes), 6.73 (1H, s, *meta*-CH Mes'), 6.70 (2H, s, *meta*-CH Mes'), 6.67 (1H, s, *meta*-CH Mes'), 3.52 (2H, br m, NCH_2), 3.18 (4H, s, NCH_2), 2.94 (2H, m, NCH_2), 2.42 (6H, s, *para*-CH_3 Mes), 2.41 (2H, br, $IrCH_2$), 2.33 (12H, s, *ortho*-CH_3 Mes), 2.18 (6H, s, *ortho*-CH_3 Mes), 1.91 (3H, s, *para*-CH_3 Mes'), 1.74 (3H, s, *ortho*-CH_3 Mes'), -32.84 (1H, s, IrH). ^{13}C NMR (C_6D_6, 75 MHz, 298 K): δ_C 210.4, 209.9 (NCN), 137.9 (NC Mes'), 137.8 (NC Mes), 137.5 (NC Mes'), 137.0 (*para*-C Mes), 136.9, 136.4 (*para*-C Mes'), 136.1 (*ortho*-C Mes'), 135.8 (*ortho*-C Mes), 133.1 (*ortho*-C Mes'), 129.6, 129.5, 129.5 (*meta*-CH Mes'), 129.2 (*meta*-CH Mes), 52.0, 51.3, 50.5, 49.4 (NCH_2), 21.3 (*para*-CH_3 Mes), 21.3, 21.2, 21.2 (*para*-CH_3 Mes'), 19.7, 19.4, 19.2 (*ortho*-CH_3 Mes'), 18.9 (*ortho*-CH_3 Mes). MS (EI +ve): *m/z* 802.4 ([M-HCl]$^+$, 1%). Elemental analysis: calc. for $C_{42}H_{52}IrN_4Cl$: C 60.40, H 6.83, N 6.13, meas. C 59.80, H 6.63, N 5.91.

*Crystallographic data for **2***

$C_{42}H_{52}IrN_4Cl$, M_r = 840.57, monoclinic, $P2_1/n$, a = 15.8693(1), b = 12.3445(1), c = 21.1450(2) Å, β = 104.6968(4) °, V = 4006.75(6) $Å^3$, Z = 4, ρ_c = 1.393 Mg m^{-3}, T = 150 K, λ = 0.710730 Å, 138077 reflections collected, 9099 independent [R(int) = 0.024], which were used in calculations. R_1 = 0.0282, wR_2 = 0.0611 for observed unique reflections [I > 2σ(I)] and R_1 = 0.0424, wR_2 = 0.0732 for all unique reflections. Max. and min. residual electron densities 1.50 and -1.43 e $Å^{-3}$.

*Preparation of (5-Mes)$_2$IrH$_2$Cl (**3**)*

In a Young's ampoule, a solution of **2** (200 mg, 0.24 mmol) in toluene (15 cm^3) was freeze-pump-thaw degassed three times. On the final cycle, the flask was immersed in liquid nitrogen under vacuum and the head-space was back-filled with hydrogen gas. The solution was allowed to warm to room temperature and stirred for 1 h. This reaction was accompanied by a colour change from red to yellow and conversion was shown to be quantitative by ^{1}H NMR. X-ray quality crystals of **3** were isolated from a concentrated solution in diethyl ether stored at -30 °C.

*Spectroscopic data for **3***

^{1}H NMR (C_6D_6, 300 MHz, 298 K): δ 6.78 (8H, s, *meta*-CH), 3.08 (8H, s, NCH_2), 2.34 (12H, s, *para*-CH_3), 2.19 (24H, s, *ortho*-CH_3), -32.81 (2H, s, IrH). ^{13}C NMR (C_6D_6, 125 MHz, 298 K): δ 210.4 (NCN), 137.9 (NC Mes), 137.0 (*para*-C Mes), 135.8 (*ortho*-C Mes), 129.2 (*meta*-CH Mes), 50.5 (NCH_2), 21.3 (*para*-CH_3), 18.9 (*ortho*-CH_3). MS (EI +ve): *m/z* 842.4 (M^+, 5%). Accurate mass ($[C_{42}H_{54}N_4{}^{191}IrCl]^+$): 840.3639 (meas.), 840.3643 (calc.). Elemental analysis: calc. for $C_{42}H_{54}IrN_4Cl$: C 59.87, H 6.46, N 6.65, meas. C 58.79, H 6.12, N 6.32.

*Crystallographic data for **3***

$C_{42}H_{54}IrN_4Cl$, M_r = 842.59, orthorhombic, *Pbca*, a = 17.0027(1), b = 19.4001(1), c = 23.4149(2) Å, V = 7723.50(9) $Å^3$, Z = 8, ρ_c = 1.449 Mg m^{-3}, T = 150 K, λ = 0.710730 Å, 158718 reflections collected, 8784 independent [R(int) = 0.033], which were used in calculations. R_1 = 0.0311, wR_2 = 0.0542 for observed unique reflections [$I > 2\sigma(I)$] and R_1 = 0.0643, wR_2 = 0.0768 for all unique reflections. Max. and min. residual electron densities 2.51 and -1.75 e $Å^{-3}$.

*Preparation of (6-Mes')$_2$IrH (**4a**)*

A solution of 6-Mes (2.8 g, 8.74 mmol) in THF (30 cm^3) was added to a stirred solution of $[Ir(COE)_2Cl]_2$ (1.3 g, 1.45 mmol) in THF (30cm^3). The orange solution was stirred overnight and darkened to an orange/brown colour. Removal of the volatiles *in vacuo* yielded a dark orange solid. The product was washed with cold hexanes (3 x 20 cm^3) and dried *in vacuo*. Extraction of the solid into toluene and subsequent removal of the solvent *in vacuo* yielded the product as an orange/red powder in 52% yield (1.25 g). Crystals suitable for X-ray crystallography were obtained by slow evaporation of a concentrated solution in diethyl ether at room temperature.

*Spectroscopic data for **4a***

^{1}H NMR (C_6D_6, 300 MHz, 298 K): δ 7.05 (2H, s, *meta*-H Mes'), 6.96 (2H, s, *meta*-H Mes), 6.85 (2H, s, *meta*-H Mes), 6.06 (2H, s, *meta*-H Mes'), 3.15 (2H, m, NCH_2), 2.78 (2H, m, NCH_2), 2.67 (4H, m, NCH_2), 2.39 (6H, s, *para*-CH_3), 2.34 (6H, s, *para*-CH_3), 2.31 (6H, s, *ortho*-CH_3), 2.25 (2H, d, $^2J_{HH}$ = 6.9 Hz, Ir-CH_2), 2.18 (6H, s, *ortho*-CH_3), 2.17 (2H, d, $^2J_{HH}$ = 6.9 Hz, Ir-CH_2), 1.85 (6H, s, *ortho*-CH_3), 1.48 (4H, m, NCH_2CH_2), -37.54 (1H, s, IrH). ^{13}C NMR (C_6D_6, 125 MHz, 298 K): δ 205.2 (NCN), 145.3 (NC Mes), 144.4 (NC Mes'),

136.4 (*para*-C Mes), 135.1 (*para*-C Mes'), 133.9 (*ortho*-C Mes), 129.7 (*ortho*-C Mes'), 128.9 (*meta*-CH Mes), 128.1 (*meta*-CH Mes'), 127.3 (*meta*-CH Mes'), 123.7 (*ortho*-C Mes'), 47.7 (NCH_2), 46.4 (NCH_2), 23.1 (NCH_2CH_2), 22.4 (*para*-CH_3 Mes), 21.2 (*para*-CH_3 Mes'), 19.7 (*ortho*-CH_3 Mes), 18.7 (*ortho*-CH_3 Mes), 18.3 (*ortho*-CH_3 Mes'), 8.3 ($IrCH_2$). MS (EI +ve): *m/z* 832.3 (M^+), 830.3 ($[M-2H]^+$). Accurate mass ($[C_{44}H_{53}N_4{}^{191}Ir]^+$): 828.3872 (meas.), 828.3893 (calc.).

*Crystallographic data for **4a***

$C_{44}H_{54}IrN_4$, M_r = 832.15, monoclinic, *C*2/*c*, a = 33.2496(3), b = 20.4868(2), c = 19.4945(2) Å, β = 121.4724(5) °, V = 11325.7(2) $Å^3$, Z = 4, ρ_c = 1.463 Mg m^{-3}, T = 150 K, λ = 0.710730 Å, 56613 reflections collected, 12909 independent [R(int) = 0.044], which were used in calculations. R_1 = 0.0541, *w*R_2 = 0.0901 for observed unique reflections [I > 2σ(I)] and R_1 = 0.0762, *w*R_2 = 0.1023 for all unique reflections. Max. and min. residual electron densities 3.45 and -1.70 e $Å^{-3}$.

*Preparation of (7-Mes')$_2$IrH (**4b**)*

A solution of 7-Mes (300 mg, 0.90 mmol) in THF (30 cm^3) was added to a stirring solution of $[Ir(COE)_2Cl]_2$ (201 mg, 0.22 mmol) in THF (20cm^3). The orange solution was stirred overnight and darkened to an orange/brown colour. Removal of the volatiles *in vacuo* yielded a dark orange solid. The product was subsequently extracted into hexanes (3 x 20 cm^3). Concentration and storage at -30 °C yielded a red precipitate in 29% yield (109 mg). Crystals obtained from a concentrated diethyl ether solution at 20 °C were suitable for X-ray crystallography.

*Spectroscopic data for **4b***

^{1}H NMR (C_6D_6, 300 MHz, 298 K): δ 6.98 (2H, s, *meta*-H Mes), 6.95 (2H, s, *meta*-H Mes), 6.88 (2H, s, *meta*-H Mes'), 6.16 (2H, s, *meta*-H Mes'), 3.76 (2H, m, NCH_2), 3.46 (2H, m, NCH_2), 2.90 (4H, m, NCH_2), 2.36 (6H, s, *para*-CH_3), 2.34 (6H, s, *ortho*-CH_3), 2.34 (6H, s, *para*-CH_3), 2.31 (2H, d, $^{2}J_{HH}$ = 7 Hz, Ir-CH_2), 2.30 (6H, s, *ortho*-CH_3), 2.22 (2H, d, $^{2}J_{HH}$ = 7 Hz, Ir-CH_2), 2.00 (6H, s, *ortho*-CH_3), 1.82 (2H, m, NCH_2CH_2), 1.33 (4H, m, NCH_2CH_2), 1.07 (2H, m, NCH_2CH_2), -31.76 (1H, s, IrH). ^{13}C NMR (C_6D_6, 125 MHz, 298 K): δ 216.4 (NCN), 147.3 (NC Mes), 141.6 (NC Mes'), 137.2 (*para*-C Mes), 135.1 (*para*-C Mes'), 134.5 (*ortho*-C Mes), 134.2 (*ortho*-C Mes'), 130.4 (*meta*-CH Mes), 130.0 (*meta*-CH Mes'), 126.2 (*meta*-CH Mes'), 125.0 (*ortho*-C Mes'), 57.8 (NCH_2), 55.2 (NCH_2), 27.3 (NCH_2CH_2), 25.5 (NCH_2CH_2), 22.8 (*para*-CH_3 Mes), 21.6 (*para*-CH_3 Mes'), 20.6 (*ortho*-CH_3-Mes), 20.3 (*ortho*-CH_3 Mes), 19.8 (*ortho*-CH_3 Mes'), 6.7 ($IrCH_2$). MS (EI +ve): *m/z* 860.5 (M^+); (CI +ve): *m/z* 861.5 ($[M+H]^+$). Accurate mass ($[CHN_4{}^{191}Ir]^+$): 859.4416 (meas.), 859.4379 (calc.).

*Crystallographic data for **4b***

$C_{46}H_{59}IrN_4$, M_r = 860.22, monoclinic, *C*2/*c*, a = 32.1355(4), b = 20.8001(3), c = 20.6871(3) Å, β = 120.2697(6)°, V = 11942.5(3) Å^3, Z = 4, ρ_c = 1.435 Mg m^{-3}, T = 150 K, λ = 0.71073 Å, 55182 reflections collected, 13541 independent [R(int) = 0.077], which were used in all calculations. R_1 = 0.0465, *w*R_2 = 0.0673 for observed unique reflections [I > 2σ(I)] and R_1 = 0.1077, *w*R_2 = 0.1022 for all unique reflections. Max. and min. residual electron densities 6.37 and -5.38 e Å^{-3}.

*Preparation of (6-Xyl')$_2$IrH (**4c**)*

A solution of 6-Xyl (900 mg, 3.10 mmol) in THF (20 cm^3) was added to a stirred solution of $[Ir(COE)_2Cl]_2$ (460 mg, 0.51 mmol) in THF (20 cm^3). The orange solution was stirred overnight and darkened to an orange/brown colour. Removal of the volatiles *in vacuo* yielded a dark orange solid, which was washed hexanes (3 x 15 cm^3). The remaining orange powder was dissolved in toluene and filtered. Layering of this yellow/orange toluene solution with pentane at -30 °C gave red crystals suitable for X-ray crystallography in 83% yield (660 mg).

*Spectroscopic data for **4c***

^{1}H NMR (C_6D_6, 300 MHz, 298 K): δ 7.22 (2H, d, $^3J_{HH}$ = 7.5 Hz, *meta*-H Xyl), 7.11 (2H, tr, $^3J_{HH}$ = 6.7 Hz, *para*-H Xyl), 7.06 (2H, d, $^3J_{HH}$ = 8.7 Hz, *meta*-H Xyl'), 6.90 (4H, tr, $^3J_{HH}$ = 7.8 Hz, *para*-H Xyl'), 6.12 (2H, d, $^3J_{HH}$ = 7.2 Hz, *meta*-H Xyl'), 3.10 (2H, m, NCH_2), 2.73 (2H, m, NCH_2), 2.60 (4H, m, NCH_2), 2.38 (6H, s, *ortho*-CH_3), 2.20 (6H, s, *ortho*-CH_3), 2.13 (2H, d, $^2J_{HH}$ = 6.9 Hz, Ir-CH_2), 2.00 (2H, d, $^2J_{HH}$ = 6.9 Hz, Ir-CH_2), 1.85 (6H, s, *ortho*-CH_3), 1.43 (4H, m, NCH_2CH_2), -36.85 (1H, s, IrH). ^{13}C NMR (C_6D_6, 125 MHz, 298 K): δ 203.8 (NCN), 147.4 (NC Xyl), 144.8 (NC Xyl'), 137.0 (*ortho*-C Xyl), 135.5 (*ortho*-C Xyl'), 130.2 (*meta*-CH Xyl), 128.7 (*meta*-CH Xyl'), 127.5 (*meta*-CH Xyl'), 126.6 (*para*-CH Xyl), 125.5 (*ortho*-CH Xyl'), 123.2 (*para*-CH Xyl'), 47.9 (NCH_2), 46.1 (NCH_2), 22.9 (s, NCH_2CH_2), 20.1 (*ortho*-CH_3 Xyl'), 18.7 (*ortho*-CH_3 Xyl), 15.6 (*ortho*-CH_3 Xyl'), 7.8 ($IrCH_2$). MS (EI +ve): *m/z* 776.4 (M^+), 774.4 ($[M-2H]^+$). Accurate mass ($[C_{40}H_{45}N_4{}^{191}Ir]^+$): 772.3238 (meas.), 772.3272 (calc.). Elemental analysis: calc. for $C_{40}H_{46}IrN_4$: C 61.91; H 6.10; N 7.22, meas. C 61.78; H 5.93; N 7.12.

*Crystallographic data for **4c***

$C_{40}H_{46}IrN_4$, M_r = 775.05, monoclinic, $P2_1$, a = 9.0172(3), b = 15.0295(6), c = 12.2995(5) Å, β = 94.9522(17)°, V = 1660.66(11) $Å^3$, Z = 2, ρ_c = 1.550 Mg m^{-3}, T = 150 K, λ = 0.71073 Å, 15631 reflections collected, 7051 independent [R(int) = 0.090], which were used in all calculations. R_1 = 0.0570, wR_2 = 0.1047 for observed unique reflections [I > 2σ(I)] and R_1 = 0.0943, wR_2 = 0.1356 for all unique reflections. Max. and min. residual electron densities 2.77 and -2.29 e $Å^{-3}$.

*Preparation of (6-Mes)$_2$IrH$_3$ (**5a**) and (7-Mes)$_2$IrH$_3$ (**5b**)*

A solution of (6-Mes')$_2$IrH (50 mg, 0.06 mmol) or (7-Mes')$_2$IrH (50 mg, 0.06 mmol) in toluene (10 cm^3) in a high pressure flask was freeze-pump-thaw degassed. The flask was then immersed in liquid nitrogen and evacuated, and the headspace back-filled with H_2 gas. After melting, the solution was stirred for 3 h, over which time a colour change was observed from orange to pale yellow. Transformation was quantitative by ^{1}H NMR spectroscopy when maintained under a H_2 atmosphere.

*Spectroscopic data for **5a***

^{1}H NMR (C_6D_6, 300 MHz, 298 K): δ 6.90 (8H, s, *meta*-CH), 2.63 (8H, tr, $^3J_{HH}$ = 5.4 Hz, NCH_2), 2.41 (12H, s, *para*-CH_3), 2.10 (24H, s, *ortho*-CH_3), 1.30 (4H, qn, $^3J_{HH}$ = 5.4 Hz, NCH_2CH_2), -9.75 (3H, s, IrH_3). ^{13}C NMR (C_6D_6, 125 MHz, 298 K): δ 188.9 (NCN), 149.0 (NC Mes), 133.4 (*para*-C Mes), 132.9 (*ortho*-C Mes), 128.1 (*meta*-CH Mes), 44.3 (NCH_2), 20.9 (NCH_2CH_2), 20.0 (*para*-CH_3 Mes), 17.9 (*ortho*-CH_3 Mes). MS (CI -ve): *m/z* 836.4 (M^+).

*Crystallographic data for **5a***

$C_{88}H_{122}Ir_2N_8$, M_r = 1676.43, orthorhombic, *Fdd*2, a = 21.4014(2) Å, b = 43.1705(4) Å, c = 8.3559(1) Å, V = 7720.09(14) Å^3, Z = 4, ρ_c = 1.442 Mg m^{-3}, T = 150 K, λ = 0.71073 Å, 35342 reflections collected, 4313 independent [R(int) = 0.060], which were used in all calculations. R_1 = 0.0343, wR_2 = 0.0895 for observed unique reflections [$I > 2\sigma(I)$] and R_1 = 0.0402, wR_2 = 0.1047 for all unique reflections. Max. and min. residual electron densities 3.55 and -0.89 e Å^{-3}.

*Spectroscopic data for **5b***

^{1}H NMR (C_6D_6, 300 MHz, 298 K): δ 6.91 (8H, s, *meta*-CH Mes), 3.17 (8H, m, NCH_2), 2.41 (12H, s, *para*-CH_3), 2.13 (24H, s, *ortho*-CH_3), 1.32 (8H, m, NCH_2CH_2), -9.51 (3H, s, IrH). ^{13}C NMR (C_6D_6, 125 MHz, 298 K): δ 190.1 (NCN), 151.9 (NC Mes), 135.6 (*para*-C Mes), 134.4 (*ortho*-C Mes), 130.2 (*meta*-CH Mes), 54.1 (NCH_2), 25.1 (NCH_2CH_2), 21.7 (*para*-CH_3), 20.6 (*ortho*-CH_3).

*Preparation of (6-Mes)(6-Mes')IrHCl (**6**)*

A solution of 2.0 M HCl in diethyl ether (0.06 cm^3, 0.12 mmol) was added to a stirred solution of (6-Mes')$_2$IrH (100 mg, 0.12 mmol) also in diethyl ether (20 cm^3). A colour change from orange to yellow was observed on addition. After 15 min, the volatiles were removed *in vacuo* to give the yellow product which was collected in 90% yield (94 mg) without further purification.

*Spectroscopic data for **6***

^{1}H NMR (C_6D_6, 300 MHz, 298 K): δ 7.04 (1H, s, *meta*-H Mes'), 6.92 (1H, s, *meta*-H Mes), 6.83 (1H, s, *meta*-H Mes), 6.74 (2H, s, *meta*-H Mes), 6.65 (2H, s, *meta*-H Mes), 6.64 (1H, s,

meta-H Mes'), 3.33 (1H, d, $^{3}J_{HH}$ = 10.9 Hz, NCH_2 Mes'), 2.97 (1H, m, NCH_2), 2.78 (2H, m, NCH_2), 2.73 (4H, m, NCH_2), 2.61 (3H, s, *para*-CH_3 Mes), 2.49 (6H, s, *para*-CH_3 Mes), 2.40 (3H, s, *para*-CH_3 Mes'), 2.36 (3H, s, *ortho*-CH_3 Mes), 2.30 (1H, d, $^{2}J_{HH}$ = 11.5 Hz, $IrCH_2$), 2.25 (6H, s, *ortho*-CH_3 Mes), 2.19 (1H, d, $^{2}J_{HH}$ = 11.5 Hz, $IrCH_2$), 2.18 (6H, s, *ortho*-CH_3 Mes), 1.87 (3H, s, *ortho*-CH_3 Mes'), 1.70 (3H, s, *ortho*-CH_3 Mes), 1.54 (2H, qn, $^{3}J_{HH}$ = 5.7 Hz, NCH_2CH_2), 1.29 (1H, m, NCH_2CH_2), 1.15 (1H, m, NCH_2CH_2), -46.50 (1H, s, IrH). ^{13}C NMR (C_6D_6, 75 MHz, 298 K): δ 207.4, 204.0 (d, $^{2}J_{CH}$ = 6.3 Hz, NCN), 144.1 (N-C Mes'), 143.5, 143.4, 143.2 (NC Mes), 137.6, 135.9 (*para*-C Mes), 135.5 (*para*-C Mes'), 134.7, 134.5, 133.7, 133.6 (*ortho*-C Mes), 129.8 (*meta*-CH Mes'), 129.3, 129.2, 129.0, 128.4 (*meta*-CH Mes), 126.6 (*meta*-CH Mes'), 126.2 (*ortho*-C Mes'), 48.8, 48.3 (NCH_2), 47.3, 47.3 (NCH_2), 22.4, 21.7 (NCH_2CH_2), 21.3, 21.1, 20.8 (*para*-CH_3), 20.6 (ortho-CH_3 Mes'), 20.1, 19.6, 18.8, 16.8 (*ortho*-CH_3), -13.2 (d, $^{2}J_{CH}$ = 10.1 Hz, $IrCH_2$). MS (EI +ve): *m/z* 868.4 (M^+, 1%). Accurate mass ($[C_{44}H_{56}N_4{}^{191}IrCl]^+$): 866.37977 (meas.), 866.37994 (calc.).

Preparation of (6-Mes)$_2$IrHCl$_2$ (7)

HCl in diethyl ether (0.03 cm^3, 0.06 mmol) was added to a stirred solution of (6-Mes')$_2$IrH (25 mg, 0.03 mmol) also in diethyl ether (10 cm^3). The solution was observed to turn from orange to yellow and back to orange in colour. Stirring was allowed to continue for 10 min after which time the volatiles were removed *in vacuo*. The product was collected as a pale orange solid in 81% yield (22 mg) without need for purification.

*Spectroscopic data for **7***

^{1}H NMR (C_6D_6, 300 MHz, 298 K): δ 6.79 (8H, s, *meta*-CH), 2.68 (8H, tr, $^{3}J_{HH}$ = 6.9 Hz, NCH_2), 2.35 (12H, s, *para*-CH_3), 2.27 (24H, s, *ortho*-CH_3), 1.40 (4H, qn, $^{3}J_{HH}$ = 6.9 Hz, -49.80 (1H, s, IrH). ^{13}C NMR (C_6D_6, 125 MHz, 298 K): δ 198.2 (d, $^{2}J_{CH}$ = 6.7 Hz, NCN), 145.4 (NC-Mes), 136.8 (*para*-C Mes), 135.3 (*ortho*-C Mes), 130.3 (*meta*-CH Mes), 50.0

(NCH_2), 22.2 (NCH_2CH_2), 20.1 (*para*-CH_3 Mes), 19.6 (*ortho*-CH_3 Mes). MS (EI +ve): *m/z* 830.3 ($[M-2HCl]^+$), 904.3 (M^+). Accurate mass ($[C_{44}H_{57}N_4{}^{191}Ir^{35}Cl_2]^+$): 902.34436 (meas.), 902.35662 (calc.).

*Preparation of (6-Mes)$_2$IrH$_2$Cl (**8**)*

A solution of (6-Mes)(6-Mes')IrHCl (50 mg, 0.06 mmol) in toluene (20 cm^3) in a high pressure flask was freeze-pump-thaw degassed. The reaction flask was then immersed in liquid nitrogen and evacuated before the headspace was back-filled with H_2 gas. After melting, the solution was then stirred for 3 h. Removal of the solvent *in vacuo* yielded the yellow solid product without need for purification collected in 84% yield (21 mg). Crystals suitable for X-ray crystallography were obtained from a concentrated solution in diethyl ether at 20°C.

*Spectroscopic data for **8***

^{1}H NMR (C_6D_6, 300 MHz, 298 K): δ_H 6.81 (8H, s, *meta*-CH), 2.57 (8H, tr, $^3J_{HH}$ = 6.0 Hz, NCH_2), 2.36 (12H, s, *para*-CH_3), 2.15 (24H, s, *ortho*-CH_3), 1.37 (4H, qn, $^3J_{HH}$ = 6.0 Hz, NCH_2CH_2) -33.05 (2H, s, IrH_2). ^{13}C NMR (C_6D_6, 126 MHz, 298 K): δ_C 205.1 (NCN), 145.7 (NC Mes), 136.3 (*para*-C Mes), 135.1 (*ortho*-C Mes), 130.6 (*meta*-CH Mes), 48.6 (NCH_2), 22.8 (NCH_2CH_2), 22.0 (*para*-CH_3 Mes), 19.9 (*ortho*-CH_3 Mes). MS (EI +ve): *m/z* 895.9 ($[M+25]^+$, 1%). Elemental analysis: calc. for $C_{44}H_{58}IrN_4Cl$: C 60.70, H 6.71, N 6.44, meas. C 60.88, H 6.60, N 7.06.

*Crystallographic data for **8***

$C_{44}H_{58}IrN_4Cl$, M_r = 870.64, orthorhombic, *Fdd*2, a = 42.9414(5), b = 21.5369(3), c = 8.42331(9) Å, V = 7790.10(15) $Å^3$, Z = 8, ρ_c = 1.485 Mg m^{-3}, T = 150 K, λ = 1.54180 Å, 21447 reflections collected, 2192 independent [R(int) = 0.029], which were used in

calculations. R_1 = 0.0205, wR_2 = 0.0560 for observed unique reflections [$I > 2\sigma(I)$] and R_1 = 0.0206, wR_2 = 0.0561 for all unique reflections. Max. and min. residual electron densities 1.04 and -1.14 e $Å^{-3}$.

3.3 Saturated 5-membered NHC Complexes

Previous work in the group utilising the unsaturated NHC IMes to support iridium complexes has yielded a series of complexes competent for the coordination and activation of B–H bonds in amine-boranes. Given that the corresponding saturated NHCs are reported to be stronger σ-donors, it seems likely that the use of 5-Mes (SIMes) should provide a more electron rich iridium centre, leading to greater back-bonding and more facile activation of the B–H bonds.

The initial synthetic approaches targeted were analogous to those documented for the related IMes complexes. Four equivalents of 5-Mes were stirred with $[Ir(COE)_2Cl]_2$, providing two equivalents of NHC per iridium centre. The ^1H NMR spectrum indicates a symmetric NHC framework and the presence of a bound alkene. As expected, the product isolated from the reaction was $(5\text{-Mes})_2Ir(COE)Cl$ (**1**, Fig 3.2), analogous to the previously reported species $(IMes)_2Ir(COE)Cl$.[49] The crystal structure shows a square planar iridium with two 5-Mes ligands coordinated in a *trans*-configuration and a bound cyclooctene opposite a chloride ligand.

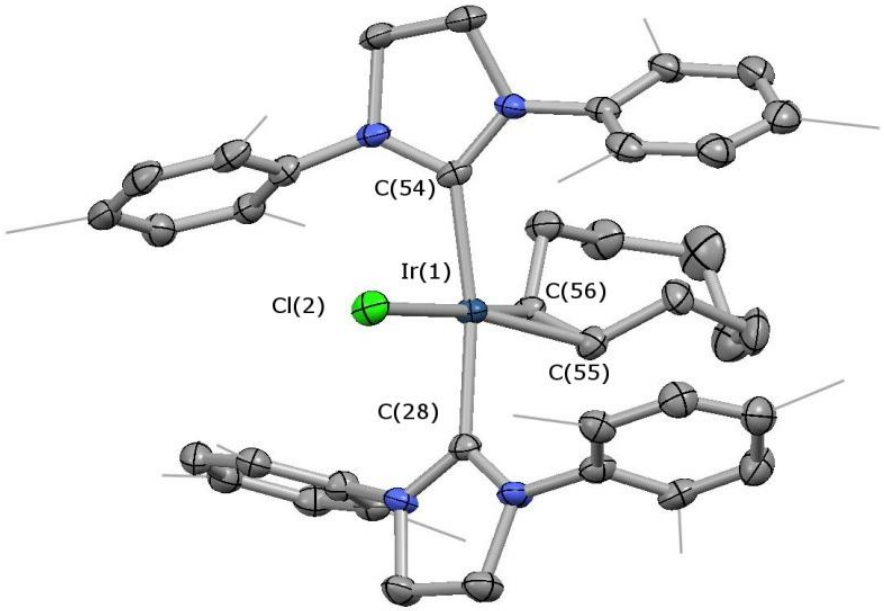

Figure 3.2: (5-Mes)$_2$Ir(COE)Cl (**1**), most H atoms omitted and Me groups shown in wireframe for clarity; thermal ellipsoids set at 50% probability level. Key bond lengths (Å) and angles (°): Ir(1)–Cl(2) 2.368(1), Ir(1)–C(28) 2.061(6), Ir(1)–C(54) 2.078(4), Ir(1)–C(55) 2.133(6), Ir(1)–C(56) 2.132(5), C(28)–Ir(1)–C(54) 167.6(2).

Compared to the unsaturated analogue (IMes)$_2$Ir(COE)Cl, the distances measured in **1** show little variation from this previously reported species. The Ir–Cl distance in **1** is marginally shorter than that reported for (IMes)$_2$Ir(COE)Cl [2.368(1) *cf.* 2.380(2) Å, respectively] despite the stronger donor power of 5-Mes. Additionally, the Ir–C_{NHC} bonds are also statistically the same [2.061(6), 2.078(4) Å *cf.* 2.040(8), 2.082(8) Å] even though we may expect shorter distances in **1** due to the increased donor ability of 5-Mes.

Consistent with the behaviour of the analogous complex (IMes)$_2$Ir(COE)Cl, heating of **1** to 65°C for 24 hours results in the displacement of the cyclooctene ligand followed by oxidative addition of the C–H bond of one of the *ortho*-methyl groups to form (5-Mes)(5-Mes')IrHCl (**2**, Fig 3.3).[49] This transformation is characterised by the appearance of a

hydride signal in the ^{1}H NMR spectrum at δ_H -32.8 ppm (similar to that of the IMes analogue observed at δ_H -33.1 ppm) and the lowering of the symmetry of signals associated with the mesityl groups.

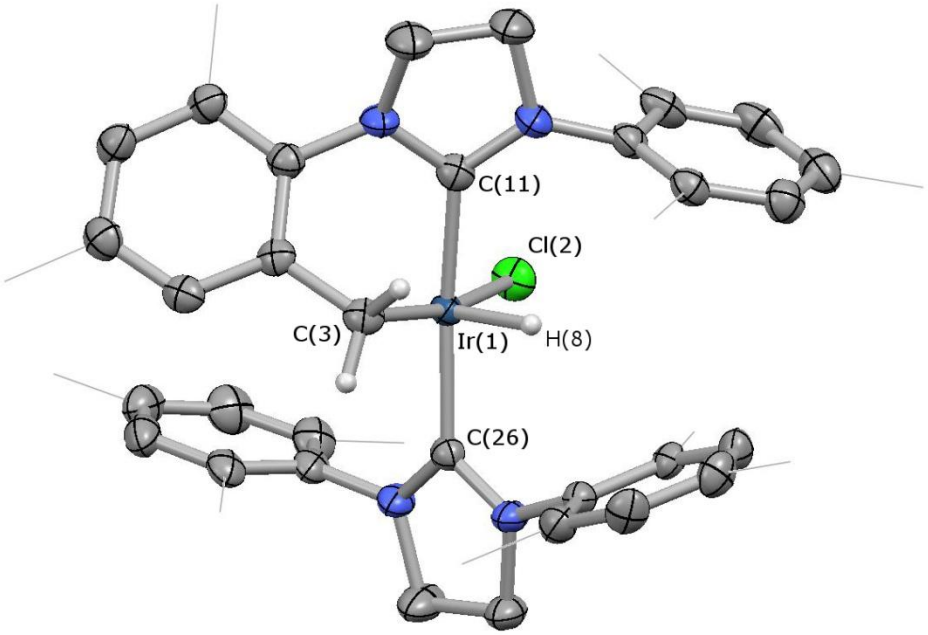

Figure 3.3: (5-Mes)(5-Mes')IrHCl (**2**), most H atoms omitted and Me groups shown in wireframe for clarity; thermal ellipsoids set at 50% probability level. Key bond lengths (Å) and angles (°): Ir(1)–Cl(2) 2.415(1), Ir(1)–C(3) 2.099(4), Ir(1)–C(11) 2.022(5), Ir(1)–C(26) 2.049(3), Ir(1)–H(8) 1.52(4), C(11)–Ir(1)–C(26) 173.1(2).

The bond lengths and angles observed in **2** are not statistically different from those reported for the unsaturated IMes analogue with the exception of the Ir–Cl distance being marginally shorter in **2** [2.415(1) *cf.* 2.422(1) Å for the IMes complex]. There also appears to be a slight distortion of the supporting heterocycle from planar suggesting an increase in conformational flexibility over the IMes ligand.

After conversion to **2**, hydrogenation then affords the precursor dihydride complex, $(5\text{-Mes})_2IrH_2Cl$ (**3**), detailed in Scheme 3.4.

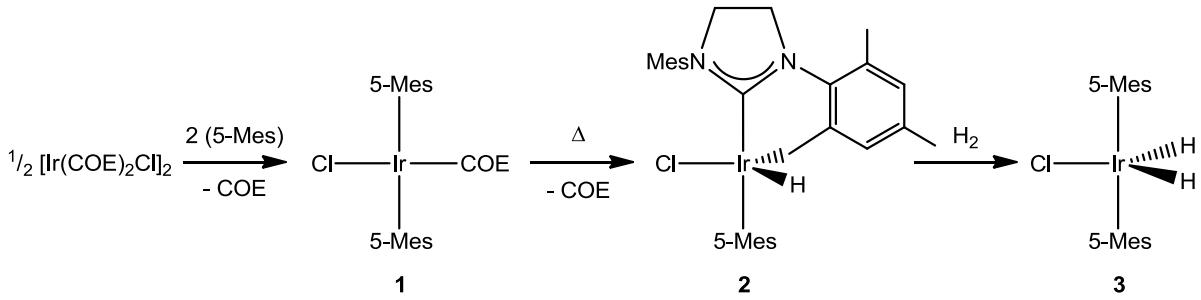

Scheme 3.4: Syntheses of complexes **1**-**3**.

Monitoring the ^{1}H NMR spectra *in situ* during the hydrogenation process shows a simplification of the signals corresponding to the 5-Mes ligand, consistent with the removal of the benzylic tether. There is also an accompanying small shift in the hydride signal, from δ_H -32.84 to -32.81 ppm. Presumably interaction with H_2 initiates reductive elimination of the previously activated C–H bond of the *ortho*-methyl group, followed by oxidative addition of the H_2. This resulting species is the target precursor to the $[(5\text{-Mes})_2IrH_2]^+$ fragment. The crystal structure (Fig 3.5) shows two *trans*-located 5-Mes ligands and a chloride ligand opposite to two areas of electron density that were assigned to be the hydrides in the system.

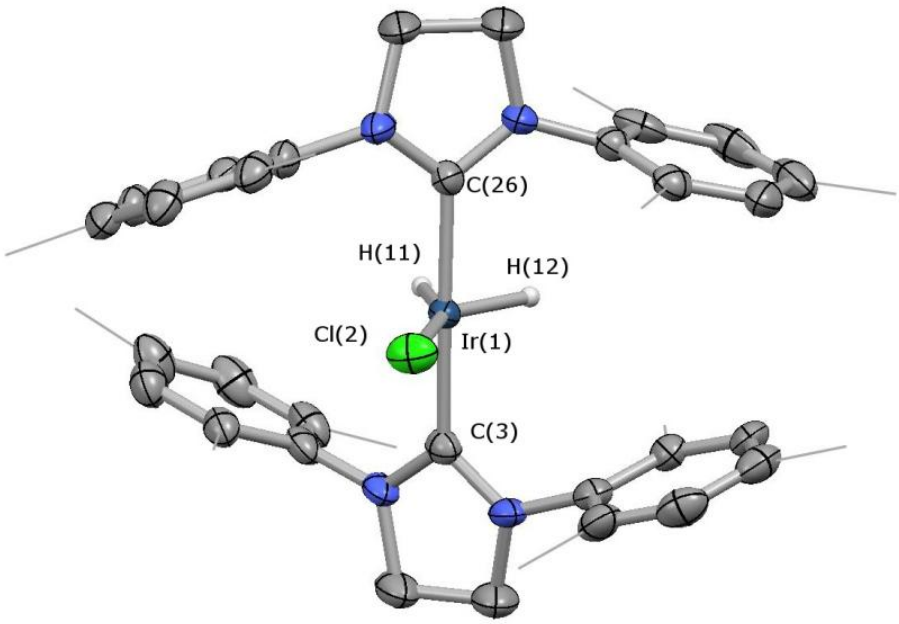

Figure 3.5: $(5\text{-Mes})_2IrH_2Cl$ (**3**), most H atoms omitted and Me groups shown in wireframe for clarity; thermal ellipsoids set at 50% probability level. Ir–H located in the Fourier difference map and refined isotropically. Key bond lengths (Å) and angles (°): Ir(1)–Cl(2) 2.404(2), Ir(1)–C(3) 2.016(6), Ir(1)–C(26) 2.009(6), Ir(1)–H(11) 1.53, Ir(1)–H(12) 1.60, C(3)–Ir(1)–C(26) 176.5(2).

In this case, the $Ir–C_{NHC}$ bonds have shortened compared to **2** suggesting a stronger interaction with the metal [2.016(6), 2.009(6) Å *cf.* 2.099(4), 2.022(5) Å]. Again there is a slight shortening of the Ir–Cl bond [from 2.415(1) to 2.404(2) Å] as the chloride now appears to have no *trans*-ligand. Although the location of hydrides from X-ray data is not reliable, this trigonal bipyramidal arrangement is sensible as it avoids the strong *trans*-influence of the hydrides acting on chloride. Conversely, calculations by Eisenstein et al. predict the structure of the model system $(PH_3)_2IrH_3$ to have two *trans*-hydride ligands in a square-based pyramidal structure.[50] Hence, it may be possible that there is a hydride located *trans*- to the chloride and the other is then *cis*-.

3.4 Expanded Ring Saturated NHC Complexes

Initial entry into 6-Mes adducts of iridium was attempted using a similar approach to that employed with IMes and 5-Mes. Four equivalents of 6-Mes were stirred with $[Ir(COE)_2Cl]_2$ in an attempt to make the *bis*-ligated product. Observation of a high-field shift hydride resonance (δ_H -37.5 ppm) in the ^1H NMR spectrum suggests spontaneous activation of a C–H bond, most likely belonging to one of the mesityl substituents. This spontaneous, facile C–H activation is attributed to the increased electron-density on the iridium via stronger σ-donation, coupled with the close approach of the mesityl rings caused by the expansion of the supporting heterocycle ring. Crystals of the product were obtained from a concentrated solution of diethyl ether at -30 °C, and X-ray crystallography analysis revealed the structure of the doubly cyclometalled system $(6\text{-Mes}')_2IrH$ (**4a**) (Fig 3.6).

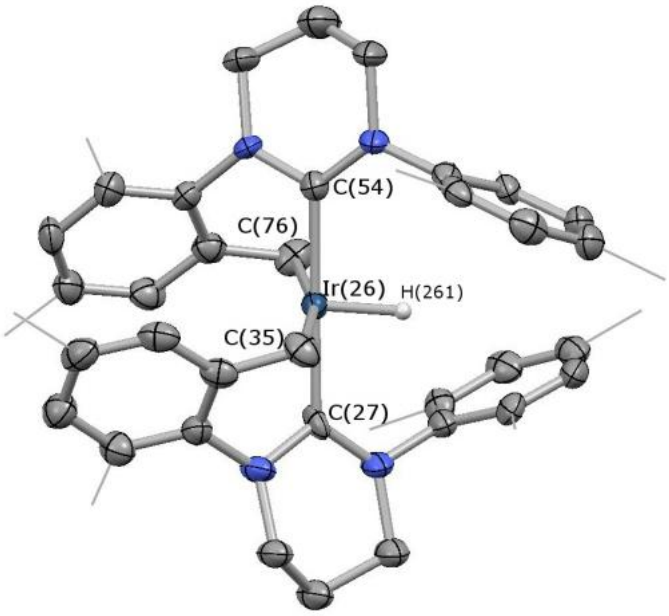

Figure 3.6: $(6\text{-Mes}')_2IrH$ (**4a**), most H atoms omitted and Me groups shown in wireframe for clarity; thermal ellipsoids set at 50% probability level. Ir–H located in the Fourier difference map and refined isotropically. Key bond lengths (Å) and angles (°): Ir(26)–H(261) 1.51, Ir(26)–C(27) 2.017(7), Ir(26)–C(54) 2.038(7), Ir(26)–C(76) 2.17(1), Ir(26)–C(35) 2.15(1), C(27)–Ir(26)–C(54) 179.2(3), C(76)–Ir(26)–C(35) 164.9(3).

For **4a**, the Ir-C_{NHC} bonds are comparable to those observed in (5-Mes)(5-Mes')IrHCl (**2**) [2.017(7), 2.038(7) Å for **4** and 2.049(3), 2.022(5) Å for **2**]. One would expect slightly longer bond lengths for (6-Mes)-iridium complexes due to the increased p-character of the donor orbital at the carbenic centre. However, we can note that the Ir-CH_2 distances are significantly longer [2.17(1) and 2.15(1) Å *cf.* 2.099(4) Å in **2**] despite the smaller angle between the N-C_{Mes} bonds. For the case of 6-Mes, the mesityl rings approach the metal closer than 5-Mes, thus the increased bond length may be attributed to increased electron density at the metal centre offered by both the expanded ring NHC and the extra alkyl ligand (compared with one alkyl ligand in **2**). This would lead to a weaker interaction between the formally negatively charged benzylic ligand.

Oxidative addition of more than one C–H bond from an NHC is not unprecedented.[51, 52] The structure reveals the activation of a C–H bond from each of the two coordinated carbene ligands, which has resulted in the loss of one equivalent of HCl. This is thought to be driven by protonation of an equivalent of 6-Mes in solution, hence the potential yield is reduced by a third. As a result, synthesis was optimised to use a ratio of 3:1 of NHC:Ir which gave increased yields of **4a**.

Effective C_2 symmetry of the complex in solution explains the relatively simple ^{1}H NMR spectrum, displaying three *ortho*-methyl and two *para*-methyl signals. The *pseudo*-trigonal bipyramidal geometry featuring an apical hydride explains the unusually high-field hydride shift due to the trans effect of the vacant site.[53]

The proposed mechanistic route by which **4a** forms (Scheme 3.7) begins with the well documented coordination of two NHC ligands (*cf.* 5-Mes and IMes).[49] Then due to the increased steric crowding at the iridium centre, the relatively loosely bound cyclooctene is ejected. This is followed by rapid oxidative addition of an *ortho*-methyl C–H bond across

the electron rich iridium centre is promoted due to the increased σ-donor strength of 6-Mes (*cf*. 5-Mes and IMes). Loss of HCl, which is captured by free 6-Mes, reduces the iridium centre allowing for subsequent oxidative addition of a second *ortho*-methyl C–H bond.

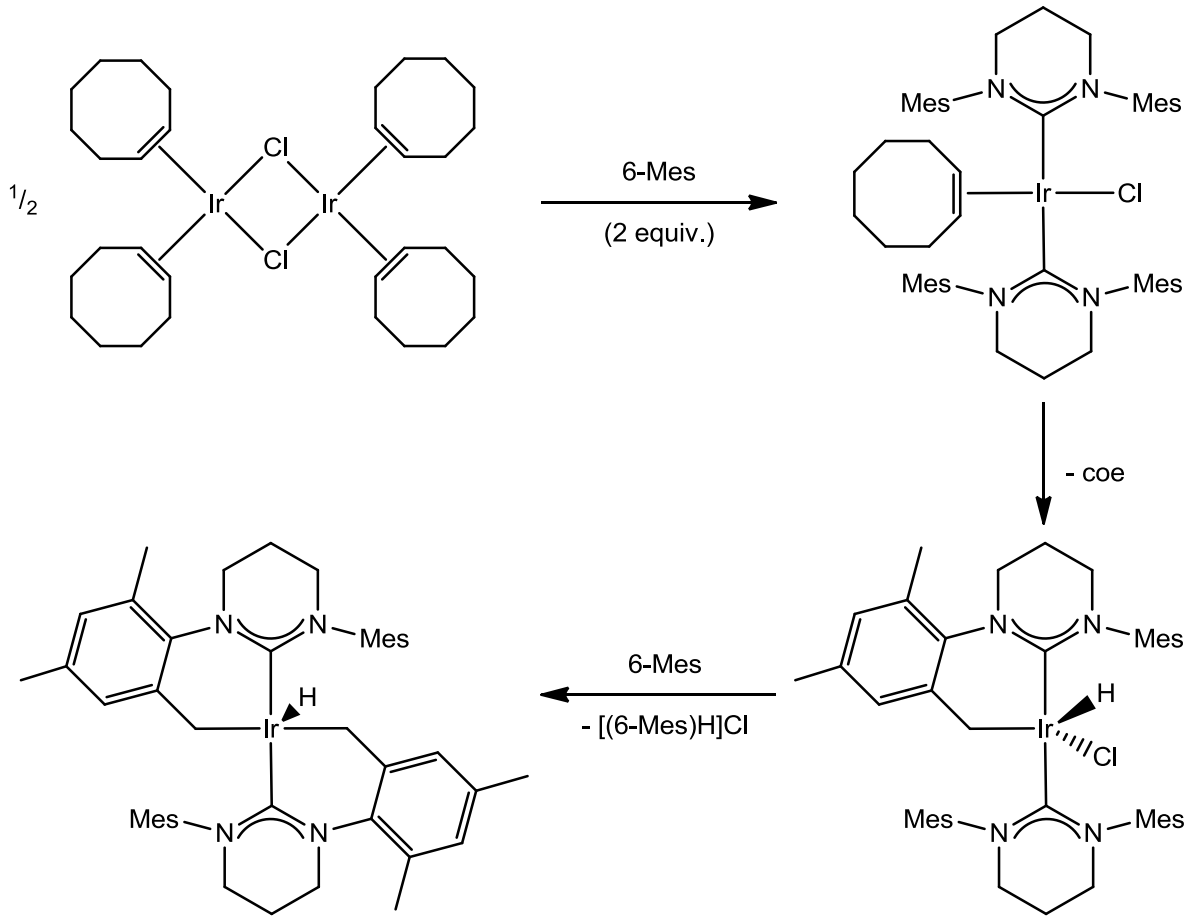

Scheme 3.7: Proposed mechanism for formation of **4a**

Analogous syntheses involving other expanded ring carbenes, 7-Mes and 6-Xyl, are presumed to proceed via the same route to give the isostructural products (7-Mes')$_2$IrH (**4b**) and (6-Xyl')$_2$IrH (**4c**), respectively (Fig 3.8).

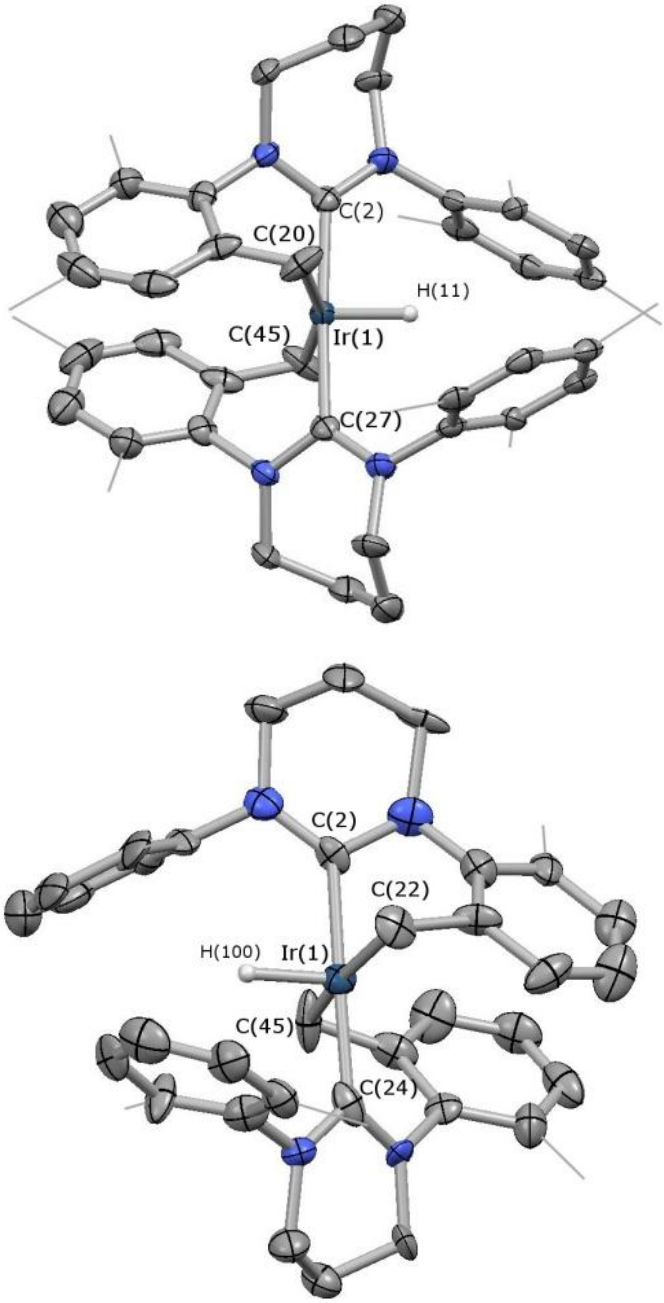

Figure 3.8: Structures of **4b** (*top*) and **4c** (*bottom*), most H atoms omitted and Me groups shown in wireframe for clarity; thermal ellipsoids set at 50% probability level. Ir–H located in the Fourier difference map and refined isotropically. Key bond lengths (Å) and angles (°): (for **4b**) Ir(1)–H(11) 1.42, Ir(1)–C(2) 2.029(8), Ir(1)–C(27) 2.029(8), Ir(1)–C(45) 2.19(1), Ir(1)–C(20) 2.13(1), C(2)–Ir(1)–C(27) 177.5(3), C(45)–Ir(1)–C(20) 163.4(4); (for **4c**) Ir(1)–H(100) 1.49, Ir(1)–C(2) 1.99(2), Ir(1)–C(24) 2.00(2), Ir(1)–C(22) 2.17(1), Ir(1)–C(45) 2.05(2), C(2)–Ir(1)–C(24) 178.1(7), C(22)–Ir(1)–C(45) 168.4(6).

Bond distances and angles reported for **4a**, **4b** and **4c** are identical within three standard deviations, suggesting that 7-Mes puckers the backbone to minimise strain energy across the NCN framework. The average NCN angles in **4a**, **4b** and **4c** are 115.7, 115.0 and 113.5° respectively. It is noticeable that the ^{1}H NMR shift of **4b** is significantly more downfield than that of **4a** and **4c** (δ_H -31.76 vs. -37.54 and -36.85 ppm respectively). This might imply that the iridium centre in **4b** pushes less electron density onto the hydride, which is in contrast to previous observations that 7-membered NHCs are stronger σ-donors than 6-membered NHCs.[14] An alternative hypothesis to explain this shift examines the C–Ir–C angles across the iridium centre. In the case of **4b**, the C_{NHC}–Ir–C_{NHC} and C_{benzyl}–Ir–C_{benzyl} angles are 177.5(3)° and 163.4(4)° respectively which are, on average, narrower than for **4a** and **4c** [179.2(3)°, 164.9(3)° and 178.1(7)°, 168.4(6)° respectively]. Hence, it could be thought that the benzylic carbon atoms in **4b** interact more with the orbital *trans* to the hydride, thus drawing electron density away from the hydride leading to a lower field ^{1}H NMR signal. This second argument remains consistent with the increased donor strength in 7-membered NHCs.

3.5 Addition of H_2

It has been reported that metal-tethered benzylic systems, such as **4a**, can be cleaved from the metal centre by addition of H_2.[54] Hence, in order to test the stability of the metallocycles and additionally with the view to forming a precursor to an active 14-electron iridium cation, **4a** was placed under pressure of H_2. In principle, sequential addition of two equivalents of hydrogen could return the ligands to a state where they are bound solely to the metal via the carbene carbon.

The hydrogenation process was monitored by ^{1}H NMR spectroscopy for **4a**, **4b** and **4c** although crystals of the final product suitable for X-ray crystallography were obtained

only from the hydrogenation of **4a** (Fig 3.9). However, due to the reversible nature of the hydrogen addition, only a small number of relatively poor quality crystals were obtained so the structure does not allow for accurate bond measurements. Crystallisations were also repeated under a hydrogen atmosphere but better quality crystals could not be obtained.

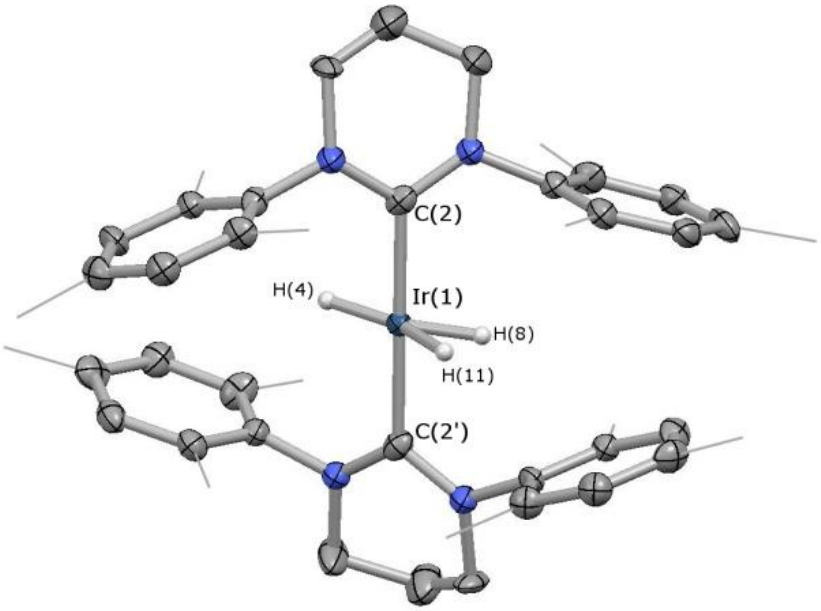

Figure 3.9: (6-Mes)$_2$IrH$_3$ (**5a**), with most H atoms omitted and Me groups shown in wireframe for clarity; thermal ellipsoids set at 50% probability level. Ir–H located in the Fourier difference map and refined isotropically. Key bond lengths (Å) and angles (°): Ir(1)–H(4) 1.39, Ir(1)–H(8) 1.38, Ir(1)–H(11) 1.44, Ir(1)–C(2) 2.1(2), C(2)–Ir(1)–C(2') 177(9).

The resulting trihydride species gives rise to a hydride resonance at δ_H -9.9 ppm which is at significantly lower field than hydrides observed for related iridium-NHC complexes earlier in this chapter (in the region of δ_H -20 to -40 ppm). This could possibly be due to an averaged chemical shift due to a fluxional process between dihydrogen coordination and dihydride formation. Moreover, **5a** is stable only when stored under an

atmosphere of H_2. Purging of H_2 from the system, either by exposure to vacuum or replacement of hydrogen with argon, results in the appearance of multiple hydride signals over a 48 h period, among which **4a** was identified. Similar reactivity was observed when **5a** was exposed to a hydrogen acceptor, TBE, with clean conversion back to **4a** occurring over a 16 h period (Fig 3.10).

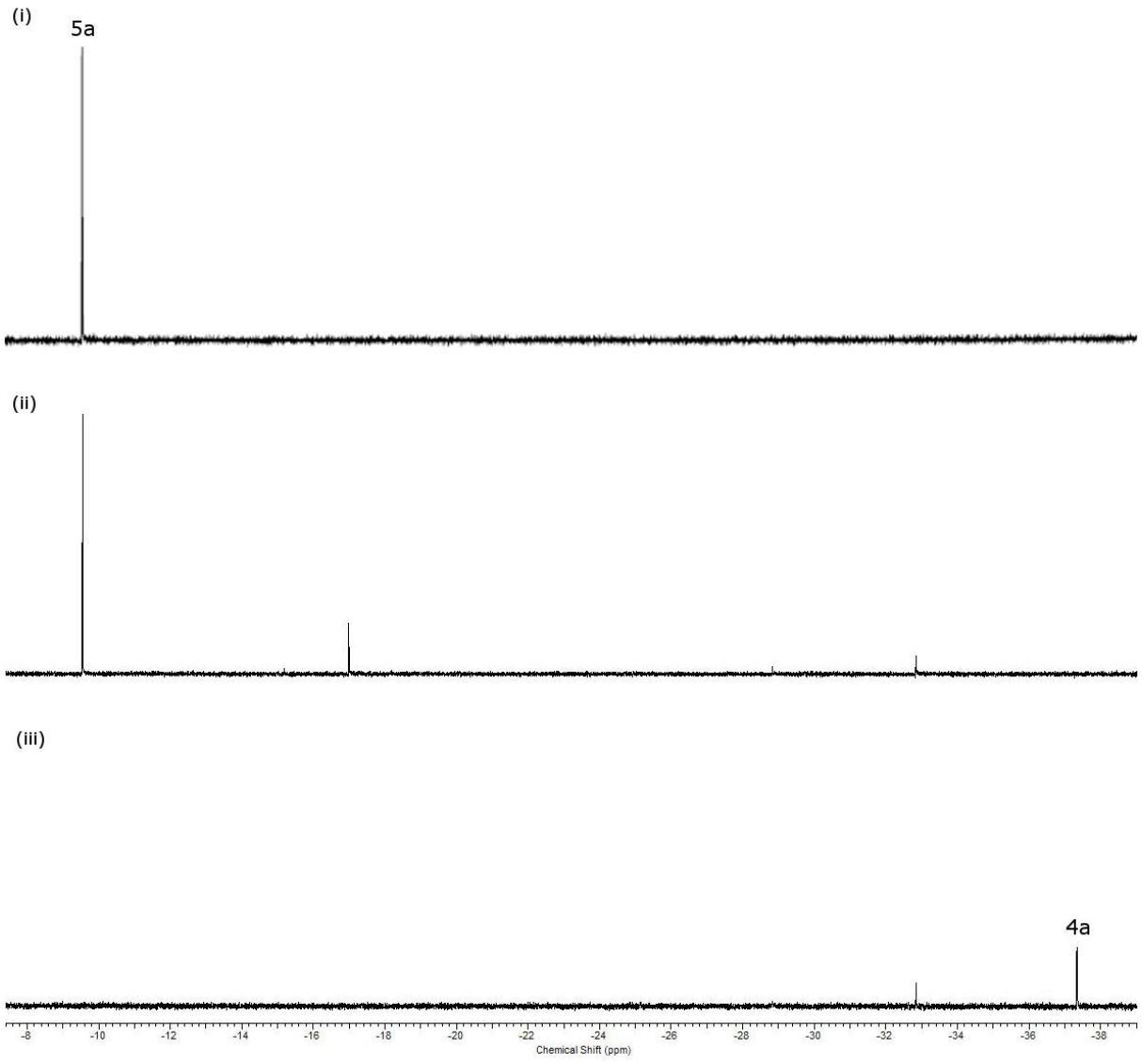

Figure 3.10: ^{1}H NMR (300 MHz) spectrum in the hydride region showing the dehydrogenation of **5a** in C_6D_6 at 20 °C; (i) **5a** under H_2 atmosphere, (ii) 30 min after addition of TBE, then (iii) after 16 h.

In order for such a phenomenon to occur, **5a** must have a thermally accessible hydride-dihydrogen complex form, or a low barrier pathway to reductive elimination of H_2. Probing this mechanism was attempted by several methods. Firstly, H_2 gas was replaced with D_2 gas to probe any coupling observed in the hydride region or in the *ortho*-methyl groups, assuming reversible C–H activation. Secondly, the spin-lattice relaxation times (T_1) were measured for the hydride signals in the ^{1}H NMR and compared to that of known dihydrogen and dihydride complexes.

3.5.1 Deuterium Labelling

Reaction with D_2 gas showed no H–D coupling in the hydride region of ^{1}H NMR although, as expected, the signal was significantly reduced in intensity and broadened due to replacement of H with D at the metal centre. This supports the notion that the system has a low barrier to the reductive elimination of hydrogen. In addition, it implies that the hydride can exchange with deuterium in either a σ-CAM type mechanism, via the trihydride species or potentially by reversible oxidative addition of the *ortho*-methyl C–H bond promoting loss of H_2 and replacement by D_2. However, this is not conclusive as evidence for any of these mechanisms.

Over a period of two weeks under pressure of D_2 the hydride signal disappeared completely. Coupling to deuterium is observed in the methyl region of the ^{1}H and ^{13}C NMR spectra suggesting involvement of the *ortho*-methyl groups in this process. This would support reversible oxidative addition and reductive elimination of the methyl groups at the metal centre.

3.5.2 T_1 Measurement

Measurements of the T_1 relaxation time (Table 3.11) for the hydride signal were carried out over the temperature range 223 K to 298 K, with a minimum value observed of 514 ms at 253 K. Known dihydrogen species typically have faster relaxation times found at lower temperatures, for example $[Cp^*Os(CO)_2(\eta^2\text{-}H_2)]^+$ has $T_{1(min)}$ = 24 ms at 180 K, and the fluxional species $[cis\text{-}CpOs(dppm)H_2]^+$ has $T_{1(min)}$ = 240 ms at 218 K.[55] On the other hand, dihydride species exhibit longer minimum relaxation times at higher temperature, thus $(\{CNC\})Fe(SiH_2Ph)_2(H)_2$ has $T_{1(min)}$ = 405 ms at 272 K,[56] and $[trans\text{-}CpOs(dppm)H_2]^+$ has $T_{1(min)}$ = 2700 ms.[55] In particular, the Ir(III) hydride system $Ir(PCy_3)_2(H)_2(\kappa^2\text{-}S_2CH)$ has $T_{1(min)}$ = 215 ms at 233 K (at 400 MHz), whereas the rapidly exchanging hydride/dihydrogen cation $[Ir(PCy_3)_2(H)(\eta^2\text{-}H_2)(\kappa^2\text{-}S_2CH)]^+$ has $T_{1(min)}$ = 29 ms at 213 K (at 400 MHz).[57, 58] The observed value of $T_{1(min)}$ determined for **5a** appears to be consistent with the system existing as a trihydride.

Temperature (K)	T_1 (ms)
298	909
273	666
253	514
233	516
223	631

Table 3.11: T_1 relaxation times at 300 MHz at intervals of 20 K.

These studies are inconclusive about the nature of **5a**. The ease of dissociation of the dihydrogen ligand leading to the slow release of hydrogen and subsequent oxidative addition of the *ortho*-methyl C–H bonds implies an energetically accessible Ir(I), hydride-dihydrogen complex. The particularly low-field hydride signal in the ^1H NMR may imply a large contribution from a dihydrogen complex which often appear at resonances closer to

free H_2 (δ_H 4.5 ppm). However, Eisenstein *et al.* calculated the structure for the model system $(PH_3)_2Ir(H)_3$ in which there existed two *trans*-located hydride ligands and one opposite a vacant site.[50] Milstein *et al.* and Brookhart *et al.* later reported that *trans*-hydride ligands appear at much lower field in the ^1H NMR spectrum [δ_H = -9.69 ppm for $(PCP)Ir(CO)(H)_2$,[59] and δ_H = -9.07 ppm for $(PONOP)Ir(CH_3)(H)_2$].[60] This supports the possibility of **5a** being a trihydride system with rapidly interconverting hydride ligands to give an averaged ^1H NMR signal.

3.5.3 DFT Calculations

Calculations of the relative Gibbs free energies of the trihydride and hydride-dihydrogen species support the existence of the hydride-dihydrogen species as the ground state system (Fig 3.12). Oxidative addition of the dihydrogen molecule to make the trihydride complex has a ΔG = +8.53 kcal/mol, suggesting this is unlikely to be present in significant amounts to dictate the shift of the ^1H NMR hydride signal.

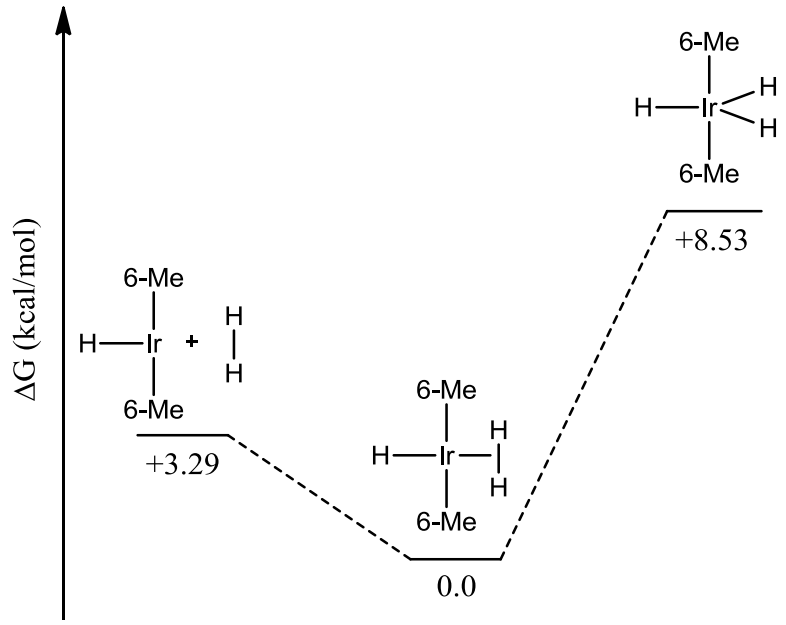

Figure 3.12: Calculated free energy changes associated with loss of hydrogen, and oxidative addition of hydrogen to $(6\text{-}Me)_2IrH$.

In further support of this system, the loss of hydrogen at room temperature is energetically accessible. This explains the relatively slow loss of hydrogen under vacuum and rapid loss with a dihydrogen acceptor (TBE). The species "$(6\text{-Me})_2IrH$" is just an intermediate and will undergo rapid oxidative addition of the *ortho*-methyl C–H bonds to make the overall process energetically favourable.

3.6 Addition of HCl

The most common method for the formation of the 14-electon cationic metal fragments of the type $[(NHC)_2M(H)_2]^+$ (NHC = IMes, IPr; M = Rh, Ir) is chloride abstraction.[47] For systems with expanded ring NHCs reported thus far, the chloride needs to be reintroduced to the system as one equivalent of HCl is lost in the final stages of formation of **4a**.

Addition of one equivalent of HCl to $(6\text{-Mes}')_2IrH$ (**4a**) is found to yield a system of the form (6-Mes)(6-Mes')IrHCl (**6**) (Scheme 3.13). Thus far this species has only been characterised by ^1H and ^{13}C NMR spectroscopy but the patterns observed are analogous to those observed for (5-Mes)(5-Mes')IrHCl (**2**).[49] This spectrum also displays an extremely high-field hydride resonance (δ_H -46.50 ppm) which suggests a similar hydride geometry to the parent complex **4a** where the hydride sits opposite a vacant site.

Addition of a further equivalent of HCl protonates the final activated methyl group and adds a second chloride. The species $(6\text{-Mes})_2Ir(H)(Cl)_2$ (**7**) has also only been characterised by NMR spectroscopy, as expected the ^1H NMR displays a similar peak pattern to that of $(6\text{-Mes})_2IrH_3$ (**5a**). The hydride shift in this species is yet further upfield from the parent complex with a single chloride (δ_H -49.80 ppm) suggesting a *trans*-arrangement of the chloride ligands, thus H *trans* to the vacant site.

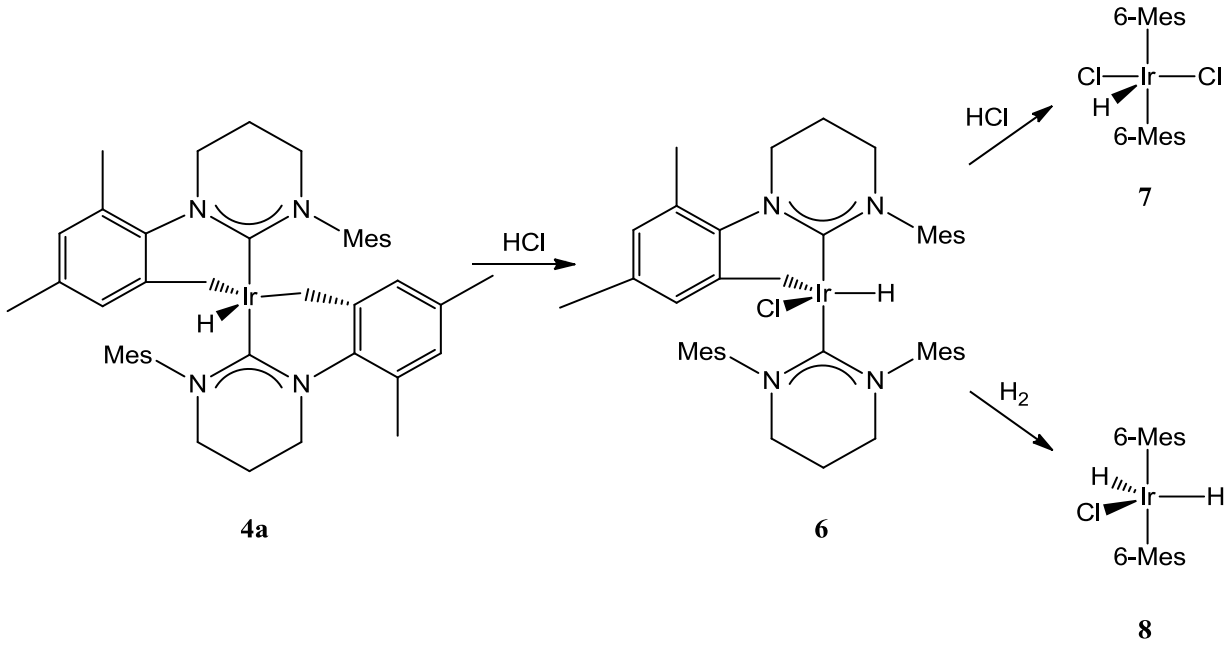

Scheme 3.13: Selective addition of HCl and H_2 under ambient conditions.

In order to synthesise a precursor of the form $(NHC)_2M(H)_2Cl$, as used extensively by Tang,[47, 48] **6** was exposed to 3 atm pressure of H_2 gas. After the reaction, the ^1H NMR spectrum resembled that of **5a** and **7** suggesting elimination of the benzylic fragment. The hydride signals appear at δ_H -33.05 ppm in the ^1H NMR, suggesting a hydridic nature with little to no dihydrogen character. This is supported by the observation that exposure of $(6\text{-}Mes)_2IrH_2Cl$ (**8**) to vacuum does not lead to loss of H_2, unlike **5a**. A crystal structure of **8** was obtained by recrystallisation from a concentrated solution of diethyl ether at -30 °C (Fig 3.14).

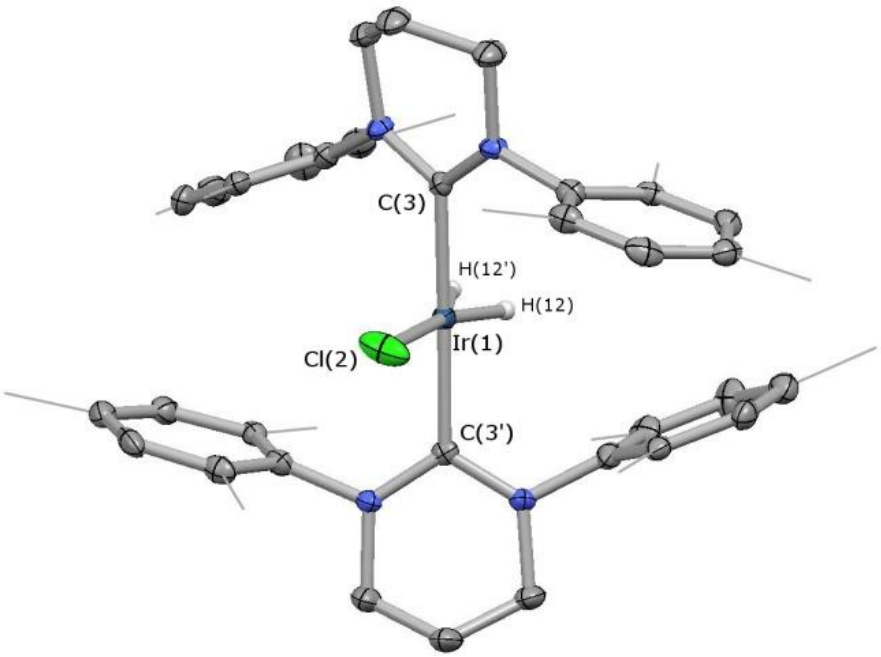

Figure 3.14: $(6\text{-Mes})_2IrH_2Cl$ (**8**), most H atoms omitted and Me groups shown in wireframe; thermal ellipsoid set at 50% probability level. Ir–H located in the Fourier difference map and refined isotropically. Key bond lengths (Å) and angles (°): Ir(1)–H(12) 1.47, Ir(1)–Cl(2) 2.401(2), Ir(1)–C(3) 2.052(3), C(3)–Ir(1)–C(3') 177.5(1).

Compared to $(5\text{-Mes})_2IrH_2Cl$ (**3**), the Ir-Cl distance in **8** is identical [2.401(2) *cf.* 2.404(2) Å], however the Ir–C_{NHC} distance is significantly longer [2.052(3) *cf.* 2.016(6), 2.009(6) Å]. This is consistent with the increased p-character of the donor orbital leading to a longer bond to the metal. Additionally, the "space-fill" representation of the structure alludes to the fact that the mesityl rings of opposing 6-Mes ligands come into relatively close contact. Hence, although we would expect the longer M–C_{NHC} bond, the steric pressure of the 6-Mes ligand may limit optimal overlap with the metal centre.

3.7 Conclusions

A range of charge-neutral, saturated 5-membered NHC complexes and expanded ring NHC complexes have been designed and synthesised. These are intended to act as precursors to 14-electron cationic metal fragments for use as dehydrogenation catalysts towards small molecules, in particular $H_3B{\cdot}NH_3$ and its alkylated derivatives.

It appears that the conformational flexibility offered by saturated 5-membered NHC ligands [demonstrated in (5-Mes)(5-Mes')IrHCl (**2**)] over their unsaturated counter-parts can lead to reduced strain in the benzylic tether of **2**, and when coordinating a substrate. This may allow for coordination of more sterically demanding substrates. Thus, the 5-Mes ligated systems (**1**-**3**) appear to have several advantages over the same IMes bearing complexes for catalytic coordination and activation of small molecules.

Expanding the NHC backbone clearly has a marked effect on the steric strain of the system. A clear result of this was the spontaneous ejection of cyclooctene and subsequent C–H activation in the synthesis of **14a**, **b** and **c**. Loss of the cyclooctene ligand may have also been promoted by an increase in electron density at the iridium due to the strong σ-donation from the 6- and 7-membered NHCs, thus donation from the alkene was not required. An advantage of this facile oxidative addition would be the electronic stabilisation of the low valent catalytic intermediates we aim to produce.

In addition, the benzylic tethers are easily removed by addition of hydrogen, or acid, hence these should act as a "hydrogen sink". The reversible nature of hydrogen addition to $(6\text{-Mes}')_2IrH$ to form $(6\text{-Mes})_2IrH_3$ suggests that this class of complex is suitable for creating a low energy pathway to dehydrogenation of small molecules, such as $H_3B{\cdot}NH_3$.

3.8 References

1. W. A. Herrmann and C. Kocher, *Angew. Chem. Int. Ed.*, 1997, **36**, 2162-2187.
2. W. A. Herrmann, *Angew. Chem. Int. Ed.*, 2002, **41**, 1290-1309.
3. J. C. Y. Lin, R. T. W. Huang, C. S. Lee, A. Bhattacharyya, W. S. Hwang and I. J. B. Lin, *Chem. Rev.*, 2009, **109**, 3561-3598.
4. P. L. Arnold and I. J. Casely, *Chem. Rev.*, 2009, **109**, 3599-3611.
5. D. Bourissou, O. Guerret, F. P. Gabbai and G. Bertrand, *Chem. Rev.*, 2000, **100**, 39-91.
6. A. J. Arduengo, *Acc. Chem. Res.*, 1999, **32**, 913-921.
7. C. M. Crudden and D. P. Allen, *Coord. Chem. Rev.*, 2004, **248**, 2247-2273.
8. S. Diez-Gonzalez and S. P. Nolan, *Coord. Chem. Rev.*, 2007, **251**, 874-883.
9. F. E. Hahn and M. C. Jahnke, *Angew. Chem. Int. Ed.*, 2008, **47**, 3122-3172.
10. P. de Fremont, N. Marion and S. P. Nolan, *Coord. Chem. Rev.*, 2009, **253**, 862-892.
11. H. W. Wanzlick, *Angew. Chem. Int. Ed.*, 1962, **1**, 75-80.
12. A. J. Arduengo, R. Krafczyk, R. Schmutzler, H. A. Craig, J. R. Goerlich, W. J. Marshall and M. Unverzagt, *Tetrahedron*, 1999, **55**, 14523-14534.
13. A. M. Magill, K. J. Cavell and B. F. Yates, *J. Am. Chem. Soc.*, 2004, **126**, 8717-8724.
14. T. Droge and F. Glorius, *Angew. Chem. Int. Ed.*, 2010, **49**, 6940-6952.
15. A. C. Hillier, W. J. Sommer, B. S. Yong, J. L. Petersen, L. Cavallo and S. P. Nolan, *Organometallics*, 2003, **22**, 4322-4326.
16. M. Iglesias, D. J. Beetstra, J. C. Knight, L. L. Ooi, A. Stasch, S. Coles, L. Male, M. B. Hursthouse, K. J. Cavell, A. Dervisi and I. A. Fallis, *Organometallics*, 2008, **27**, 3279-3289.
17. R. W. Alder, M. E. Blake, C. Bortolotti, S. Bufali, C. P. Butts, E. Linehan, J. M. Oliva, A. G. Orpen and M. J. Quayle, *Chem. Comm.*, 1999, 241-242.
18. P. Bazinet, G. P. A. Yap and D. S. Richeson, *J. Am. Chem. Soc.*, 2003, **125**, 13314-13315.
19. M. Mayr, K. Wurst, K. H. Ongania and M. R. Buchmeiser, *Chem. Eur. J.*, 2004, **10**, 1256-1266.
20. L. R. Yang, M. Mayr, K. Wurst and M. R. Buchmeiser, *Chem. Eur. J.*, 2004, **10**, 5761-5770.
21. J. Yun, E. R. Marinez and R. H. Grubbs, *Organometallics*, 2004, **23**, 4172-4173.
22. B. Bantu, D. R. Wang, K. Wurst and M. R. Buchmeiser, *Tetrahedron*, 2005, **61**, 12145-12152.
23. N. Imlinger, K. Wurst and M. R. Buchmeiser, *Monatsh. Chem.*, 2005, **136**, 47-57.
24. C. C. Scarborough, M. J. W. Grady, I. A. Guzei, B. A. Gandhi, E. E. Bunel and S. S. Stahl, *Angew. Chem. Int. Ed.*, 2005, **44**, 5269-5272.
25. C. C. Scarborough, B. V. Popp, I. A. Guzei and S. S. Stahl, *J. Organomet. Chem.*, 2005, **690**, 6143-6155.
26. Y. Zhang, D. R. Wang, K. Wurst and M. R. Buchmeiser, *J. Organomet. Chem.*, 2005, **690**, 5728-5735.

27. R. Jazzar, H. Z. Liang, B. Donnadieu and G. Bertrand, *J. Organomet. Chem.*, 2006, **691**, 3201-3205.
28. G. C. Lloyd-Jones, R. W. Alder and G. J. J. Owen-Smith, *Chem. Eur. J.*, 2006, **12**, 5361-5375.
29. M. Iglesias, D. J. Beetstra, A. Stasch, P. N. Horton, M. B. Hursthouse, S. J. Coles, K. J. Cavell, A. Dervisi and I. A. Fallis, *Organometallics*, 2007, **26**, 4800-4809.
30. D. M. Khramov, E. L. Rosen, V. M. Lynch and C. W. Bielawski, *Angew. Chem. Int. Ed.*, 2008, **47**, 2267-2270.
31. V. Cesar, N. Lugan and G. Lavigne, *J. Am. Chem. Soc.*, 2008, **130**, 11286-11287.
32. C. C. Scarborough, A. Bergant, G. T. Sazama, I. A. Guzei, L. C. Spencer and S. S. Stahl, *Tetrahedron*, 2009, **65**, 5084-5092.
33. M. Iglesias, D. J. Beetstra, B. Kariuki, K. J. Cavell, A. Dervisi and I. A. Fallis, *Eur. J. Inorg. Chem.*, 2009, 1913-1919.
34. U. Siemeling, C. Farber and C. Bruhn, *Chem. Comm.*, 2009, 98-100.
35. A. Binobaid, M. Iglesias, D. J. Beetstra, B. Kariuki, A. Dervisi, I. A. Fallis and K. J. Cavell, *Dalton Trans.*, 2009, 7099-7112.
36. R. Armstrong, C. Ecott, E. Mas-Marzá, M. J. Page, M. F. Mahon and M. K. Whittlesey, *Organometallics*, 2010, **29**, 991-997.
37. A. Binobaid, M. Iglesias, D. Beetstra, A. Dervisi, I. Fallis and K. J. Cavell, *Eur. J. Inorg. Chem.*, 2010, 5426-5431.
38. M. Iglesias, D. J. Beetstra, K. J. Cavell, A. Dervisi, I. A. Fallis, B. Kariuki, R. W. Harrington, W. Clegg, P. N. Horton, S. J. Coles and M. B. Hursthouse, *Eur. J. Inorg. Chem.*, 2010, 1604-1607.
39. C. J. E. Davies, M. J. Page, C. E. Ellul, M. F. Mahon and M. K. Whittlesey, *Chem. Comm.*, 2010, **46**, 5151-5153.
40. A. J. Arduengo, H. V. R. Dias, R. L. Harlow and M. Kline, *J. Am. Chem. Soc.*, 1992, **114**, 5530-5534.
41. H. Clavier and S. P. Nolan, *Chem. Comm.*, 2010, **46**, 841-861.
42. W. Y. Lu, K. J. Cavell, J. S. Wixey and B. Kariuki, *Organometallics*, 2011, **30**, 5649-5655.
43. J. J. Dunsford, K. J. Cavell and B. M. Kariuki, *Organometallics*, 2012, **31**, 4118-4121.
44. X. H. Cui and K. Burgess, *Chem. Rev.*, 2005, **105**, 3272-3296.
45. G. E. Dobereiner and R. H. Crabtree, *Chem. Rev.*, 2010, **110**, 681-703.
46. A. C. Cooper, E. Clot, J. C. Huffman, W. E. Streib, F. Maseras, O. Eisenstein and K. G. Caulton, *J. Am. Chem. Soc.*, 1999, **121**, 97-106.
47. C. Y. Tang, A. L. Thompson and S. Aldridge, *J. Am. Chem. Soc.*, 2010, **132**, 10578-10591.
48. C. Y. Tang, A. L. Thompson and S. Aldridge, *Angew. Chem. Int. Ed.*, 2010, **49**, 921-925.
49. C. Y. Tang, W. Smith, A. L. Thompson, D. Vidovic and S. Aldridge, *Angew. Chem. Int. Ed.*, 2011, **50**, 1359-1362.
50. J. F. Riehl, Y. Jean, O. Eisenstein and M. Pelissier, *Organometallics*, 1992, **11**, 729-737.

51. N. M. Scott, V. Pons, E. D. Stevens, D. M. Heinekey and S. P. Nolan, *Angew. Chem. Int. Ed.*, 2005, **44**, 2512-2515.
52. J. Navarro, O. Torres, M. Martin and E. Sola, *J. Am. Chem. Soc.*, 2011, **133**, 9738-9740.
53. A. C. Cooper, W. E. Streib, O. Eisenstein and K. G. Caulton, *J. Am. Chem. Soc.*, 1997, **119**, 9069-9070.
54. J. K. Huang, E. D. Stevens and S. P. Nolan, *Organometallics*, 2000, **19**, 1194-1197.
55. J. D. Egbert, R. M. Bullock and D. M. Heinekey, *Organometallics*, 2007, **26**, 2291-2295.
56. D. Pugh, N. J. Wells, D. J. Evans and A. A. Danopoulos, *Dalton Trans.*, 2009, 7189-7195.
57. H. V. Nanishankar, S. Dutta, M. Nethaji and B. R. Jagirdar, *Inorg. Chem.*, 2005, **44**, 6203-6210.
58. M. Findlater, K. M. Schultz, W. H. Bernskoetter, A. Cartwright-Sykes, D. M. Heinekey and M. Brookhart, *Inorg. Chem.*, 2012, **51**, 4672-4678.
59. B. Rybtchinski, Y. BenDavid and D. Milstein, *Organometallics*, 1997, **16**, 3786-3793.
60. M. Findlater, W. H. Bernskoetter and M. Brookhart, *J. Am. Chem. Soc.*, 2010, **132**, 4534-4535.

Chapter IV

Increasing Electron Density at Low Valent Metal Cations: Steric and Electronic Stabilisation

4.1 Introduction

Low valent, cationic metal complexes have been widely exploited in E–H bond activation chemistry.[1-6] Often the active species is a 14-electron complex to which the substrate can coordinate through a σ-bond interaction and, if the metal provides sufficient back-bonding, the bond can be cleaved.[7] Fragments of the type $[(L)_2M(H)_2]^+$ (L = tertiary phosphine, NHC; M = Rh, Ir) have been extensively investigated for the dehydrogenation of $H_3B{\cdot}NHR_2$ (R = H, alkyl) systems.[8-12] Previous NHC metal complexes exploited in the Aldridge group for the dehydrogenation of amine-borane species have been shown to only undergo a limited number of turnovers before the catalyst degrades. In the case of ammonia-borane, a target molecule for hydrogen storage applications, unpublished work in our group has shown by NMR spectroscopy that $[(IMes)_2IrH_2][BAr^f_4]$ degrades by cleavage of the metal–NHC bond (Scheme 4.1).

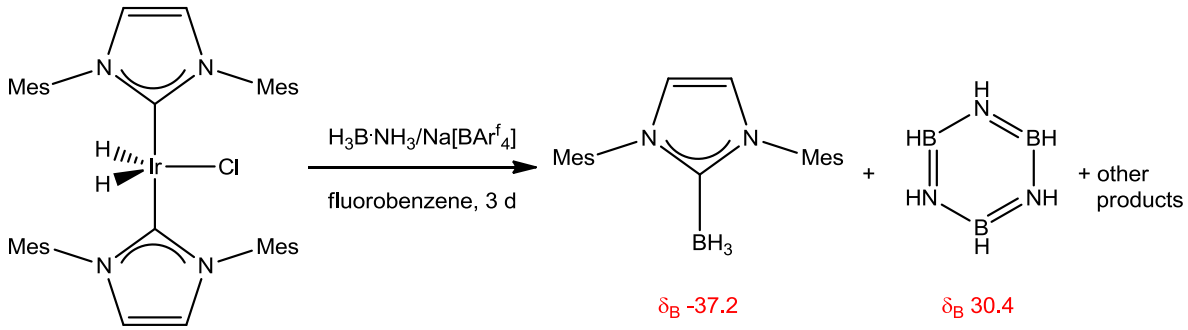

Scheme 4.1: Degradation of NHC–Ir bonds observed by ^{11}B NMR experiments.

The increased donor power of these saturated carbene ligands will lead to a stronger M–NHC bond and reduce lability of the ligand. Furthermore, this increased donation will lead to a more electron-rich metal centre to aid in oxidative addition of E–H bonds of a substrate.

As observed in Chapter III, saturated NHC ligands appear to promote relatively facile oxidative addition processes to increase the metal electron count, as well as offering a degree of conformational flexibility to allow substrates to access the metal. Equally, relatively facile reductive elimination will be required to allow for oxidative addition of the E–H bonds in the substrate. This has been demonstrated to an extent by the reversible addition of H_2 to (6-Mes')$_2$IrH (Scheme 4.2).

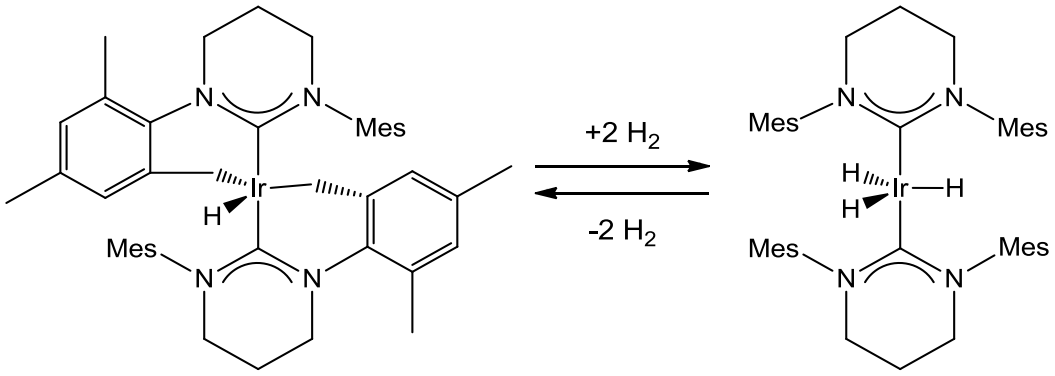

4a **5a**

Scheme 4.2: Reversible C-H bond activation in 6-Mes by addition and removal of hydrogen.

The larger %V_{bur} of the expanded ring NHCs will offer greater steric protection of the metal centre, perhaps allowing for more reactive species to be isolated. In addition to this, the close approach of the *N*-based substituents in the expanded ring NHCs should favour stabilisation of these low valent centres through agostic or other intramolecular

interactions. It has also been reported that expanded ring NHCs can offer electronic stabilisation via interaction of the arene ring with the metal centre (Fig 4.3).[13, 14]

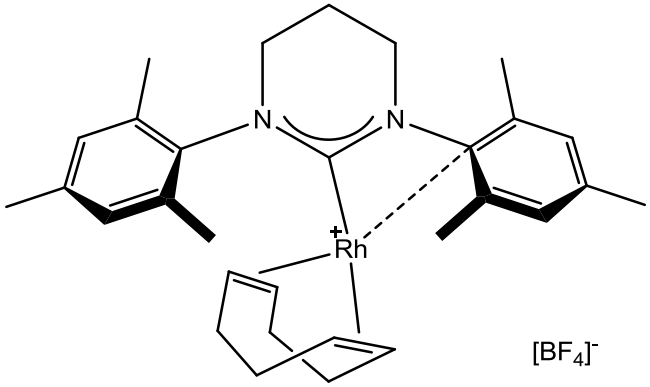

Figure 4.3: Arene stabilisation of low valent centres offered by expanded ring NHCs.

The aim of the work reported in this chapter is to synthesise 14-electron iridium complexes with enhanced stability such that the lifetime of such species in catalytic processes may be increased. Changing the NHC to a saturated and/or expanded ring donor should increase the strength of the metal-NHC interaction, and hence reduce the lability of the system. In addition, the increased donor power of this class of NHC should increase the electron density at the metal, thus providing the possibility for increased back-bonding to activate the coordinated E–H bond.

4.2 Experimental

*Preparation of [(5-Mes)$_2$IrH$_2${H$_3$BNMe$_3$}][BAr$^f_4$] (**11**)*

A solution of Na[BAr$^f_4$] (53 mg, 0.06 mmol) in THF (10 cm^3) was added to a stirred solution of (5-Mes)$_2$IrH$_2$Cl (50 mg, 0.06 mmol) and H$_3$B·NMe$_3$ (43 mg, 0.6 mmol) also in THF (20 cm^3) at -30°C. The mixture was stirred whilst warming to room temperature over 1 h, during which time the yellow colour paled. The precipitated solid was removed by filtration and volatiles were removed *in vacuo*. The remaining pale yellow solid was

washed with hexanes (2 x 10 cm^3), dried *in vacuo* and collected in 52% yield (54 mg). Crystals suitable for X-ray crystallography were obtained from a fluorobezene/pentane layering at 20 °C.

*Spectroscopic data for **11***

^{1}H NMR (CD_2Cl_2, 300 MHz, 298 K): δ_H 7.73 (8H, s, *ortho*-CH $[BAr^f_4]^-$), 7.57 (4H, s, *para*-CH $[BAr^f_4]^-$), 6.80 (8H, s, *meta*-CH), 3.67 (8H, s, NCH_2), 2.36 (24H, s, *ortho*-CH_3), 2.24 (12H, s, *para*-CH_3), 1.93 (9H, br, NMe_3), -2.11 (3H, br, BH_3), -21.86 (2H, s, IrH). ^{13}C NMR (CD_2Cl_2, 75 MHz, 298 K): δ_C 198.8 (NCN), 162.1 (q, $^1J_{CB}$ = 49.6 Hz, CB $[BAr^f_4]^-$), 137.9 (NC Mes), 137.7 (*para*-C Mes), 135.1 (br, *ortho*-CH $[BAr^f_4]^-$), 129.8 (*meta*-CH Mes), 129.2 (m, *meta*-C $[BAr^f_4]^-$), 124.9 (q, $^1J_{CF}$ = 271.0 Hz, CF_3 $[BAr^f_4]^-$), 117.8 (m, *para*-CH $[BAr^f_4]^-$), 52.7 (NCH_2), 51.4 (NMe_3), 21.1 (*para*-CH_3 Mes), 18.9 (*ortho*-CH_3 Mes). ^{11}B NMR (CD_2Cl_2, 96 MHz, 298 K): δ_B 13.01 (s, BH_3), -6.87 (s, $[BAr^f_4]^-$). ^{19}F NMR (CD_2Cl_2, 282 MHz, 298 K): δ_F -62.87 (s, CF_3 $[BAr^f_4]$). MS (ESI +ve): *m/z* 807.4 ($[M\text{-}H_3BNMe_3]^+$, 45%), 880.5 (M^+, 50%). Accurate mass ($[C_{45}H_{66}N_5{}^{11}B^{191}Ir]^+$): 880.5180 (meas.), 880.5045 (calc.) Elemental analysis: calc. for $C_{77}H_{78}IrN_5B_2F_{24}$: C 53.05, H 4.51, N 4.02, meas. C 50.85, H 4.82, N 3.61.

*Crystallographic data for **11***

$C_{77}H_{78}IrN_5B_2F_{24}$, M_r = 1743.29, triclinic, *P* -1, a = 12.5841(2), b = 17.9389(3), c = 18.2196(3) Å, α = 86.8231(6), β = 69.9280(7), γ = 87.6703(6) °, V = 3856.21(11) $Å^3$, Z = 2, ρ_c = 1.501 Mg m^{-3}, T = 150 K, λ = 0.710730 Å, 60623 reflections collected, 17332 independent [R(int) = 0.070], which were used in calculations. R_1 = 0.0552, wR_2 = 0.0877 for observed unique reflections [I > 2σ(I)] and R_1 = 0.1004, wR_2 = 0.1205 for all unique reflections. Max. and min. residual electron densities 6.73 and -4.41 e $Å^{-3}$.

*Preparation of [(5-Mes)$_2$IrH$_2${H$_2$BNMe$_2$}][BAr$^f_4$] (**12**)*

A solution of Na[BAr$^f_4$] (53 mg, 0.06 mmol) in THF (10 cm^3) was added to a stirred solution of (5-Mes)$_2$IrH$_2$Cl (50 mg, 0.06 mmol) and H$_3$B·NHMe$_2$ (35 mg, 0.6 mmol) in THF (10 cm^3) at -78°C. The mixture was stirred whilst warming to room temperature, during which time the yellow colour paled. The solution was filtered and volatiles removed *in vacuo*. The residue was washed with hexanes (2 x 10 cm^3), dried *in vacuo* and collected a pale yellow powder in 59% yield (61 mg). Crystals suitable for X-ray and neutron diffraction studies were obtained from a fluorobezene/pentane layering at 20 °C.

*Spectroscopic data for **12***

^{1}H NMR (CD_2Cl_2, 300 MHz, 298 K): δ_H 7.72 (8H, s, *ortho*-CH [BAr$^f_4$]$^-$), 7.56 (4H, s, *para*-CH [BAr$^f_4$]$^-$); (i) signals corresponding to **12i**: 6.84 (8H, s, *meta*-CH Mes), 3.74 (8H, s, NCH_2), 2.46 (6H, s, NMe_2), 2.36 (12H, s, *para*-CH_3 Mes), 1.87 (24H, s, *ortho*-CH_3 Mes), -6.18 (2H, br, BH_2), -15.70 (2H, d, $^2J_{HH}$ = 13.5 Hz, IrH) ; (i) signals corresponding to **12ii**: 6.88 (8H, s, *meta*-CH), 3.78 (8H, s, NCH_2), 2.46 (6H, s, NMe_2), 2.33 (12H, s, *para*-CH_3), 1.90 (24H, s, *ortho*-CH_3), -20.51 (2H, s IrH). ^{13}C NMR (CD_2Cl_2, 75 MHz, 298 K): δ_C 187.5 (NCN), 162.1 (q, $^1J_{CB}$ = 49.6 Hz, CB [BAr$^f_4$]$^-$), 138.4 (NC Mes), 137.4 (*para*-C Mes), 135.9 (*ortho*-C Mes), 135.2 (br, *ortho*-CH [BAr$^f_4$]$^-$), 129.9 (*meta*-CH Mes), 129.2 (m, *meta*-C [BAr$^f_4$]$^-$), 124.9 (q, $^1J_{CF}$ = 271.0 Hz, CF_3 [BAr$^f_4$]$^-$), 117.8 (m, *para*-CH [BAr$^f_4$]$^-$), 50.5 (NCH_2), 41.1 (NCH_3), 21.2 (*para*-CH_3 Mes), 17.8 (*ortho*-CH_3 Mes). ^{11}B NMR (CD_2Cl_2, 96 MHz, 298 K): δ_B 48.1 (br, BH_2), 10.8 (s, BH_3), -6.9 (s, [BAr$^f_4$]$^-$). ^{19}F NMR (CD_2Cl_2, 282 MHz, 298 K): δ_F -62.89 (s, CF_3 [BAr$^f_4$]$^-$). MS (ESI +ve): *m/z* 864.5 (M$^+$, 100%). Accurate mass ([$C_{44}H_{62}N_5{}^{11}B^{192}Ir$]$^+$): 864.4834 (meas.), 864.4732 (calc.). Elemental analysis: calc. for $C_{76}H_{74}IrN_5B_2F_{24}$: C 52.85, H 4.32, N 4.05, meas. C 50.73, H 4.76, N 3.68.

*Crystallographic data for **12***

$C_{76}H_{74.86}IrN_5B_2F_{24}$, M_r = 1728.11, triclinic, *P*-1, a = 12.7291(1), b = 17.5467(2), c = 18.0265(2) Å, α = 88.2727(4), β = 70.2021(5), γ = 87.5305(4) °, V = 3784.27(7) $Å^3$, Z = 2, ρ_c = 1.517 Mg m^{-3}, T = 150 K, λ = 0.710730 Å, 66843 reflections collected, 17238 independent [R(int) = 0.027], which were used in calculations. R_1 = 0.0411, wR_2 = 0.0947 for observed unique reflections [I > 2σ(I)] and R_1 = 0.0486, wR_2 = 0.1042 for all unique reflections. Max. and min. residual electron densities 2.80 and -1.22 e $Å^{-3}$.

*Neutron diffraction data for **12***

$C_{76}H_{74.70}IrN_5B_2F_{24}$, M_r = 1727.96, triclinic, *P* -1, a = 12.689(3), b = 17.555(1), c = 17.948(4) Å, α = 88.275(19), β = 70.175(17), γ = 87.82(2) °, V = 3757.7(14) $Å^3$, Z = 2, ρ_c = 1.527 Mg m^{-3}, T = 100(2) K, λ = Laue, 7639 reflections collected, 6529 independent, which were used in calculations. R_1 = 0.0937, wR_2 = 0.2053 for observed unique reflections [I > 2σ(I)] and R_1 = 0.1060, wR_2 = 0.2162 for all unique reflections.

*Preparation of [(6-Mes)(6-Mes')IrH][BAr^f_4] (**14a**)*

A solution of $[H(OEt_2)_2][BAr^f_4]$ (Brookhart's acid) (120 mg, 0.120 mmol) in fluorobenzene (15 cm^3) was added to a stirred solution of $(6\text{-Mes}')_2IrH$ (100 mg, 0.120 mmol) also in fluorobenzene (15 cm^3). On stirring for 30 min the solution turned from orange/red to yellow/orange. Removal of volatiles *in vacuo* yielded a pale orange solid that was subsequently washed with hexanes (3 x 20 cm^3). The powder was dried *in vacuo* for 2 h, and the pale orange product isolated in 88% yield (180 mg). Crystals suitable for X-ray crystallography were obtained from a dichloromethane/hexane layering at -30°C.

*Spectroscopic data for **14a***

^{1}H NMR (CD_2Cl_2, 300 MHz, 298 K): δ_H 7.73 (8H, s, *ortho*-CH $[BAr^f_4]^-$), 7.56 (4H, s, *para*-CH $[BAr^f_4]^-$), 7.04, 7.03 (each 2H, s, *meta*-CH Mes), 6.92 (2H, br, s, *meta*-CH Mes'), 6.70 (2H, s, *meta*-CH Mes'), 3.34 (2H, m, NCH_2), 3.24 (4H, m, NCH_2), 2.89 (2H, m, NCH_2), 2.36 (6H, s, *para*-CH_3 Mes), 2.31 (6H, s, *para*-CH_3 Mes'), 2.26 (6H, s, *ortho*-CH_3 Mes), 2.02 (6H, s, *ortho*-CH_3 Mes'), 1.88 (4H, br, NCH_2CH_2), $IrCH_2$, agostic CH_3 and IrH not observed. ^{13}C NMR (CD_2Cl_2, 75 MHz, 298 K): δ_C 188.3 (NCN), 162.1 (q, $^{1}J_{CB}$ = 49.6 Hz, NC $[BAr^f_4]^-$), 141.8 (NC Mes), 138.6 (*para*-C Mes), 138.5 (*para*-C Mes'), 136.6, 136.5 (*ortho*-C Mes), 135.2 (br, *ortho*-CH $[BAr^f_4]^-$), 134.9 (*ortho*-C Mes'), 134.2 (NC Mes'), 131.8, 130.8 (*meta*-CH Mes'), 130.4 (*ortho*-C Mes'), 130.1 129.5 (*meta*-C Mes), 129.2 (m, *meta*-C $[BAr^f_4]^-$), 125.0 (q, $^{1}J_{CF}$ = 270.5 Hz, CF_3 $[BAr^f_4]^-$), 117.8 (m, *para*-CH $[BAr^f_4]^-$), 48.5, 46.7 (NCH_2), 21.5 (NCH_2CH_2), 21.1 (*para*-CH_3 Mes), 21.0 (*para*-CH_3 Mes'), 19.0 (*ortho*-CH_3 Mes'), 18.4, 18.0 (*ortho*-CH_3 Mes), 1.1 ($IrCH_2$). ^{11}B NMR (CD_2Cl_2, 96 MHz, 298 K): δ_B -6.66 ($BAr^f_4^-$). ^{19}F NMR (CD_2Cl_2, 282 MHz, 298 K): δ_F -62.89 (CF_3). MS (ESI +ve): *m/z* 833.4 (M^+, 100%). Accurate mass ($[C_{44}H_{56}N_4{}^{191}Ir]^+$): 831.4125 (meas.), 831.4105 (calc.). IR (CH_2Cl_2, ν(C-H, agostic)/cm^{-1}): 2548.02. Elemental analysis: calc. for $C_{76}H_{68}IrN_4BF_{24}$: C 53.81, H 4.04, N 3.30, meas. C 53.36, H 3.83, N 2.95.

*Low Temperature Spectroscopic data for **14a***

^{1}H NMR (CD_2Cl_2, 500 MHz, 213 K): δ_H 7.73 (8H, s, *ortho*-CH $[BAr^f_4]^-$), 7.56 (4H, s, *para*-CH $[BAr^f_4]^-$), 7.01 (1H, s, *meta*-CH Mes'), 6.99 (1H, s, *meta*-CH Mes), 6.98 (1H, s, *meta*-CH Mes), 6.96, 6.96 (1H, s, *meta*-CH Mes), 6.66 (1H, s, *meta*-CH Mes), 6.62 (1H, s, *meta*-CH Mes'), 6.47 (1H, s, *meta*-CH Mes), 3.44 (1H, ddd, $^{2}J_{HH}$ = 13.3, $^{3}J_{HH}$ = 10.0, 3.8 Hz, NCH_2), 3.38-3.30 (1H, m, NCH_2), 3.30-3.24 (1H, m, NCH_2), 3.26-3.20 (1H, m, NCH_2), 3.21-3.14 (1H, m, NCH_2), 2.95 (1H, ddd, $^{2}J_{HH}$ = 12.1, $^{3}J_{HH}$ = 8.0, 4.3 Hz, NCH_2), 2.83-2.77

(1H, m, NCH_2), 2.32 (1H, d, $^2J_{HH}$ = 7.3 Hz, $IrCH_2$) 2.32 (3H, s, *para*-CH_3 Mes), 2.31 (3H, s, *para*-CH_3 Mes'), 2.27 (3H, s, *para*-CH_3 Mes'), 2.26 (3H, s, *ortho*-CH_3 Mes), 2.18 (3H, s, *ortho*-CH_3 Mes), 2.16 (3H, s, *para*-CH_3 Mes), 2.12-2.08 (1H, m, NCH_2CH_2), 2.08 (3H, s, *ortho*-CH_3 Mes'), 2.05-2.00 (1H, m, NCH_2CH_2), 2.03-1.95 (1H, m, NCH_2CH_2), 1.84 (3H, s, *ortho*-CH_3 Mes), 1.80 (3H, s, *ortho*-CH_3 Mes), 1.77-1.72 (1H, m NCH_2CH_2), 1.70 (3H, s, *ortho*-CH_3 Mes), 1.65 (1H, d, $^2J_{HH}$ = 7.3 Hz, $IrCH_2$), 0.61 (3H, s, *agostic*-CH_3 Mes), -31.06 (1H, s, IrH). ^{13}C NMR (CD_2Cl_2, 125 MHz, 213 K): signals due to cation: δ_C 194.0, 182.9 (s, NCN), 142.2, 140.7 (s, NC Mes), 137.9, 137.7, 137.6 (s, *para*-C Mes), 136.8 (s, NC Mes'), 136.5 (s, *ortho*-C Mes), 136.2 (s, *para*-C Mes'), 136.2, 136.1, 135.6, 134.5, 134.2 (s, *ortho*-C Mes), 131.0 (s, *meta*-CH Mes), 130.9 (s, *ortho*-C Mes'), 130.9 (s, *meta*-CH Mes'), 130.9 (s, *meta*-CH Mes), 129.5, 129.4, 128.9, 128.6 (s, *meta*-CH Mes), 127.4 (s, *meta*-CH Mes'), 125.2 (s, *ortho*-C Mes'), 120.6 (s, NC Mes *agostic*), 48.2, 47.2, 46.1, 46.0 (s, NCH_2), 21.5 (s, NCH_2CH_2), 20.9, 20.9, 20.8 (s, *para*-CH_3 Mes), 20.7 (s, *para*-CH_3 Mes'), 20.5 (NCH_2CH_2), 19.2 (s, *ortho*-CH_3 Mes'), 18.9, 18.2, 18.1, 17.9, 17.5 (s, *ortho*-CH_3 Mes), 15.8 (s, *agostic*-CH_3 Mes), -4.6 (s, $IrCH_2$); signals due to $[BAr^f_4]^-$ anion: δ_C 162.1 (q, $^1J_{CB}$ = 49.6 Hz, NC), 135.2 (br, *ortho*-CH), 129.2 (q, $^2J_{CF}$ = 31.4 Hz, *meta*-C), 125.0 (q, $^1J_{CF}$ = 270.5 Hz, CF_3), 117.8 (m, *para*-CH).

Crystallographic data for ***14a***

$C_{44}H_{56}IrN_4 \cdot C_{32}H_{12}BF_{24}$, M_r = 1696.39, triclinic, *P*-1, a = 15.1100(3) Å, b = 17.1158(4) Å, c = 17.3974(4) Å, α = 63.004(2) °, β = 66.1775(19) °, γ = 75.0989(19) °, V = 3652.42(16) Å^3, Z = 2, ρ_c = 1.542 Mg m^{-3}, T = 150 K, λ = 1.54184 Å, 38689 reflections collected, 15191 independent [R(int) = 0.028], which were used in calculations. R_1 = 0.0337, wR_2 = 0.087 for observed unique reflections [I > 2σ(I)] and R_1 = 0.0355, wR_2 = 0.0895 for all unique reflections. Max. and min. residual electron densities 2.42 and -1.64 e Å^{-3}.

*Preparation of [(7-Mes)(7-Mes')IrH][BAr$^f_4$] (**14b**)*

A solution of [H(OEt$_2$)$_2$][BAr$^f_4$] (116 mg, 0.116 mmol) in fluorobenzene (15 cm^3) was added to a stirred solution of (7-Mes')$_2$IrH (100 mg, 0.116 mmol) also in fluorobenzene (15 cm^3). After 30 mins the solution turned from orange/red to yellow. Removal of the volatiles *in vacuo* yielded a yellow solid that was subsequently washed with hexanes (3 x 15 cm^3). The resulting powder was dried *in vacuo* for 2 h, and the yellow product isolated in 65% yield (130 mg). Crystals suitable for X-ray crystallography were obtained from a dichloromethane/hexane layering at -30 °C.

*Spectroscopic data for **14b***

^{1}H NMR (CD_2Cl_2, 300 MHz, 298 K): δ_H 7.72 (8H, s, *ortho*-CH [BAr$^f_4$]$^-$), 7.56 (4H, s, *para*-CH [BAr$^f_4$]$^-$), 7.03, 7.00 (each 2H, s, *meta*-H Mes), 6.83 (2H, br, *meta*-H Mes'), 6.73 (2H, s, *meta*-CH Mes'), 4.01, 3.75, 3.52, 3.03 (each 2H, m, NCH_2), 2.38 (6H, s, *para*-CH_3 Mes), 2.30 (6H, s, *para*-CH_3 Mes'), 2.29, 2.02 (each 6H, s, *ortho*-CH_3 Mes), 1.98 (6H, s, *ortho*-CH_3 Mes'), 1.85, 1.26 (8H, m, NCH_2CH_2). ^{13}C NMR (CD_2Cl_2, 125 MHz, 298 K): δ_C (NCN-not observed), 162.6 (q, $^1J_{CB}$ = 49.4 Hz, BC [BAr$^f_4$]$^-$), 157.7 (*ipso*-C Mes'), 144.3 (*ipso*-C Mes), 138.4 (*para*-C Mes), 137.8 (*para*-C Mes'), 136.7 (*ortho*-C Mes), 135.4 (*ortho*-CH [BAr$^f_4$]$^-$), 135.4 (*ortho*-C Mes'), 134.5 (*ortho*-C Mes'), 131.6 (*meta*-CH Mes), 130.6 (*meta*-CH Mes'), 130.5 (*meta*-CH Mes'), 129.5 (m, *meta*-C [BAr$^f_4$]$^-$), 125.1 (q, $^1J_{CF}$ = 272.3 Hz, CF_3 [BAr$^f_4$]$^-$), 118.0 (*para*-CH [BAr$^f_4$]$^-$) 57.6, 54.9 (NCH_2), 26.3, 25.4 (NCH_2CH_2), 21.3 (*para*-CH_3 Mes'), 20.2 (br, *ortho*-CH_3 Mes'), 19.3 (*ortho*-CH_3 Mes), 18.7 (*para*-CH_3 Mes), 1.4 (Ir-CH_2). ^{11}B NMR (CD_2Cl_2, 96 MHz, 298 K): δ_B -6.7 ([BAr$^f_4$]$^-$). ^{19}F NMR (CD_2Cl_2, 282 MHz, 298 K): δ_F -62.9 (CF_3 [BAr$^f_4$]$^-$). MS (ESI +ve) *m*/*z*: 861.4 (M$^+$, 100 %); accurate mass: calc. for [$C_{46}H_{60}IrN_4$]$^+$ 861.4445, meas. 861.4469. Elemental analysis: calc. for $C_{78}H_{72}BF_{24}IrN_4$: C 54.33, H 4.21, N 3.25, meas. C 54.37, H 4.53, N 3.52.

*Crystallographic data for **14b**·½CH_2Cl_2*

$C_{78}H_{72}BF_{24}IrN_4 \cdot 0.5(CH_2Cl_2)$, M_r = 1766.90, triclinic, *P*-1, a = 12.6230(2) Å, b = 16.3790(3) Å, c = 19.2977(3) Å, α = 100.9174(8)°, β = 104.0419(7)°, γ = 94.8383°, V = 3764.84(11) $Å^3$, Z = 2, ρ_c = 1.559 Mg m^{-3}, T = 150 K, λ = 0.71073 Å, 57468 reflections collected, 17157 independent [R(int) = 0.066], which were used in all calculations. R_1 = 0.0575, *w*R_2 = 0.0958 for observed unique reflections [I > 2σ(I)] and R_1 = 0.0988, *w*R_2 = 0.1289 for all unique reflections. Max and min. residual electron densities 4.19 and -3.41 e $Å^{-3}$.

*Preparation of [(6-Mes)$_2$Ir(H)$_2$][BAr$^f_4$] (**15a**)*

A solution of [(6-Mes)(6-Mes')IrH][BAr^f_4] (180 mg, 0.106 mmol) in fluorobenzene (20 cm^3) was thoroughly degassed by the freeze-pump-thaw method. When the solution was frozen for the final time, the flask was immersed in liquid nitrogen and the head space back-filled with H_2 gas. The solution was allowed to melt and stirred for 2 h, during which time a colour change from orange to yellow was observed. Removal of the volatiles *in vacuo* yielded a yellow solid which is washed with hexanes (3 x 15 cm^3). The resulting yellow powder was dried *in vacuo* and collected in 78% yield (140 mg). Crystals suitable for X-ray crystallography were obtained from a fluorobenzene/pentane layering at 20 °C.

*Spectroscopic data for **15a***

^{1}H NMR (CD_2Cl_2, 300 MHz, 298 K): δ_H 7.72 (8H, br, *ortho*-CH [BAr^f_4]$^-$), 7.56 (4H, s, *para*-CH [BAr^f_4]$^-$), 6.95 (8H, s, *meta*-CH Mes), 3.11 (8H, tr, $^3J_{HH}$ = 5.7 Hz, NCH_2), 2.35 (12H, s, *para*-CH_3 Mes), 2.10 (4H, qn, $^3J_{HH}$ = 5.7 Hz, $NCH_2C\underline{H}_2$), 1.78 (24H, s, *ortho*-CH_3 Mes), -43.57 (2H, s, IrH_2). ^{13}C NMR (CD_2Cl_2, 75 MHz, 298 K): δ_C 200.6 (NCN), 162.1 (q, $^1J_{CB}$ = 49.6 Hz, BC [BAr^f_4]$^-$), 139.1 (NC Mes), 136.5 (*para*-C Mes), 135.9 (*ortho*-C Mes), 135.2 (*ortho*-CH [BAr^f_4]$^-$), 130.2 (*meta*-CH Mes), 129.4 (m, *meta*-C [BAr^f_4]$^-$), 125.0 (q, $^1J_{CF}$

= 271 Hz, CF_3 $[BAr^f_4]^-$), 117.8 (m, *para*-CH $[BAr^f_4]^-$), 46.4 (NCH_2), 21.2 (NCH_2CH_2), 18.0 (CH_3 Mes). ^{11}B NMR (CD_2Cl_2, 96 MHz, 298 K): δ_B -5.81 ($[BAr^f_4]^-$). ^{19}F NMR (CD_2Cl_2, 282 MHz, 298 K): δ_F -62.03 (CF_3 $[BAr^f_4]^-$). MS (ESI +ve): *m/z* 835.4 (M^+, 100%). Accurate mass ($[C_{44}H_{58}N_4{}^{191}Ir]^+$): 833.4314 (meas.), 833.4262 (calc.). Elemental analysis: calc. for $C_{76}H_{70}IrN_4BF_{24}$: C 53.75, H 4.15, N 3.30, meas. C 53.64, H 4.07, N 3.22.

*Crystallographic data for **15a***

$C_{76}H_{70}IrN_4BF_{24}$, M_r = 1696.10, triclinic, *P*-1, a = 13.83290(10) Å, b = 16.2697(2) Å, c = 17.7359(2) Å, α = 91.7424(4) °, β = 110.8926(4) °, γ = 90.7674(7) °, V = 3726.17(7) $Å^3$, Z = 2, ρ_c = 1.512 Mg m^{-3}, T = 150 K, λ = 0.710730 Å, 51811 reflections collected, 16839 independent [R(int) = 0.024], which were used in calculations. R_1 = 0.0426, wR_2 = 0.0980 for observed unique reflections [$I > 2\sigma(I)$] and R_1 = 0.0533, wR_2 = 0.1077 for all unique reflections. Max. and min. residual electron densities 1.63 and -1.29 e $Å^{-3}$.

*Preparation of $[(7\text{-Mes})_2Ir(H)_2][BAr^f_4]$ (**15b**)*

A solution of [(7-Mes)(7-Mes')IrH][BAr^f_4] (200 mg, 0.116 mmol) in fluorobenzene (20 cm^3) was thoroughly degassed by the freeze-pump-thaw method. When the solution was frozen for the final time, the flask was immersed in liquid nitrogen and the head space back-filled with H_2 gas. The solution was allowed to melt and stirred for 2 h. Removal of the volatiles *in vacuo* yielded a yellow solid which was washed with hexanes (3 x 15 cm^3). The resulting yellow powder was dried *in vacuo* and collected in 97% yield (194 mg). Crystals suitable for X-ray crystallography were obtained from a fluorobenzene/pentane layering at 20 °C.

*Spectroscopic data for **15b***

^{1}H NMR (300 MHz, CD_2Cl_2, 298 K): δ_H 7.71 (8H, s, *ortho*-CH $[BAr^f_4]^-$), 7.55 (4H, s, *para*-CH $[BAr^f_4]^-$), 6.94 (8H, s, *meta*-CH Mes), 3.48 (8H, t, $^{3}J_{HH}$ = 5.4 Hz, NCH_2), 2.36 (12H, s, *para*-CH_3 Mes), 2.00 (8H, m, NCH_2CH_2), 1.85 (24H, s, *ortho*-CH_3 Mes), -41.68 (2H, s, IrH). ^{13}C NMR (75 MHz, CD_2Cl_2, 25°C): δ_C 162.6 (q, $^{1}J_{CB}$ = 49.4 Hz, BC $[BAr^f_4]^-$), 139.0 (*ortho*-C Mes), 137.6 (*para*-C Mes), 136.5 (*meta*-CH Mes), 135.4 (br, *ortho*-C $[BAr^f_4]^-$), 129.5 (q, $^{2}J_{CF}$ = 32.1 Hz, *meta*-C $[BAr^f_4]^-$), 125.2 (q, $^{1}J_{CF}$ = 270.3 Hz, CF_3 $[BAr^f_4]^-$), 118.0 (m, *para*-C $[BAr^f_4]^-$), 54.8 (NCH_2), 25.8 ($NCH_2\underline{C}H_2$), 21.4 (*para*-CH_3 Mes), 19.0 (*ortho*-CH_3-Mes). ^{11}B NMR (CD_2Cl_2, 96 MHz, 298 K): δ_B -6.7 ($[BAr^f_4]^-$). ^{19}F NMR (CD_2Cl_2, 282 MHz, 298 K): δ_F -62.9 (CF_3 $[BAr^f_4]^-$). Elemental microanalysis: calc. for $C_{78}H_{74}BF_{24}IrN_4$: C 54.26, H 4.32, N 3.25, meas. C 54.36, H 4.18, N 3.20.

*Crystallographic data for **15b***

$C_{78}H_{74}BF_{24}IrN_4$, M_r = 1726.45, triclinic, *P*-1, *a* = 13.0310(2), *b* = 14.9560(2), *c* = 19.9381(3) Å, α = 99.3037(5), β = 104.8178(6), γ = 91.3768(5)°, V = 3698.41(9) Å^3, Z = 2, ρ_c = 1.550 Mg m^{-3}, T = 150 K, λ = 0.710730 Å, 61453 reflections collected, 16739 independent [R(int) = 0.048], which were used in all calculations. R_1 = 0.0478, *w*R_2 = 0.0838 for observed unique reflections [I > 2σ(I)] and R_1 = 0.0816, *w*R_2 = 0.1143 for all unique reflections. Max. and min. residual electron densities 3.89 and -3.27 e Å^{-3}.

*In situ generation of [(6-Mes)$_2$Ir(H)$_4$][BAr$^f_4$] (**16**)*

A solution of **15a** in CD_2Cl_2 was placed under an atmosphere of H_2 gas using the standard freeze-pump-thaw method. The formation of **16** was observed by ^{1}H NMR spectroscopy. Complex **15a** reforms upon replacement of H_2 with argon, so no solid product has been isolated.

*Spectroscopic data for **16***

^{1}H NMR (300 MHz, CD_2Cl_2, 298 K): δ_H 7.72 (8H, s, *ortho*-CH $[BAr^f_4]^-$), 7.55 (4H, s, *para*-CH $[BAr^f_4]^-$), 6.94 (8H, s, *meta*-CH Mes), 3.11 (8H, t, $^{3}J_{HH}$ = 5.7 Hz, NCH_2), 2.35 (12H, s, *para*-CH_3 Mes), 2.10 (8H, m, NCH_2CH_2), 1.78 (24H, s, *ortho*-CH_3 Mes), no signal below δ_H 0 ppm observed.

*Preparation of [(6-Mes)$_2$Ir(CO)$_2$][BAr$^f_4$] (**17**)*

A solution of **14a** (40 mg, 0.02 mmol) in CD_2Cl_2 was placed under 1 atm of CO gas and sonicated for 4 d. Over this time the colour rapidly paled to almost colourless and then became bright orange. Volatiles were then removed *in vacuo* to leave a bright orange powder in 81% yield (33 mg). Attempts were made to crystallise the product from a range of solvents under a variety of conditions, however no solid product was ever obtained.

*Spectroscopic data for **17***

^{1}H NMR (300 MHz, CD_2Cl_2, 298 K): δ_H 7.72 (8H, s, *ortho*-CH $[BAr^f_4]^-$), 7.56 (4H, s, *para*-CH $[BAr^f_4]^-$), 6.88 (8H, s, *meta*-CH Mes), 3.18 (8H, t, $^{3}J_{HH}$ = 5.8 Hz, NCH_2), 2.43 (12H, s, *para*-CH_3 Mes), 2.15 (8H, qn, $^{3}J_{HH}$ = 5.9 Hz, NCH_2CH_2), 1.80 (24H, s, *ortho*-CH_3 Mes). ^{13}C NMR (CD_2Cl_2, 75 MHz, 298 K): δ_C 186.6 (NCN), 182.0 (CO), 162.1 (q, $^{1}J_{CB}$ = 49.7 Hz, BC $[BAr^f_4]^-$), 142.3 (NC Mes), 138.0 (*para*-C Mes), 135.2 (br, *ortho*-CH $[BAr^f_4]^-$), 134.8 (*ortho*-C Mes), 130.9 (*meta*-CH Mes), 129.4 (m, *meta*-C $[BAr^f_4]^-$), 124.9 (q, $^{1}J_{CF}$ = 270.8 Hz, CF_3 $[BAr^f_4]^-$), 117.8 (m, *para*-CH $[BAr^f_4]^-$), 49.8 (NCH_2), 21.3 (NCH_2CH_2), 21.2 (*para*-CH_3 Mes), 18.0 (*ortho*-CH_3 Mes). Accurate mass ($[C_{46}H_{56}N_4{}^{191}IrO_2]^+$): 889.4033 (meas.), 889.4030 (calc.). IR (CD_2Cl_2, ν(CO)/cm^{-1}): 1985.

*Preparation of [(6-Mes)$_2$Ir(CO)$_2$(H)$_2$][BAr$^f{}_4$] (**18**)*

A solution of **17** (33 mg, 0.02 mmol) in CD_2Cl_2 (0.6 cm^3) was degassed by the freeze-pump-thaw method. The tube was then immersed in liquid nitrogen, and the head space back-filled with H_2 gas. After sealing, the tube was allowed to warm to room temperature accompanied by a colour change from bright orange to pale yellow. Due to spontaneous hydrogen loss in an argon atmosphere, this complex was not isolated as a solid but ^{1}H NMR spectroscopy suggested quantitative conversion.

*Spectroscopic data for **18***

^{1}H NMR (CD_2Cl_2, 300 MHz, 298 K): δ 7.71 (8H, s, *ortho*-CH [BAr$^f{}_4$]$^-$), 7.55 (4H, s, *para*-CH [BAr$^f{}_4$]$^-$), 6.92 (8H, s, *meta*-CH Mes), 3.31 (8H, tr, $^3J_{HH}$ = 6.2 Hz, NCH_2), 2.33 (12H, s, *para*-CH_3 Mes), 2.11 (4H, m, NCH_2CH_2), 1.89 (24H, s, *ortho*-CH_3 Mes), -9.83 (2H, s, IrH). IR (CD_2Cl_2, ν(CO)/cm^{-1}): 2058, 2017.

*Preparation of [(6-Mes)(6-Mes')Ir(H)(CN^{t}Bu)$_2$][BAr$^f{}_4$] (**19**)*

Tert-butyl isocyanide (0.019 cm^3, 0.17 mmol) was added to a stirred solution of **14a** (117 mg, 0.07 mmol) in fluorobenzene (15 cm^3). The solution paled from orange to yellow rapidly and was stirred for a further 10 min. Volatiles were removed *in vacuo* and the residue was washed with hexanes (2 x 15 cm^3). Drying *in vacuo* yielded the product as a pale yellow powder in 63% yield (82 mg). Crystals suitable for X-ray crystallography were obtained from a dichloromethane/hexane layering at -30 °C.

*Spectroscopic data for **19***

^{1}H NMR (CD_2Cl_2, 400 MHz, 298 K): δ_H 7.73 (8H, s, *ortho*-CH [BAr$^f{}_4$]$^-$), 7.57 (4H, s, *para*-CH [BAr$^f{}_4$]$^-$), 7.08 (1H, s, *meta*-CH Mes'), 7.04, 6.92, 6.86, 6.85, 6.78, 6.60 (1H, s, *meta*-CH Mes), 6.43 (1H, s, *meta*-CH Mes'), 3.75 (1H, m, NCH_2), 3.56 (1H, m, NCH_2), 3.38 (1H,

m, NCH_2), 3.27 (2H, m, NCH_2), 3.15 (1H, m, NCH_2), 3.06 (2H, m, NCH_2), 2.70 (3H, s, *para*-CH_3 Mes), 2.41 (3H, s, *para*-CH_3 Mes'), 2.36 (3H, s, *para*-CH_3 Mes), 2.32 (1H, obscured signal, $IrCH_2$), 2.27 (3H, s, *para*-CH_3 Mes), 2.27 (6H, s, *ortho*-CH_3 Mes), 2.20 (1H, obscured signal, $IrCH_2$), 2.18 (3H, s, *ortho*-CH_3 Mes), 2.14 (3H, s, *ortho*-CH_3 Mes), 2.09 (3H, s, *ortho*-CH_3 Mes'), 1.99 (2H, m, NCH_2CH_2), 1.75 (3H, s, *ortho*-CH_3 Mes), 1.47 (3H, s, *ortho*-CH_3 Mes), 1.43 (2H, m, NCH_2CH_2), 1.37 (9H, s, CH_3 ^{t}Bu), 1.02 (9H, s, CH_3 ^{t}Bu), -12.10 (1H, s, IrH). ^{13}C NMR (CD_2Cl_2, 125 MHz, 298 K): δ_C 192.2 (s, NCN), 185.0 (s, NCN), 162.3 (q, $^1J_{CB}$ = 49.6 Hz, CB $[BAr^f_4]^-$), 153.1 (s, CN ^{t}BuNC), 150.4 (s, CN ^{t}BuNC), 146.3, 146.0 (s, NC Mes), 145.0 (s, NC Mes'), 137.4, 137.0 (s, *para*-C Mes), 136.5 (s, *para*-C Mes'), 136.3 (s, *para*-C Mes), 135.7, 135.6 (s, *ortho*-C Mes), 135.4 (m, *ortho*-CH $[BAr^f_4]^-$), 134.5, 134.0 (s, *ortho*-C Mes), 133.9 (s, *ortho*-C Mes'), 131.6 (s, *meta*-CH Mes'), 131.0, 130.4, 130.3 (s, *meta*-CH Mes), 129.4 (m-qt, $^2J_{CF}$ = 31.3 Hz, *meta*-C $[BAr^f_4]^-$), 128.1 (s, *meta*-CH Mes), 126.7 (s, *meta*-CH Mes'), 125.2 (qt, $^1J_{CF}$ = 271 Hz, CF_3 $[BAr^f_4]^-$), 123.6 (s, *ortho*-C Mes'), 118.1 (m, *para*-CH $[BAr^f_4]^-$), 57.5 (s, C-^{t}Bu), 56.1 (s, C-^{t}Bu), 51.5, 50.9, 50.3, 48.2 (s, NCH_2), 30.9 (s, CH_3-^{t}Bu), 30.0 (s, CH_3-^{t}Bu), 24.9, 23.6, 23.2 (s, *para*-CH_3 Mes), 21.3 (s, *para*-CH_3 Mes'), 21.3 (s, NCH_2CH_2), 21.1 (s, *ortho*-CH_3 Mes'), 20.7 (s, *ortho*-CH_3 Mes), 20.5 (s, NCH_2CH_2), 20.0, 19.3, 19.0, 18.7, 17.9 (s, *ortho*-CH_3 Mes), -9.6 (s, $IrCH_2$). MS (ESI +ve): *m/z* calc. for $C_{67}H_{81}IrN_6$ 999.5603; meas. 999.5601 (M^+, 65%), 916.49 ([M-^{t}BuNC]$^+$, 80%), 833.41 ([M-2(^{t}BuNC)]$^+$, 100%);. Elemental analysis: calc. for $C_{89}H_{93}IrN_6BF_{24}$: C 55.45, H 4.65, N 4.51, meas. C 54.52, H 4.67, N 4.47.

*Crystallographic data for **19***

$C_{89}H_{93}IrN_6BF_{24}$, M_r = 1905.74, triclinic, *P*-1, a = 12.8704(2), b = 17.9170(2), c = 20.7465(2) Å, α = 88.3024(9), β = 88.3952(9), γ = 79.2935(10) °, V = 4697.54(10) Å^3, Z = 2, ρ_c = 1.347 Mg m^{-3}, T = 150 K, λ = 1.54180 Å, 19495 reflections collected, 19495

independent [R(int) = 0.034], which were used in calculations. R_1 = 0.0459, wR_2 = 0.1078 for observed unique reflections [$I > 2\sigma(I)$] and R_1 = 0.0471, wR_2 = 0.1088 for all unique reflections. Max. and min. residual electron densities 1.92 and -1.62 e $Å^{-3}$.

4.3 Reactivity of 5-Mes Supported Iridium Cations

4.3.1 Attempted Isolation of the 'Naked' Cationic Species

Attempts were made to try and isolate the active 14-electron fragments resulting from halide abstraction from (5-Mes)(5-Mes')IrHCl (**2**) and $(5\text{-Mes})_2IrH_2Cl$ (**3**) in the absence of any coordinating species. Initial attempts in CD_2Cl_2 resulted in a darkening of the solution and a highly complex ^1H NMR spectrum, suggesting possible reaction with the solvent. Reaction of **2** with $Na[BAr^f_4]$ in C_6D_5Br led to more promising observations. The solution colour paled from red to orange, and this was accompanied by a downfield shift of the hydride signal in the ^1H NMR spectrum to δ_H -16.28 ppm (from δ_H -32.81). Perhaps more interestingly, a broad signal emerged at δ_H 1.49 ppm as a potential indication of the presence of an agostic interaction with the metal centre involving a mesityl *ortho*-methyl group (*vide infra*). However a species of the type $[(5\text{-Mes})(5\text{-Mes}')IrH][BAr^f_4]$ (**9**) has not yet been isolated due to its extreme instability towards air, moisture and chlorinated solvents, so precise details cannot be confirmed. However, DFT calculations by Miss Lucy Treasure support the proposal of an agostically stabilised species like **9**.

Halide abstraction was also attempted from complex **3** in the absence of any coordinating species. Previous chemistry reported by our group using the related IMes complex, show that the sodium ion from $Na[BAr^f_4]$ is retained and lies between the mesityl rings in forming $[(IMes)_2Ir(H)_2(Cl)\{Na\}][BAr^f_4]$.[9] In an attempt to abstract the chloride from **3**, $Na[BAr^f_4]$ was introduced and the system was heated to 60 °C for 24 h as no change in spectroscopic data was observed at ambient temperatures. ^1H NMR spectra revealed a

broadening of the hydride signal over this time; however, the complex appeared to degrade in CD_2Cl_2 solution. A crude X-ray structure was obtained of a complex which appears to be a decomposition product. This featured a square-planar iridium centre bearing two NHCs and two *trans*-atoms, postulated to be chlorides although this structure could not be refined fully. This serves as indication for the potential synthesis of a highly reactive species, potentially of the type $[(5\text{-Mes})_2IrH_2][BAr^f_4]$ (**10**), unfortunately the structure collected does not confirm the formation of **10**.

4.3.2 Trapping 14-electron Fragments with Amine-Boranes

Fragments of the type $[(NHC)_2IrH_2]^+$ have been reported to coordinate and dehydrogenate amine-borane species, of the type $H_3B{\cdot}NHR_2$.[9] The complex $(5\text{-Mes})_2IrH_2Cl$ (**3**) is a potential precursor to such a fragment when taken with a halide abstraction agent, such as $Na[BAr^f_4]$. In order to compare reactivity with the previously reported complexes $[(IMes)_2Ir(H)_2\{H_3B{\cdot}NRMe_2\}][BAr^f_4]$ (R = H, Me),[9, 15] the reactions of **3**/$Na[BAr^f_4]$ were therefore investigated with $H_3B{\cdot}NMe_3$ and $H_3B{\cdot}NHMe_2$.

The reaction of **3**/$Na[BAr^f_4]$ with $H_3B{\cdot}NMe_3$ results in a shift in the ^{11}B NMR signal from δ_B -8.1 to 13.0 ppm and in the observation of a broad hydride resonance at δ_H -2.11 ppm in the ^1H NMR spectrum suggesting coordination of the borane at iridium through the B-H bonds. Elucidation of the structure via X-ray crystallography confirmed the formation of a κ^2-coordination complex (Fig 4.4). Due to the lack of β-hydrogens the amine borane fragment shows no sign of dehydrogenation.

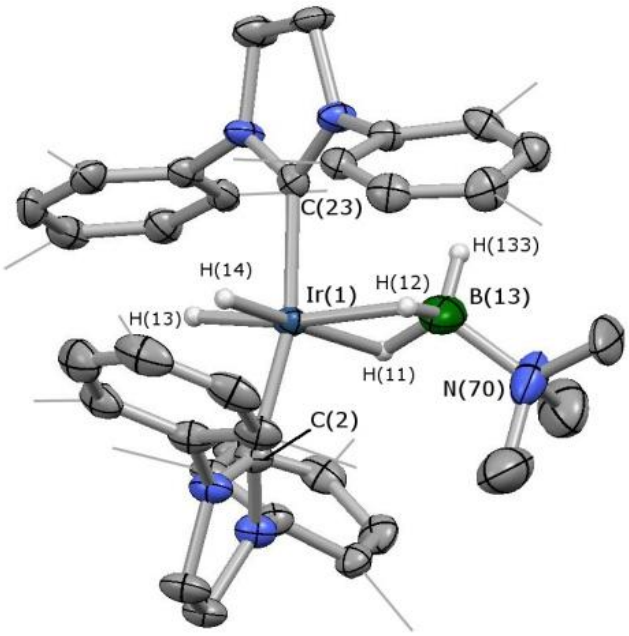

Figure 4.4: $[(5\text{-Mes})_2IrH_2\{H_3BNMe_3\}][BAr^f{}_4]$ (**11**), with $[BAr^f{}_4]^-$ anion omitted, most H atoms omitted and Me groups shown in wireframe for clarity; thermal ellipsoids set at 50% probability level. Ir-H located in the Fourier difference map and refined isotropically. Key bond lengths (Å) and angles (°): Ir(1)–C(2) 2.039(7), Ir(1)–C(23) 2.042(7), Ir(1)···B(13) 2.24(1), B(13)–N(70) 1.55(1), Ir(1)–H(11) 1.87, Ir(1)–H(12) 1.85, Ir(1)–H(13) 1.60, Ir(1)–H(14) 1.66, C(2)–Ir(1)–C(23) 166.2(3), Ir(1)···B(13)–N(70) 138.8(8).

The structural metrics for **11** (Fig 4.4) are statistically identical to those of the corresponding IMes complex, $[(IMes)_2IrH_2\{H_3BNMe_3\}][BAr^f{}_4]$.[9] The Ir···B separation 2.24(1) Å [*cf.* 2.230(2) Å] suggests no significant increase in interaction between the iridium and boron centres for **11** over the IMes supported system. In support of the inert nature of the coordination of tertiary amineboranes to metal centres, the B–N distance of 1.55(1) Å [*cf.* 1.581(1) Å] implies there is no change in bond order. In further support of an intact amine-borane ligand, the Ir···B–N angle is found to be significantly deviated from linear [138.8(8)°] implying a tetrahedral borane centre. The presence of the amine-borane ligand causes a distortion of the geometry around the iridium from octahedral, characterised

by a non-linear C_{NHC}–Ir–C_{NHC} angle of 166.2(3)° consistent with a relatively crowded metal centre.

Reaction of $H_3B{\cdot}NHMe_2$ also proceeded in a fashion consistent with previously reported observations of dehydrogenation chemistry.[15] In the ^{11}B NMR spectrum there is evidence for coordination of the secondary amineborane fragment (δ_B 10.8 ppm) as well as a component corresponding to coordinated aminoborane (very broad resonance at δ_B 48.2 ppm). The ^{1}H NMR spectrum is consistent with highly symmetrical NHC environments, suggesting no interaction of the 5-Mes with the metal or the boron via agostic or C–H activation. The two components observed in the ^{11}B NMR spectrum co-crystallised; thus, both complexes were fully characterised by both X-ray and neutron diffraction (Fig 4.5).

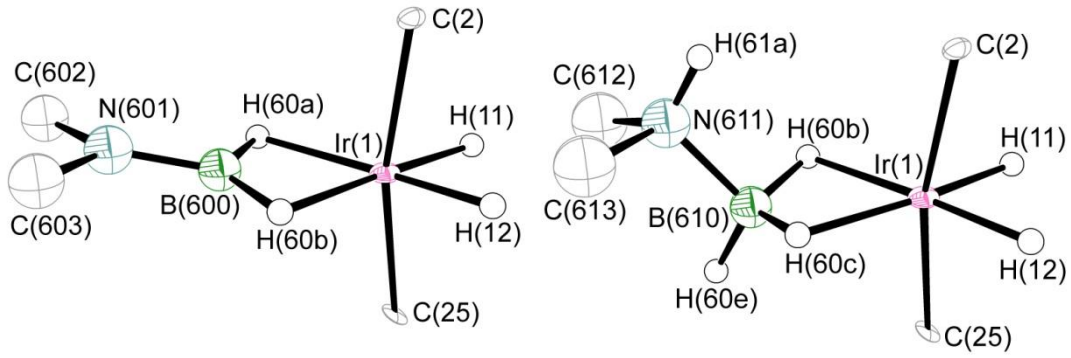

Figure 4.5: Neutron diffraction structures for $[(5\text{-Mes})_2IrH_2\{H_2BNMe_2\}][BAr^f{}_4]$ (*left*, **12i**) and $[(5\text{-Mes})_2IrH_2\{H_3B{\cdot}NHMe_2\}][BAr^f{}_4]$ (*right*, **12ii**), with $[BAr^f{}_4]^-$ anion and most H atoms omitted, Me groups shown in wireframe for clarity; thermal ellipsoids set at 50% probability level. Hydrogen atoms accurately located and refined anisotropically. Key bond lengths (Å) and angles (°) are reported below (Table 4.6) for both X-ray and neutron diffraction studies.

	12i		**12ii**	
	X-ray	Neutron	X-ray	Neutron
Ir(1)–C(2)	2.050(4)	2.039(7)	2.050(4)	2.039(7)
Ir(1)–C(25)	2.047(3)	2.041(6)	2.047(3)	2.041(6)
Ir(1)–H(11)	-	1.55(2)	-	1.55(2)
Ir(1)–H(12)	-	1.53(2)	-	1.53(2)
Ir(1)–H(60)	-	1.83(3), 1.87(3)	-	1.87(6), 1.75(7)
Ir(1)···B	2.15(1)	2.07(2)	2.19(2)	2.21(4)
B–H(60)	-	1.33(4), 1.28(3)	-	1.21(6), 1.29(8)
B–N	1.26(1)	1.40(2)	1.51(2)	1.55(3)
C(2)–Ir(1)–C(25)	167.9(1)	167.5(3)	167.9(1)	167.5(3)
Ir(1)···B–N	174(1)	171(1)	127(1)	125(2)

Table 4.6: Key bond lengths (Å) and angles (°) for the coordinated H_2BNMe_2 and $H_3B{\cdot}NHMe_2$ components in **12i** and **12ii**.

Modelling of the two borane components in the crystal structure is consistent with a ratio of aminoborane to amineborane adduct of 57:43 by X-ray crystallography and 65:35 by neutron diffraction. There are very few examples of neutron diffraction studies of the coordination and activation of B–H bonds at metal centres.[15-17] The structure of the coordinated amineborane component is, to our knowledge, the first example of such a system to be characterised by neutron diffraction.

Inspection of the X-ray structure reveals that the amineborane component has a B–N distance [1.51(2) Å] which is longer than that found in the coordinated aminoborane [1.26(1) Å], but identical to the coordinated $H_3B{\cdot}NMe_3$ fragment found in **11** [1.55(1) Å]. This is largely as expected, due to the hybridisation in the aminoborane being *ca.* sp^2; thus the B–N bond has some double bond character due to donation from N to B. Consistent with previously reported examples, the amineborane complex has a bent Ir···B–N framework [127(1)°], compared to the near linear aminoborane coordination [174(1)°].

Interestingly, there appears to be no significant change in the bridging B–H and Ir–H distances between the coordination of the aminoborane [*d*(B–H) = 1.33(4), 1.28(3) Å and *d*(Ir–H) = 1.83(3), 1.87(3) Å] and amineborane ligands [*d*(B–H) = 1.21(6), 1.29(8) Å and *d*(Ir–H) = 1.87(6), 1.75(7) Å]. Thus, the κ^2-coordination defined by the Ir(μ-H)$_2$B unit is essentially identical in both **12i** and **12ii**. Additionally, the Ir···B separations are statistically identical [2.07(2) and 2.21(4) Å]. These may suggest that the two ligands bind to the metal with similar strength and might compete for coordination.

4.3.3 Ammonia-Borane Dehydrogenation

When taking a mixture of **3**/Na[BAr$^f_4$] with ammonia-borane ($H_3B{\cdot}NH_3$), monitoring by ^{11}B NMR showed rapid formation of borazine (δ_B 30.4 ppm) resulting from the removal of 2 equivalents of H_2. A broad signal at δ_B 3.9 ppm was also identified, and assigned to coordinated ammonia-borane or an oligomer of ammonia-borane. After 12 h, there was an additional signal forming at δ_B -37.2 ppm due to (5-Mes)BH_3. Unfortunately, it appears that this system degrades in a similar fashion observed with the IMes ligated complex.

After 7 d, the signal in the ^{11}B NMR spectrum at δ_B -37.2 ppm had increased in intensity significantly indicating continued NHC–Ir cleavage. The ^{11}B NMR signal at δ_B

3.9 ppm had disappeared, supporting the notion that this was due to coordinated ammonia-borane or related species. It was also suggested that there was complete degradation of the catalyst as residual ammonia-borane starting material could still be observed at δ_B -21.2 ppm. An even stronger NHC–Ir bond appears to be necessary to maintain the stability of the catalyst during this process.

4.4 Cationic Fragments from Expanded Ring NHC Complexes

Given the ability of CH_2–Ir bonds to act as a hydrogen sink, it was an initial aim to maintain the metallocycles observed in (6-Mes')$_2$IrH (**4a**) to aid in the dehydrogenation of amine-borane substrates. A cationic fragment similar to the doubly cyclometallated complex [(I^{t}Bu')$_2$Ir]PF_6 reported by Nolan *et al.* was a target system.[18] Starting with a system such as **4a** means that to form a cationic species, a hydride abstraction agent is required. The widely available trityl (Ph_3C^+) cation was used in an attempt to remove the hydride ligand from **4a** (Scheme 4.7).

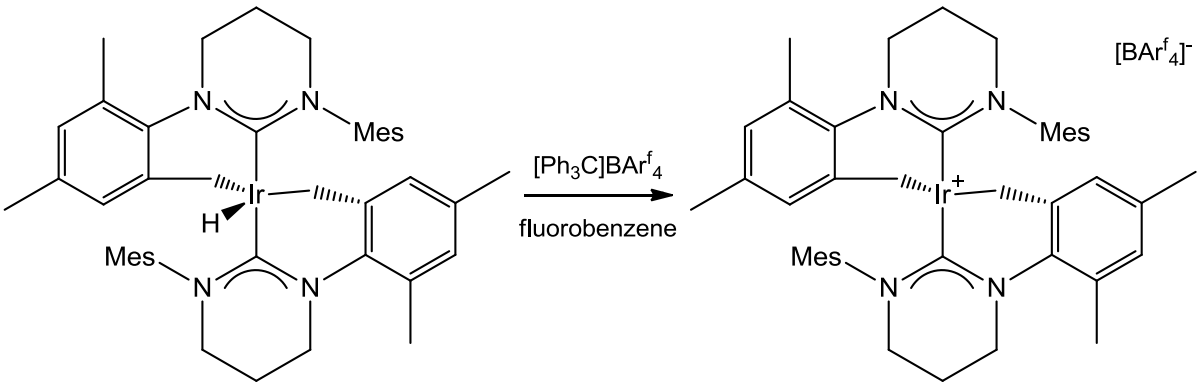

4a

Scheme 4.7: Attempt at hydride abstraction from **4a** to form the cationic product.

Monitoring the reaction by ^{1}H NMR showed the appearance of two new, low field hydride resonances (δ_H -17.59 and -30.87 ppm) and an increased number of resonances corresponding to the methyl protons, from five to twelve. For the hydride abstraction product, one would expect a spectrum not dissimilar from **4a**, hence it was to be believed

this was not a simple abstraction reaction. Subsequent isolation and X-ray analysis of single crystals provides a rationale for the spectroscopic observations. The structure shows an iridium centre bearing two hydride ligands and two *trans*-(6-Mes) ligands, one of which has a "Ph_3C" fragment incorporated into an *ortho*-methyl group.

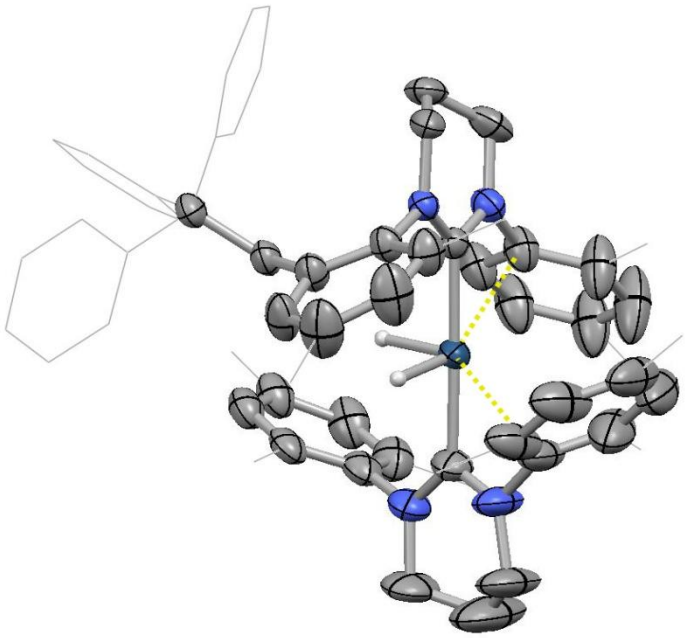

Figure 4.8: [(6-Mes^{CPh_3})(6-Mes)IrH_2][BAr^F_4] (**13**), with [BAr^F_4]$^-$ anion omitted, most H atoms omitted, and Ph of Ph_3C fragment and Me groups shown in wireframe for clarity; thermal ellipsoids set at 50% probability level. Ir–H located in the Fourier difference map and refined isotropically. Poor data does not allow accurate measurements of metrics.

This structure is of poor quality, however it does allow the connectivity to be determined and shows the incorporation of the trityl fragment into the *ortho*-methyl group of one of the mesityl rings. This reactivity can be rationalised if the trityl cation acts as an electron acceptor (it is widely used as an oxidising agent) with metal hydrides as in the mechanism proposed by Bullock *et al*. for hydride abstraction from molybdenum hydrides (Scheme 4.9).[19] Further evidence for this postulate is the identification of Gomberg's dimer

in the ^{1}H NMR spectrum, which is presumably formed in the termination step when two trityl radicals combine.[20]

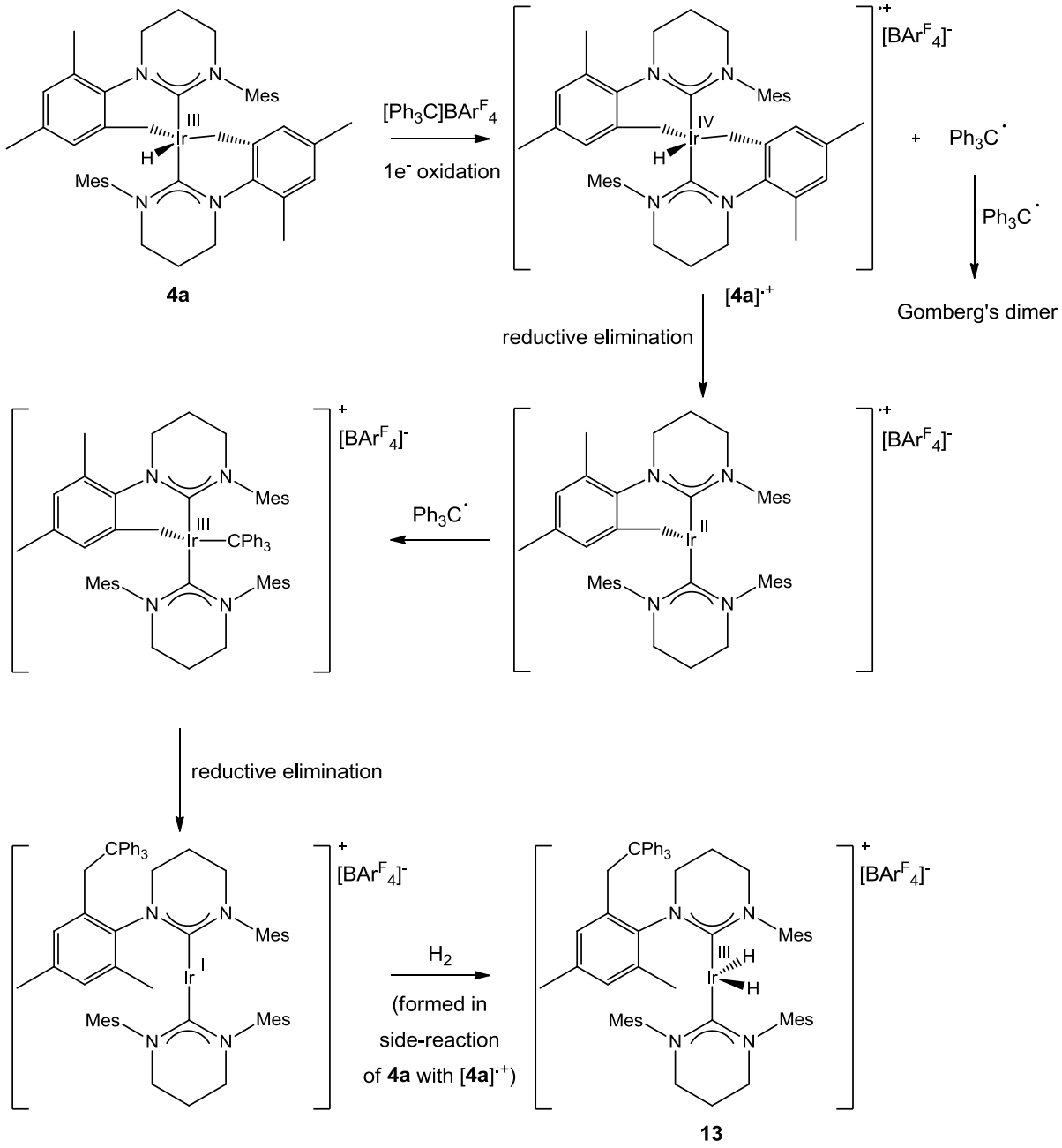

Scheme 4.9: Proposed mechanism for the inclusion of the trityl fragment based on the mechanism reported by Bullock *et al*. for abstraction from Mo-H complexes.

Clearly, this is not an efficient route for the formation of a 14-electron cation as it was isolated in poor yield. Inclusion of the trityl fragment also adds to the steric congestion at the metal, hence this is not a suitable system to carry forward. Abstraction of a hydride using Ph_3C^+ was also attempted from $(6\text{-Mes})_2IrH_3$ (**5a**) which appeared to proceed more cleanly by ^1H NMR. Although the product of this precise reaction was not structurally characterised by X-ray crystallography, it was identified as **15a** (reported later in §4.6) by ^1H NMR spectroscopy. The lack of M–CH_2 bonds in this system presumably reduces the number of alternative reaction pathways.

4.5 Addition of $[H(OEt_2)_2]^+[BAr^f_4]^-$ to $(NHC')_2IrH$

Precursors to 14-electron metal fragments bearing 5-membered NHCs were each of the form $(NHC)_2IrH_2Cl$, much like complex **8,** $(6\text{-Mes})_2IrH_2Cl$. However, initial halide abstraction reactions from **8** in the presence of an aminoborane did not provide conclusive evidence of a coordination complex, thus a different approach was employed.

Protonation of systems of the type $(NHC')_2IrH$ using HCl was shown to reintroduce a chloride ligand to the metal. The standard approach to the 14-electron metal cation involves abstraction of this chloride, but if the acid did not deliver a halide then abstraction would not be necessary. Brookhart's acid, $[H(OEt_2)_2][BAr^f_4]$, is a source of H^+ but contains a weakly-coordinating anion. Therefore, we hypothesised that the product of the protonation of $(6\text{-Mes}')_2IrH$ (**4a**) should be similar to that of halide abstraction from (6-Mes)(6-Mes')IrHCl (**6**).

The ^1H NMR spectrum of the product of protonation of **4a** is consistent with a highly symmetrical system and no hydride signal is observed. One would expect the spectrum to be similar to that of **6**, but the observed pattern is closer to that of **4a**. It was then found that on cooling the sample to below -20 °C resulted in the emergence of a

hydride resonance and increased complexity of the entire ^{1}H NMR spectrum. In the low temperature limit, the resonance for the iridium bound H is located at δ_H -31.06 ppm. An upfield-shifted methyl signal is apparent at δ_H 0.61 ppm consistent with an agostic interaction with the iridium centre.

It is apparent that in solution [(6-Mes)(6-Mes')IrH][BAr$^f_4$] (**14a**) exhibits rapid fluxional interconversion between the agostic interaction and C–H activation resulting in a simple ^{1}H NMR spectrum with broadening of some methyl signals and an absent hydride resonance (Fig 4.10).

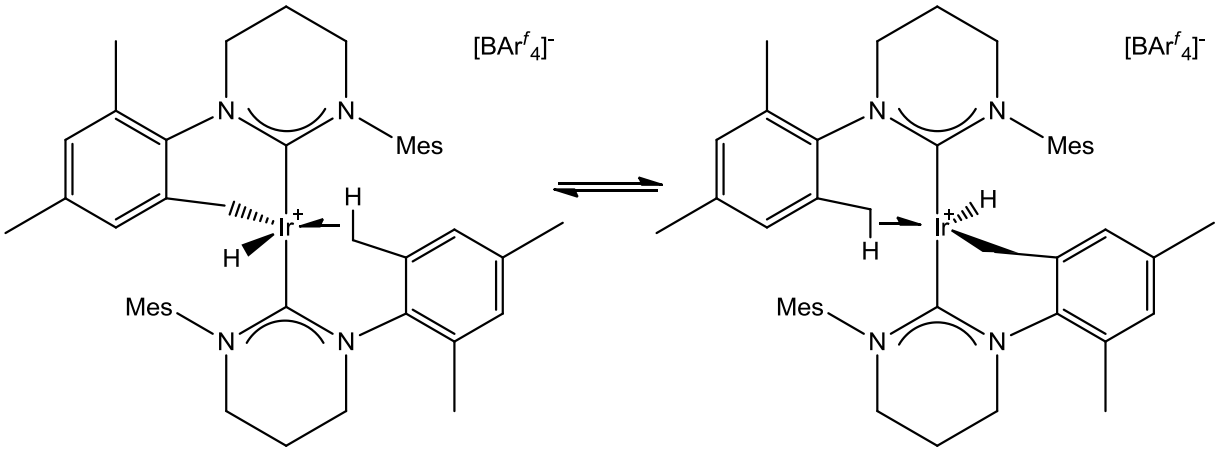

Figure 4.10: Dynamic equilibrium between structures of **14a**.

Despite this fluxionality being observed implying agostic stabilisation and a signal in the ^{1}H NMR spectrum (δ_H = 0.61 ppm) as evidence for an agostic interaction, the crystal structure does not initially appear to support the ^{1}H NMR data (Fig 4.11). There is no clear evidence of any potential agostic C–H bond interacting with the metal cation. In fact, there appears to be close approach of the aryl system of the mesityl ring to the metal centre. This could be the result of crystal packing forces contradicting the observation of agostic interactions in solution.

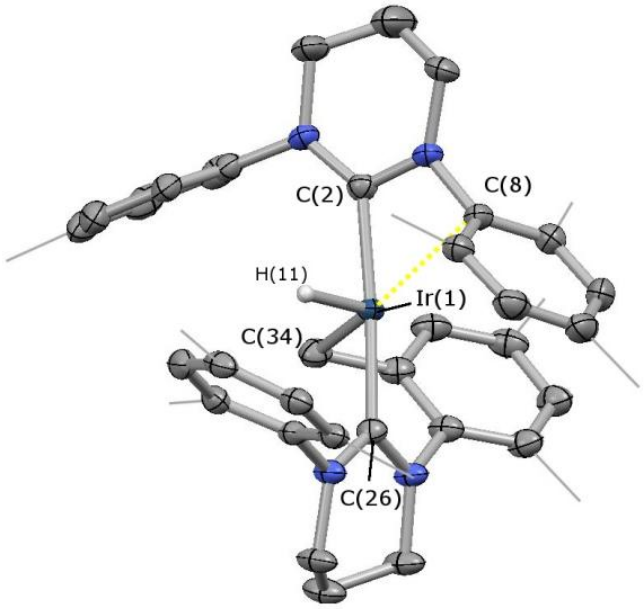

Figure 4.11: [(6-Mes)(6-Mes')IrH][BAr^f_4] (**14a**), with [BAr^f_4]$^-$ anion omitted, most H atoms omitted and Me groups shown in wireframe for clarity; thermal ellipsoids set at 50% probability level. Ir–H located in the Fourier difference map and refined isotropically. Key bond lengths (Å) and angles (°): Ir(1)–H(11) 1.50, Ir(1)–C(2) 2.059(3), Ir(1)–C(26) 2.049(3), Ir(1)–C(34) 2.066(4), Ir(1)$^{\cdots}$C(8) 2.512(3), C(2)–Ir(1)–C(26) 174.7(1).

In the solid state, the structure adopted displays a 14-electron cationic metal centre stabilised by an interaction with the π-system of one of the mesityl rings as manifested by a short Ir$^{\cdots}C_{ipso}$ contact of 2.512(3) Å [for C(8)]. Solution phase infra-red data obtained from **14a** showed a weak absorption at 2548 cm^{-1}, supporting the existence of an agostic interaction in solution.[21] Low temperature protonation of (6-Mes')$_2$IrH **4a** with Brookhart's acid displayed a signal at δ_H 0.54 ppm, consistent with the presence of the agostic interaction in the ^{1}H NMR spectrum. This experiment additionally confirms that the benzylic tether is protonated and not the hydride, which would form a dihydrogen complex.

Somewhat surprisingly, this complex was able to be recrystallised from wet, bench solvents. A crystal structure was obtained and the structure is identical to that obtained from dry solvents. It is remarkable that this 14-electron species is resistant to the coordination of water, although it is less promising for its role as a catalytic species.

Similar behaviour was observed for the protonation of (7-Mes')$_2$IrH (**4b**) and (6-Xyl')$_2$IrH (**4c**), although the structure obtained in the case of 7-Mes confirms the presence of an agostic interaction in the solid state. Perhaps the increased size of the ligand allows for more movement of the mesityl ring within the lattice, or crystal packing forces act differently on this complex.

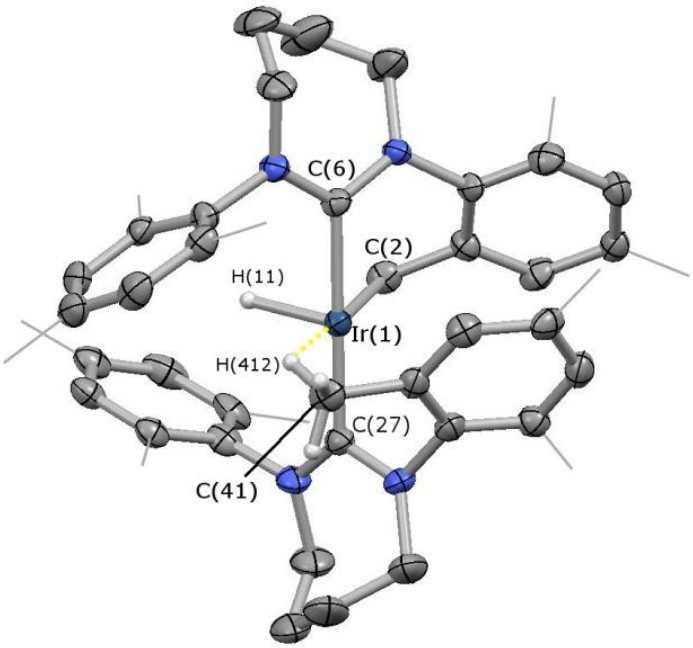

Figure 4.12: [(7-Mes)(7-Mes')IrH][BAr$^f_4$] (**14b**), with [BAr$^f_4$]$^-$ anion omitted, most H atoms omitted and Me groups shown in wireframe for clarity; thermal ellipsoids set at 50% probability level. Ir–H located in the Fourier difference map and refined isotropically. Key bond lengths (Å) and angles (°): Ir(1)–H(11) 1.66, Ir(1)–C(2) 2.063(8), Ir(1)–C(6) 2.072(6), Ir(1)–C(27) 2.051(7), Ir(1)$^{\cdots}$H(412) 1.98, Ir(1)$^{\cdots}$C(41) 2.546(8), C(6)–Ir(1)–C(27) 177.7(3), C(2)–Ir(1)$^{\cdots}$H(412) 177.8(2).

The ^{1}H and ^{13}C spectra display distinct resonances for the 7-Mes ligands below -35 °C suggesting that the barrier to activation of a C–H bond in this system must be relatively low. Variable temperature ^{1}H NMR studies were carried out on **14a** and **14b** to establish and compare the kinetics of the interconversion between the degenerate complexes stabilised by agostic interactions from opposite NHCs. Three potential mechanisms were postulated for consideration against the thermodynamic parameters found from the full variable temperature analysis.[22]

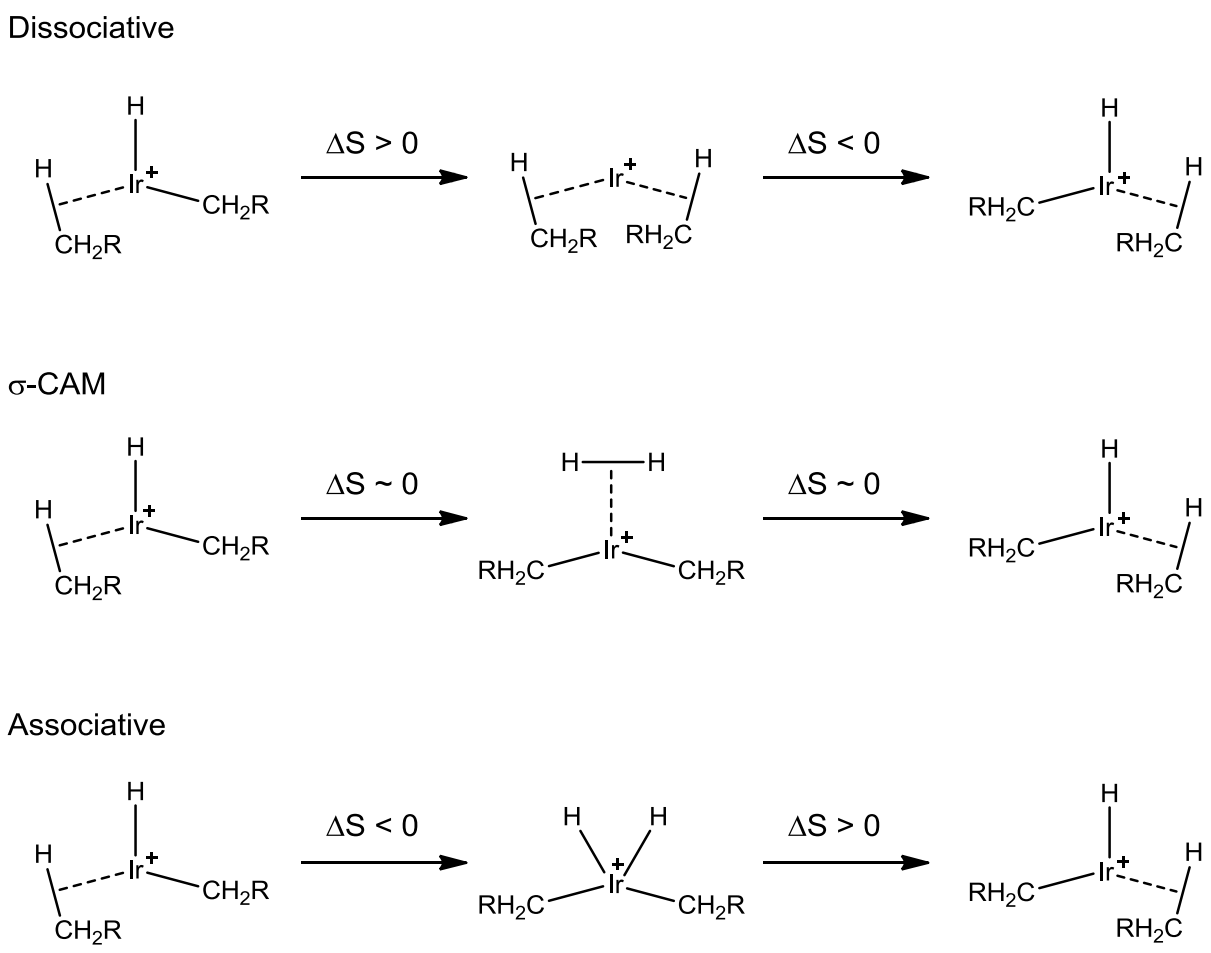

Scheme 4.13: Possible mechanisms for the exchange involving Ir(I), Ir(III) and Ir(V) intermediate species.

Coalescence temperatures for the aromatic signals in **14a** and **14b** varied slightly, T_c was found to be -20°C and -35°C respectively. In the low temperature limit, resonances for the iridium bound H and CH_2 groups are resolved at δ_H -31.06, -28.59 and 1.65/2.32, 1.83/2.38 ppm for **14a** and **14b** respectively. For both cations, an upfield-shifted methyl signal is also apparent (at δ_H 0.61 and -0.24 ppm respectively), consistent with an agostic interaction with the iridium centre.

Correlation experiments, conducted by Dr Nick Rees, reveal that this exchange process only involves two of the eight possible methyl groups, i.e. there is no rotation of the mesityl rings or carbene unit during the timescale of the process. Line shape analysis allows exchange rates to be determined in the temperature range -25 to -55°C,[23] yielding an Eyring plot from which thermodynamic data could be extracted.

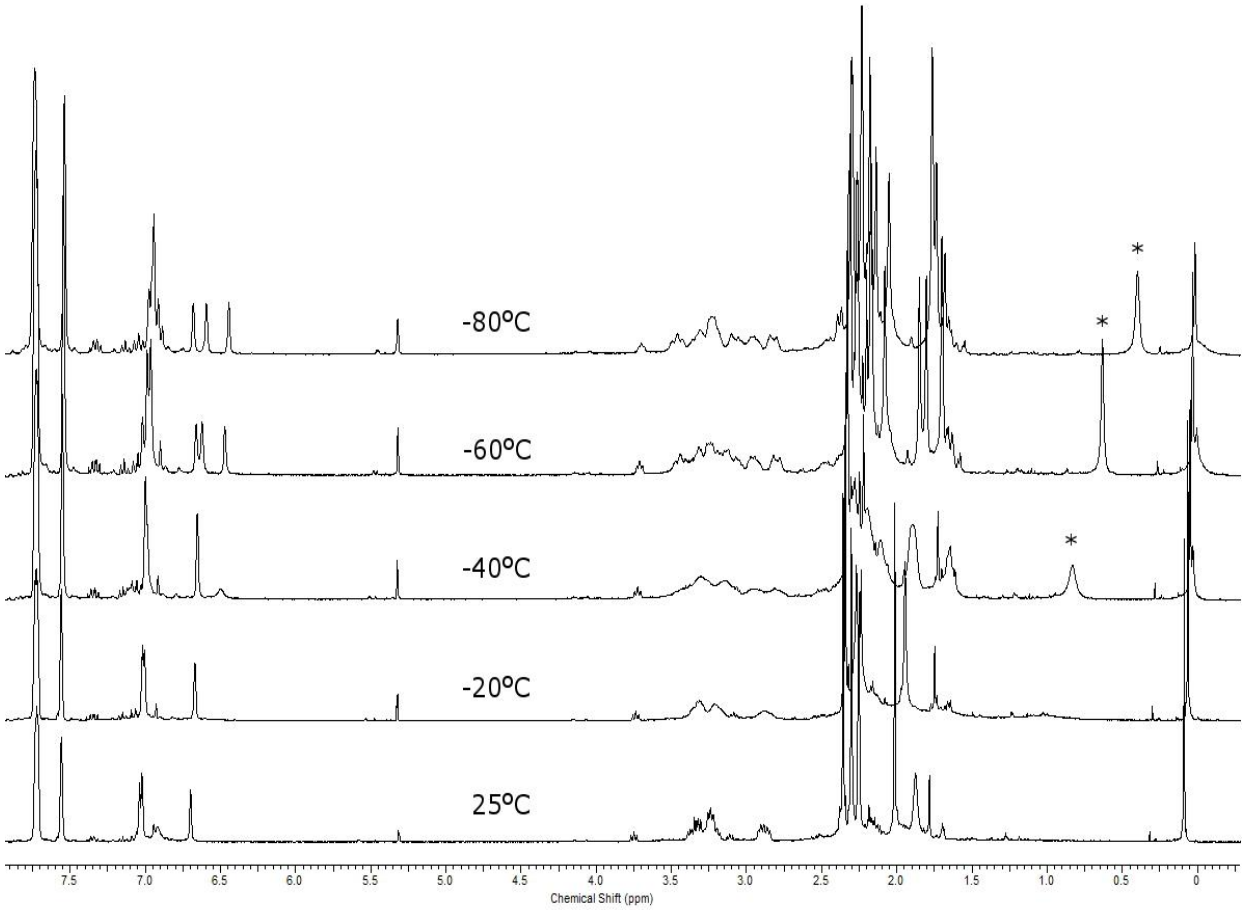

Figure 4.14: Stack plot of VT-^{1}H NMR spectra for **14a**; signal for emerging agostic CH_3 marked with *.

Analysis of this data for **14a** gave values for $\Delta H^{\ddagger}$ and $\Delta S^{\ddagger}$ of 8.8(0.4) kcal mol^{-1} and -12.2(1.7) eu, respectively. For **14b**, $\Delta H^{\ddagger}$ and $\Delta S^{\ddagger}$ were found to be 7.8(0.3) kcal mol^{-1} and -16.2(1.2) eu, respectively.

Given negative transition state entropies, and under the assumption that the rate limiting step is formation of the intermediate, this mechanism is postulated to be associative, with oxidative cleavage of the agostic C–H bond preceding, to some extent, reductive elimination of the CH_2–Ir–H unit. Comparative work by Bergman *et al.* has shown the conversion of rhodium alkane complexes to alkyl-hydrides proceeds with $\Delta H^{\ddagger}$ = 2.7±1 to 4.6±0.4 kcal mol^{-1} and $\Delta S^{\ddagger}$ = -7±6 to -16±5 eu.[24] However, our findings do not eliminate

the possibility of a σ-CAM mechanism taking place,[22] i.e. a concerted mechanism for hydride exchange as in $(PEtPh_2)_3Fe(H)_2(H_2)$.[25]

4.5.1 DFT Calculations

DFT calculations were carried out and represented graphically (in Fig 4.15 and 4.16) by Miss Lucy Treasure on **14a** and **14b** to provide support for the proposed mechanisms using PBE0 level of theory. An SDD basis set was used for iridium, SVP on atoms in the immediate coordination sphere and SV on all other atoms. A model system was used where one aromatic group was omitted and the aromatic group involved in the activation phenomenon contained just one *ortho*-methyl group, which is justified by the observation by ^{1}H NMR that there was no rotation or exchange of the methyl groups involved.

Initially, a dissociative pathway was considered beginning with the arene stabilised structure defined as the ground state (Fig 4.15). As predicted, in the case of **14b**, the agostic stabilisation provides a marginally lower ground state energy species. The mechanism then moves towards a reductive elimination transition state (TS_{RE}) ending at a *bis*-arene stabilised intermediate (P_{RE}).

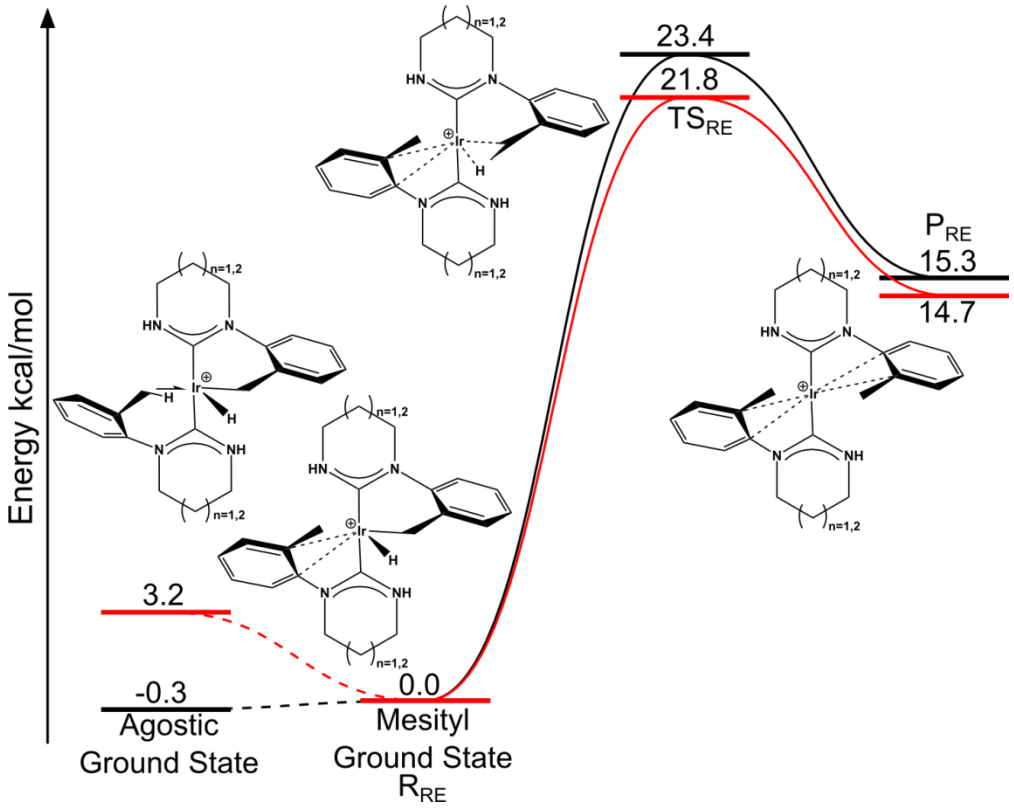

Figure 4.15: Energy pathway for the dissociative process, **14a** – black, **14b** – red.

For this mechanism, the calculated activation barriers ($\Delta H^{\ddagger}$) for **14a** and **14b** are 23.4 and 21.8 kcal mol^{-1}, respectively. Clearly, these values are significantly above the experimental values of 8.8 and 7.8 kcal mol^{-1}. In addition, the entropy changes ($\Delta S^{\ddagger}$) calculated by the DFT analyses are much less negative than the experimental data (-0.4 and 1.9 eu for **14a** and **14b** respectively, *cf.* -12.2 and -16.2 eu). This data supports the hypothesis that the mechanism is not a dissociative-type mechanism.

Attempts to find the 6-coordinate Ir(V) intermediate required for an associative mechanism failed to converge, however a dihydrogen type intermediate was found. This serves as a weak argument against the full associative process. Hence, the σ-CAM mechanism was analysed (Fig 4.16) starting from an agostic species; this C–H bond is observed to break early in the reaction profile ($TS1_{CAM}$). There is a shallow intermediate

0.9 kcal mol^{-1} below the transition state (I_{CAM}), but this is not dissimilar to the transition states.

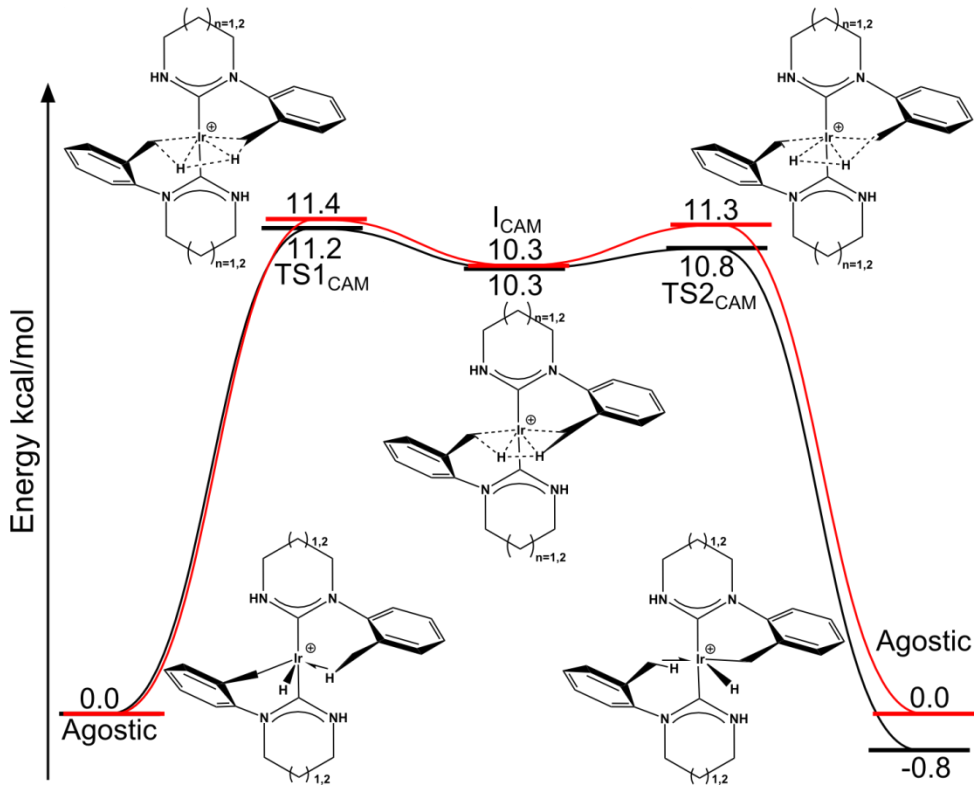

Figure 4.16: Energy profile for the σ-CAM mechanism, **14a** – black, **14b** – red.

The activation barriers here are much less endothermic than the dissociative case, 11.2 and 11.4 kcal mol^{-1} for **14a** and **14b**, respectively. In further support of this mechanism, the calculated activation entropies for **14a** and **14b** were -3.7 and -4.4 eu, respectively. Calculations indicate that the exchange process is likely to be a σ-CAM type mechanism.

4.6 Coordination of Amine-Boranes

Given the facile and reversible C–H activation of the *ortho*-methyl groups, the 14-electron fragments **14a** and **14b** may act as suitable hydrogen atom shuttles to aid the dehydrocoupling of amine-boranes. *N*,*N*-dimethyl amine-borane, $H_3B{\cdot}NHMe_2$, was reacted

with the two complexes and in each case no ^{11}B NMR signal remained, except for $[BAr^f_4]^-$, after washing the product with hexane. Sharp hydride resonances were observed in the ^{1}H NMR spectrum at δ_H -43.57 and -41.68 ppm respectively. Crystallisation of the reaction products explained the apparent lack of boron and simplified ^{1}H NMR spectrum (Fig 4.17).

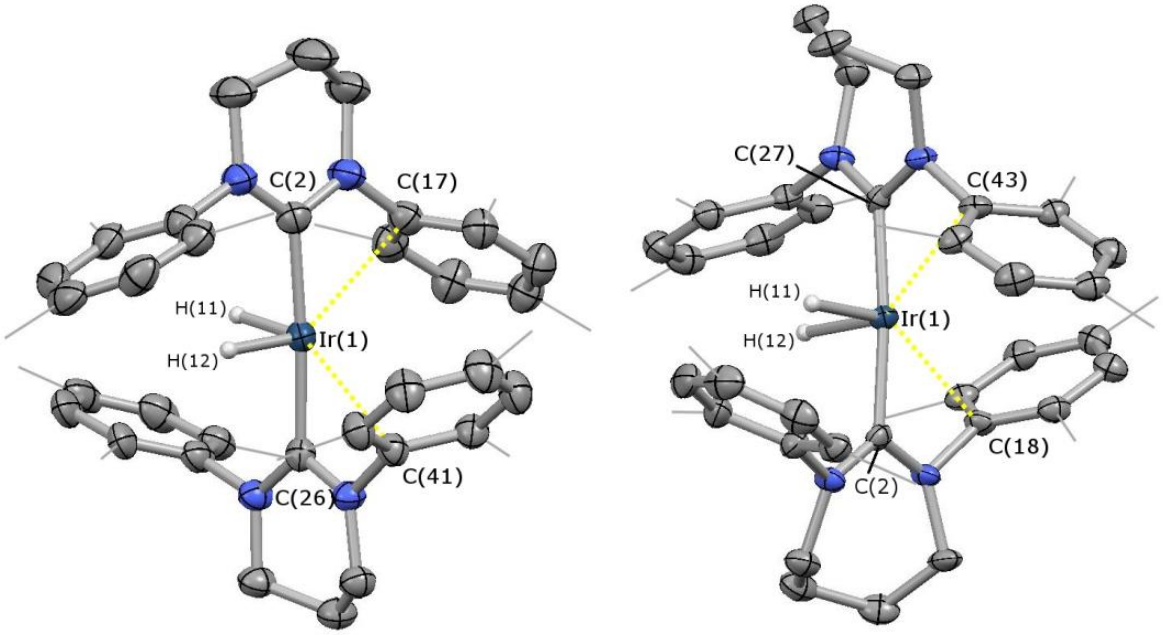

Figure 4.17: $[(6\text{-Mes})_2IrH_2][BAr^f_4]$ (*left*, **15a**) and $[(7\text{-Mes})_2IrH_2][BAr^f_4]$ (*right*, **15b**), with $[BAr^f_4]^-$ anion omitted, most H atoms omitted and Me groups shown in wireframe for clarity; thermal ellipsoids set at 50% probability level. Ir–H located in the Fourier difference map and refined isotropically. Key bond lengths (Å) and angles (°): (for **15a**) Ir(1)–H(11) 1.43, Ir(1)–H(12) 1.47, Ir(1)–C(2) 2.046(6), Ir(1)–C(26) 2.036(6), Ir(1)···C(17) 2.876(5), Ir(1)···C(41) 2.814(5), C(2)–Ir(1)–C(26) 176.0(2); (for **15b**) Ir(1)–H(11) 1.85, Ir(1)–H(12) 1.58, Ir(1)–C(2) 2.053(6), Ir(1)–C(27) 2.042(6), Ir(1)···C(18) 2.732(7), Ir(1)···C(43) 2.755(5), C(2)–Ir(1)–C(27) 174.8(2).

The amine-borane acts on the Ir–CH_2 fragment in fashion analogous to dihydrogen to produce this 14-electron iridium dihydride cation. C_{NHC}–Ir distances for **15a** and **15b** [2.046(6), 2.036(6) and 2.053(6), 2.042(6) Å respectively] are identical to those of their

precursors **14a** and **14b** [2.059(3), 2.049(3) and 2.063(8), 2.072(6) Å respectively]. Close approach of the aryl rings *trans* to the hydrides coupled with a significant distortion of the coordination angle of the NHC–Ir fragment supports the notion of π-stabilisation of the iridium centre. When there is no additional interaction of the NHC with the metal, coordination of the NHC would be expected to be symmetrical about the C_{NHC}–M bond. However, unsymmetrical coordination can occur when the NHC additionally interacts with the metal through the aryl system,[13] or even the nitrogens (Fig 4.18).[26]

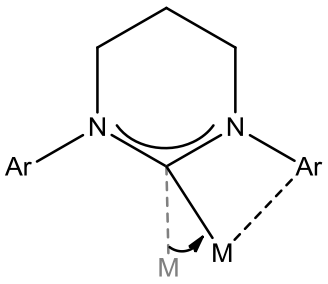

Figure 4.18: Deviation of the metal centre from symmetric coordination of the NHC.

Approach of the C_{ipso} to the iridium centre is on average 0.1 Å closer for **15b** than **15a** (2.845 and 2.744 Å; mean values for **15a** and **15b** respectively). This implies there is a stronger π-interaction from the 7-Mes ligand forming at the expense of optimal orbital overlap of the carbene centre with the metal (Fig 4.19).

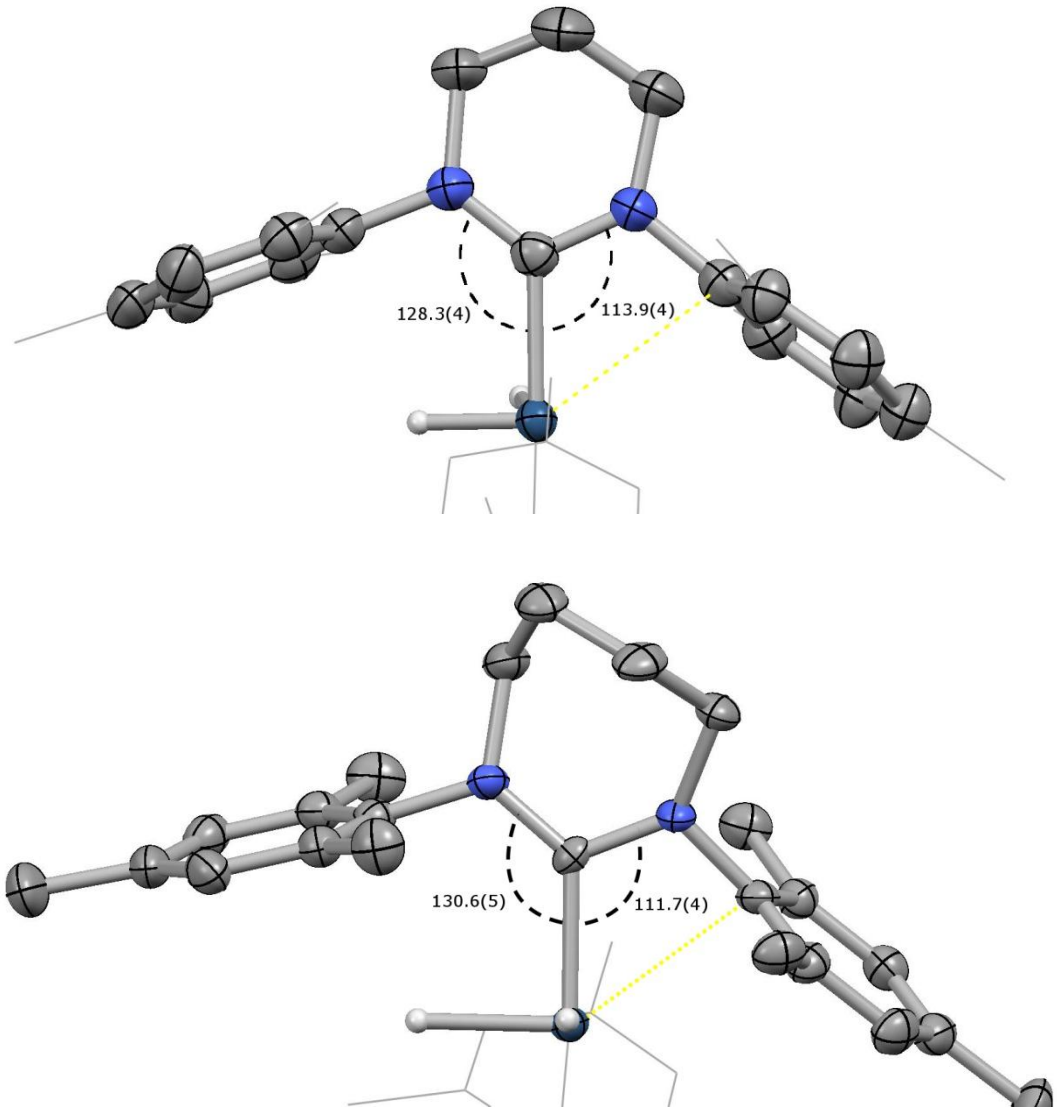

Figure 4.19: Cut-off images depicting the distortion of Ir-NCN framework from trigonal in **15a** (*top*) and **15b** (*bottom*), angles in degrees (°).

Interaction of the π-system with the iridium centre leads to a deviation of ~7° from ideal in **15a**, and ~9.5° for **15b**. This suggests that optimal orbital overlap of the carbene lone pair with the iridium d_{z^2}-orbital may be sacrificed in order to increase stabilisation by the π-system.

Coordination of two B–H bonds from an amine-borane, or aminoborane, would displace the arene interaction allowing the NHC–Ir framework to become more

symmetrical. Even so, the steric demands of the 6-Mes and 7-Mes ligands are so great that the lack of space in the cavity outweighs the electronic stabilisation gained by B–H coordination.

The peripheral steric shielding and electronic stabilisation provided by these expanded ring carbenes lead to a remarkably stable 14-electron, cationic metal centre. Monitoring a solution in "wet" bench *d*-chloroform exposed to air showed no degradation of the complex over a period of >10 days.

It was suspected that the *para*-methyl groups on such a sterically demanding system may clash and significantly restrict rotation of the NHC–Ir bond. Allowing rotation here would provide the opportunity for a larger cavity. Hence, the analogous complex [(6-Xyl)(6-Xyl')IrH][BAr^f_4] (**14c**) was tested with $H_3B{\cdot}NHMe_2$ to see if coordination of B–H bonds would be favoured over the π-interactions. Interestingly, this was not observed to be the case and the isolated complex from the reaction was in keeping with previous results, i.e. [$(6\text{-Xyl})_2IrH_2$][BAr^f_4] (**15c**).

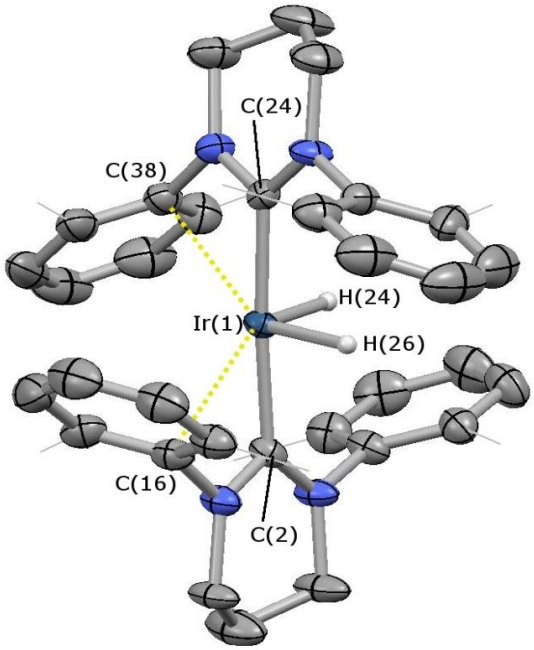

Figure 4.20: $[(6\text{-Xyl})_2IrH_2][BAr^f{}_4]$ (**15c**), with $[BAr^f{}_4]^-$ anion omitted, most H atoms omitted and Me groups shown in wireframe for clarity; thermal ellipsoids set at 50% probability level. Ir–H located in the Fourier difference map and refined isotropically. Key bond lengths (Å) and angles (°): Ir(1)–H(24) 1.68, Ir(1)–H(26) 1.72, Ir(1)–C(2) 2.042(6), Ir(1)–C(24) 2.049(6), Ir(1)···C(16) 2.818(7), Ir(1)···C(38) 2.809(5), C(2)–Ir(1)–C(24) 176.1(3).

Comparison of **15c** with the 6-Mes analogue (**15a**) shows that removing the *para*-methyl substituents allows for slightly closer approach of the aromatic rings to the metal centre [2.818(7), 2.809(5) Å *cf.* 2.876(5), 2.814(5) Å]. As expected, the C_{NHC}–Ir distances are statistically identical at 2.042(6), 2.049(6) Å *cf.* 2.046(6), 2.036(6) Å.

These systems are clearly in the limits of the steric bulk that can be accommodated around the iridium centre. Displaying the crystal structure of **15c** in "space-filling" mode shows the extent of the hindrance at the metal centre despite the smaller aryl groups (Fig 4.21). This inaccessibility of the iridium centre supports the observations that **15a**, **15b** and **15c** are resistant to interaction of H_2O and amine-boranes.

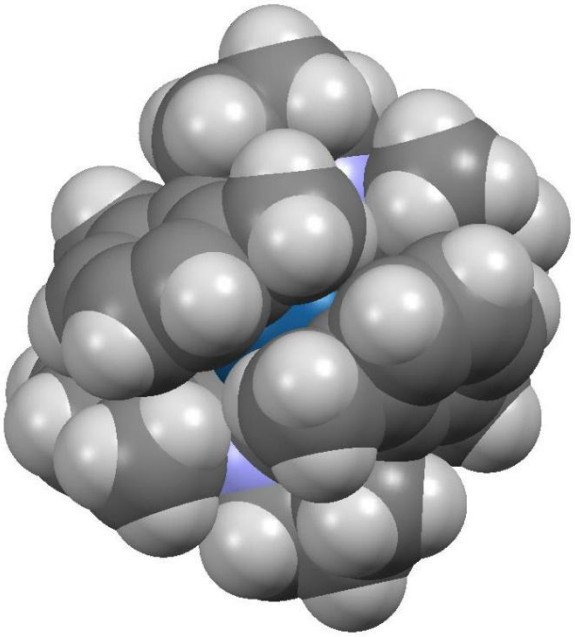

Figure 4.21: Space-fill representation of **15c**. Accessible surface of the iridium cation is only just visible as a dark blue-green area at the centre of the structure.

4.6.1 Addition of H_2

Amine-boranes apparently act as a source of hydrogen in reactions with **14a**, **14b** and **14c**, hence the addition of H_2 gas to [(6-Mes)(6-Mes')IrH][BAr^f_4] (**14a**) was explored. Exposure of **14a** to an excess of hydrogen led to a ^{1}H NMR spectrum similar to **15a**, however no signal was observed in the hydride region. As the pressure is released and the system is placed back under an argon environment, a signal in the hydride region appears at δ_H -43.6 ppm.

This is postulated to be due to the formation of a dihydrogen complex of **15a**, similar to the iridium-phosphine analogue reported by Caulton[27] and the corresponding ruthenium system investigated by Chaudret.[28] In the postulated complex, [$(6\text{-Mes})_2IrH_2(H_2)_2$][$BAr^f_4$] (**16**), σ-coordination of two equivalents of dihydrogen lead to an 18-electron species, but

these appear to be readily displaced in favour of π-interactions of the mesityl rings when the hydrogen atmosphere is replaced with argon.

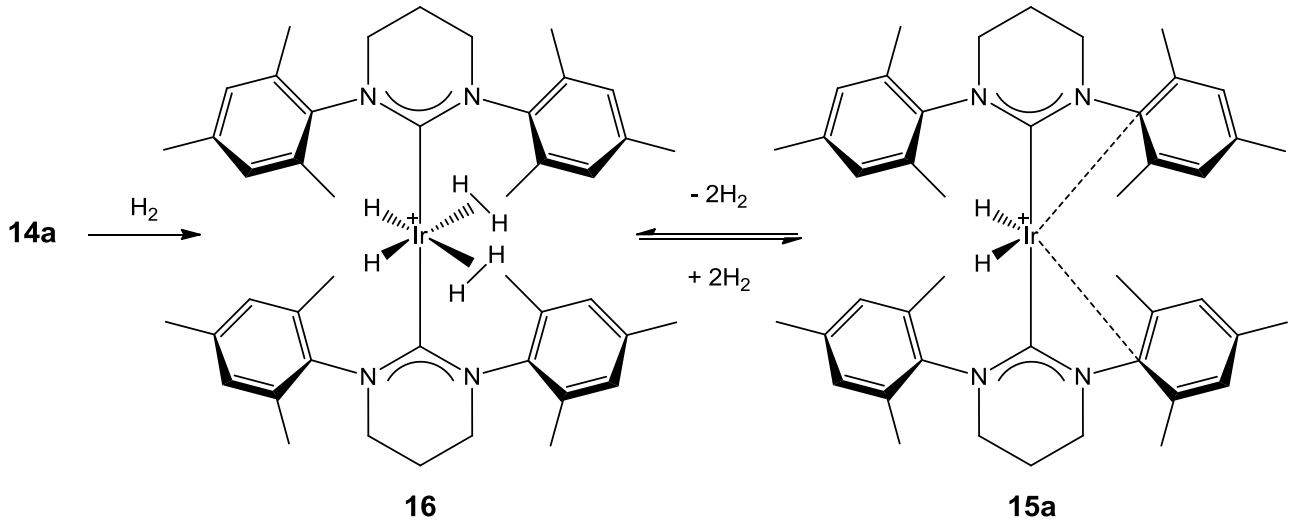

Scheme 4.22: Proposed equilibrium between **16** and **15a**.

The disappearance of the hydride signal in the ^{1}H NMR spectrum would suggest that there is rapid exchange of the hydrides with the bound H_2 molecules. Cooling the sample to -85 °C resulted in a very broad signal appearing in the ^{1}H NMR spectrum at δ_H -8.0 ppm potentially due to interaction of H_2 with the metal centre. The position of this signal suggests some exchange between dihydrogen and hydride ligands.

4.6.2 DFT Analysis of H_2 Coordination

Calculations were performed by Dr Josh Bates to determine the extent of the coordination of the dihydrogen ligand to the metal centre. A model system of **15a** was used bearing 6-Me ligands with methyl groups in place of mesityl rings, thus no secondary stabilising aryl interactions were taken into account.

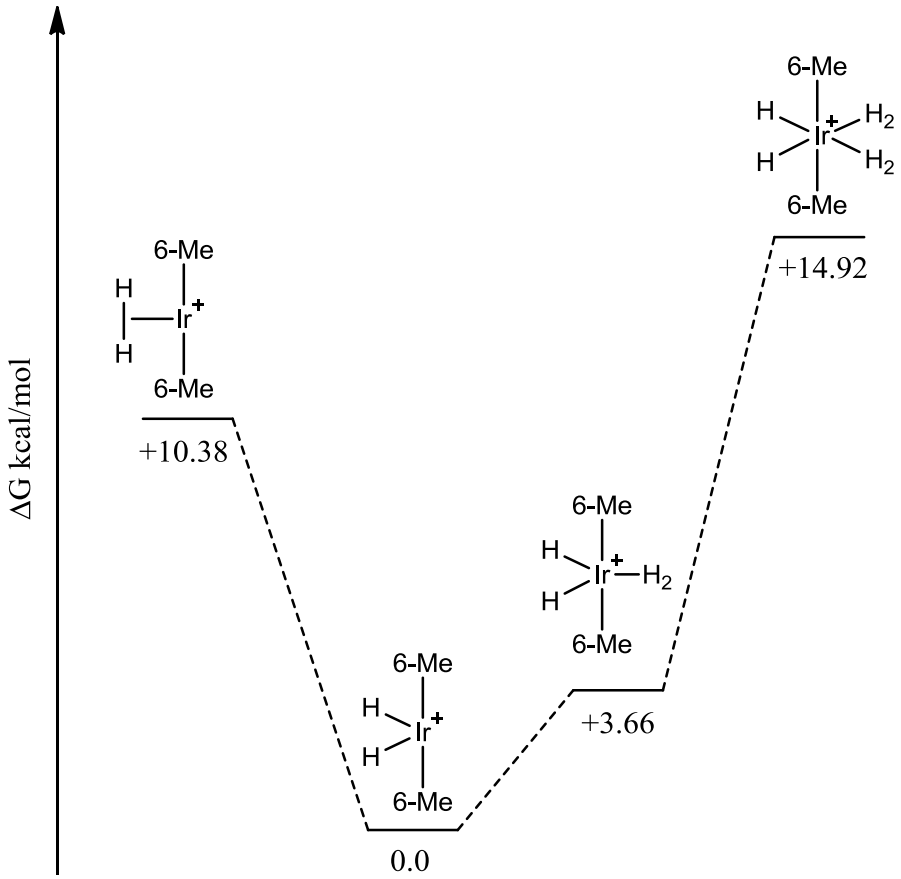

Figure 4.23: Calculations for the coordination of dihydrogen to the model complex $[(6\text{-Me})_2IrH_2]^+$. ΔG values account for the free energy of uncoordinated H_2.

Calculations imply that complex **16** may contain only one molecule of dihydrogen which only exists under a hydrogen atmosphere as loss of H_2 is energetically favourable for the model system (-3.66 kcal/mol). The barrier to reductive elimination of H_2 from the model $[(6\text{-Me})_2IrH_2]^+$ is large enough (10.38 kcal/mol), hence $[(6\text{-Mes})_2IrH_2][BAr^f{}_4]$ (**15a**) may be dried under vacuum without decomposition unlike $(6\text{-Mes})_2IrH_3$ (**5a**).

4.7 Addition of CO

Extensive work on cationic, expanded ring NHC systems (such as **14a**) has shown a remarkable stability to a range of substrates that would not normally be described as "large". It was then considered to attempt coordination and activation of some smaller species, such

as carbon monoxide. It has been shown that similar group 9 cationic *bis*-NHC systems have been able to coordinate CO.[29-31] When [(6-Mes)(6-Mes')IrH][BAr^f_4] (**14a**) was placed under an excess of carbon monoxide gas, the solution paled in colour from yellow to a salmon pink within 5 min. This is thought to be the coordination of a CO ligand to displace the agostic interaction form the *ortho*-methyl group, supported by the appearance of a relatively low-field hydride resonance (at δ_H -10.10 ppm) as well as an increase in complexity of the ^{1}H NMR spectrum similar to that of the lower temperature spectrum of **14a**, implying the system is no longer fluxional.

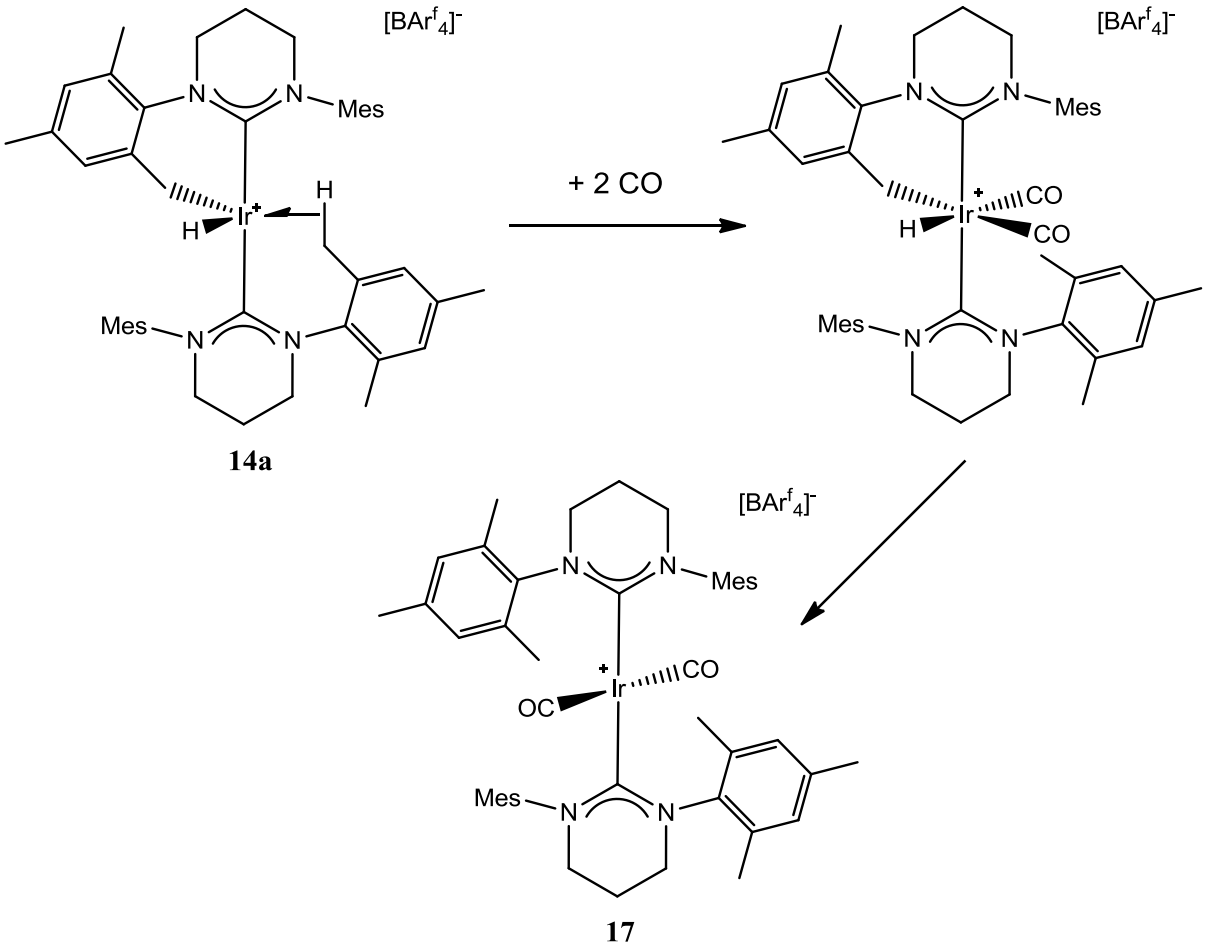

Scheme 4.24: Coordination of CO to **14a**.

Over a period of 7 days, the solution gains intensity in colour to end up as an intense, bright orange. During this time, the hydride signal is observed to reduce in intensity to zero

and the ^{1}H NMR spectrum simplifies to resemble that of **15a**. The process is thought to yield the species [(6-Mes)$_2$Ir(CO)$_2$][BAr$^f_4$] (**17**), supported by ^{13}C NMR (δ_C 186.6 and 182.0 ppm for CO and NCN respectively), an accurate mass spectrometry measurement of 889.4033 for [(6-Mes)$_2$Ir(CO)$_2$]$^+$ (calc. 889.4030) and a strong IR stretch at 1985 cm^{-1}.[29, 31]

Assuming this now to be an iridium(I) complex, it has the potential to undergo the oxidative addition of H_2. This would then lead to a potential precursor to the formation of formyl groups for subsequent elimination or hydrolysis as formaldehyde or formic acid respectively. Addition of excess H_2 causes a rapid paling of colour back to a salmon pink accompanied by the re-emergence of a low field hydride signal (at δ_H -9.83 ppm), similar to the intermediate in Scheme 4.24. As a result, it is thought that this species is formed by the reverse route to yield [(6-Mes)$_2$Ir(CO)$_2$H$_2$][BAr$^f_4$] (**18**).

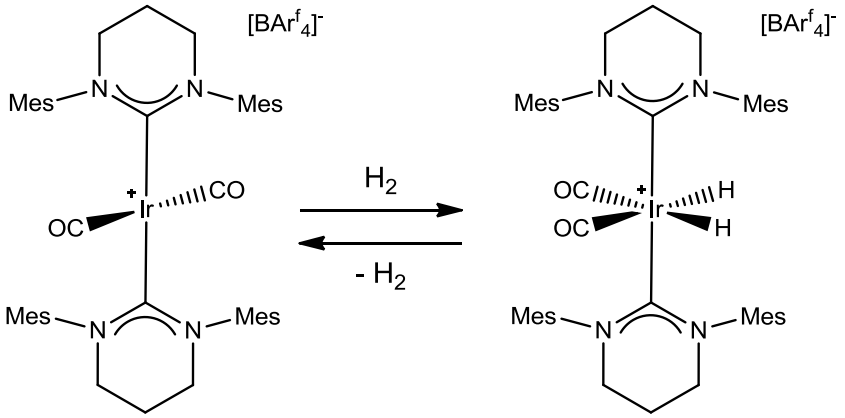

Scheme 4.25: Addition of H_2 to **17**.

This process can then be reversed by applying vacuum for several minutes, or by replacing the hydrogen atmosphere with argon to return to **17**, as monitored by ^{1}H NMR spectroscopy (Fig 4.26). As observed previously with expanded ring NHC-based systems, there appears to be a low barrier to oxidative addition and reductive elimination of the H_2 molecule.

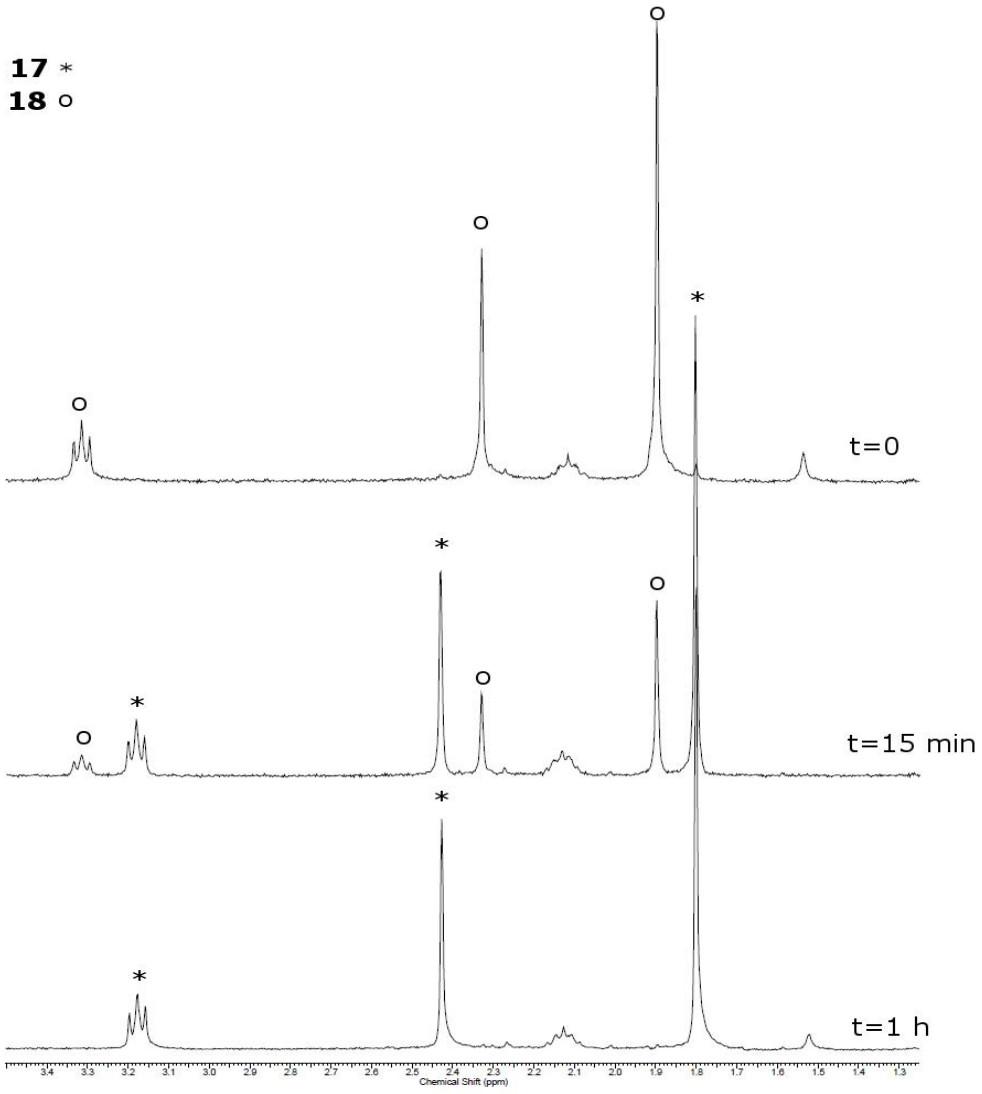

Figure 4.26: ^{1}H NMR spectra (300 MHz) showing return of **18** to **17** under an argon atmosphere in CD_2Cl_2 at 20 °C.

4.7.1 Trapping with ^{t}BuNC

In an attempt to model the intermediate formed via CO addition to **14a**, a stoichiometric amount of a less reducing analogue (^{t}BuNC) was utilised. Monitoring by ^{1}H NMR suggested a static structure, as a hydride signal was observed in the expected region (δ_H -12.10 ppm) and the colour of the solution paled to yellow, similar to the intermediate observed during addition of CO. As a result of the crowded nature of complex **19**, there is little free rotation in the structure and hence the NMR spectra are relatively complex.

Assignments of the ^{1}H and ^{13}C NMR spectra for this complex were aided by the comparison with the limiting low temperature spectra for [(6-Mes)(6-Mes')IrH][BAr^{f}_{4}] (**14a**) as the agostic interaction also restricts rotation of the 6-Mes ligand.

Attempts to add a single equivalent of ^{t}BuNC resulted in the coordination of two molecules of ^{t}BuNC, yielding [(6-Mes)(6-Mes')Ir(H){CN^{t}Bu}$_2$][BAr^{f}_{4}] (**19**) (Fig 4.27). As a result, the synthesis of **19** was altered accordingly to maximise the yield and purity. The structure is similar to that of [(6-Mes)(6-Mes')Ir(H)][BAr^{f}_{4}] (**14a**) but with the aryl ring interaction replaced with 2 ^{t}BuNC ligands.

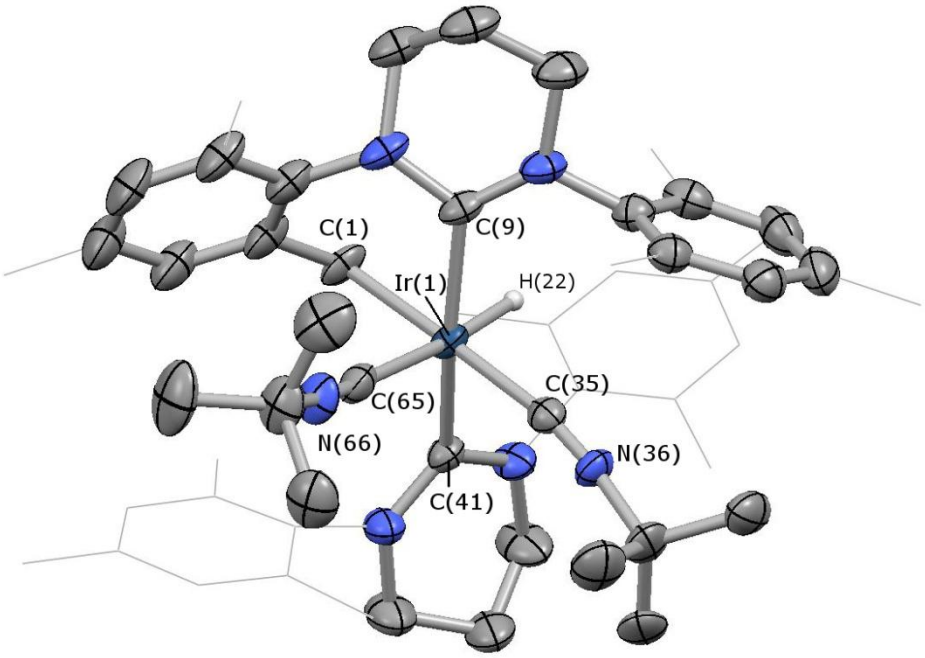

Figure 4.27: [(6-Mes)(6-Mes')Ir(H){CN^{t}Bu}$_2$][BAr^{f}_{4}] (**19**), with [BAr^{f}_{4}]$^{-}$ anion omitted for clarity, most H atoms omitted, and Me and lower Mes groups shown in wireframe; thermal ellipsoids set at 50% probability level. Ir–H located in the Fourier difference map and refined isotropically. Key bond lengths (Å) and angles (°): Ir(1)–C(1) 2.150(4), Ir(1)–C(9) 2.125(3), Ir(1)–C(41) 2.127(3), Ir(1)–C(35) 2.000(4), Ir(1)–C(65) 2.041(4), C(35)–N(36) 1.155(5), C(65)–N(66) 1.146(6), C(9)–Ir(1)–C(41) 165.0(1), Ir(1)–C(35)–N(36) 170.5(3), Ir(1)–C(65)–N(66) 166.8(4), C(35)–N(36)–C(37) 173.8(4), C(65)–N(66)–C(67) 168.6(4).

The Ir-C distances to the ^{t}BuNC ligands are 2.000(4) Å when *trans* to the benzylic ligand and 2.041(4) Å when *trans* to hydride. Adducts of ^{t}BuNC to cationic iridium centres reported in the literature quote Ir-C bond distances *trans* to a carbon donor in the range 2.004(6) to 2.034(6) Å.[32-34] Hence, the relatively short distance for **19** of 2.000(4) Å implies an electron-rich centre providing significant back-donation to the C≡N. Additionally, the ^{t}BuNC *trans* to hydride has a short Ir-C distance [2.041(4) *cf.* 2.061(6), 2.117(6) Å].[32, 35]

Further evidence of this back-donation is manifested in the elongation of the C≡N bond in **19**. For the *trans*-C ligand, the C≡N bond is found to be 1.155(5) Å [*cf.* 1.133(8) Å] and for *trans*-H the C≡N bond is 1.146(6) Å [*cf.* 1.132(6), 1.108 Å].[32, 35]

The C_{NHC}–Ir–C_{NHC} angle is significantly more bent than in **14a** [165.0(1)° *cf.* 174.7(1)°], most likely due to the steric demand of the two ^{t}BuNC ligands at the metal. This steric pressure also has a marked effect on the ^{t}BuNC ligands themselves, both ligands are not coordinated perfectly "end-on" [Ir-C≡N angles of 170.5(3)° and 173.8(4)°] hence optimal orbital overlap is sacrificed. In a similar *bis*(phosphine)-based system, these Ir-C≡N angles are reported to be 177.6(6)° and 175.6(4)°.[35] In addition, the angles about the isocyanide-nitrogens in **19** deviate significantly from linear [166.8(4)° and 168.6(4)°], potentially due to the decrease in C≡N bond order by back-donation (i.e. more sp^2 character) as well as steric demands from the 6-Mes ligands.

4.8 Conclusions

Despite the increased donor strength and apparent flexibility of the saturated 5-Mes ligands, $[(5\text{-Mes})_2Ir(H)_2\{H_3B{\cdot}NHMe_2\}][BAr^f{}_4]$ (**12**) displayed similar levels of amineborane activation to its unsaturated NHC counter-parts. However, from the neutron diffraction structures obtained for **12i** and **12ii**, we were able to study the hydride locations of a coordinated amineborane to a metal centre in a solid state structure for the first time. This has given insight into the degree of activation of the B-H bonds when complexed to the metal in both amineborane and aminoborane ligands. Given that the $Ir(\mu\text{-}H)_2B$ fragment appears to remain essentially unchanged on dehydrogenation of the amineborane, it appears there is no thermodynamic preference to coordinate either substrate. Thus, competition for coordination of the aminoborane and amineborane may slow the rate of dehydrogenation of the amineborane.

Complexes bearing the 6- and 7-Mes ligands gave entirely different modes of reactivity. Close approach the aryl rings to the metal centre in complexes of the type $[(NHC)(NHC')IrH][BAr^f{}_4]$ and $[(NHC)_2IrH_2][BAr^f{}_4]$ (NHC = expanded ring NHC) led to strong arene and agostic interactions with the low valent centres. The facile nature of the subsequent oxidative addition of the agostic bond was exemplified in the room temperature spectra of **14a** and **b**. Analysis of this process gives us a good insight into activation processes of C-H bonds at late transition metal centres.

Complexes **14a** and **b**, and **15a** and **b** showed remarkable stability to a range of external reagents, including water. This highlights how easily and efficiently these expanded ring NHCs can stabilise 14-electron metal cations. Unfortunately, this extreme stability rendered the complexes inactive towards borane substrates. Reactivity could only be achieved with extremely small ligands, such as H_2, or with linear, strong σ-donor/π-

acceptor ligands, such as CO and isonitriles. Further work in this area would be hindered by the remarkable stability of these 14-electron cations.

4.9 References

1. W. A. Herrmann and C. Kocher, *Angew. Chem. Int. Ed.*, 1997, **36**, 2162-2187.
2. J. F. Hartwig, *Nature*, 2008, **455**, 314-322.
3. D. A. Colby, R. G. Bergman and J. A. Ellman, *Chem. Rev.*, 2010, **110**, 624-655.
4. T. Bolano, M. L. Buil, M. A. Esteruelas, S. Izquierdo, R. Lalrempuia, M. Olivan and E. Onate, *Organometallics*, 2010, **29**, 4517-4523.
5. J. Campos, J. Lopez-Serrano, E. Alvarez and E. Carmona, *J. Am. Chem. Soc.*, 2012, **134**, 7165-7175.
6. J. M. Meredith, R. Robinson, K. I. Goldberg, W. Kaminsky and D. M. Heinekey, *Organometallics*, 2012, **31**, 1879-1887.
7. C. E. Johnson and R. Eisenberg, *J. Am. Chem. Soc.*, 1985, **107**, 3148-3160.
8. A. Staubitz, M. E. Sloan, A. P. M. Robertson, A. Friedrich, S. Schneider, P. J. Gates, J. Gunne and I. Manners, *J. Am. Chem. Soc.*, 2010, **132**, 13332-13345.
9. C. Y. Tang, A. L. Thompson and S. Aldridge, *J. Am. Chem. Soc.*, 2010, **132**, 10578-10591.
10. C. Y. Tang, A. L. Thompson and S. Aldridge, *Angew. Chem. Int. Ed.*, 2010, **49**, 921-925.
11. A. B. Chaplin and A. S. Weller, *Acta Cryst. C*, 2011, **67**, M355-M358.
12. C. J. Stevens, R. Dallanegra, A. B. Chaplin, A. S. Weller, S. A. Macgregor, B. Ward, D. McKay, G. Alcaraz and S. Sabo-Etienne, *Chem. Eur. J.*, 2011, **17**, 3011-3020.
13. N. Imlinger, K. Wurst and M. R. Buchmeiser, *J. Organomet. Chem.*, 2005, **690**, 4433-4440.
14. V. Cesar, N. Lugan and G. Lavigne, *J. Am. Chem. Soc.*, 2008, **130**, 11286-11287.
15. C. Y. Tang, N. Phillips, J. I. Bates, A. L. Thompson, M. J. Gutmann and S. Aldridge, *Chem. Comm.*, 2012, **48**, 8096-8098.
16. T. J. Hebden, M. C. Denney, V. Pons, P. M. B. Piccoli, T. F. Koetzle, A. J. Schultz, W. Kaminsky, K. I. Goldberg and D. M. Heinekey, *J. Am. Chem. Soc.*, 2008, **130**, 10812-10820.
17. W. H. Lam, S. Shimada, A. S. Batsanov, Z. Y. Lin, T. B. Marder, J. A. Cowan, J. A. K. Howard, S. A. Mason and G. J. McIntyre, *Organometallics*, 2003, **22**, 4557-4568.
18. N. M. Scott, R. Dorta, E. D. Stevens, A. Correa, L. Cavallo and S. P. Nolan, *J. Am. Chem. Soc.*, 2005, **127**, 3516-3526.
19. T. Y. Cheng, D. J. Szalda, J. Zhang and R. M. Bullock, *Inorg. Chem.*, 2006, **45**, 4712-4720.
20. M. Gomberg, *J. Am. Chem. Soc.*, 1900, **22**, 757-771.
21. M. Brookhart and M. L. H. Green, *J. Organomet. Chem.*, 1983, **250**, 395-408.
22. R. N. Perutz and S. Sabo-Etienne, *Angew. Chem. Int. Ed.*, 2007, **46**, 2578-2592.

23. gNMR5.0 and P. H. M. Budezelaar, *http://home.cc.umanitoba.ca/~budzelaa/gNMR/gNMR.html*.
24. B. K. McNamara, J. S. Yeston, R. G. Bergman and C. B. Moore, *J. Am. Chem. Soc.*, 1999, **121**, 6437-6443.
25. L. S. Vandersluys, J. Eckert, O. Eisenstein, J. H. Hall, J. C. Huffman, S. A. Jackson, T. F. Koetzle, G. J. Kubas, P. J. Vergamini and K. G. Caulton, *J. Am. Chem. Soc.*, 1990, **112**, 4831-4841.
26. W. A. Herrmann, K. Ofele, D. von Preysing and E. Herdtweck, *J. Organomet. Chem.*, 2003, **684**, 235-248.
27. A. C. Cooper, W. E. Streib, O. Eisenstein and K. G. Caulton, *J. Am. Chem. Soc.*, 1997, **119**, 9069-9070.
28. M. L. Christ, S. Saboetienne and B. Chaudret, *Organometallics*, 1994, **13**, 3800-3804.
29. M. V. Baker, S. K. Brayshaw, B. W. Skelton, A. H. White and C. C. Williams, *J. Organomet. Chem.*, 2005, **690**, 2312-2322.
30. S. Burling, S. Douglas, M. F. Mahon, D. Nama, P. S. Pregosin and M. K. Whittlesey, *Organometallics*, 2006, **25**, 2642-2648.
31. F. Chen, J. F. Sun, T. Y. Li, X. T. Chen and Z. L. Xue, *Organometallics*, 2011, **30**, 2006-2011.
32. P. Lacey and A. G. Sykes, *J. Coord. Chem.*, 2003, **56**, 141-145.
33. J. Li, P. I. Djurovich, B. D. Alleyne, M. Yousufuddin, N. N. Ho, J. C. Thomas, J. C. Peters, R. Bau and M. E. Thompson, *Inorg. Chem.*, 2005, **44**, 1713-1727.
34. N. M. Shavaleev, F. Monti, R. Scopelliti, N. Armaroli, M. Gratzel and M. K. Nazeeruddin, *Organometallics*, 2012, **31**, 6288-6296.
35. J. T. Mague, *Polyhedron*, 1992, **11**, 677-686.

Chapter V

Exploring the Limits of Steric Bulk:

Dipp-Functionalized NHCs

5.1 Introduction

Work outlined in previous chapters has highlighted the protection offered by mesityl-functionalized expanded ring NHCs. A common alternative substituent is the 2,6-diisopropylphenyl (Dipp) group, which has been used extensively to offer steric protection for highly reactive, low valent complexes bearing a number of ancillary ligand types.[1-5] When applied in expanded ring NHC cases, Dipp groups result in $\%V_{bur}$ values of over 50% (Fig 5.1),[6] meaning the ligand will occupy over half of the coordination sphere of the metal. This suggests that coordination of two such species to a metal should be disfavoured. Thus, in the current study, we aim to synthesise unsaturated metal centres stabilised by coordination of just one NHC. This would avoid the inertness provided by coordination of two 6-Mes ligands, for example $[(6\text{-Mes})_2IrH_2][BAr^f_4]$ (**15a**; Chapter IV) which was found to be resistant to a range of substrates including water, primarily on steric grounds.

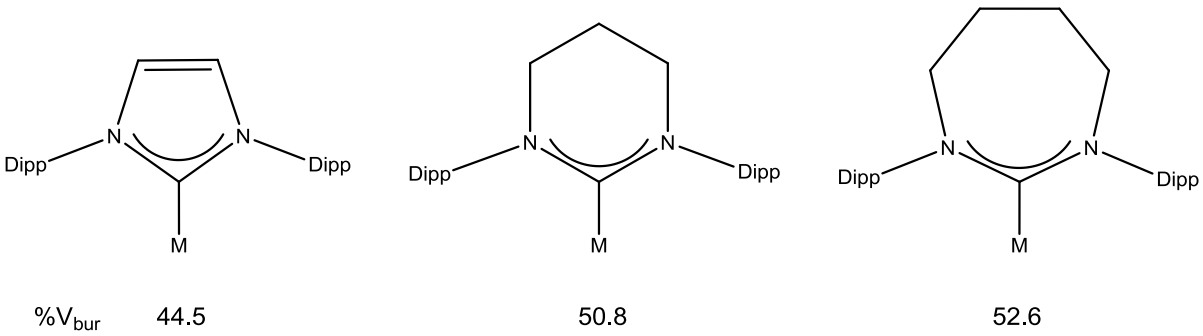

Figure 5.1: $\%V_{bur}$ of NHCs in linear (NHC)AuCl complexes.

In addition, coordination of Dipp-functionalized NHCs to low valent metal centres has enabled a variety of mechanistic routes to increase the electron count above those facilitated by simple oxidative addition.[7] In 5-membered systems, the ^{i}Pr group is observed to be dehydrogenated by Ir(I) due to its close proximity to the metal centre and existence of a β-hydride. So far there have been no examples of ligand activation by this route for Dipp-functionalized expanded ring NHCs.

Interest in sterically demanding, anionic ligands has been pioneered by work on terphenyl ligands (e.g. 2,6-Dipp-C_6H_3), principally by Power *et al.* (Fig 5.2).[1, 8, 9] This extremely bulky class of anionic ligand has been used to stabilise a variety of low valent main group and transition metal species, including the first Cr–Cr quintuple bond. In 2006, Yamashita *et al.* reported the synthesis of an anionic boryl ligand which is isoelectronic with IPr (Fig 5.2).[10] This ligand has been able to stabilise a series of compounds with unusual oxidation states, for example an acyclic silylene, Si(II),[11] and a range of M(II) complexes for M = Ga, In, Tl.[12]

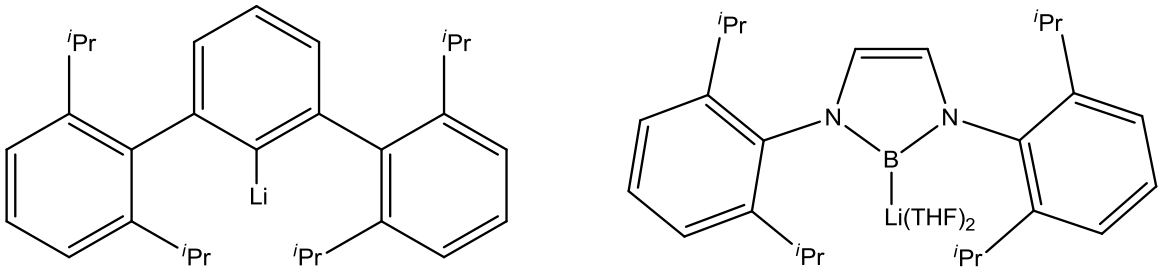

Figure 5.2: Power's Dipp-terphenyl ligand (*left*) and Yamashita's Dipp-boryl ligand (*right*).

A major problem with these anionic ligands is their high reduction potential, which leads in many cases to electron transfer rather than metathesis chemistry with the metal electrophile. There have been some reports of zwitterionic NHCs which are expected to be much less reducing as the negative charge is not involved in the donor orbital, resulting in a lower lying HOMO.[13, 14] In 2013, Tamm *et al.* utilised a range of anionic NHCs bearing

integrated weakly coordinating anions in coordination chemistry with rhodium and iridium cations (Fig 5.3).[15]

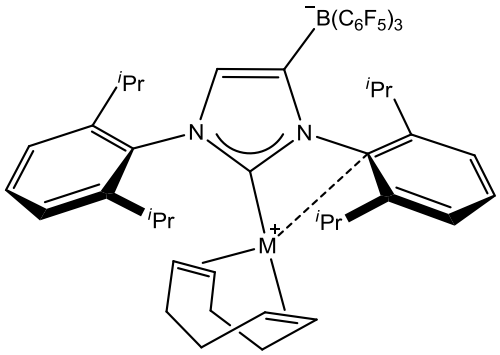

Figure 5.3: Tamm's zwitterionic metal-NHC complexes containing a weakly coordinating anion moiety (M = Rh, Ir).

Moreover, it appears that the inclusion of the bulky borate moiety on the heterocycle backbone increases the steric profile of the ligand, allowing interaction of the pendant arene rings with the metal centre. Although these are not hugely sterically demanding ligands, this does allow the complexes to be manipulated in non-polar solvents. Utilising this approach, the authors were able to monitor the behaviour of reactive intermediates without interaction with polar solvents, and even carry out hydrogenation chemistry in neat alkene solvent.

This chapter reports on attempts to investigate the effect of creating highly hindered, low valent metal centres and the consequences for subsequent reactivity. Due to the extremely bulky nature of the Dipp-substituted expanded ring NHCs, coordination of two ligands may result in M-C bond elongation or lability of the second NHC, leaving the system with a degree of unquenched reactivity. An expanded ring NHC containing a weakly coordinating anionic fragment is also a target, with the view to stabilising a variety of cationic metal fragments as zwitterionic species. These should have the added benefit of

solubility in less coordinating, non-polar solvents leading to the ability to study potential catalytic intermediates.

5.2 Experimental

*Preparation of (6'-Dipp)Ir(COE)Cl (**20**)*

6-Dipp (100 mg, 0.24 mmol) was dissolved in THF (30 cm^3) and added to a stirred solution of $[Ir(COE)_2Cl]_2$ (111 mg, 0.12 mmol) also in THF (20 cm^3). The reaction mixture was allowed to stir for 1 h then the volatiles were removed *in vacuo*. Extraction of the residue into hexanes (3 x 20 cm^3), concentration and storage at -30 °C yielded yellow-orange crystalline product. X-ray quality crystals were obtained from a concentrated solution in diethyl ether at -30 °C. The isolated yield of crystals was 72% (132 mg).

*Spectroscopic data for **20***

^{1}H NMR (300 MHz, C_6D_6, 298 K): δ_H 7.23-7.97 (6H, m, CH Dipp), 7.18 (1H, s, NCHN), 5.05 (1H, v br, CH alkene), 4.44 (1H, br, CH ^{i}Pr), 4.37 (1H, d, $^2J_{HH}$ = 15.6 Hz, NCH_2), 3.40 (2H, sept, $^3J_{HH}$ = 6.9 Hz, CH ^{i}Pr), 3.11 (2H, br, CH COE), 2.95 (1H, br, CH ^{i}Pr), 2.82 (1H, d, $^2J_{HH}$ = 15.6 Hz, NCH_2), 2.57 (2H, br, CH_2 alkene), 1.79 (3H, d, $^3J_{HH}$ = 6.9 Hz, CH_3 ^{i}Pr), 1.72 (6H, d, $^3J_{HH}$ = 6.9 Hz, CH_3 ^{i}Pr), 1.44-1.65 (6H, m, CH_2 COE), 1.33 (3H, d, $^3J_{HH}$ = 6.9 Hz, CH_3 ^{i}Pr), 1.31 (2H, br, CH_2 COE), 1.17 (3H, d, $^3J_{HH}$ = 6.9 Hz, CH_3 ^{i}Pr), 1.13 (3H, d, $^3J_{HH}$ = 6.9 Hz, CH_3 ^{i}Pr), 1.09, 1.04 (6H, d, $^3J_{HH}$ = 6.9 Hz, CH_3 ^{i}Pr), 0.96 (2H, tr, $^3J_{HH}$ = 6.8 Hz, CH_2 COE). ^{13}C NMR (75 MHz, C_6D_6, 298 K): δ_C 155.2 (NCHN), 147.2, 146.6 (NC Dipp), 146.3, 145.1, 142.6, 140.0 (*ortho*-C Dipp), 129.6, 126.7 (*para*-CH Dipp), 125.0, 124.6, 123.3, 123.2 (*meta*-CH Dipp), 54.1 (NCH_2), 43 (br, CH alkene), 31.9 (CH COE), 29.1 (CH ^{i}Pr), 28.9 (CH ^{i}Pr), 28.6 (CH ^{i}Pr), 28.0, 26.8, 26.4, 26.3 (CH_2 COE), 25.1, 24.8, 24.6, 24.2, 23.0, 22.9 (CH_3 ^{i}Pr), 14.3 (s, CH_2 COE). MS (EI +ve): *m/z* 388.9 ([(6'-Dipp)-

$CH_4]^+$, 40%), 402.9 ([(6'-Dipp)-2H]$^+$, 15%). Elemental analysis: calcd. for $C_{36}H_{54}N_2IrCl{\cdot}C_4H_{10}O$: C 58.83% H 7.90% N 3.43%, meas. C 59.12% H 7.28% N 3.64%.

*Crystallographic data for **20***

$C_{36}H_{54}N_2IrCl{\cdot}C_4H_{10}O$, M_r = 816.63, triclinic, *P -1*, a = 11.8594(1), b = 12.9290(1), c = 13.4021(1) Å, α = 109.3254(5), β = 93.2260(5), γ = 95.6324(5)°, V = 1921.16(3) Å^3, Z = 2, ρ_c = 1.412 Mg/m^3, T = 150 K, λ = 0.71073 Å. 8758 independent reflections [R(int) = 0.033], used in all calculations. R_1 = 0.0306, wR_2 = 0.0713 for observed reflections [I > 2σ (I)] and R_1 = 0.0399, wR_2 = 0.0823 for all unique reflections. Max. and min. residual electron densities 1.56 and -1.50 e Å^{-3}.

*Preparation of (6'-Dipp)$_2$IrCl **(21)***

6-Dipp (181 mg, 0.44 mmol) was dissolved in THF (40 cm^3) and added to a stirred solution of $[Ir(COE)_2Cl]_2$ (100 mg, 0.11 mmol) also in THF (20 cm^3). The reaction mixture was allowed to stir for 30 min then the volatiles were removed *in vacuo*. Extraction of the residue into hexanes (3 x 20 cm^3), concentration and storage at -30 °C yielded yellow crystalline product. X-ray quality crystals were obtained from a concentrated solution in Et_2O at -30 °C, and the product was collected in 66% yield (150 mg).

*Spectroscopic data for **21***

^{1}H NMR (300 MHz, C_6D_6, 298 K): δ_H 6.85-7.24 (14H, m, CH Dipp and NCHN), 5.65 (1H, d, $^3J_{HH}$ = 14.7 Hz, CH alkene), 4.36 (2H, m, CH ^{i}Pr), 4.25 (2H, m, NCH_2), 4.09 (1H, m, NCH_2), 3.64 (2H, sept, $^3J_{HH}$ = 6.9 Hz, CH ^{i}Pr), 3.27 (4H, m, CH ^{i}Pr), 3.05 (1H, m, CH alkene), 2.80 (1H, s, CH_2 alkene), 2.75 (2H, s, CH_2 alkene), 2.69 (1H, d, $^3J_{HH}$ = 8.1 Hz, NCH_2), 2.52 (1H, d, $^3J_{HH}$ = 7.5 Hz, CH_2 alkene), 1.78, 1.57, 1.40, 1.35, 1.32, 1.23, 1.22, 1.10, 1.05, 1.01, 0.99, 0.93 (3H, d, $^3J_{HH}$ = 6.9 Hz, CH_3 ^{i}Pr). ^{13}C NMR (75 MHz, C_6D_6, 298

K): δ_C 155.8, 151.5 (NCHN), 148.9, 148.3, 147.7, 146.6, 146.4, 146.2, 144.9, 142.7, 139.9 (NC and *ortho*-C), 129.7, 128.6, 126.9 (*para*-CH), 124.9, 124.8, 124.6, 124.1, 123.5, 123.2, 123.0, 122.9 (*meta*-CH), 64.0 (alkene), 54.6, 54.4 (NCH_2), 53.6, 39.9, 32.9 (alkene), 29.2, 28.9, 28.6, 28.4, 28.3, 28.1 (CH ^{i}Pr), 26.5, 26.4 (alkene), 25.7, 24.9, 24.8, 24.7, 24.6, 24.4, 24.2, 23.9, 23.8, 23.7, 22.8 (CH_3 ^{i}Pr). MS (EI +ve): *m/z* 389.3 ([6'-Dipp-CH_3]$^+$, 20%). Elemental analysis: calcd. for $C_{56}H_{80}N_4IrCl$: C 64.86% H 7.78% N 5.40%, meas. C 64.10% H 7.04% N 5.11%.

*Crystallographic data for **21***

$C_{56}H_{80}N_4IrCl{\cdot}2(C_4H_{10}O)$, M_r = 1185.20, triclinic, *P -1*, a = 11.9203(2), b = 14.7777(2), c = 19.6398(3) Å, α = 77.5709(5), β = 82.4992(6), γ = 70.3071(8)°, V = 3174.62(9) Å^3, Z = 2, ρ_c = 1.240 Mg m^{-3}, T = 150 K, λ = 0.71073 Å. 14237 independent reflections [R(int) = 0.024], used in all calculations. R_1 = 0.0381, wR_2 = 0.0793 observed reflections [I > 2σ (I)] and R_1= 0.0469, wR_2 = 0.0834 for all unique reflections. Max. and min. residual electron densities 1.68 and -1.79 e Å^{-3}.

*Preparation of bis-N,N'-Dipp-N-allylformamidine (**22**)*

A flask was charged with *bis-N,N'*-di-isopropylphenyl-formamidine (4.1 g, 12 mmol), allyl-bromide (1 cm^3, 12 mmol), and K_2CO_3 (0.8 g, 6 mmol). Acetonitrile (250 cm^3) was added and the mixture stirred at 50 °C for 2 h. Volatiles were removed *in vacuo* and the residue dissolved in CH_2Cl_2 (80 cm^3) and filtered through silica. The solvent was removed *in vacuo* and the product extracted in hexanes (3 x 30 cm^3), subsequent concentration and storage at -30 °C yielded the product as colourless blocks in 41% yield (2.0 g).

*Spectroscopic data for **22***

^{1}H NMR (300 MHz, $CDCl_3$, 298 K): δ_H 7.35-6.95 (m, 7H, arom-CH and NCHN), 6.17 (m, 1H, alkene CH), 5.16 (m, 2H, alkene CH_2), 4.39 (d, 2H, $^{3}J_{HH}$ = 6.6 Hz NCH_2), 3.22 (overlapping m, 4H, CH ^{i}Pr), 1.28 (d, 6H, $^{3}J_{HH}$ = 6.3 Hz CH_3 ^{i}Pr), 1.20 (d, 12H, $^{3}J_{HH}$ = 6.6 Hz CH_3 ^{i}Pr), 1.13 (d, 6H, $^{3}J_{HH}$ = 7.2 Hz CH_3 ^{i}Pr). ^{13}C NMR (75 MHz, $CDCl_3$, 298 K): δ_C 150.9 (NCHN), 148.2, 147.2 (NC), 139.9, 138.2 (*ortho*-C), 133.2 (alkene CH), 128.7 (*para*-CH), 124.2, 122.6 (*meta*-CH), 118.1 (alkene CH_2), 52.8 (NCH_2), 28.3, 27.8 (CH ^{i}Pr), 25.2, 24.2, 23.6 (CH_3 ^{i}Pr). MS (EI +ve): *m/z* 403.30 ($[M-H]^+$, 100%). Elemental analysis: calcd. for $C_{28}H_{40}N_2$: C 83.11% H 9.96% N 6.92%, meas. C 82.93% H 9.57% 6.98%.

*Preparation of H(5-Dipp^{BArF}) (**23**)*

Tris(pentafluorophenyl)borane (154 mg, 0.3 mmol) was added to a stirred solution of **22** (121 mg, 0.3 mmol) in toluene (15 cm^3). The mixture was allowed to stir for 1 h, then the volatiles were removed *in vacuo*. Washing with hexanes and drying *in vacuo* yielded the crude product as a white powder. X-ray quality crystals were obtained in 62% yield (170 mg) from a concentrated solution of toluene stored at -30 °C.

*Spectroscopic data for **23***

^{1}H NMR ($CDCl_3$, 300 MHz, 298 K): δ 7.32-7.04 (7H, m, CH Dipp and NCHN), 4.34 (1H, m, NCH), 3.80 (1H, apparent tr, $^{2}J_{HH}$ = 10.8 Hz, NCH_2), 3.61 (1H, apparent tr, $^{2}J_{HH}$ = 10.8 Hz, NCH_2), 3.15 (1H, sept, $^{3}J_{HH}$ = 5.9 Hz, CH-^{i}Pr), 2.80 (1H, sept, $^{3}J_{HH}$ = 5.9 Hz, CH ^{i}Pr), 2.62 (1H, sept, $^{3}J_{HH}$ = 6.7 Hz, CH ^{i}Pr), 2.48 (1H, sept, $^{3}J_{HH}$ = 5.3 Hz, CH ^{i}Pr), 2.16 (1H, apparent tr, $^{2}J_{HH}$ = 14.7 Hz, CH_2-B), 1.51 (1H, apparent d, $^{2}J_{HH}$ = 12.3 Hz, CH_2-B), 1.33 (3H, d, $^{3}J_{HH}$ = 6.9 Hz, CH_3 ^{i}Pr), 1.20 (3H, d, $^{3}J_{HH}$ = 6.9 Hz, CH_3 ^{i}Pr), 1.13 (3H, overlapping d, CH_3 ^{i}Pr), 1.11 (3H, overlapping d, CH_3 ^{i}Pr), 1.00 (12H, overlapping d, CH_3 ^{i}Pr). ^{13}C

NMR ($CDCl_3$, 100 MHz, 298 K): δ 155.6 (NCHN), 148.0 (dm, $^1J_{CF}$ = 240.1 Hz, *ortho*-CF), 147.6, 146.4 (NC Dipp), 146.0, 146.0 (*ortho*-C Dipp), 138.2 (dm, $^1J_{CF}$ = 243.0 Hz, *para*-CF), 136.6 (dm, $^1J_{CF}$ = 245.0 Hz, *meta*-CF), 131.7, 131.6 (*para*-CH Dipp), 127.4, 125.1, 125.0, 124.8 (*meta*-CH Dipp), 71.0 (NCH), 58.8 (NCH_2), 29.5, 29.4, 29.3, 29.0 (CH ^{i}Pr), 26.4, 25.2, 24.9, 24.8, 24.0, 23.6, 22.6 (CH_3 ^{i}Pr), (CH_2B not observed). ^{11}B NMR ($CDCl_3$, 128 MHz, 298 K): δ -14.65 (s). ^{19}F NMR ($CDCl_3$, 282 MHz, 298 K): δ -131.44 (d, $^3J_{FF}$ = 28.8 Hz, *ortho*-F), -161.64 (tr, $^3J_{FF}$ = 21.3 Hz, *para*-F), -165.36 (m, *meta*-F). MS (EI +ve): *m/z* 403.3 ([M-BCF]+, 100%), 512.0 ([BCF]+, 30%). Elemental analysis: calcd. for $C_{46}H_{40}BF_{15}N_2$: C 60.28, H 4.40, N 3.06, meas. C 61.12, H 4.22, N 3.58.

*Crystallographic data for **23***

$C_{46}H_{40}BF_{15}N_2 \cdot C_7H_8$, M_r = 1008.76, monoclinic, *C* 2/*c*, a = 35.4499(3), b = 11.1438(1), c = 25.1650(2) Å, β = 104.2861(3)°, V = 9633.92(14) Å^3, Z = 8, ρ_c = 1.391 Mg m^{-3}, T = 150 K, λ = 0.710730 Å, 21331 reflections collected, 10963 independent [R(int) = 0.027], which were used in calculations. R_1 = 0.0603, *w*R_2 = 0.1340 for observed unique reflections [I > 2σ(I)] and R_1 = 0.0875, *w*R_2 = 0.1603 for all unique reflections. Max. and min. residual electron densities 0.89 and -0.52 e Å^{-3}.

*Preparation of [K(18-crown-6)][(5-Dipp^{BArF})] (**24**)*

K[$N(SiMe_3)_2$] (24 mg, 0.12 mmol) in THF (10 cm^3) was added to a stirred solution of **23** (100 mg, 0.11 mmol) also in THF (15 cm^3). The mixture was allowed to stir for 30 min, then the mixture transferred onto 18-crown-6 (29 mg, 0.11 mmol) and stirred for a further 10 min. Removal of the volatiles *in vacuo* and washing with hexanes yielded product as a white powder. Green oil can form on the surface of the product, which can be washed away using diethyl ether. X-ray quality crystals were obtained in 54% yield (73 mg) from a concentrated solution of THF layered with pentane at 20 °C.

*Spectroscopic data for **24***

^{1}H NMR ($C_6D_5CD_3$, 400 MHz, 298 K): δ_H 7.11-6.76 (6H, m, CH Dipp), 4.45 (1H, m, NCH), 4.19 (1H, tr, $^{2}J_{HH}$ = 12.6 Hz, NCH_2), 3.61 (1H, tr, $^{2}J_{HH}$ = 11.4 Hz, NCH_2), 3.26 (1H, sept, $^{3}J_{HH}$ = 7.0 Hz, CH ^{i}Pr), 2.75 (1H, sept, $^{3}J_{HH}$ = 6.8 Hz, CH ^{i}Pr), 2.68 (1H, overlapping tr, $^{2}J_{HH}$ = 13.2 Hz, CH_2-B), 2.56 (1H, sept, $^{3}J_{HH}$ = 6.6 Hz, CH ^{i}Pr), 2.43 (1H, sept, $^{3}J_{HH}$ = 6.8 Hz, CH ^{i}Pr), 1.72 (1H, br d, $^{2}J_{HH}$ = 13.6 Hz, CH_2-B), 1.44 (3H, d, $^{3}J_{HH}$ = 6.9 Hz, CH_3 ^{i}Pr), 1.18 (3H, d, $^{3}J_{HH}$ = 6.8 Hz, CH_3 ^{i}Pr), 1.08 (3H, d, $^{3}J_{HH}$ = 6.8 Hz, CH_3 ^{i}Pr), 1.01, 0.99 (3H, overlapping d, CH_3 ^{i}Pr), 0.91 (6H, overlapping d, CH_3 ^{i}Pr), 0.89 (3H, overlapping d, CH_3 ^{i}Pr). ^{13}C NMR ($C_6D_5CD_3$, 125 MHz, 298 K): δ_C 165.5 (NCN), 148.8 (dm, $^{1}J_{CF}$ = 236.9 Hz, *ortho*-CF), 147.8, 146.3 (NC Dipp), 146.1, 146.0, 143.7, 141.5 (*ortho*-C Dipp), 138.6 (dm, $^{1}J_{CF}$ = 240.6 Hz, *para*-CF), 137.3 (dm, $^{1}J_{CF}$ = 194.1 Hz, *meta*-CF), 131.7, 129.6 (*para*-CH Dipp), 125.6, 124.8, 123.8 (*meta*-CH Dipp), 71.5 (NCH), 58.8 (NCH_2), 30.4, 29.7, 29.5, 29.1 (CH ^{i}Pr), 27.8 (CH_2B), 26.2, 25.9, 24.4, 23.8, 23.5, 23.1, 22.8 (CH_3 ^{i}Pr). ^{11}B NMR ($C_6D_5CD_3$, 128 MHz, 298 K): δ -14.4 (s). ^{19}F NMR ($C_6D_5CD_3$, 376 MHz, 298 K): δ -130.89 (d, $^{3}J_{FF}$ = 21.8 Hz, *ortho*-F), -161.24 (tr, $^{3}J_{FF}$ = 20.3 Hz, *para*-F), -165.09 (m, *meta*-F). MS (ESI -ve): *m/z* 933.3 ($[M+H_2O]^-$, 100%).

*Crystallographic data for **24***

$C_{58}H_{63}BF_{15}N_2KO_6$, M_r = 1219.03, monoclinic, *P* $2_1/n$, a = 10.5956(2), b = 22.6260(3), c = 24.4132(4) Å, β = 98.9391(6)°, V = 5781.64(16) Å^3, Z = 4, ρ_c = 1.400 Mg m^{-3}, T = 150 K, λ = 0.710730 Å, 70863 reflections collected, 13012 independent [R(int) = 0.037], which were used in calculations. R_1 = 0.0689, wR_2 = 0.1251 for observed unique reflections [I > 2σ(I)] and R_1 = 0.1062, wR_2 = 0.1453 for all unique reflections. Max. and min. residual electron densities 1.01 and -0.69 e Å^{-3}.

5.3 Coordination of Extremely Sterically Demanding Ligands

Offering as a comparison with the coordination chemistry of 6-Mes with iridium reported in Chapters III and IV, the reactivity of the 6-Dipp ligand was probed towards $[Ir(COE)_2Cl]_2$. Given the predicted $\%V_{bur}$ for this system being >50%, the addition of both one and two equivalents of NHC per Ir centre was investigated.

The products of both reactions yielded highly unsymmetrical ^1H NMR spectra suggesting potential activation of the Dipp substituent as reported previously in the chemistry of IPr. Signals were observed in the ^1H NMR spectra of both reaction mixtures at δ_H 5.05 and 5.65 ppm, suggesting the formation of an alkenic species. Additionally, there was no signal corresponding to a hydride present in either spectrum which would have resulted from oxidative addition. In both cases, there is no carbenic signal in the ^{13}C NMR spectrum (δ_C <190 ppm); instead there are resonances at δ_C 155.8, and 155.2/151.5 ppm, for one and two equivalents respectively, which indicate the existence of a NC(H)N fragment. It was found, upon crystallisation, that the metal containing species resulting from these reactions features allyl-functionalised formamidine ligands, presumably resulting from ring opening of the 6-Dipp ligand (Scheme 5.4).

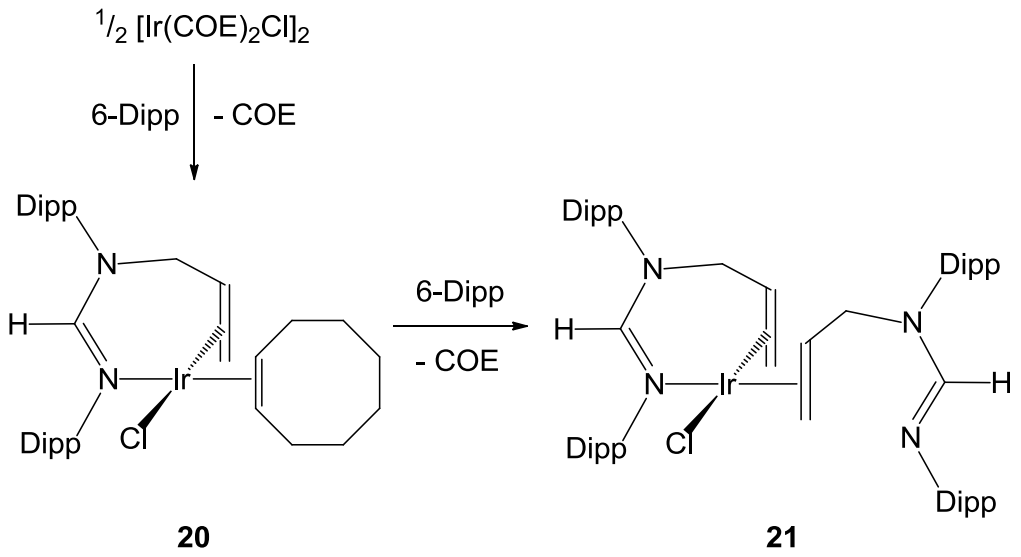

20 **21**

Scheme 5.4: Synthesis of iridium complexes bearing ring-opened 6-Dipp ligands.

These ligands formally result from the transfer of a proton from the C5 position to the C2 position and cleavage of an N-C bond in the original cyclic 6-Dipp ligand. Addition of a second equivalent of 6-Dipp to the iridium centre results in the cleavage of the N–C bond in a similar fashion to yield a system with an allyl-formamidine bound solely via the alkene, in addition to the *N*,alkene-chelating ligand. ^{1}H NMR spectroscopy data supports the observed structures, displaying signals consistent with metal-bound alkene moieties (multiplets in the range δ_H 3.1-2.5 ppm) for both **20** and **21**. In addition, for complex **21** there are 12 distinct ^{i}Pr CH_3 signals, indicating a low symmetry structure with no fluxional behaviour at room temperature. Crystals obtained from a concentrated diethyl ether solution at -30 °C were analysed by X-ray crystallography. The resulting structure featured the open chain, chelating 6-Dipp ligand with the alkene moiety *cis*- to the remaining cyclooctene ligand and *trans*- to the chloride ligand.

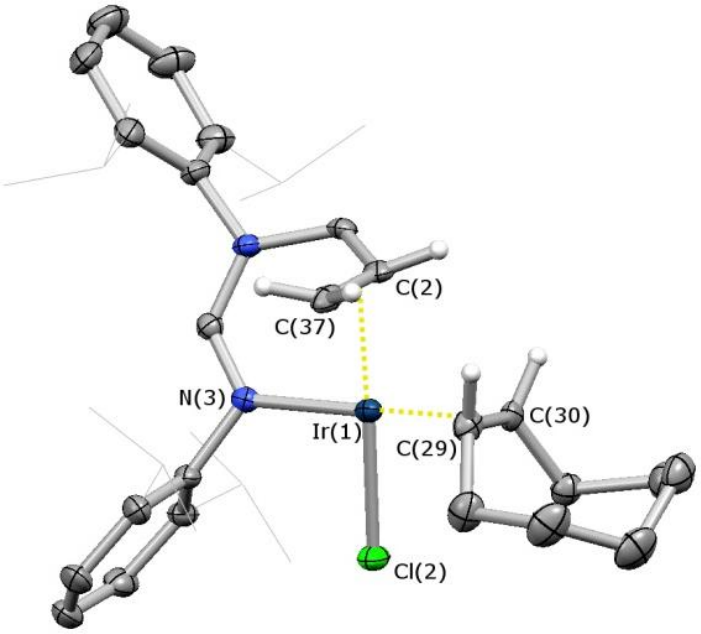

Figure 5.5: (6'-Dipp)Ir(COE)Cl (**20**), with most H atoms and ether solvent omitted and Dipp groups shown in wireframe for clarity; thermal ellipsoids set at 50% probability level. Key bond lengths (Å) and angles (°): Ir(1)–Cl(2) 2.344(1), Ir(1)–N(3) 2.103(4), Ir(1)–{C(2)–C(37)}centroid 1.981, Ir(1)–{C(29)–C(30)}centroid 2.039, C(2)–C(37) 1.419(7).

The Ir-Cl distance in **20** is somewhat shorter than the equivalent distance in (5-Mes)$_2$Ir(COE)Cl (**1**) [2.344(1) *cf.* 2.368(1) Å, respectively] presumably due to the relatively poor electron donation to the iridium offered by the imine and alkene substituents compared to NHC ligands. The alkene bond length is elongated from a free C=C bond [1.419(7) Å *cf.* 1.33 Å], which is in the typical range for an alkene coordinated to a neutral iridium-chloride fragment [1.37-1.43 Å].[16-19]

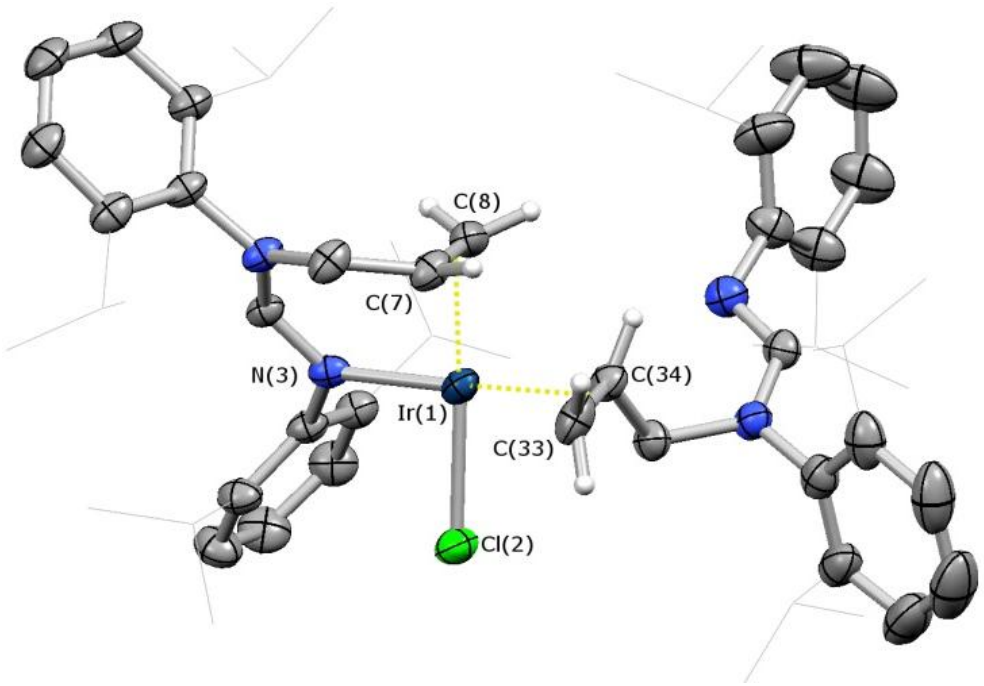

Figure 5.6: (6'-Dipp)$_2$IrCl (**21**), with most H atoms and ether solvent omitted and Dipp groups shown in wireframe for clarity; thermal ellipsoids set at 50% probability level. Key bond lengths (Å) and angles (°): Ir(1)–Cl(2) 2.3451(8), Ir(1)–N(3) 2.098(3), Ir(1)–{C(7)–C(8)}centroid 1.977, Ir(1)–{C(33)–C(34)}centroid 2.005, C(7)–C(8) 1.413(7), C(33)–C(34) 1.410(6).

As one might expect, the bond lengths observed for the 6'-Dipp ligand in **21** are essentially identical to those found in **20**. The second 6'-Dipp ligand is κ^1-coordinated through the alkene with no interaction via the formamidine presumably due to the alkene being a better donor to Ir(I) than the sp^2 nitrogen coupled with the ability to receive back bonding from the metal centre. The structure of **21** exhibits relatively short metal-alkene distances [1.977 and 2.005 Å], indicating a high amount of back-bonding from the electron rich metal to the alkenes. This is further supported by the elongation of the C=C bonds [1.413(7) and 1.410(6) Å], as observed in **20**.

In order to produce **20** and **21** via a more logical route, an alternative, targeted synthesis was devised via the open chain formamidine ligand. A straightforward synthesis, was employed involving the reaction of allyl bromide with *bis*-*N*,*N'*-Dipp-formamidine in the presence of a base. The temperature was maintained at 50 °C in order to minimise volatilisation of allyl-bromide. This produced the free *bis*-*N*,*N'*-Dipp-*N*-allylformamidine ligand (**22**) in good yield (Scheme 5.7). Addition of half an equivalent of $[Ir(COE)_2Cl]_2$ then afforded complex **20** in near quantitative yield (by ^{1}H NMR) after 30 min. Addition of a further equivalent of **22** to **20** leads to the formation of **21** as expected.

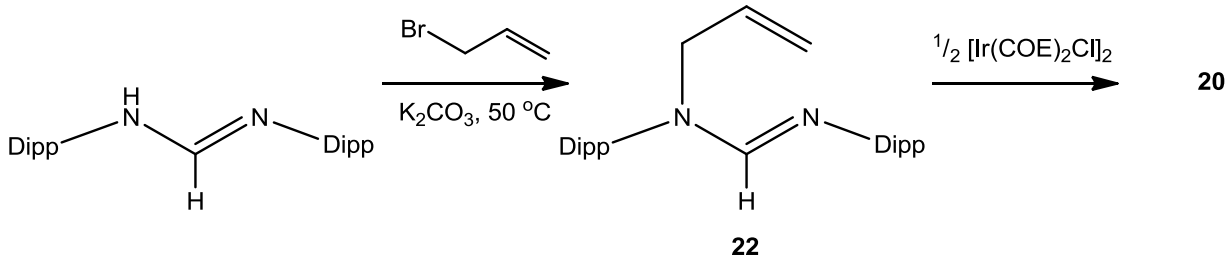

Scheme 5.7: Synthesis of ligand **22**, and subsequent reaction to form **20**.

5.4 Ring Opening Mechanism

Observation of the C–N cleavage of a heterocyclic carbene by metal coordination has not been previously reported. However, this process is not without precedent. In 2009, a report by Necheav *et al.* proposed the cleavage of the C–N bond in a 7-membered NHC bearing a double bond across the backbone by the action of a strong base (outlined in Fig 1.35, Chapter I).[20] In 2010, Whittlesey *et al*. reported the thermolysis of 6-Mes and 7-Mes where the carbene centre is close enough to the ortho-CH_3 group to oxidatively add a C-H bond (Scheme 5.8).[21] Trace amounts of acid, e.g. which are present in $CHCl_3$, are then enough to result in C-N cleavage in the backbone.

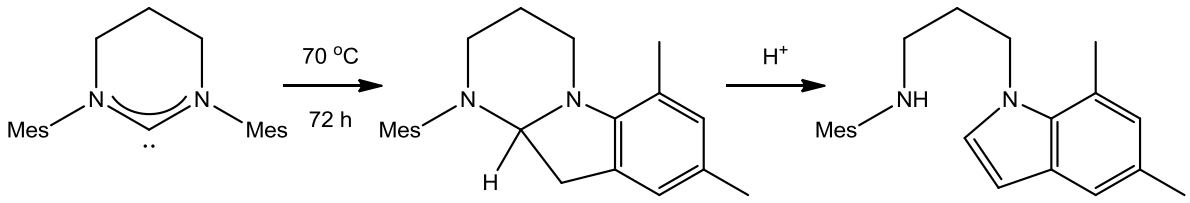

Scheme 5.8: Thermally induced intramolecular C–H activation followed by acid-catalysed C–N cleavage in 6-Mes observed by Whittlesey *et al.*[21]

Bearing in mind the deprotonation mechanism reported by Necheav *et al.*, we postulate an analogous metal-mediated route leading to the cleavage of the N–C bond and net proton migration using catalytic amounts of free NHC as a base (Scheme 5.9).

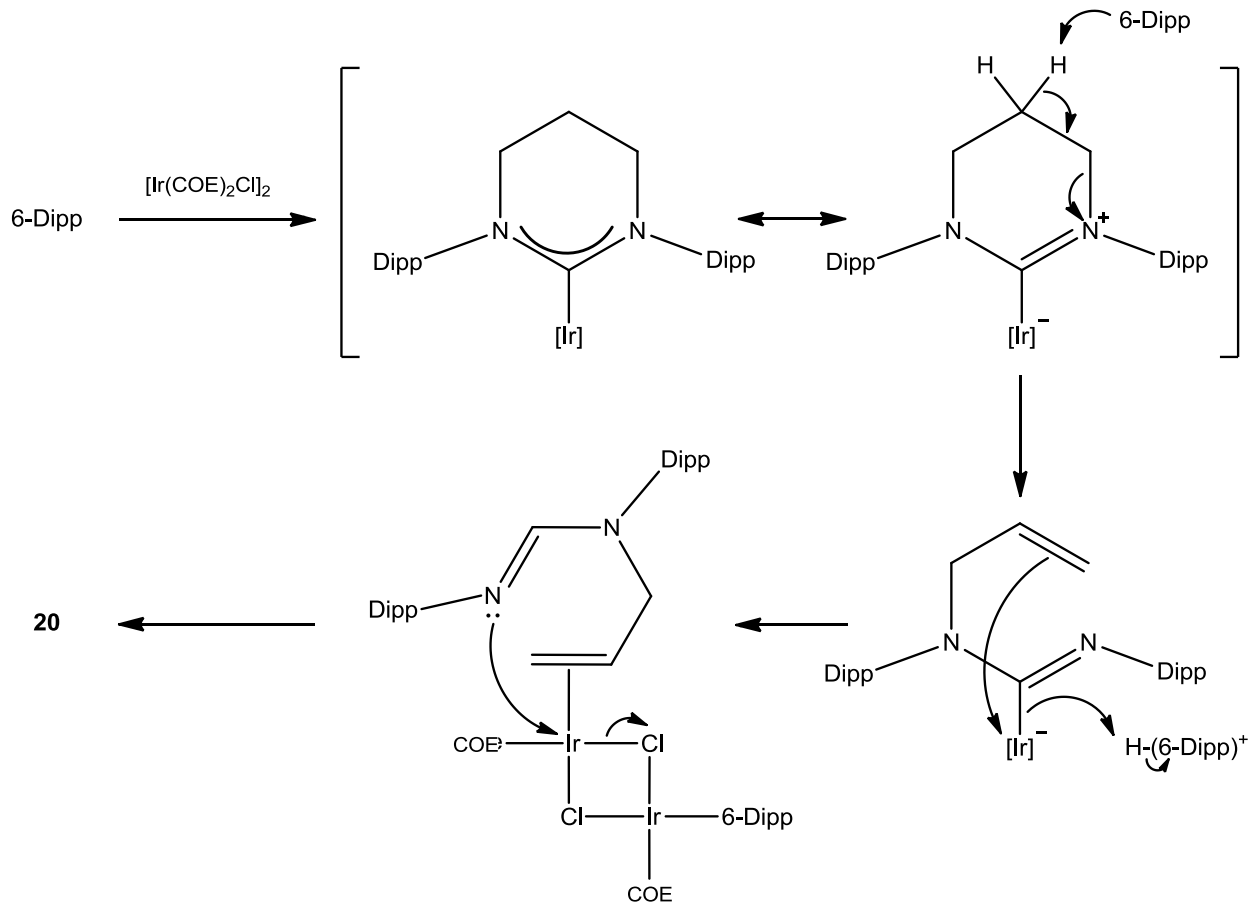

Figure 5.9: Postulated mechanism for the metal-mediated cleavage of the N–C linkage in 6-Dipp leading to the formation of **20**. [Ir] = [Ir(COE)(μ-Cl)$_2$Ir(COE)(6-Dipp)].

Coordination of the NHC to the metal allows the formation of a formally zwitterionic form which increases the acidity of the C5 proton. A free equivalent of 6-Dipp can then act as a strong base to remove this proton leading to a Hoffman-type elimination mechanism with consequent cleavage of the C–N bond. The newly formed alkene can wrap round to coordinate at the metal, replacing the metal-carbon bond which can deprotonate $[(6\text{-Dipp})H]^+$ to reform the catalytic 6-Dipp. Finally, we can envisage displacement of the chloride bridge by the amidine sp^2-nitrogen donor resulting in a chelating allyl-formamidine ligand.

5.4.1 Protonation Study

A comparative study was carried out using sub-stoichiometric amounts of methyl iodide and hydrochloric acid, as sources of Me^+ and H^+ respectively. Initially, we attempted to add one equivalent of methyl iodide to a solution of 6-Dipp in order to study [(6-Dipp)Me]I. This, unfortunately, resulted in a mixture of products observed by ^{1}H NMR in which both allyl-formamidine species and protonated [(6-Dipp)H]I were observed as well as methylated analogues.

A clean reaction, as observed by ^{1}H NMR spectroscopy, could be obtained by the addition of 0.5 equivalents of methyl iodide (Scheme 5.10). Both the NHC salt and open chain formamidine could be separated by hexane extraction of the neutral allyl-formamidine, and their ^{1}H NMR spectrum measured to confirm their identity.

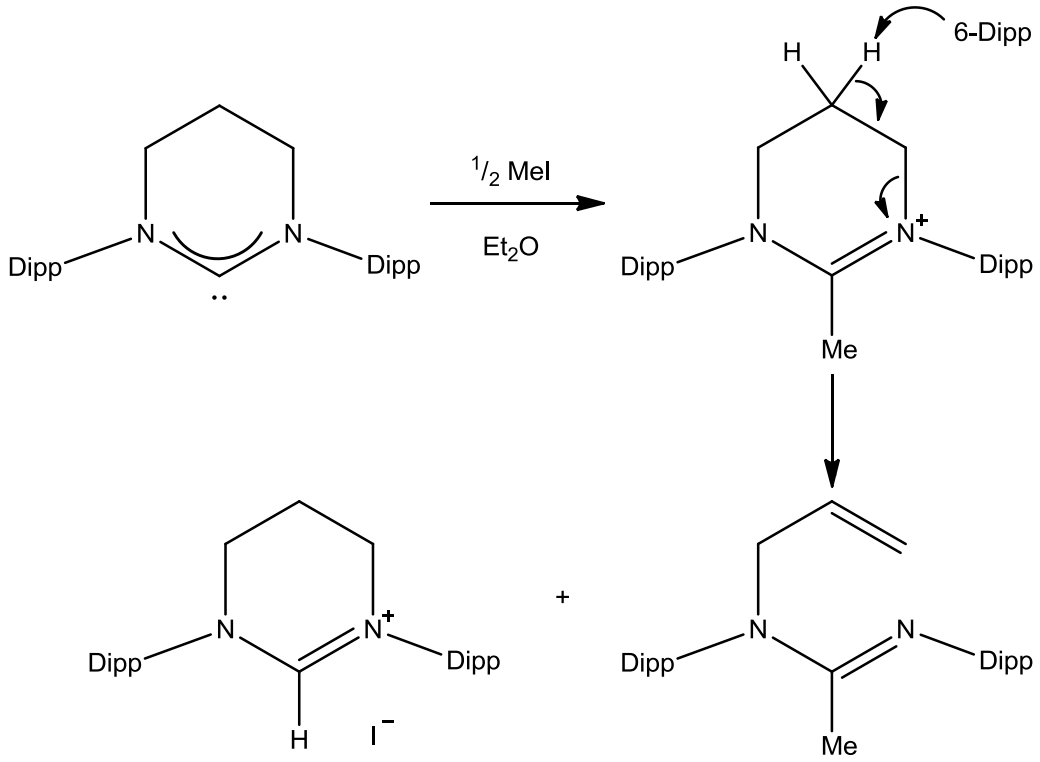

Scheme 5.10: Cleavage of the N–C bond in 6-Dipp with stoichiometric control.

It transpired that this ring opening process can also be effected using catalytic amounts of acid. Addition of 10 mol% of hydrochloric acid resulted in the isolation in nearly 90% yield of the allyl-formamidine product (**22**). This would suggest that protonation of one NHC results in the deprotonation of its C5 proton by a second molecule of the free carbene; this is then activated to attack by a third molecule and so on.

In 1995, Arduengo *et al.* reported and structurally characterised the interaction of IMes with corresponding imidazolium salt [(IMes)H][PF_6] where, in this case, the free NHC "coordinates" to the imidazolium proton to give a proton bridged species.[22] For 6-Dipp, the C2 position is more hindered by the flanking Dipp groups, but it likely that the C2-proton in $[(6\text{-Dipp})H]^+$ may be removed by free 6-Dipp. However, this process is unproductive whereas acting as a base at the C5 position leads to Hoffman-type elimination chemistry to produce **22**. Deprotonation is further favoured as the C–H bond at C5 also aligns perfectly

with the σ^*(C–N) (Fig 5.11); hence, these hindered 6-membered NHCs are well set up for this ring opening mechanism.

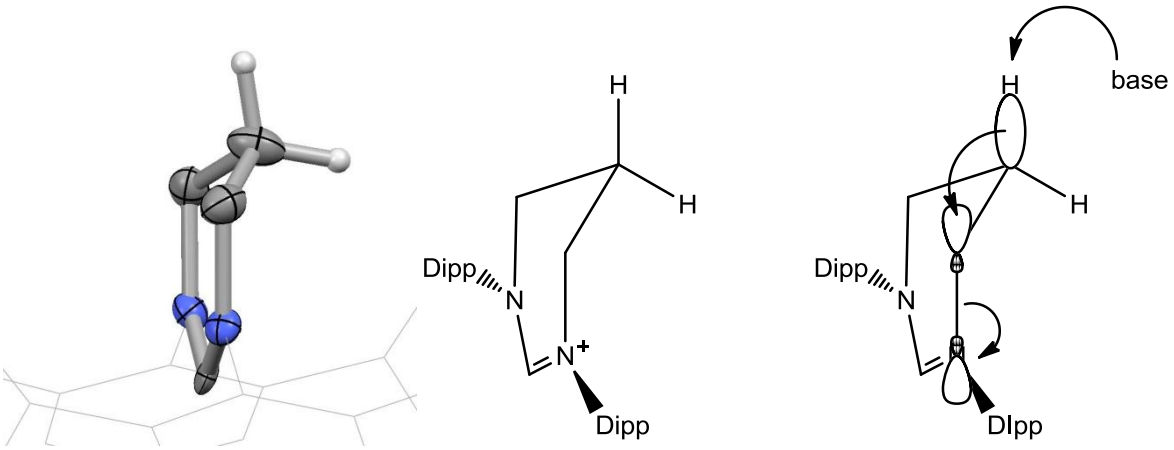

Figure 5.11: Alignment of the σ(C–H) orbital with the σ^*(C–N) orbital in 6-membered NHCs. Crystal structure (*left*) was taken from the structure of (6-Dipp)AgBr reported by Fallis *et al*.[23]

5.5 Formation of Saturated Anionic NHCs

Basic species facilitate the ring opening mechanism of the 6-Dipp ligand, yet as reported later in this thesis (Chapter VI) the electrophilic $[(NHC)Au]^+$ fragment will promote ring closing of the allyl-formamidine **22**. Hence, use of a neutral Lewis acid should in theory lead to a ring closed product bearing an anionic substituent on the backbone. A bulky system would be required to reduce the propensity for coordination through the nitrogen of the formamidine. In an attempt to form an expanded ring analogue of Tamm's anionic NHC,[24] *tris*(pentafluorophenyl)borane was added to **22** in toluene. Aside from coordination through nitrogen, there are two potential ring closing mechanisms leading to different products (Scheme 5.12).

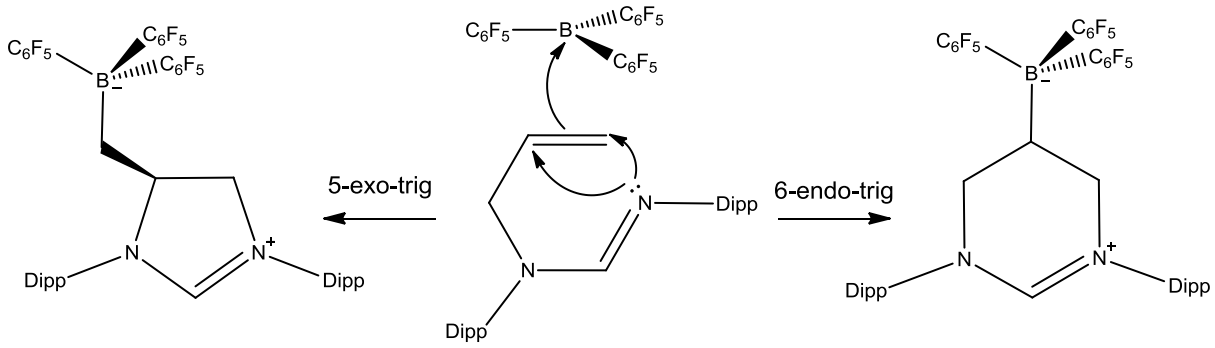

Scheme 5.12: Two ring closing mechanisms leading to different sizes of a saturated NHC precursor.

Monitoring of the reaction by ^{11}B and ^{19}F NMR spectroscopies suggested coordination through a primary carbon, characterised by a ^{11}B NMR signal at -14.7 ppm,[25] compared with δ_B -3.3 ppm reported for coordination of imine type species to $B(C_6F_5)_3$.[26] The ^{11}B NMR implies a small degree of coordination through the imine nitrogen, suggesting that this site is sufficiently hindered that the major reaction occurs through the alkene. Collection of crystals from a concentrated toluene solution at -30 °C and X-ray crystallography revealed the precise structure of the heterocycle formed (Fig 5.13). The structure displays a 5-membered heterocycle with a $–CH_2B(C_6F_5)_3$ unit attached at the C4 position.

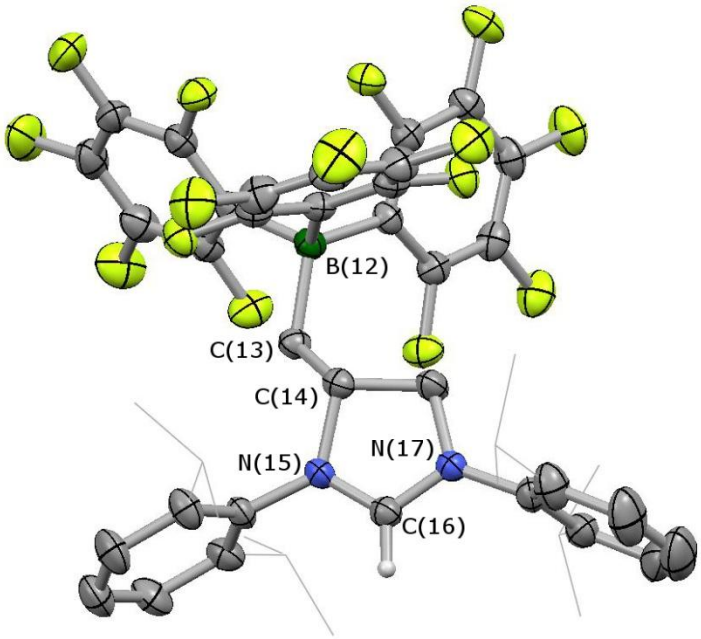

Figure 5.13: H(5-Dipp^{BArF}) (**23**), with most H atoms and toluene solvent omitted and Dipp groups shown in wireframe for clarity; thermal ellipsoids set at 50% probability level. Key bond lengths (Å) and angles (°): B(12)–C(13) 1.664(4), N(15)–C(16) 1.311(3), C(16)–N(17) 1.309(3), B(12)–C(13)–C(14) 116.8(2), N(15)–C(16)–N(17) 114.0(2), sum of angles around B(12) to (C_6F_5) rings – 329.4(6).

It appears that reaction of **22** with $B(C_6F_5)_3$ leads to a 5-exo-trig ring closure resulting in a 5-membered, saturated NHC precursor. By Baldwin's rules, the 6-endo-trig ring closing mechanism is also favourable, however there is only one signal observed in the ^{11}B NMR spectrum. Reaction of $B(C_6F_5)_3$ with (6'-Dipp)$_2$IrCl (**21**) led to coordination occurring exclusively through the pendant formamidine nitrogen, as characterised by ^{11}B NMR. This is perhaps unsurprising as this nitrogen is the most available reaction site.

5.5.1 Deprotonation of 23

Interestingly, it is possible to deprotonate **23** with one equivalent of K[N(SiMe$_3$)$_2$] to give the potassium salt of the corresponding anionic NHC, which can be crystallised as the

18-crown-6 adduct (Fig 5.14). In comparison, Tamm *et al.* had discovered that deprotonation of their unsaturated NHC zwitterions was not possible.[24]

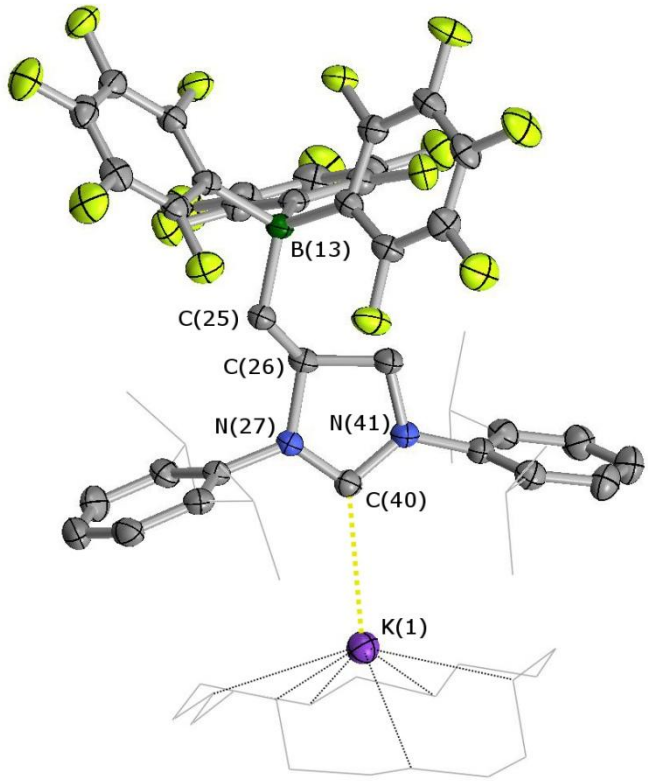

Figure 5.14: [K(18-crown-6)][(5-Dipp^{BArF})] (**24**), with H atoms omitted and Dipp groups and crown-ether shown in wireframe for clarity; thermal ellipsoids set at 50% probability level. Key bond lengths (Å) and angles (°): B(13)–C(25) 1.669(4), N(27)–C(40) 1.353(4), C(40)–N(41) 1.353(3), C(40)···K(1) 3.234(3), B(13)–C(25)–C(26) 115.9(2), N(27)–C(40)–N(41) 104.7(2), sum of angles around B(13) to (C_6F_5) rings – 328.0(6).

The main structural difference observed on deprotonation of **23** to form **24** is the narrowing of the NCN angle [104.7(2)° from 114.0(2)°] accompanied by the lengthening of the N–C bonds around the carbene [1.353(4) Å from 1.310(3) Å]. This is consistent with a reduction in the bond order witnessed with deprotonation in NHCs.[27, 28] The K···C_{NHC} distance is much longer [3.234(3) Å] than Alder *et al.* reported for their potassium complex

of 6-^{i}Pr [3.00 Å].[28] This is perhaps due to the steric demand of the Dipp groups clashing with 18-crown-6, whereas the ^{i}Pr groups on Alder's NHC can rotate out of the way.

5.6 Conclusions

It is clear that the coordination of a saturated, expanded ring NHC to a metal atom enhances the acidity of the C–H bonds at the C5 position. This has not been previously observed with less sterically demanding NHCs, presumably due to the ability of the second NHC equivalent to coordinate to the metal in preference to acting as a base. The steric demands of the 6-Dipp ligand at the metal centre mean that a second equivalent of free 6-Dipp cannot coordinate and so instead acts as a base. This is an alternative pathway to the observations of *bis*-coordination observed in Chapter III due to the inability of iridium to fit two, intact 6-Dipp ligands in the coordination sphere.

The ring closing mechanism of these open chain allyl-formamidine systems using a bulky Lewis acid [such as $B(C_6F_5)_3$], appears to favour the 5-exo-trig pathway even though the 6-endo-trig route is also possible. This has offered opportunities for the development of saturated, anionic NHCs. In contrast to Tamm's imidazolium-based NHC, **24** has the anion electronically separated from the carbenic centre such that the donor properties should not be dissimilar to those of 5-Dipp. **24** will have many applications for the formation and study of low valent cations in non-polar, non-donor solvents. Initial attempts to form a coordination complex with (THT)AuCl have resulted in a colour change consistent with coordination of a NHC, but spectroscopic data thus far have proved inconclusive.

5.7 References

1. T. Nguyen, A. D. Sutton, M. Brynda, J. C. Fettinger, G. J. Long and P. P. Power, *Science*, 2005, **310**, 844-847.
2. S. P. Green, C. Jones and A. Stasch, *Science*, 2007, **318**, 1754-1757.
3. N. Marion and S. P. Nolan, *Chem. Soc. Rev.*, 2008, **37**, 1776-1782.
4. N. Marion and S. P. Nolan, *Acc. Chem. Res.*, 2008, **41**, 1440-1449.

5. H. Braunschweig, R. D. Dewhurst, K. Hammond, J. Mies, K. Radacki and A. Vargas, *Science*, 2012, **336**, 1420-1422.
6. J. J. Dunsford, K. J. Cavell and B. M. Kariuki, *Organometallics*, 2012, **31**, 4118-4121.
7. C. Y. Tang, A. L. Thompson and S. Aldridge, *J. Am. Chem. Soc.*, 2010, **132**, 10578-10591.
8. Z. L. Zhu, R. J. Wright, M. M. Olmstead, E. Rivard, M. Brynda and P. P. Power, *Angew. Chem. Int. Ed.*, 2006, **45**, 5807-5810.
9. E. Rivard and P. P. Power, *Inorg. Chem.*, 2007, **46**, 10047-10064.
10. Y. Segawa, M. Yamashita and K. Nozaki, *Science*, 2006, **314**, 113-115.
11. A. V. Protchenko, K. H. Birjkumar, D. Dange, A. D. Schwarz, D. Vidovic, C. Jones, N. Kaltsoyannis, P. Mountford and S. Aldridge, *J. Am. Chem. Soc.*, 2012, **134**, 6500-6503.
12. A. V. Protchenko, D. Dange, J. R. Harmer, C. Y. Tang, A. D. Schwarz, M. J. Kelly, N. Phillips, R. Tirfoin, K. H. Birjkumar, C. Jones, N. Kaltsoyannis, P. Mountford and S. Aldridge, *Nature Chem.*, 2014, **6**, 315-319.
13. V. Cesar, N. Lugan and G. Lavigne, *J. Am. Chem. Soc.*, 2008, **130**, 11286-11287.
14. M. G. Hobbs, C. J. Knapp, P. T. Welsh, J. Borau-Garcia, T. Ziegler and R. Roesler, *Chem. Eur. J.*, 2010, **16**, 14520-14533.
15. E. L. Kolychev, S. Kronig, K. Brandhorst, M. Freytag, P. G. Jones and M. Tamm, *J. Am. Chem. Soc.*, 2013, **135**, 12448-12459.
16. R. J. Restivo, G. Ferguson, T. L. Kelly and C. V. Senoff, *J. Organomet. Chem.*, 1975, **90**, 101-109.
17. T. Makino, Y. Yamamoto and K. Itoh, *Organometallics*, 2004, **23**, 1730-1737.
18. T. Yamagata, K. Nakajima, K. Arimitsu, A. Iseki and K. Tani, *Acta Cryst. E*, 2008, **64**, M579-U592.
19. J. Langer and H. Gorls, *Inorg. Chem. Comm.*, 2011, **14**, 1612-1615.
20. E. L. Kolychev, I. A. Portnyagin, V. V. Shuntikov, V. N. Khrustalev and M. S. Nechaev, *J. Organomet. Chem.*, 2009, **694**, 2454-2462.
21. R. S. Holdroyd, M. J. Page, M. R. Warren and M. K. Whittlesey, *Tet. Lett.*, 2010, **51**, 557-559.
22. A. J. Arduengo, S. F. Gamper, M. Tamm, J. C. Calabrese, F. Davidson and H. A. Craig, *J. Am. Chem. Soc.*, 1995, **117**, 572-573.
23. M. Iglesias, D. J. Beetstra, J. C. Knight, L. L. Ooi, A. Stasch, S. Coles, L. Male, M. B. Hursthouse, K. J. Cavell, A. Dervisi and I. A. Fallis, *Organometallics*, 2008, **27**, 3279-3289.
24. S. Kronig, E. Theuergarten, C. G. Daniliuc, P. G. Jones and M. Tamm, *Angew. Chem. Int. Ed.*, 2012, **51**, 3240-3244.
25. N. Bavarian and M. C. Baird, *Dalton Trans.*, 2004, 4089-4091.
26. J. M. Blackwell, W. E. Piers, M. Parvez and R. McDonald, *Organometallics*, 2002, **21**, 1400-1407.
27. A. J. Arduengo, R. L. Harlow and M. Kline, *J. Am. Chem. Soc.*, 1991, **113**, 361-363.
28. R. W. Alder, M. E. Blake, C. Bortolotti, S. Bufali, C. P. Butts, E. Linehan, J. M. Oliva, A. G. Orpen and M. J. Quayle, *Chem. Comm.*, 1999, 241-242.

Chapter VI

Attempting to Isolate the Gold Cation:

Stabilising a Highly Electrophilic Centre

6.1 Introduction

In recent years, reactions involving ring closing of alkenes and alkynes as well as nucleophilic addition to alkynes have been catalysed by gold(I) cations, and this has become a highly researched and exploited area.[1-5] Due to the closed shell configuration of Au(I), the catalytic behaviour of $[LAu]^+$ (L = phosphine, NHC) is analogous to that of a soft proton.[6] A variety of supporting ligands have been exploited for the synthesis of a variety of catalyst precursors. In particular, NHCs have been well documented to stabilise a variety of reactive gold species.[7-12] There is a wealth of literature on the activity of the gold species and the products produced,[3, 4] however, most attempts to isolate the reactive intermediates have been futile.[13] The closest examples to a one-coordinate gold cation were reported in 2007 by Bertrand *et al.*,[14] and in 2012 by Straub *et al*. where the NHC supported gold cation were coordinated by a toluene molecule (Fig 6.1).[15]

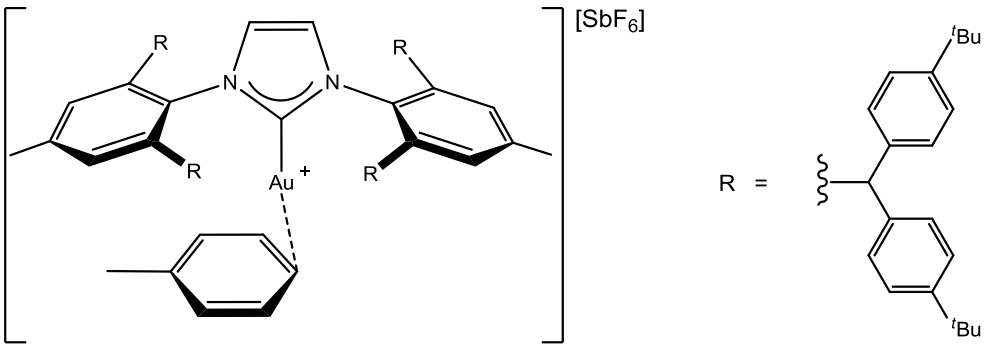

Figure 6.1: Coordination of toluene to a one-coordinate gold cation.

Another class of gold species that has been suggested as an intermediate in catalytic cycles is a gold hydride.[1, 16, 17] The parent species AuH and extended AuH_n systems have been studied theoretically,[18, 19] as well as in the gas phase[20] and by matrix isolation.[21, 22] However, these are typically highly reactive species and reported examples of complexes containing AuH bonds are most often supported by an ancillary phosphine or NHC donor. There are several examples of heterometallic hydride bridges,[23-26] but very few examples of monomeric and homometallic gold hydrides (Fig 6.2).[27-29]

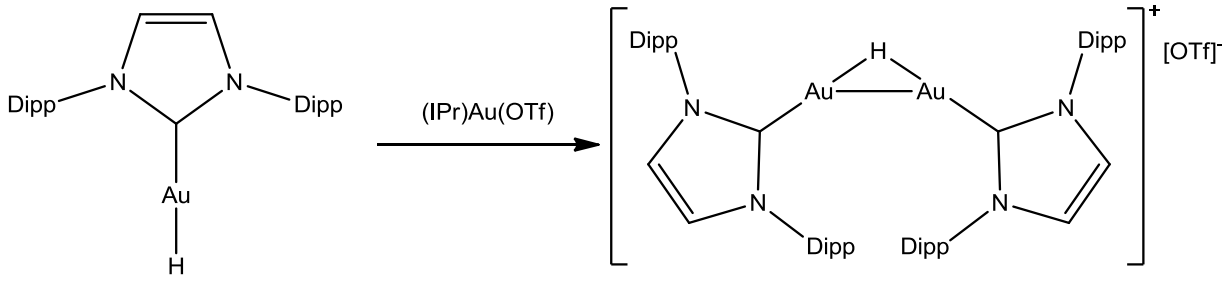

Figure 6.2: First examples of NHC-supported monomeric and homonuclear gold hydrides.

In this chapter, we aim to exploit the increased donor properties of the sterically demanding expanded ring NHCs such as 6-Mes, 7-Mes and 6-Dipp to electronically and sterically stabilise a one-coordinate gold cation. This increased donor strength should help to reduce the electrophilicity of the gold cation such that solvent molecules will interact less strongly allowing for a more relevant study of the catalytic species. Additionally, expanded ring NHCs will be exploited to alter the properties of gold hydride systems, potentially increasing the hydridic nature of the Au–H fragment.

6.2 Experimental

*Preparation of [(6-Mes)$_2$Au][BAr$^f_4$] (**25**)*

A suspension of Na[BAr$^f_4$] (40 mg, 0.05 mmol) in fluorobenzene (10 cm^3) was added to a stirred mixture of (6-Mes)AuCl (25 mg, 0.05 mmol) and 6-Mes (15 mg, 0.05 mmol) also in fluorobenzene (20 mL) at -30 °C. After warming to 20 °C, the solution was filtered and the solvent removed *in vacuo*. The off-white product was washed with hexanes (2 x 20 mL), and crystals suitable for X-ray diffraction obtained by layering a fluorobenzene solution with hexane and storage at 20 °C. Crystals were isolated in only 34% yield (29 mg) due to the accompanying formation of colloidal gold.

*Spectroscopic data for **25***

^{1}H NMR (CD_2Cl_2, 300 MHz, 298 K): δ_H 7.73 (8H, s, *ortho*-CH [BAr$^f_4$]$^-$), 7.57 (4H, s, *para*-CH [BAr$^f_4$]$^-$), 6.92 (8H, s, *meta*-CH Mes), 3.13 (8H, tr, $^3J_{HH}$ = 5.7 Hz, NCH_2), 2.33 (12H, s, *para*-CH_3), 2.06 (4H, qn, $^3J_{HH}$ = 5.7 Hz, NCH_2CH_2), 1.74 (24H, s, *ortho*-CH_3). ^{13}C NMR (CD_2Cl_2, 75 MHz, 298 K): δ_c 202.1 (NCN), 162.1 (qt, $^1J_{CB}$ = 49.1 Hz, BC [BAr$^f_4$]$^-$), 141.4 (NC Mes), 138.7 (*para*-C Mes), 135.2 (br, *ortho*-CH [BAr$^f_4$]$^-$), 135.2 (*ortho*-C Mes), 129.8 (*meta*-CH Mes), 129.2 (m, *meta*-C [BAr$^f_4$]$^-$), 125.0 (qt, $^1J_{CF}$ = 270 Hz, CF_3 [BAr$^f_4$]$^-$), 117.8 (m, *para*-CH [BAr$^f_4$]$^-$), 45.5 (NCH_2), 21.1 (NCH_2CH_2), 20.6 (*para*-CH_3 Mes), 17.9 (*ortho*-CH_3 Mes). MS (ESI +ve): *m/z* calc. for $[C_{44}H_{56}AuN_4]^+$ 837.4165; meas. 837.4197.

*Crystallographic data for **25***

$C_{76}H_{68}AuN_4BF_{24}$, M_r = 1701.13, triclinic, *P*-1, a = 13.7243(1), b = 16.2782(1), c = 17.8607(1) Å, α = 91.6666(4), β = 109.7994(4), γ = 91.2678(3)°, V = 3750.56(4) Å^3, Z = 2, ρ_c = 1.506 Mg m^{-3}, T = 150 K, λ = 0.710730 Å, 67690 reflections collected, 17050 independent [R(int) = 0.025], which were used in calculations. R_1 = 0.0409, *w*R_2 = 0.0882

for observed unique reflections [$I > 2\sigma(I)$] and $R_1 = 0.0478$, $wR_2 = 0.0924$ for all unique reflections. Max. and min. residual electron densities 1.19 and -1.03 e $Å^{-3}$.

*Preparation of (Xyl7-Mes)AuCl (**26**)*

(THT)AuCl (50 mg, 0.02 mmol) was added to a stirred solution of (Xyl7-Mes)AgBr (98 mg, 0.02 mmol) in dichloromethane (10 cm^3) in the absence of light and stirred for 3 h. Activated charcoal (150 mg) was added to the dark blue solution which was stirred for a further 30 min. The solution was filtered through Celite and concentrated *ca*. 2 cm^3. Addition of pentane (40 cm^3) stimulated the precipitation of the white product, which was collected in 52% yield (50 mg). Crystals suitable for X-ray crystallography were obtained from a layering of dichloromethane solution with pentane stored at 20 °C.

*Spectroscopic data for **26***

^{1}H NMR ($CDCl_3$, 300 MHz, 298 K): δ_H 7.40 (2H, m, CH Xyl), 7.22 (2H, m, CH Xyl), 6.91 (4H, s, *meta*-CH Mes), 4.96 (4H, s, NCH_2), 2.27 (6H, s, *para*-CH_3 Mes), 2.22 (12H, s, *ortho*-CH_3 Mes). ^{13}C NMR ($CDCl_3$, 100 MHz, 298 K): δ_C 202.5 (NCN), 140.5 (NC Mes), 140.2 (*para*-C Mes), 134.3 (*ortho*-C Mes), 134.0 (C Xyl), 130.4 (CH Xyl), 130.2 (*meta*-CH Mes), 129.3 (CH Xyl), 56.5 (NCH_2), 20.9 (*para*-CH_3 Mes), 18.2 (*ortho*-CH_3 Mes). MS (ESI +ve): *m/z* 637.2 (M^+, 100%). Accurate mass: calc. for $[C_{27}H_{30}AuN_2Na]^+$ 637.1655, meas. 637.1650.

*Crystallographic data for **26***

$C_{27}H_{30}AuN_2Cl$, M_r = 614.97, monoclinic, $P2_1/c$, a = 9.6600(1), b = 16.9304(2), c = 16.0749(2) Å, β = 106.2737(6)°, V = 2523.68(5) $Å^3$, Z = 4, ρ_c = 1.618 Mg m^{-3}, T = 150 K, λ = 0.710730 Å, 34506 reflections collected, 5749 independent [R(int) = 0.030], which were used in calculations. $R_1 = 0.0349$, $wR_2 = 0.0760$ for observed unique reflections [$I > 2\sigma(I)$]

and R_1 = 0.0584, wR_2 = 0.0961 for all unique reflections. Max. and min. residual electron densities 1.79 and -1.54 e $Å^{-3}$.

*Preparation of [{(6-Dipp)Au}$_2$(μ-Cl)][BAr$^f_4$] (**27a**)*

Na[BAr$^f_4$] (21 mg, 0.024 mmol) in fluorobenzene was added to a stirred solution of (6-Dipp)AuCl (30 mg, 0.047 mmol) also in fluorobenzene (5 cm^3) at -5 °C. After stirring for 1 h at -5 °C, the solution was warmed to room temperature and the mixture was filtered and the solvent removed *in vacuo*. Washing with hexanes (2 x 10 cm^3) and drying *in vacuo* yielded a white solid. X-ray quality crystals were obtained in 54% yield (27 mg) by layering a fluorobenzene solution with hexane at -30 °C.

*Spectroscopic data for **27a***

^{1}H NMR (CD_2Cl_2, 300 MHz, 298 K): δ 7.72 (8H, s, *ortho*-CH [BAr$^f_4$]$^-$), 7.56 (4H, s, *para*-CH [BAr$^f_4$]$^-$), 7.38 (4H, tr, $^3J_{HH}$ = 7.5 Hz, *para*-CH Dipp), 7.12 (8H, d, $^3J_{HH}$ = 7.5 Hz, *meta*-CH Dipp), 3.46 (8H, tr, $^3J_{HH}$ = 5.7 Hz, NCH_2), 2.78 (8H, sept, $^3J_{HH}$ = 6.9 Hz, CH ^{i}Pr), 2.30 (4H, qn, $^3J_{HH}$ = 5.7 Hz, NCH_2CH_2), 1.23 (12H, d, $^3J_{HH}$ = 6.9 Hz, CH_3 ^{i}Pr) , 1.10 (12H, d, $^3J_{HH}$ = 6.9 Hz, CH_3 ^{i}Pr). ^{13}C NMR (CD_2Cl_2, 125 MHz, 298 K): δ_C 199.8 (NCN), 162.3 (q, $^1J_{CB}$ = 50 Hz, CB [BAr$^f_4$]$^-$), 145.7 (NC Dipp), 141.3 (*ortho*-C Dipp), 135.4 (br, *ortho*-CH [BAr$^f_4$]$^-$), 130.4 (*para*-CH Dipp), 129.4 (m, *meta*-C [BAr$^f_4$]$^-$), 125.2 (q, $^1J_{CF}$ = 270 Hz, CF_3 [BAr$^f_4$]$^-$), 125.2 (*meta*-CH Dipp), 118.0 (m, *para*-CH [BAr$^f_4$]$^-$), 48.2 (NCH_2), 29.2 (CH ^{i}Pr), 25.0, 24.9 (CH_3 ^{i}Pr), 20.5 (s, NCH_2CH_2). MS (ESI +ve): *m/z* calc. for $[C_{56}H_{80}Au_2N_4Cl]^+$ 1237.5397, meas. 1322.56 (100%), 1350.59 (50%), 1415.58 (80%). Elemental analysis: calc. for $C_{88}H_{92}Au_2N_4BClF_{24}$: C 50.29, H 4.41, N 2.67, meas. C 49.20, H 4.63, N 2.59.

*Crystallographic data for **27a***

$C_{88}H_{92}Au_2N_4BClF_{24}$, M_r = 2101.88, triclinic, *P*-1, a = 15.1842(3), b = 17.8881(4), c = 20.7715(5) Å, α = 113.748(2), β = 106.436(2), γ = 97.034(2)°, V = 4770.2(2) Å^3, Z = 2, ρ_c = 1.463 Mg m^{-3}, T = 150 K, λ = 0.710730 Å, 44244 reflections collected, 22921 independent [R(int) = 0.031], which were used in calculations. R_1 = 0.0327, wR_2 = 0.725 for observed unique reflections [I > 2σ(I)] and R_1 = 0.0448, wR_2 = 0.0797 for all unique reflections. Max. and min. residual electron densities 1.80 and -1.42 e Å^{-3}.

*Preparation of [{(7-Dipp)Au}$_2$(μ-Cl)][BAr$^f{}_4$] (**27b**)*

(7-Dipp)AuCl (40 mg, 0.061 mmol) was dissolved in fluorobenzene (2 cm^3) at -5 °C. In a similar fashion, Na[BAr$^f{}_4$] (27 mg, 0.031 mmol) was slurried in fluorobenzene (1 cm^3), cooled to -5 °C and added dropwise to the solution of (7-Dipp)AuCl. After stirring at -5 °C for 1 h, the solution was allowed to warm to room temperature. Colourless crystals suitable for X-ray crystallography were obtained by layering the reaction mixture with hexanes at room temperature, isolated by filtration, washed with hexane and dried *in vacuo*. Yield: 58% (38 mg).

*Spectroscopic data for **27b***

^{1}H NMR (300 MHz, CD_2Cl_2, 298 K) δ_H 7.72 (8H, s, [BAr$^f{}_4$]$^-$), 7.56 (4H, s, [BAr$^f{}_4$]$^-$), 7.31 (4H, dd, $^3J_{HH}$ = 15.9, 7.1 Hz, *para*-CH Dipp), 7.12 (8H, d, $^3J_{HH}$ = 7.7 Hz, *meta*-CH Dipp), 3.94 (8H, m, NCH_2), 2.99 (8H, sept, $^3J_{HH}$ = 7.2 Hz, CH ^{i}Pr), 2.26 (8H, br s, NCH_2CH_2), 1.27 (24H, d, $^3J_{HH}$ = 6.4 Hz, CH_3 ^{i}Pr), 1.13 (24H, d, $^3J_{HH}$ = 5.9 Hz, CH_3 ^{i}Pr). ^{13}C NMR (100 MHz, CD_2Cl_2, 298 K) δ_C 195.6 (NCN), 162.4 (qt, $^1J_{CB}$ = 49.3 Hz, CB [BAr$^f{}_4$]$^-$), 145.5 (NC Dipp), 135.5 (br, *ortho*-CH [BAr$^f{}_4$]$^-$), 132.2 (*ortho*-C Dipp), 130.0 (*para*-CH Dipp), 129.7 (m, *meta*-C [BAr$^f{}_4$]$^-$), 125.4 (*meta*-CH Dipp), 125.2 (qt, $^1J_{CF}$ = 271.2 Hz, CF_3 [BAr$^f{}_4$]$^-$),

118.1 (m, *para*-CH $[BAr^f_4]^-$), 55.6 (NCH_2), 29.4 (CH ^{i}Pr) 25.1 (br, CH_3 ^{i}Pr), 24.7 (NCH_2CH_2). MS (ESI +ve): *m/z* calc. for $[C_{58}H_{84}Au_2N_4Cl]^+$ 1265.57, meas. 1396.57 (8%), 1378.62 (50%), 1350.59 (100%).

*Crystallographic data for **27b***

$C_{90}H_{96}Au_2N_4ClBF_{24}$, M_r = 2129.94, monoclinic, $P2_1/c$, a = 18.7614(1) Å, b = 12.8765(1) Å, c = 37.9083(3) Å, β = 97.5228(3)°, V = 9079.11(11) Å^3, Z = 4, ρ_c = 1.558 Mg m^{-3}, T = 150 K, λ = 0.710730 Å, 119619 reflections collected, 20659 independent [R(int) = 0.064], which were used in calculations. R_1 = 0.0418, wR_2 = 0.0536 for observed unique reflections [I > 2σ(I)] and R_1 = 0.0913, wR_2 = 0.0753 for all unique reflections. Max. and min. residual electron densities 2.40 and -3.17 e Å^{-3}.

*Preparation of [{(6-Dipp)Au}$_2$Ar^f][BAr$^f_4$] (**28a**)*

A stirred solution of (6-Dipp)AuCl (30 mg, 0.047 mmol) in dichloromethane (5 cm^3) at -78 °C was transferred onto Na[BAr^f_4] (42 mg, 0.047 mmol) and the reaction mixture allowed to warm to -5 °C. After stirring for 30 min at -5 °C, the solution was warmed to room temperature and stirred for 4 d. The mixture was then filtered and the solvent removed *in vacuo*. Washing with hexanes (2 x 10 cm^3) and drying *in vacuo* yielded a white solid. X-ray quality crystals were obtained in 61% yield (32 mg) by layering a fluorobenzene solution with pentane at 20 °C.

*Spectroscopic data for **28a***

^{1}H NMR (CD_2Cl_2, 300 MHz, 298 K): δ_H 7.73 (1H, s, *para*-CH Ar^f), 7.72 (8H, s, *ortho*-CH $[BAr^f_4]^-$), 7.56 (4H, s, *para*-CH $[BAr^f_4]^-$), 7.37 (4H, tr, $^3J_{HH}$ = 7.5 Hz, *para*-CH Dipp), 7.09 (8H, d, $^3J_{HH}$ = 7.5 Hz, *meta*-CH Dipp), 6.37 (2H, s, *ortho*-CH Ar^f), 3.36 (8H, tr, $^3J_{HH}$ = 5.7 Hz, NCH_2), 2.69 (8H, sp, $^3J_{HH}$ = Hz, CH ^{i}Pr), 2.24 (4H, qn, $^3J_{HH}$ = 5.7 Hz, NCH_2CH_2), 1.16

(24H, d, $^{3}J_{HH}$ = 6.9 Hz, CH_3 ^{i}Pr) , 0.83 (24H, d, $^{3}J_{HH}$ = 6.9 Hz, CH_3 ^{i}Pr). ^{13}C NMR (CD_2Cl_2, 100 MHz, 298 K): δ_c 199.9 (NCN), 162.4 (q, $^{1}J_{CB}$ = 49.6 Hz, CB $[BAr^f_4]^-$), 145.7 (NC Dipp), 145.1 (*ortho*-CH Ar^f), 141.4 (*ortho*-C Dipp), 135.4 (*para*-CH Ar^f), 135.4 (br, *ortho*-CH $[BAr^f_4]^-$), 130.5 (*para*-CH Dipp), 129.3 (m, *meta*-C $[BAr^f_4]^-$), 129.0 (m, *meta*-C Ar^f), 125.4 (meta-CH Dipp), 125.2 (q, $^{1}J_{CF}$ = 270.8 Hz, CF_3 $[BAr^f_4]^-$), (CF_3 Ar^f not obs.), 118.1 (m, *para*-CH $[BAr^f_4]^-$), 49.2 (NCH_2), 29.1 (CH ^{i}Pr), 25.0, 24.8 (CH_3 ^{i}Pr), 20.6 (s, NCH_2CH_2). ^{19}F NMR (282 MHz, CD_2Cl_2, 298 K) δ_F = -62.4 (Ar^f), -62.9 ($[BAr^f_4]^-$). MS (ESI +ve): *m/z* calc. for $[C_{64}H_{83}Au_2N_4F_6]^+$ 1415.5847, meas. 1415.6073 (M^+, 100%). Elemental analysis: calc. for $C_{96}H_{95}Au_2N_4BF_{30}$: C 50.58, H 4.20, N 2.46, meas. C 50.48, H 4.33, N 2.46.

*Crystallographic data for **28a***

$C_{96}H_{95}Au_2N_4BF_{30}$, M_r = 2279.53, monoclinic, $P2_1$, a = 13.9845(1), b = 16.5811(2), c = 22.3309(2) Å, β = 100.3429(5)°, V = 5093.91(9) Å^3, Z = 2, ρ_c = 1.486 Mg m^{-3}, T = 150 K, λ = 0.710730 Å, 72464 reflections collected, 22271 independent [R(int) = 0.067], which were used in calculations. R_1 = 0.0619, wR_2 = 0.1545 for observed unique reflections [I > 2σ(I)] and R_1 = 0.0697, wR_2 = 0.1669 for all unique reflections. Max. and min. residual electron densities 1.10 and -1.48 e Å^{-3}.

*Preparation of [{(7-Dipp)Au}$_2$Ar^f][BAr$^f_4$] (**28b**)*

(7-Dipp)AuCl (30 mg, 0.046 mmol) was dissolved in dichloromethane-d_2 (0.65 cm^3), cooled to -78 °C and the resulting solution added to solid Na[BAr^f_4] (41 mg, 0.046 mmol) and allowed to warm to room temperature. After 14 d, volatiles were removed *in vacuo* and the residue dissolved in fluorobenzene (2 cm^3). Colourless crystals suitable for X-ray crystallography were obtained by layering with hexanes at room temperature, and isolated

by filtration, washed with hexane and dried *in vacuo*. The crystalline product was collected in 49% yield (52 mg).

*Spectroscopic data for **28b***

^{1}H NMR (300 MHz, CD_2Cl_2, 298 K) δ_H 7.72 (8H, s, *ortho*-CH $[BAr^f_4]^-$), 7.56 (4H, s, *para*-CH $[BAr^f_4]^-$), 7.33 (4H, t, $^3J_{HH}$ = 7.7 Hz, *para*-CH Dipp), 7.23 (1H, s, *para*-CH Ar^f), 7.06 (8H, d, $^3J_{HH}$ = 8.2 Hz, *meta*-CH Dipp), 6.40 (2H, s, *ortho*-CH Ar^f), 3.80 (8H, m, NCH_2), 2.86 (8H, sept, $^3J_{HH}$ = 6.9 Hz, CH ^{i}Pr), 2.14 (8H, m, NCH_2CH_2), 1.19 (24H, d, $^3J_{HH}$ = 6.5 Hz, CH_3 ^{i}Pr), 0.87 (24H, d, $^3J_{HH}$ = 7 Hz, CH_3 ^{i}Pr). ^{13}C NMR (100 MHz, CD_2Cl_2, 298 K) δ_C 207.8 (NCN), 162.5 (q, $^1J_{CB}$ = 49.3 Hz, CB $[BAr^f_4]^-$), 145.4 (NC Dipp), 144.9 (*ortho*-CH Ar^f), 143.7 (*ortho*-C Dipp), 135.6 (*para*-CH Ar^f), 135.5 (br, *ortho*-CH $[BAr^f_4]^-$), 130.4 (*para*-CH Dipp), 129.5 (m, *meta*-C $[BAr^f_4]^-$), 127.1 (m, *meta*-C Ar^f), 125.6 (meta-CH Dipp), 125.3 (q, $^1J_{CF}$ = 271.2 Hz, CF_3 $[BAr^f_4]^-$), (CF_3 Ar^f not obs.), 118.1 (m, *para*-CH $[BAr^f_4]^-$), 57.4 (NCH_2), 29.2 (CH ^{i}Pr), 25.6 (CH_3 ^{i}Pr), 24.9 (NCH_2CH_2), 24.6 (CH_3 ^{i}Pr). ^{19}F NMR (282 MHz, CD_2Cl_2, 298 K) δ_F = -62.2 (Ar^f), -62.9 ($[BAr^f_4]^-$). MS (ESI +ve) *m/z* calc. for $[C_{66}H_{87}Au_2N_4F_6]^+$ 1443.6160, meas. 1443.6104 (M^+, 100%). Elemental analysis: calc. for $C_{98}H_{99}Au_2N_4BF_{30}$: C 51.01, H 4.32, N 2.43, meas. C 50.97, H 4.33, N 2.67.

*Crystallographic data for **28b***

$C_{98}H_{99}Au_2N_4BF_{30}$, M_r = 2307.59, orthorhombic, $P2_12_12_1$, a = 12.4694(1), b = 23.1957(1), c = 33.5245(3) Å, V = 9696.51(12) Å^3, Z = 4, ρ_c = 1.581 Mg m^{-3}, T = 150 K, λ = 0.710730 Å, 146729 reflections collected, 22058 independent [R(int) = 0.130], which were used in calculations. R_1 = 0.0537, wR_2 = 0.0828 for observed unique reflections [I > 2σ(I)] and R_1 = 0.0921, wR_2 = 0.1098 for all unique reflections. Max. and min. residual electron densities 4.95 and -3.26 e Å^{-3}.

*Preparation of [(6-Dipp)Au(6^a-Dipp)][BAr$^f_4$] (**29**)*

A suspension of Na[BAr$^f_4$] (32 mg, 0.04 mmol) in fluorobenzene (10 cm^3) was added to a stirred mixture of (6-Dipp)AuCl (23 mg, 0.04 mmol) and 6-Dipp (15 mg, 0.04 mmol) also in fluorobenzene (20 cm^3). After 10 min, the solution was filtered and the solvent removed *in vacuo*. The crude product was washed with hexanes (2 x 20 cm^3), and crystals suitable for X-ray crystallography obtained by layering a fluorobenzene solution with hexane and storage at 20 °C. Crystals were isolated in 46% yield (31 mg).

*Spectroscopic data for **29***

^{1}H NMR (300 MHz, CD_2Cl_2, 298 K): δ_H 7.72 (8H, s, *ortho*-CH [BAr$^f_4$]$^-$), 7.56 (4H, s, *para*-CH [BAr$^f_4$]$^-$), 7.41-7.12 (13H, overlapping m, arom-CH and NCHN), 3.44 (4H, tr, $^3J_{HH}$ = 5.8 Hz, NCH_2 6-Dipp), 3.25 (2H, app tr, H of NCH_2 6^a-Dipp), 2.99 (6H, overlapping m, H of NCH_2 6^a-Dipp and CH ^{i}Pr 6-Dipp), 2.77, 2.74 (2H, sept, $^3J_{HH}$ = 6.6 Hz, CH ^{i}Pr 6^a-Dipp), 2.35 (2H, qn, $^3J_{HH}$ = 5.8 Hz, CH_2 6-Dipp), 1.56 (1H, m, AuCH), 1.28 (24H, d, $^3J_{HH}$ = 6.6 Hz, CH_3 ^{i}Pr 6-Dipp), 1.28, 1.18, 1.12, 1.08 (6H, d, $^3J_{HH}$ = 6.6 Hz, CH_3 ^{i}Pr 6-Dipp'). ^{13}C NMR (75 MHz, CD_2Cl_2, 298 K): δ_C 209.2 (NCN 6-Dipp), 162.1 (qt, $^1J_{CB}$ = 50 Hz, CB [BAr$^f_4$]$^-$), 153.4 (NCHN 6^a-Dipp), 146.3 (NC 6-Dipp), 145.7, 145.4 (NC 6^a-Dipp), 141.6 (*ortho*-C 6-Dipp), 136.6 (*ortho*-C 6^a-Dipp), 135.2 (br, *ortho*-CH [BAr$^f_4$]$^-$), 131.0 (*para*-CH 6^a-Dipp), 129.2 (m, *meta*-C [BAr$^f_4$]$^-$), 129.1 (*para*-CH 6-Dipp), 125.5, 125.0 (*meta*-CH 6^a-Dipp), 125.0 (q, $^1J_{CF}$ = 271 Hz, CF_3 [BAr$^f_4$]$^-$), 124.6 (*meta*-CH 6-Dipp), 117.8 (m, *para*-CH [BAr$^f_4$]$^-$), 59.3 (NCH_2 6^a-Dipp), 47.8 (NCH_2 6-Dipp), 29.2, 29.2 (CH ^{i}Pr 6^a-Dipp), 28.9 (CH ^{i}Pr 6-Dipp), 25.3 (AuCH), 24.7 (CH_3 ^{i}Pr 6-Dipp), 24.5, 24.4, 24.3, 24.1 (CH_3 ^{i}Pr 6^a-Dipp), 20.5 (CH_2 6-Dipp). MS (ESI +ve): *m/z* calc. for $[C_{56}H_{80}AuN_4]^+$ 1005.6043, meas. 1005.6050 (M^+, 100%). Elemental analysis: calc. for $C_{88}H_{92}N_4AuBF_{24}$: C 56.54%, H 4.96%, N 3.00%, meas. C 56.20%, H 4.59%, N 3.10%.

*Crystallographic data for **29***

$C_{88}H_{92}N_4AuBF_{24}$, M_r = 1869.45, monoclinic, $P2_1/c$, a = 13.2907(1), b = 27.0645(2), c = 24.7244(2) Å, β = 105.5210(2)°, V = 8569.19(12) $Å^3$, Z = 4, ρ_c = 1.449 Mg m^{-3}, T = 150 K, λ = 0.71073 Å, 263868 reflections collected, 19531 independent [R(int) = 0.053], which were used in calculations. R_1 = 0.0489, wR_2 = 0.0826 for observed unique reflections [I > 2σ(I)] and R_1 = 0.0868, wR_2 = 0.1150 for all unique reflections. Max. and min. residual electron densities 4.77 and -2.72 e $Å^{-3}$.

*Preparation of [(6-Dipp)Au(CsCl)][$HCB_{11}Me_{11}$](**30**)*

A solution of (6-Dipp)AuCl (30 mg, 0.047 mmol) in dichloromethane-d_2 (0.5 cm^3) was transferred on to a suspension of Cs[$HCB_{11}Me_{11}$] (20 mg, 0.047 mmol) also in dichloromethane-d_2 (0.1cm^3) at -78 °C. ^{1}H NMR spectroscopy was used to monitor the transformation as the solution was warmed to room temperature. The reaction was observed to be complete in quantitative yield by the time the reaction mixture had warmed to -50 °C. Subsequent removal of the solvent *in vacuo* and washing with hexanes (2 x 10 cm^3) yielded the product as a white powder, collected in 64% yield (32 mg). Crystals suitable for X-ray crystallography were obtained by layering a fluorobenzene solution with hexane at 20 °C.

*Spectroscopic data for **30***

^{1}H NMR (CD_2Cl_2, 300 MHz, 298 K): δ_H 7.45 (2H, tr, $^3J_{HH}$ = 7.6 Hz, *para*-CH Dipp), 7.25 (4H, d, $^3J_{HH}$ = 7.6 Hz, *meta*-CH Dipp), 3.53 (4H, tr, $^3J_{HH}$ = 5.9 Hz, NCH_2), 3.01 (4H, sept, $^3J_{HH}$ = 6.9 Hz, CH ^{i}Pr), 2.41 (2H, qn, $^3J_{HH}$ = 5.9 Hz, NCH_2CH_2), 1.37 (12H, d, $^3J_{HH}$ = 6.9 Hz, CH_3 ^{i}Pr), 1.32 (12H, d, $^3J_{HH}$ = 6.9 Hz, CH_3 ^{i}Pr), 1.18 (1H, s, B_5CH), -0.17 (15H, s, BCH_3), -0.42 (15H, s, BCH_3), -0.53 (3H, s, BCH_3). ^{13}C NMR (C_6D_6, 125 MHz, 298 K): δ_C 191.5 (NCN), 146.8 (NC Dipp), 142.4 (*ortho*-C Dipp), 130.1 (*para*-CH Dipp), 125.4 (*meta*-

CH Dipp), 61.0 (br, CH $[HCB_{11}Me_{11}]^-$), 48.2 (NCH_2), 29.3 (CH ^{i}Pr), 25.0, 24.8 (CH_3 ^{i}Pr), 20.6 (NCH_2CH_2), -2.61 (m br, BCH_3 $[HCB_{11}Me_{11}]^-$). ^{11}B NMR (C_6D_6, 96 MHz, 298 K): δ_B -1.11 (1B), -9.01 (5B), -12.06 (5B). MS (ESI +ve): *m/z* calc. for $[C_{56}H_{80}Au_2N_4Cs_2Cl_2]^{2+}$ 769.1595, meas. 768.2695 ($[M-2H]^{2+}$, 7%), 1322.5593 (17%).

*Crystallographic data for **30***

$C_{40}H_{78}AuN_2B_{11}ClCs$, M_r = 1071.32, monoclinic, *C*2/*m*, a = 28.8545(5), b = 16.2390(4), c = 14.0985(3) Å, β = 107.6971(8)°, V = 6293.5(2) Å^3, Z = 4, ρ_c = 1.131 Mg m^{-3}, T = 150 K, λ = 0.710730 Å, 39986 reflections collected, 7390 independent [R(int) = 0.020], which were used in calculations. R_1 = 0.0592, *w*R_2 = 0.1533 for observed unique reflections [I > 2σ(I)] and R_1 = 0.0614, *w*R_2 = 0.1549 for all unique reflections. Max. and min. residual electron densities 3.64 and -3.06 e Å^{-3}.

*Preparation of [(6-Dipp)Au(C_6H_5F)][Al(pftb)$_4$] (**31**)*

A solution of (6-Dipp)AuCl (25 mg, 0.04 mmol) in fluorobenzene (10 cm^3) was transferred on to a solution of Li[Al(ptfb)$_4$] (38 mg, 0.04 mmol) also in fluorobezene (5 cm^3) at -35 °C. The reaction was stirred and allowed to warm to 20 °C. After stirring at room temperature for 15 min, the solution was filtered and the solvent was removed *in vacuo*. Washing with hexanes (2 x 10 cm^3) and drying *in vacuo* gave the crude product as a white powder in 65% yield (40 mg). Crystals suitable for X-ray crystallography were grown by layering a fluorobenzene solution with hexane at 20 °C.

*Spectroscopic data for **31***

^{1}H NMR (C_6D_5Br, 400 MHz, 298 K): δ_H 7.10 (2H, m, *para*-CH Dipp), 6.88 (4H, m, *meta*-CH Dipp), 3.00 (4H, tr, $^3J_{HH}$ = 5.7 Hz, NCH_2), 2.57 (4H, br, CH ^{i}Pr), 1.75 (2H, m, NCH_2CH_2), 1.06 (12H, d, $^3J_{HH}$ = 6.8 Hz, CH_3 ^{i}Pr), 1.00 (12H, d, $^3J_{HH}$ = 6.8 Hz, CH_3 ^{i}Pr).

^{13}C NMR (C_6D_5Br, 100 MHz, 298 K): δ_C 172.1 (NCN), 145.4 (NC Dipp), 140.8 (*ortho*-C Dipp), 130.6 (*para*-CH Dipp), 125.0 (*meta*-CH Dipp), 121.9 (q, $^1J_{CF}$ = 290.7 Hz, CF_3 $[Al(pftb)_4]^-$), 47.3 (NCH_2), 28.7 (CH ^{i}Pr), 24.6, 24.6 (CH_3 ^{i}Pr), 19.2 (NCH_2CH_2). ^{19}F NMR (C_6D_5Br, 376 MHz, 298 K): δ_F -74.6 (CF_3). MS (ESI +ve): *m/z* calc. for $[C_{34}H_{45}AuN_2F]^+$ 697.3227, meas. 768.27 (8%), 1322.56 (13%).

*Crystallographic data for **31***

$C_{50}H_{45}AuN_2AlO_4F_{37}$, M_r = 1664.79, monoclinic, $P2_1/c$, a = 12.7060(1), b = 16.3750(1), c = 29.3285(2) Å, β = 93.2967(7)°, V = 6092.01(7) Å^3, Z = 4, ρ_c = 1.815 Mg m^{-3}, T = 150 K, λ = 1.54180 Å, 25332 reflections collected, 12733 independent [R(int) = 0.035], which were used in calculations. R_1 = 0.1199, wR_2 = 0.3866 for observed unique reflections [I > 2σ(I)] and R_1 = 0.1243, wR_2 = 0.3987 for all unique reflections. Max. and min. residual electron densities 6.25 and -3.98 e Å^{-3}.

*Preparation of (6-Mes)AuH (**32**)*

A stirred solution of (6-Mes)AuCl (60 mg, 0.11 mmol) in THF (10 cm^3) was cooled to -78°C, and a 1.0 M solution of K[$HBEt_3$] (0.11 cm^3, 0.11 mmol) in THF was then added dropwise. The reaction mixture was allowed to stir at low temperature for 30 min before warming to 20°C and stirring for a further 4 h. Filtration and removal of volatiles *in vacuo* yielded a white solid which was washed with hexane (2 x 10 cm^3) and isolated in 63% yield (36 mg). Crystals suitable for X-ray diffraction were obtained by layering a THF solution with pentane at 20°C.

*Spectroscopic data for **32***

^{1}H NMR (C_6D_6, 300 MHz, 298 K): δ 6.78 (4H, s, *meta*-CH), 3.36 (1H, s, AuH), 2.51 (4H, tr, $^3J_{HH}$ = 5.7 Hz, NCH_2), 2.19 (12H, s, *ortho*-CH_3), 2.10 (6H, s, *para*-CH_3), 1.36 (2H, qn,

$^3J_{HH}$ = 5.7 Hz, NCH_2CH_2). ^{13}C NMR (C_6D_6, 75 MHz, 298 K): δ 218.6 (NCN), 142.2 (NC Mes), 137.5 (*para*-C Mes), 134.8 (*ortho*-C Mes), 129.7 (*meta*-CH Mes), 44.9 (NCH_2), 21.0 (NCH_2CH_2), 20.6 (*para*-CH_3 Mes), 18.0 (*ortho*-CH_3 Mes). MS (EI +ve): *m/z* 517.2 ([M-H]$^+$, 1%). Elemental analysis: calc. for $C_{22}H_{29}AuN_2$: C 50.97, H 5.64, N 5.40, meas. C 50.62, H 5.59, N 5.51.

*Crystallographic data for **32***

$C_{22}H_{29}AuN_2$, M_r = 518.45, monoclinic, $P2_1/n$, a = 8.2544(1), b = 15.8234(2), c = 15.5082(2) Å, β = 94.0501(5)°, V = 2020.51(4) Å^3, Z = 4, ρ_c = 1.704 Mg m^{-3}, T = 150 K, λ = 0.710730 Å, 33627 reflections collected, 4612 independent [R(int) = 0.022], which were used in calculations. R_1 = 0.0349, wR_2 = 0.0785 for observed unique reflections [I > 2σ(I)] and R_1 = 0.0581, wR_2 = 0.1044 for all unique reflections. Max. and min. residual electron densities 4.23 and -1.92 e Å^{-3}.

*Preparation of (6-Dipp)AuH (**33a**) and (7-Dipp)AuH (**33b**)*

Compounds **33a** and **33b** were prepared by a common method. A stirred solution of (6-Dipp)AuCl (55 mg, 0.09 mmol) or (7-Dipp)AuCl (44 mg, 0.068 mmol) in THF (10 cm^3) was cooled to -78 °C, and a 1.0 M solution of K[$HBEt_3$] (0.09 cm^3, 0.09 mmol; 0.08 cm^3, 0.08 mmol, respectively) also in THF was then added dropwise. The reaction mixture was allowed to stir at -78 °C for 30 min before warming to 20 °C and stirring for a further 4 h. Volatiles were removed *in vacuo* resulting in a white solid from which the product was extracted with hexane (3 x 10 cm^3). Crystals of **33a** and **33b** suitable for X-ray diffraction were obtained from a solution of Et_2O at -30 °C in 56% (29 mg) and 45% yield (19 mg) respectively.

*Spectroscopic data for **33a***

^{1}H NMR (C_6D_6, 300 MHz, 298 K): δ 7.19 (2H, tr, $^{3}J_{HH}$ = 7.5 Hz, *para*-CH), 7.08 (4H, d, $^{3}J_{HH}$ = 7.5 Hz, *meta*-CH), 3.57 (1H, s, AuH), 3.08 (4H, sept, $^{3}J_{HH}$ = 6.9 Hz, CH ^{i}Pr), 2.73 (4H, tr, $^{3}J_{HH}$ = 5.7 Hz, NCH_2), 1.59 (12H, d, $^{3}J_{HH}$ = 6.9 Hz, CH_3 ^{i}Pr), 1.47 (2H, qn, $^{3}J_{HH}$ = 5.7 Hz, NCH_2CH_2), 1.21 (12H, d, $^{3}J_{HH}$ = 6.9 Hz, CH_3 ^{i}Pr). ^{13}C NMR (C_6D_6, 75 MHz, 298 K): δ 218.0 (NCN), 146.0 (NC-Dipp), 142.4 (*ortho*-C Dipp), 129.3 (*para*-CH Dipp), 124.8 (*meta*-CH Dipp), 47.8 (NCH_2), 29.3 (CH ^{i}Pr), 25.1, 25.0 (CH_3 ^{i}Pr), 20.6 (NCH_2CH_2). MS (EI +ve): *m/z* 601.3 ($[M-2H]^+$, 3%), 602.3 (M^+, 2%). Elemental analysis: calc. for $C_{28}H_{41}AuN_2$: C 55.81, H 6.86, N 4.65, meas. C 55.42, H 6.57, N 4.42.

*Crystallographic data for **33a***

$C_{28}H_{41}AuN_2$, M_r = 602.61, monoclinic, $P2_1/n$, a = 12.4954(1), b = 15.5603(2), c = 13.6979(2) Å, β = 99.2359(5)°, V = 2628.78(6) Å^3, Z = 4, ρ_c = 1.523 Mg m^{-3}, T = 150 K, λ = 0.710730 Å, 43555 reflections collected, 5974 independent [R(int) = 0.037], which were used in calculations. R_1 = 0.0318, wR_2 = 0.0739 for observed unique reflections [I > 2σ(I)] and R_1 = 0.0530, wR_2 = 0.0945 for all unique reflections. Max. and min. residual electron densities 2.70 and -1.87 e Å^{-3}.

*Spectroscopic data for **33b***

^{1}H NMR (300 MHz, C_6D_6, 298 K): δ_H 7.18 (2H, m, *para*-CH Dipp), 7.08 (4H, d, $^{3}J_{HH}$ = 8.2 Hz, *meta*-CH Dipp), 3.30 (4H, m, NCH_2), 3.28 (4H, m, CH ^{i}Pr), 3.15 (1H, s, AuH), 1.65 (4H, m, NCH_2CH_2), 1.60 (12H, d, $^{3}J_{HH}$ = 7.0 Hz, CH_3-^{i}Pr), 1.23 (12H, d, $^{3}J_{HH}$ = 7.0 Hz, CH_3-^{i}Pr). ^{13}C NMR (75 MHz, C_6D_6, 298 K): δ_c 229.1 (NCN), 145.6 (NC Dipp), 129.1 (*ortho*-C Dipp), 125.9 (*para*-CH Dipp), 124.9 (*meta*-CH Dipp), 55.3 (NCH_2), 29.4 (CH ^{i}Pr)

25.4, 25.2 (CH_3 ^{i}Pr), 25.0 (NCH_2CH_2). MS (EI +ve) *m/z* 615.3 (M^+). Elemental analysis: calc. for $C_{29}H_{43}AuN_2$: C 56.49, H 7.03, N 4.54, meas. C 55.53, H 7.25, N 4.35.

*Crystallographic data for **33b***

$C_{29}H_{43}AuN_2$, M_r = 616.64, monoclinic, $P2_1/n$, a = 12.4372(1), b = 15.9767(1), c = 13.7945(1) Å, β = 97.1847(4)°, V = 2719.52(3) Å^3, Z = 4, ρ_c = 1.506 Mg m^{-3}, T = 150 K, λ = 0.710730 Å, 77295 reflections collected, 6199 independent [R(int) = 0.026], which were used in calculations. R_1 = 0.0271, wR_2 = 0.0631 for observed unique reflections [I > 2σ(I)] and R_1 = 0.0378, wR_2 = 0.0744 for all unique reflections. Max. and min. residual electron densities 2.04 and -1.45 e Å^{-3}.

*Preparation of [{(6-Dipp)Au}$_2$H][BAr$^f_4$] (**34a**)*

A mixture of (6-Dipp)AuCl (37 mg, 0.06 mmol) and (6-Dipp)AuH (35 mg, 0.06 mmol) in fluorobenzene (10 cm^3) was cooled to -30 °C. Na[BAr$^f_4$] (51 mg, 0.06 mmol) in fluorobenzene (10 cm^3) was added, and the stirred mixture was allowed to warm to room temperature over 30 min. The solvent was then removed *in vacuo* and the residue was washed with hexanes (2 x 10 cm^3). X-ray diffraction quality crystals were obtained in 48% yield (57 mg) by layering a fluorobenzene solution with hexane at 20 °C.

*Spectroscopic data for **34a***

^{1}H NMR (C_6D_5Br, 300 MHz, 298 K): δ 8.14 (8H, br, *ortho*-CH [BAr$^f_4$]$^-$), 7.51 (8H, br, *para*-CH [BAr$^f_4$]$^-$), 7.07 (4H, tr, $^3J_{HH}$ = 7.9 Hz, *para*-CH Dipp), 6.84 (8H, d, $^3J_{HH}$ = 7.9 Hz, *meta*-CH Dipp), 2.91 (8H, tr, $^3J_{HH}$ = 5.4 Hz, NCH_2), 2.56 (8H, sept, $^3J_{HH}$ = 6.8 Hz, CH ^{i}Pr), 1.70 (4H, qn, $^3J_{HH}$ = 5.4 Hz, NCH_2CH_2), 1.02 (24H, d, $^3J_{HH}$ = 6.8 Hz, CH_3 ^{i}Pr), 0.86 (24H, d, $^3J_{HH}$ = 6.8 Hz, CH_3 ^{i}Pr), -1.47 (1H, s, Au_2H). ^{13}C NMR (C_6D_5Br, 75 MHz, 298 K): δ 204.0 (NCN), 162.4 (qt, $^1J_{CB}$ = 49.6 Hz, BC [BAr$^f_4$]$^-$), 145.2 (NC Dipp), 140.3 (*ortho*-C

Dipp), 135.2 (br, *ortho*-CH $[BAr^f_4]^-$), 129.7 (*para*-CH Dipp), 124.9 (qt, $^1J_{CF}$ = 271.1 Hz, CF_3 $[BAr^f_4]^-$) 124.6 (*meta*-CH Dipp), 117.8 (m, *para*-CH $[BAr^f_4]^-$), 47.6 (NCH_2), 28.6 (CH ^{i}Pr), 24.9, 24.6 (CH_3 ^{i}Pr), 19.8 (NCH_2CH_2). ^{19}F NMR (C_6D_6, 282 MHz, 298 K): δ -61.75 (s, CF_3 $[BAr^f_4]^-$). MS (ESI +ve): *m/z* calc. for $[C_{56}H_{81}Au_2N_4]^+$ 1203.5787, meas. 1203.5789 (M^+, 100%). Elemental analysis: calc. for $C_{88}H_{93}Au_2N_4BF_{24}$: C 51.12, H 4.53, N 2,71, meas. C 50.76, H 4.36, N 2.35.

*Crystallographic data for **34a***

$C_{88}H_{93}Au_2N_4BF_{24}$, M_r = 2067.43, monoclinic, $P2_1/n$, a = 10.9229(1), b = 33.2601(2), c = 26.6573(2) Å, β = 96.4867(2)°, V = 9622.25(13) Å^3, Z = 4, ρ_c = 1.427 Mg m^{-3}, T = 150 K, λ = 0.710730 Å, 21819 reflections collected, 21819 independent [R(int) = 0.038], which were used in calculations. R_1 = 0.0455, wR_2 = 0.0847 for observed unique reflections [I > 2σ(I)] and R_1 = 0.0686, wR_2 = 0.1014 for all unique reflections. Max. and min. residual electron densities 2.38 and -1.53 e Å^{-3}.

*Preparation of [{(7-Dipp)Au}$_2$H][BAr$^f_4$] (**34b**)*

(7-Dipp)AuH (20 mg, 0.032 mmol) was dissolved in dichloromethane-d_2 (0.65 cm^3) and cooled to -78 °C, the solution was added to solid Brookhart's acid (17 mg, 0.017 mmol) and the reaction mixture allowed to warm to -5 °C. Volatiles were then removed *in vacuo* and the residue dissolved in fluorobenzene (2 cm^3). Colourless crystals suitable for X-ray crystallography were obtained by layering with hexanes at room temperature, and isolated by filtration, washed with hexane and dried *in vacuo*. Yield: 57% (19 mg).

*Spectroscopic data for **34b***

^{1}H NMR (300 MHz, CD_2Cl_2, 268 K): δ_H 7.72 (8H, s, *ortho*-CH $[BAr^f_4]^-$), 7.56 (4H, s, *para*-CH $[BAr^f_4]^-$), 7.24 (4H, t, $^3J_{HH}$ = 7.7 Hz, *para*-CH Dipp), 7.01 (8H, d, $^3J_{HH}$ = 7.7 Hz, *meta*-

CH Dipp), 3.84 (8H, m, NCH_2), 2.90 (8H, sept, $^3J_{HH}$ = 7.0 Hz, CH ^{i}Pr), 2.21 (8H, br, NCH_2CH_2), 1.20 (24H, d, $^3J_{HH}$ = 6.9 Hz, CH_3 ^{i}Pr), 0.95 (24H, d, $^3J_{HH}$ = 7.0 Hz, CH_3 ^{i}Pr), -1.95 (1H, s, Au_2H). ^{13}C NMR (100 MHz, $C_6H_4F_2/C_6D_5CD_3$, 298 K): δ_C 213.3 (NCN), 163.2 (q, $^1J_{CB}$ = 49.6 Hz, CB $[BAr^f_4]^-$), 151.6 (NC Dipp), 145.7 (*ortho*-C Dipp), 135.8 (br, *ortho*-CH $[BAr^f_4]^-$), 130.2 (m, *meta*-C $[BAr^f_4]^-$), 129.7 (*para*-CH Dipp), 125.6 (q, $^1J_{CF}$ = 271.2 Hz, CF_3 $[BAr^f_4]^-$), 124.9 (*meta*-CH Dipp), 118.3 (m, *para*-CH $[BAr^f_4]^-$), 55.8 (NCH_2), 29.5 (CH ^{i}Pr), 25.3 (CH_3 ^{i}Pr), 24.5 (NCH_2CH_2), 24.4 (CH_3 ^{i}Pr). MS (ESI +ve) *m/z* calc. for $[C_{58}H_{85}Au_2N_4]^+$ 1231.6100, meas. 1231.6069 (M^+, 100%).

*Crystallographic data for **34b***

$C_{90}H_{97}Au_2N_4BF_{24}$, M_r = 2095.49, monoclinic, $P2_1$, a = 12.7581(1), b = 27.0138(2), c = 13.0695(1) Å, β = 97.5636(5) °, V = 4465.14(6) Å^3, Z = 2, ρ_c = 1.558 Mg m^{-3}, T = 150 K, λ = 1.54180 Å, 50050 reflections collected, 17926 independent [R(int) = 0.024], which were used in calculations. R_1 = 0.0249, wR_2 = 0.0613 for observed unique reflections [I > 2σ(I)] and R_1 = 0.0254, wR_2 = 0.0627 for all unique reflections. Max. and min. residual electron densities 0.77 and -1.14 e Å^{-3}.

*Preparation of (6-Dipp)Au(C_6F_5) (**35a**) and (7-Dipp)Au(C_6F_5) (**35b**)*

Compounds **35a** and **35b** were prepared by a common method. To a stirred solution of (6-Dipp)AuH (47 mg, 0.08 mmol) or (7-Dipp)AuH (48 mg, 0.08 mmol) in toluene (10 cm^3) was added $B(C_6F_5)_3$ (40 mg, 0.08 mmol) also in toluene (5 cm^3). The reaction mixture was allowed to stir for 12 h, after which the volatiles were removed *in vacuo*. The white residue was washed with pentane (10 cm^3) and redissolved in a toluene/pentane mixture (5 cm^3 of each). Crystalline solid formed after storage at -30 °C. Subsequent isolation and drying *in vacuo* gave the products in 58% (36 mg) and 53% yields (33 mg) respectively. Crystals

suitable for X-ray crystallography were obtained for **35b** by layering a fluorobenzene solution with pentane and storage at 20 °C.

*Spectroscopic data for **35a***

^{1}H NMR (C_6D_6, 400 MHz, 298 K): δ_H 7.19 (2H, tr, $^{3}J_{HH}$ = 7.6 Hz, *para*-CH Dipp), 7.07 (4H, d, $^{3}J_{HH}$ = 8.0 Hz, *meta*-CH Dipp), 3.19 (4H, sept, $^{3}J_{HH}$ = 6.8 Hz, CH ^{i}Pr), 2.77 (4H, tr, $^{3}J_{HH}$ = 5.8 Hz, NCH_2), 1.57 (12H, d, $^{3}J_{HH}$ = 6.8 Hz, CH_3 ^{i}Pr), 1.46 (4H, m, NCH_2CH_2), 1.19 (12H, d, $^{3}J_{HH}$ = 6.8 Hz, CH_3 ^{i}Pr). ^{13}C NMR (C_6D_6, 125 MHz, 298 K): δ_C 208.8 (NCN), 150.0 (dm, $^{1}J_{CF}$ = 227.4 Hz, *ortho*-CF), 146.0 (NC Dipp), 141.9 (*ortho*-C Dipp), 138.8 (dm, $^{1}J_{CF}$ = 227.5 Hz, *para*-CF), 137.4 (dm, $^{1}J_{CF}$ = 247.3 Hz, *meta*-CF), 130.0 (*para*-CH Dipp), 125.1 (*meta*-CH Dipp), 47.6 (NCH_2), 29.3 (CH ^{i}Pr), 25.2, 25.0 (CH_3 ^{i}Pr), 20.1 (NCH_2CH_2). ^{19}F NMR (C_6D_6, 376 MHz, 298 K): δ -115.84 (m, *ortho*-CF), -161.64 (tr, $^{3}J_{FF}$ = 20.5 Hz, *para*-CF), -163.92 (tr-m, $^{3}J_{FF}$ = 20.5 Hz, *meta*-CF). MS (EI +ve): *m/z* 768.3 ($[M-H]^+$, 10%).

*Spectroscopic data for **35b***

^{1}H NMR (C_6D_6, 300 MHz, 298 K): δ_H 7.20 (2H, tr, $^{3}J_{HH}$ = 7.7 Hz, *para*-CH Dipp), 7.07 (4H, d, $^{3}J_{HH}$ = 6.9 Hz, *meta*-CH Dipp), 3.29 (4H, m, NCH_2), 3.19 (4H, sept, $^{3}J_{HH}$ = 7.0 Hz, CH ^{i}Pr), 1.62 (4H, m, NCH_2CH_2), 1.56 (12H, d, $^{3}J_{HH}$ = 7.0 Hz, CH_3 ^{i}Pr), 1.21 (12H, d, $^{3}J_{HH}$ = 7.0 Hz, CH_3 ^{i}Pr). ^{13}C NMR (C_6D_6, 125 MHz, 298 K): δ 217.3 (NCN), 149.4 (dm, $^{1}J_{CF}$ = 224.5 Hz, *ortho*-CF), 145.4 (NC Dipp), 144.6 (*ortho*-C Dipp), 138.3 (dm, $^{1}J_{CF}$ = 236.9 Hz, *para*-CF), 136.9 (dm, $^{1}J_{CF}$ = 223.5 Hz, *meta*-CF), 129.6 (*para*-CH Dipp), 125.2 (*meta*-CH Dipp), 54.9 (NCH_2), 29.5 (CH ^{i}Pr), 25.1 (CH_3 ^{i}Pr), 25.1 (NCH_2CH_2), 25.0 (CH_3 ^{i}Pr). ^{19}F NMR (C_6D_6, 282 MHz, 298 K): δ -115.56 (m, *ortho*-CF), -161.67 (tr, $^{3}J_{FF}$ = 21.7 Hz, *para*-CF), -163.94 (tr-m, $^{3}J_{FF}$ = 20.2 Hz, *meta*-CF). MS (EI +ve): *m/z* 782.3 ($[M-H]^+$, 8%).

*Crystallographic data for **35b***

$C_{35}H_{42}AuN_2F_5$, M_r = 782.69, orthorhombic, *Pna*2_1, a = 19.5762(1), b = 13.6085(1), c = 12.0882(1) Å, V = 3220.33(4) Å^3, Z = 4, ρ_c = 1.614 Mg m^{-3}, T = 150 K, λ = 0.710730 Å, 7092 reflections collected, 3835 independent [R(int) = 0.046], which were used in calculations. R_1 = 0.0242, *w*R_2 = 0.0594 for observed unique reflections [I > 2σ(I)] and R_1 = 0.0253, *w*R_2 = 0.0608 for all unique reflections. Max. and min. residual electron densities 1.62 and -1.86 e Å^{-3}.

6.3 Expanded Ring NHC Gold Chloride Complexes

6.3.1 Use of Mesityl-Functionalized NHCs

Expanded ring NHC ligands have proved to be extremely effective at stabilising low coordinate metal cations, as outlined in Chapter IV in the case of iridium systems. It follows then that similar NHCs would be suitable candidates for isolating the reactive intermediates in Au(I) catalysed processes. Conveniently, a recent paper reported the syntheses of (6-Mes)AuCl and (7-Mes)AuCl which were to be used as starting materials.[30]

However, the product of halide abstraction, i.e. the Au(I) cation $[LAu]^+$, had not been reported so attempts were made to isolate this species. Abstraction was repeated many times, each time controlling conditions carefully: low temperature, fluorobenzene solvent and the absence of light were all routinely employed. ^{1}H and ^{13}C NMR spectra for these compounds were consistent with highly symmetrical species, similar to signals observed for the NHC in $[(NHC)_2IrH_2][BAr^f_4]$ (NHC = 6-Mes, 7-Mes). The reaction was often accompanied by the evolution of a purple colour, attributed to colloidal gold, and the isolated cationic species was typically of the form $[(NHC)_2Au]^+$ (NHC = 6-Mes, 7-Mes). X-ray analysis of crystals obtained from a layering of fluorobenzene with hexane reveal a cationic gold centre with two *trans*-(6-Mes) ligands (Fig 6.3).

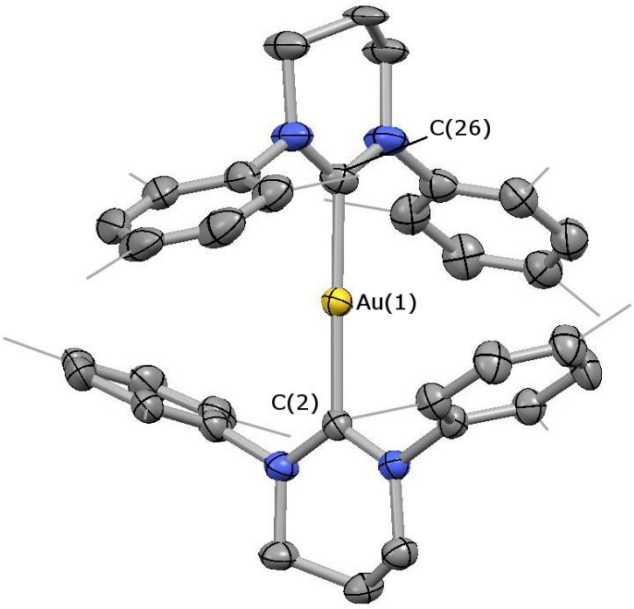

Figure 6.3: $[(6\text{-Mes})_2Au][BAr^f{}_4]$ (**25**), $[BAr^f{}_4]^-$ anion omitted, with H atoms omitted and Me groups shown in wireframe for clarity; thermal ellipsoids set at 50% probability level. Key bond lengths (Å) and angles (°): Au(1)–C(2) 2.039(4), Au(1)–C(26) 2.039(4), C(2)–Au(1)–C(26) 178.8(2).

The metrics of this compound are unremarkable, and this is a relatively stable complex as it shows no degradation on exposure to air and moisture. Complexes of this type have been reported to undergo oxidative addition of halogens (Br_2 and Cl_2),[31, 32] perhaps not unsurprisingly, this compound does not react with hydrogen gas. However, reaction with $K[HBEt_3]$ gives, what has been identified by comparison of the ^1H NMR spectrum with (6-Mes)AuH (**32**), to be (6-Mes)AuH and (6-Mes)·BEt_3.

Synthetic chemistry was previously attempted using the NHC known as Xyl7-Mes (containing a 7-membered backbone with a fused phenyl ring) via substitution at iridium by Fallis *et al.* (privately communicated). They had found it impossible to observe any evidence of coordination, even with smaller metal fragments. Hence, this may be a good

starting point to try and avoid coordination of two carbenes to the cation. ^{1}H NMR spectroscopy indicates a symmetrical NHC environment. Crystals of the chloride complex were isolated from a layering of a dichloromethane solution with pentane (Fig 6.4).

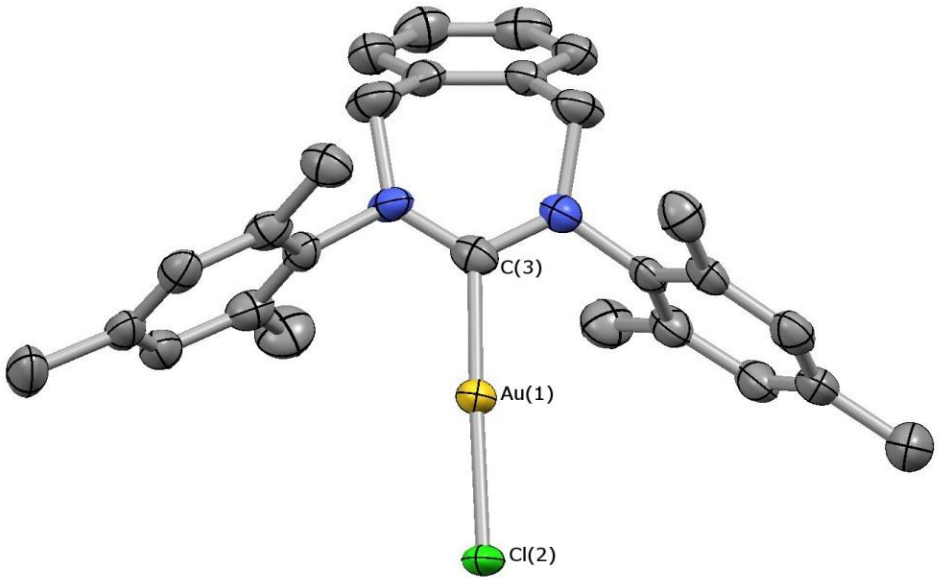

Figure 6.4: (Xyl7-Mes)AuCl (**26**), H atoms omitted for clarity; thermal ellipsoid set at 50% probability level. Key bond lengths (Å) and angles (°): Au(1)–Cl(2) 2.320(1), Au(1)–C(3) 2.013(7), C(3)–Au(1)–Cl(2) 178.1(2).

In the case of **26**, the Au(1)–C(3) distance [2.013(7) Å] is identical to those of previously reported expanded ring NHC adducts, whereas Au(1)–Cl(2) shows a slight elongation [2.320(1) *cf*. 2.303(2), 2.305(1) Å for (6-Mes)AuCl and (7-Mes)AuCl, respectively].[30] All attempts to abstract the halide from **26** have so far led to an unidentified mixture of products but no precipitation of colloidal gold was observed.

6.3.2 Use of Dipp-Functionalized NHCs

In light of the extreme steric bulk provided by 6-Dipp (%V_{bur} 50.6) as outlined in Chapter V, this ligand seems a suitable candidate to prevent degradation of "$[LAu]^{+}$" to $[L_2Au]^{+}$ and colloidal Au. The known complex (6-Dipp)AuCl was taken with $Na[BAr^{f}_{4}]$ in

CD_2Cl_2 at -78 °C in order to monitor reactivity by ^1H VT-NMR (Fig 6.5). Gradual warming of the sample revealed little reaction from -78 °C to -20 °C. From this point the transformation appeared to proceed more rapidly with increasing temperature, and at -5 °C, the reaction appeared to complete in around 20 min. This intially formed species persists at -5 °C and even at room temperature for up to 6 h.

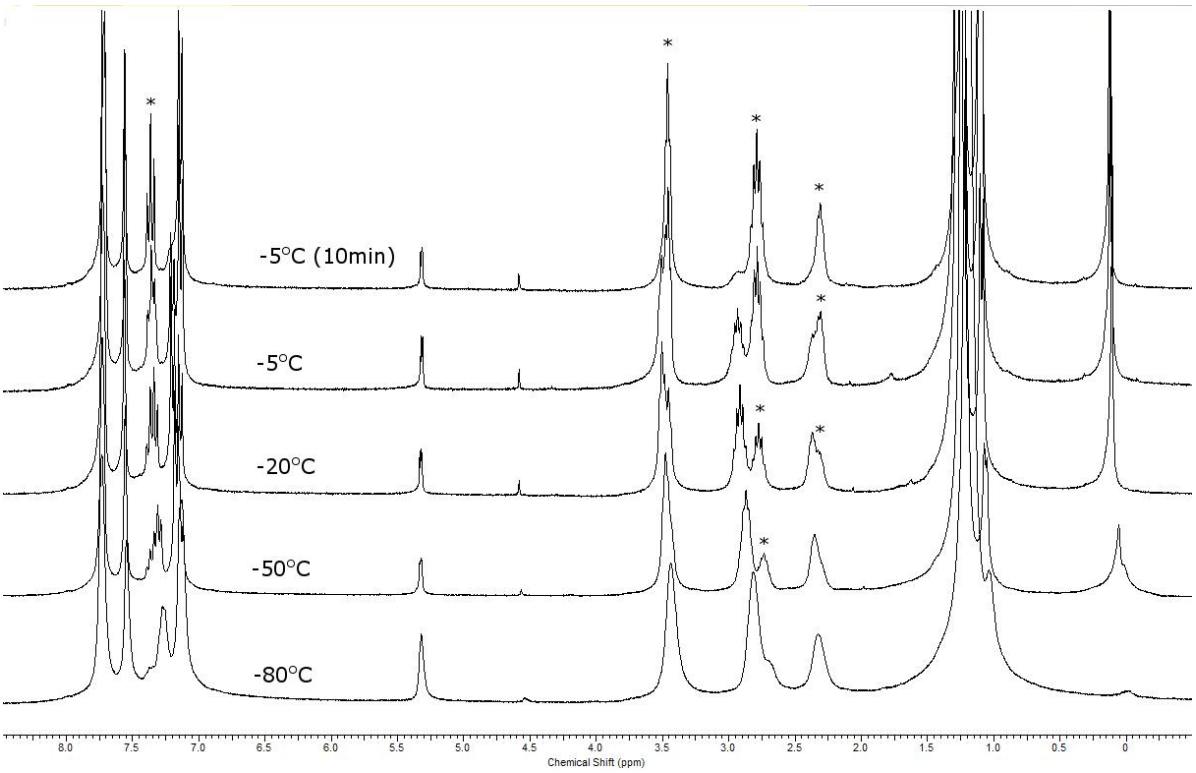

Figure 6.5: ^1H VT-NMR (300 MHz) tracing the warming of (6-Dipp)AuCl in the presence of $Na[BAr^f_4]$ in CD_2Cl_2 (selection of emerging signals indicated with *).

Upon extended storage at room temperature, however, further reaction was observed. Clean degradation was observed over several days and found to be complete after 4 days (Fig 6.6). This was accompanied by the emergence of signals assigned to BAr^f_3.[33]

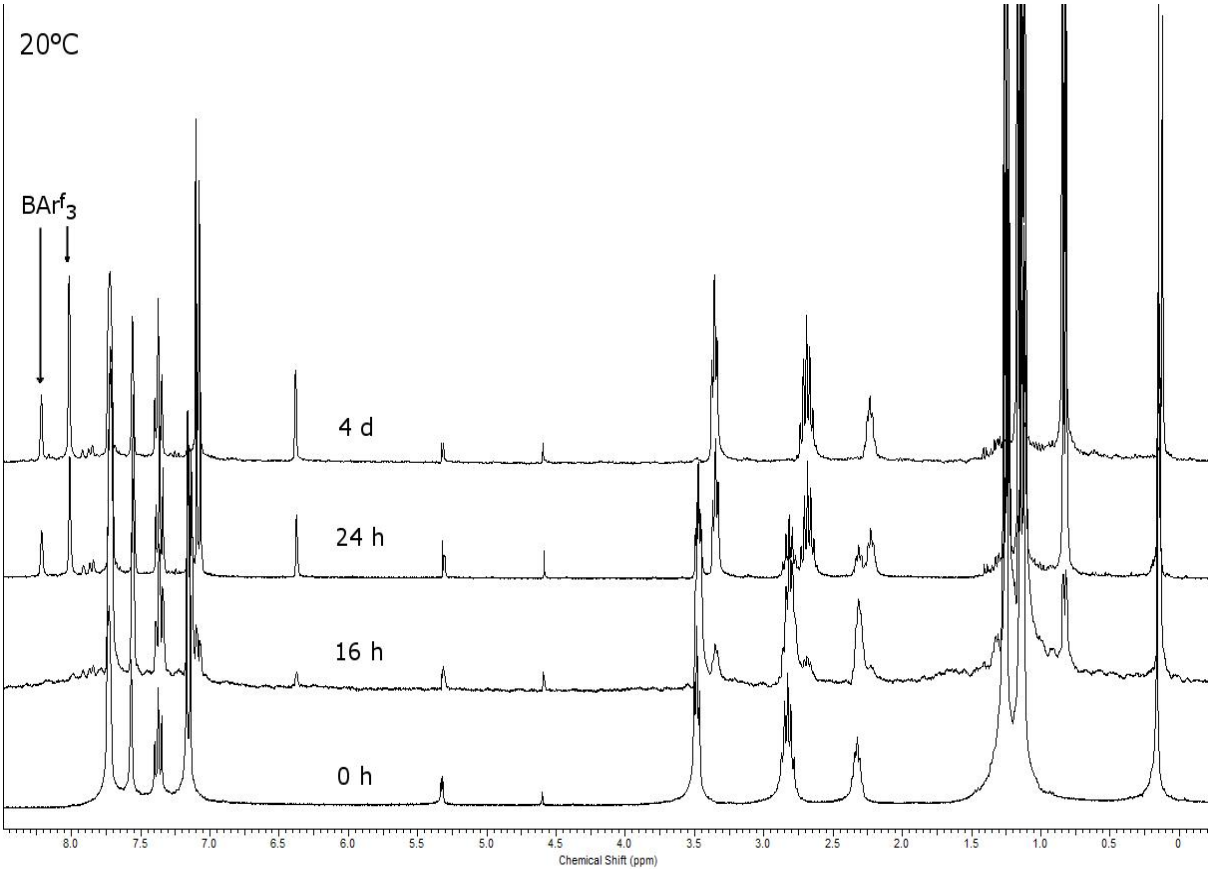

Figure 6.6: Degradation of intermediate species over 4 days in CD_2Cl_2.

Formation of BAr^f_3 is indicative of the cleavage of a B–C_{Ar} bond from the $[BAr^f_4]^-$ anion, which is unusual but has been previously reported with $[(NHC)Au]^+$, $[(PPh_3)_2Pt(Me)(OEt_2)]^+$ and $[(PCP)Rh(N_2)]^+$.[13, 34, 35] Activation of a B–C bond suggests the formation of a highly reactive gold fragment by further reaction with $Na[BAr^f_4]$. By repeating this reaction, maintaining the solution at -5 °C and carrying out crystallisation at -30 °C, the intermediate species was successfully isolated and identified as [(6-Dipp)Au(μ-Cl)Au(6-Dipp)][BAr^f_4] (**27a**) (Fig 6.7), resulting from the trapping of $[(6\text{-Dipp})Au]^+$ by (6-Dipp)AuCl. The structure reveals two $[(6\text{-Dipp})Au]^+$ fragments bridged by a single chloride ligand, with no significant interaction with the $[BAr^f_4]^-$ counter-ion.

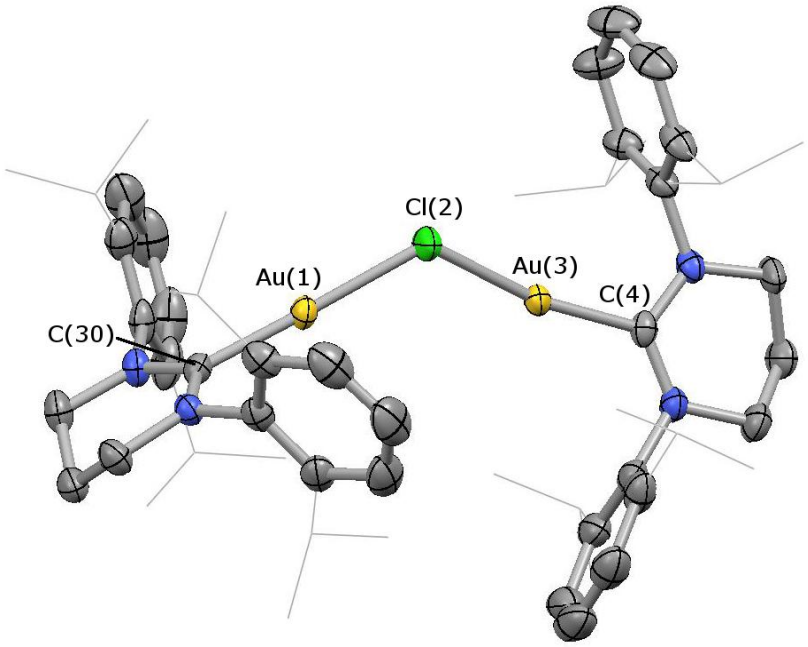

Figure 6.7: [{(6-Dipp)Au}$_2$(μ-Cl)][BAr$^f_4$] (**27a**), with [BAr$^f_4$]$^-$ anion omitted, H atoms omitted and ^{i}Pr groups shown in wireframe for clarity; thermal ellipsoids set at 50% probability level. Key bond lengths (Å) and angles (°): Au(1)–Cl(2) 2.310(1), Au(3)–Cl(2) 2.316(1), Au(1)–C(30) 1.989(4), Au(3)–C(4) 1.988(4), Au(1)···Au(3) 4.0207(2), Au(1)–Cl(2)–Au(3) 120.71(5), C(30)–Au(1)–Cl(2) 173.0(1), C(4)–Au(3)–Cl(2) 168.7(1).

The structure of **27a** displays a significant elongation of the Au-Cl bond over the parent (6-Dipp)AuCl [2.310(1), 2.316(1) *cf*. 2.277(2) Å, respectively] consistent with the bridging nature of the chloride ligand. One might expect this elongation to be accompanied by a shortening of the Au-C_{NHC} bonds as the effective *trans*-influence of the chloride is decreased, however this is not a significant effect [1.989(4), 1.988(4) *cf*. 2.009(7) Å]. An analogous complex, [{(PPh_3)Au}$_2$(μ-Cl)][ClO_4], was structurally characterised by Sheldrick *et al*. in 1980.[36] However the gold-gold separation in **27a** is significant longer than the PPh_3 system [4.021(1) *cf*. 3.085(2), 3.035(2) Å], and is well outside the typical range for aurophilic interactions [2.7-3.0 Å].[37] This is consistent with aggregation through the

chloride ligand alone. The angles at Au(1) and Au(3) can still be considered linear [173.0(1)° and 168.7(1)°], perhaps with some minor distortion coming from crystal packing forces.

It appears that this chloride must be held relatively tightly by **27a** due to the slow nature of the degradation to the final product. This degradation probably occurs due to the abstraction of the chloride from the binuclear complex by $Na[BAr^f_4]$ concurrent with activation of the B–C bond. Much of gold-mediated catalysis proceeds via the interaction of $[LAu]^+$ with the π-system of C–C multiple bonds, in this case the aromatic system in Ar^f. It seems that the gold-species generated *in situ* instantly cleaves a B–C bond from the anion to form a binuclear gold complex bridged by an aryl ring (Fig 6.8). This Wheland-type complex is of interest due to reports of similar species being intermediates in gold catalysed ring closing and aromatic electrophilic substitution.[38-40]

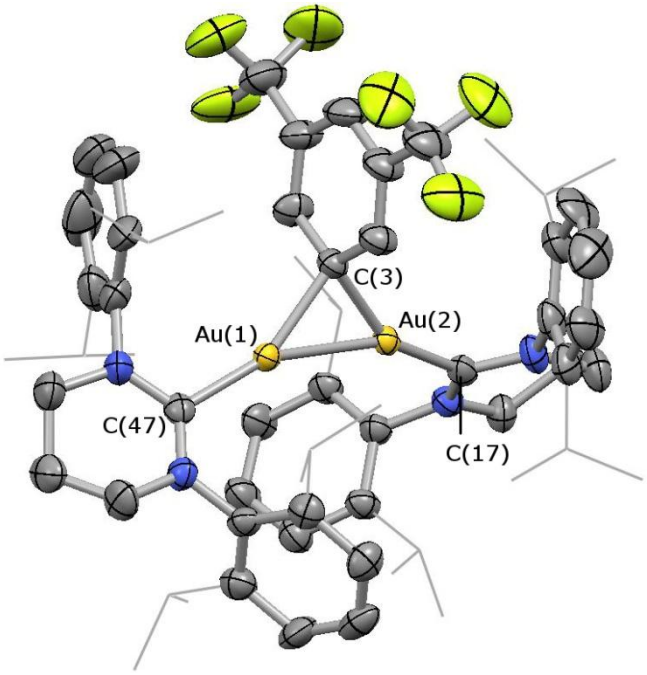

Figure 6.8: [{(6-Dipp)Au}$_2$(μ-Ar^f)][BAr$^f_4$] (**28a**), with [BAr$^f_4$]$^-$ anion omitted, H atoms omitted and ^{i}Pr groups shown in wireframe for clarity; thermal ellipsoids set at 50% probability level. Key bond lengths (Å) and angles (°): Au(1)–Au(2) 2.807(2), Au(1)–C(47) 2.07(1), Au(2)–C(17) 2.02(1), Au(1)–C(3) 2.13(1), Au(2)–C(3) 2.14(1), Au(1)–Au(2)–C(17) 157.6(3), Au(2)–Au(1)–C(47) 157.7(3), Au(1)–C(3)–Au(2) 82.1(3).

It is of note that the Au–Au separation [2.807(2) Å] compared to the chloride-bridged complex **27a** [4.0207(2) Å]. This is due to a change in nature of the bonding, the chloride bridge in **27a** bonds through the chloride lone pair, whereas the aryl bridge in **28a** is a 3-centre-2-electron bond. As a result, there is some degree of orbital overlap between the gold atoms. Compared to previously reported *gem*-diaurated aromatics (such as [{(IPr)Au}$_2$(μ-Ph)][BF$_4$][40]), **28a** varies only in the Au–Au separation being slightly elongated [2.807(2) Å] but still well in the range for an aurophilic interaction of 2.7-3.0 Å.[37] This can be attributed to the increase in steric demand of the 6-Dipp ligands, previous examples have been supported by smaller IPr NHCs. A second artefact of this steric pressure is the increased degree of linearity of the C_{NHC}–Au–Au–C_{NHC} framework. Nolan *et*

al. reported the complex [{(IPr)Au}$_2$(μ-Ph)][BF_4] containing angles across the gold centres of 154.8(2)° and 148.9(3)°,[40] compared with 157.6(3)° and 157.7(3)° for **28a**.

Expansion of the ring further to 7-Dipp leads to even greater steric strain in the system, and it is thought that this may disfavour the formation of the binuclear complexes. However, a targeted synthesis of [{(7-Dipp)Au}$_2$(μ-Cl)][BAr^f_4] (**27b**) via addition of 0.5 equivalents of Na[BAr^f_4] to (7-Dipp)AuCl at -5 °C was successful in producing the binuclear product (Fig 6.9).

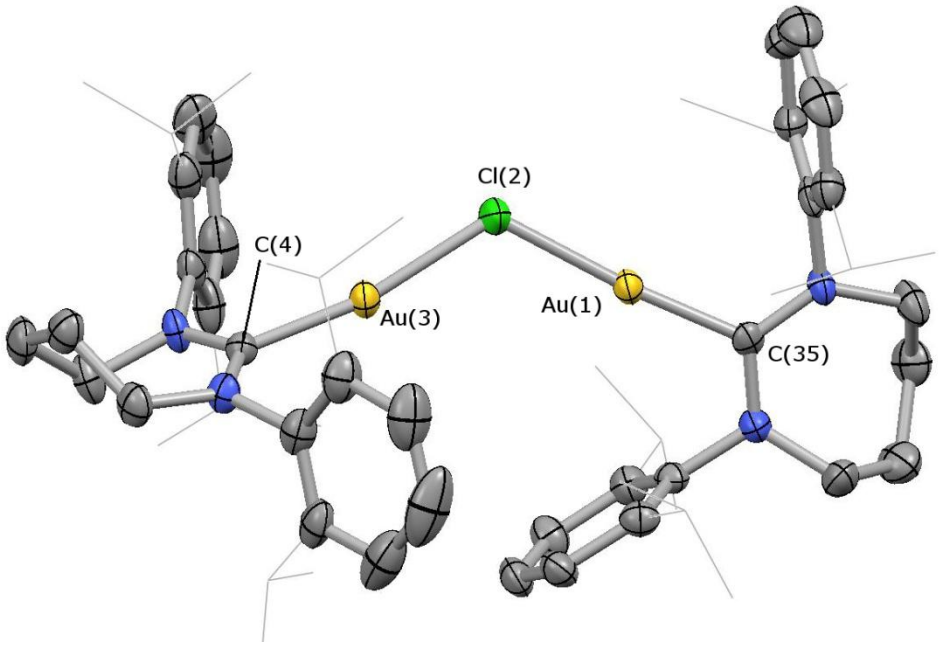

Figure 6.9: [(7-Dipp)Au}$_2$(μ-Cl)][BAr^f_4] (**27b**), with [BAr^f_4]$^-$ anion omitted, H atoms omitted and ^{i}Pr groups shown in wireframe for clarity; thermal ellipsoids set at 50% probability level. Key bond lengths (Å) and angles (°): Au(1)–Cl(2) 2.307(2), Au(3)–Cl(2) 2.319(2), Au(1)–C(35) 1.994(6), Au(2)–C(4) 2.007(6), Au(1)···Au(3) 4.0280(3), Au(1)–Cl(2)–Au(3) 121.07(7), C(35)–Au(1)–Cl(2) 175.7(2), C(4)–Au(3)–Cl(2) 169.4(2).

Comparison between **27b** and **27a** shows no significant change in the Au–Cl distances [2.307(2), 2.319(2) *cf.* 2.310(1), 2.316(1) Å] or the Au–C_{NHC} bond lengths

[1.994(6), 2.007(6) *cf*. 1.989(4), 1.988(4) Å]. However, due to the increased steric demands of 7-Dipp over 6-Dipp (%V_{bur} 52.6% *cf*. 50.8% for LAuCl), the Au···Au separation has increased slightly [4.0280(3) *cf*. 4.0207(2) Å] to give a more linear Au–Cl–Au framework.

Similarly, addition of a full equivalent of Na[BAr^f_4] led to the analogous *gem*-diaurated aryl complex. X-ray crystallography was also used to characterise [{(7-Dipp)Au}$_2$(μ-Ar^f)][BAr^f_4] (**28b**) for comparison with **28a** (Fig 6.10).

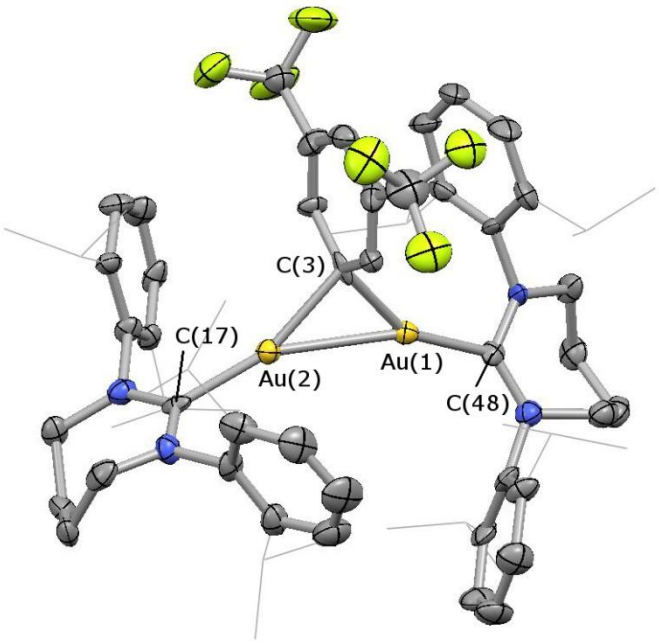

Figure 6.10: [{(7-Dipp)Au}$_2$(μ-Ar^f)][BAr^f_4] (**28b**), with [BAr^f_4]$^-$ anion omitted, H atoms omitted and ^{i}Pr groups shown in wireframe for clarity; thermal ellipsoids set at 50% probability level. Key bond lengths (Å) and angles (°): Au(1)–Au(2) 2.8410(5), Au(1)–C(48) 2.07(1), Au(2)–C(17) 2.03(1), Au(1)–C(3) 2.13(1), Au(2)–C(3) 2.13(1), Au(1)–Au(2)–C(17) 153.1(3), Au(2)–Au(1)–C(48) 158.2(3), Au(1)–C(3)–Au(2) 83.6(4).

As one might expect, compared to **28a**, the Au–Au distance in **28b** is slightly elongated due to the increased steric demands of the 7-Dipp ligands over 6-Dipp [2.841(1)

cf. 2.807(2) Å]. However, the linearity across the C_{NHC}–Au–Au–C_{NHC} framework is similar to that in **28a** [angles at Au: 158.2(3), 153.1(3) *cf*. 157.7(3), 157.6(3)°].

Due to the extremely crowded nature of these complexes, the exact nature of the B–C bond cleavage is not obvious as it seems unlikely that the gold centre is available enough to interact directly with the B–C bond in $[BAr^f_4]^-$. However, it has been postulated by Straub *et al.* that the $[(NHC)Au]^+$ cation is formed *in situ* and interacts directly with the B–C bond of $[BAr^f_4]^-$ (Scheme 6.11).[13]

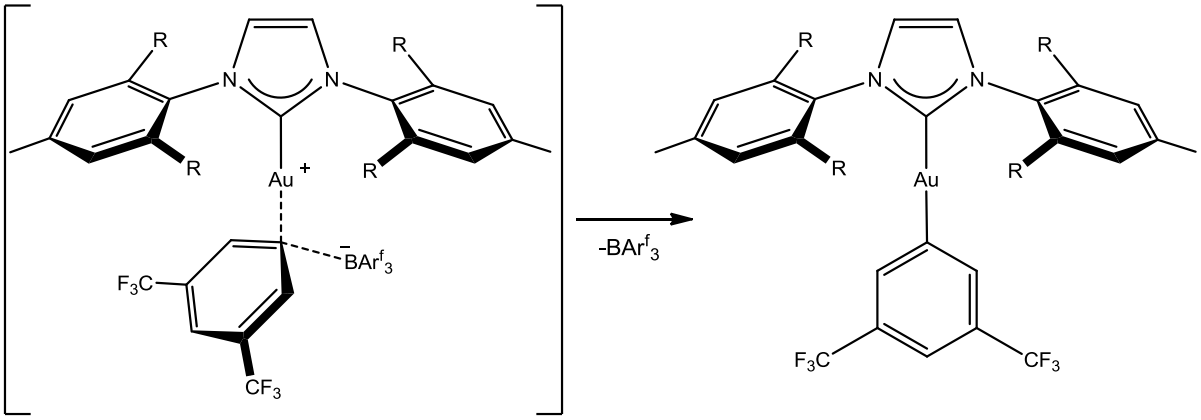

Scheme 6.11: Straub's proposed mechanism of B–C bond cleavage in $[BAr^f_4]^-$ by $[(NHC)Au]^+$, where R = $CH(4\text{-}^t\text{Bu-}C_6H_4)_2$.

However, due to the extremely bulky nature of the ligand used (IPr^{**}) approach of the gold centre to the B–C bond is likely to be highly disfavoured. This also results in the monomeric structure observed, as opposed to the binuclear species **28a** and **28b** reported here. The B–C bond cleavage observed in Straub's system occurred over a period of 7 days. Given most reactions/degradations of cationic gold species happen rapidly, this timescale would support a relatively kinetically unfavourable route. In the case of **28a**, formation occurs over 4 days, and **28b** forms over 14 days suggesting a similar mechanism to that proposed by Straub *et al*. occurs. The space-filling model of **28a** shows how inaccessible

the gold centres are (Fig 6.12), and that this is unlikely to be a concerted process where both gold centres interact simultaneously with the $[BAr^f_4]^-$.

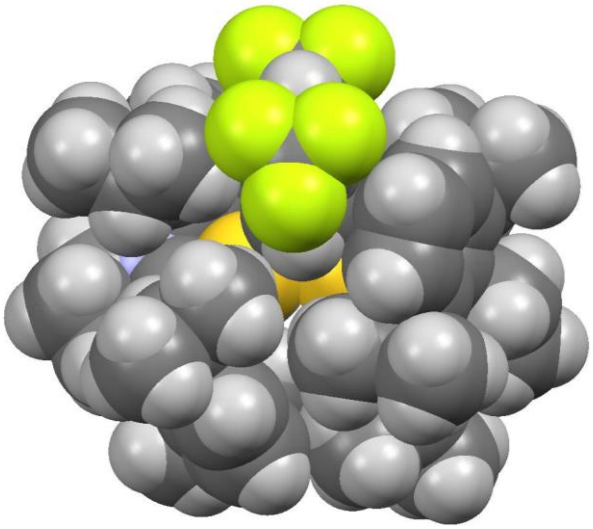

Figure 6.12: Space-filling model of $[\{(6\text{-Dipp})Au\}_2(\mu\text{-}Ar^f)]^+$ (cation of **28a**). Au-Au framework appears to be completely buried within the ligand structure.

6.3.3 Coordination of Two 6-Dipp Ligands

We have previously observed the coordination of two 6-Mes ligands at a gold centre, $[(6\text{-Mes})_2Au][BAr^f_4]$ (**25**), but 6-Dipp offers a much increased steric profile. As observed in Chapter V with iridium, coordination of two 6-Dipp ligands cannot occur even at a 5d transition metal centre. Hence, to probe the extreme steric protection provided by 6-Dipp, halide abstraction from (6-Dipp)AuCl was carried out in the presence of free 6-Dipp. This reaction was carried out a low temperature to avoid unwanted side reactions. The ^{1}H NMR spectrum appears to increase in complexity with a large number of multiplets. In the ^{13}C NMR spectrum, the carbenic signal at δ_C 209.2 ppm supports the coordination of the NHC but there is also a signal associated with the protonated NHC (δ_C 153.4 ppm for NCHN). Crystallisation of the resulting species revealed an extremely interesting complex (Fig 6.13),

where coordination of the second 6-Dipp occurs through the C5 carbon of the heterocycle backbone.

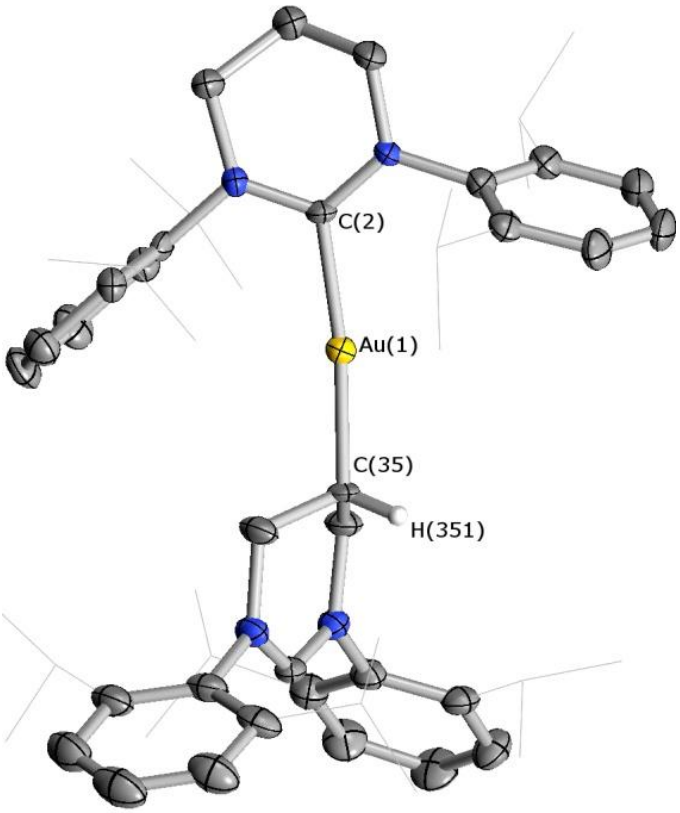

Figure 6.13: [(6-Dipp)Au(6^{a}-Dipp)][BAr$^{f}_{4}$] (**29**), with [BAr$^{f}_{4}$]$^{-}$ anion omitted, most H atoms omitted and ^{i}Pr groups shown in wireframe for clarity; thermal ellipsoids set at 50% probability level. Key bond lengths (Å) and angles (°): Au(1)–C(2) 2.054(5), Au(1)–C(35) 2.081(5), C(2)–Au(1)–C(35) 172.4(2).

The Au–C_{NHC} bond length is unremarkable, and the Au–C_{alkyl} distance of 2.081(5) Å is similar to previously reported alkyl compounds; 2.039(5) Å for (IPr)AuMe,[41] 2.107(11) Å for (IPr)Au[C(H)(CN)($CH_2N^{i}Pr_2$)].[42] It appears that the C–Au–C framework is slightly bent from linear, 172.4(2)°, despite no apparent steric clashes based upon the space-fill model.

For the imidazole-based NHCs, abnormal coordination is now well documented. Such systems are relatively simple to synthesise due to the *pseudo*-aromaticity of the system allowing the formation of a carbene at the C4 position (Fig 6.14).

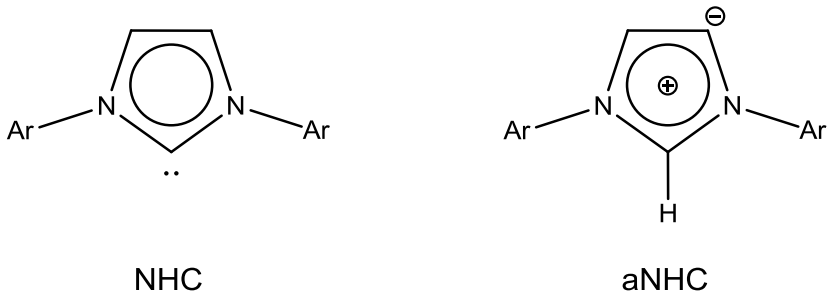

Figure 6.14: Structure of NHCs versus abnormal NHCs

This is the first example of a saturated NHC exhibiting abnormal-type coordination, although the 6^{a}-Dipp ligand in complex **29** is not a carbene, its coordination mode now is effectively an alkyl substituent. Overall, the process involves a proton migration from the C5 position on the backbone to the C2 (carbene) centre. The details of the mechanism involve processes analogous to those observed with iridium in Chapter V (Scheme 6.15).

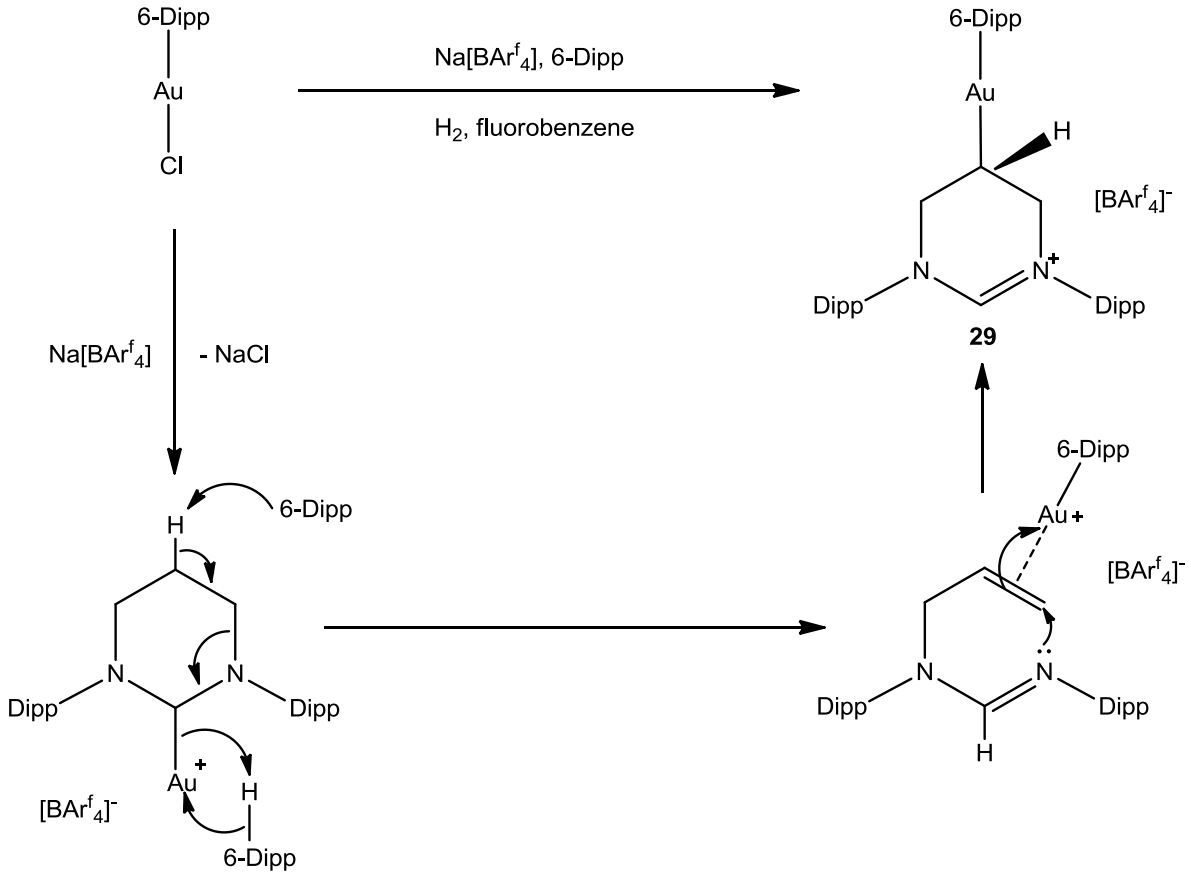

Scheme 6.15: Potential mechanism to form the "abnormal" 6-Dipp ligand.

To support this mechanism, one equivalent of *bis-N,N'*-Dipp-*N*-allylformamidine (**22**) was mixed with (6-Dipp)AuCl and Na[BAr$^f_4$] was then added. Within 5 minutes, the formation of **29** was complete. Given the observations from Chapter V involving the C–H/C–N cleavage in 6-Dipp and this observation here, the mechanism in Scheme 6.15 seems entirely feasible.

This ring closing mechanism by the Lewis acidic gold centre is analogous to the formation of H(5-Dipp^{BArF}) (**23**) reported in Chapter V. However, in the formation of **29** we observe a 6-endo-trig ring closure as opposed to the 5-exo-trig for **23**. This can be attributed to the propensity of the gold cation to form long lived complexes with alkenes (as postulated in Scheme 6.15). Hence, the overall rate of ring closure is reduced compared to the

formation of **23** so the imine lone pair attacks the slightly more δ+ primary alkene, due its lack of inductively donating alkyl groups. Formation of the 6-membered transition state also requires more pre-organisation than the 5-membered transition state. Thus, we observe the thermodynamic product of ring closing as opposed to the kinetic product for **23**.

6.4 Alternative Weakly Coordinating Anions

It is evident that a methodology should be pursued, which utilises a more robust counter-anion than $[BAr^f_4]^-$. There are many examples of weakly coordinating anions in the literature, one class of which are carborane mono-anions. Carborane anions are considered to be extremely weakly coordinating as well as being highly robust and unlikely to degrade in the presence of highly reactive species. Initial attempts used $Cs[HCB_{11}Me_{11}]$ as an abstraction agent to remove Cl^- from (6-Dipp)AuCl. Perhaps unsurprisingly, due to the relatively low lattice enthalpy of CsCl, the Cs^+ does not abstract the chloride but instead sits between the aryl rings on the NHCs (Fig 6.16) in a CsCl inclusion complex. **30** has a dimeric structure with Cs^+ ions lying between two Dipp groups and close to the chlorides which are still bound to the gold centres.

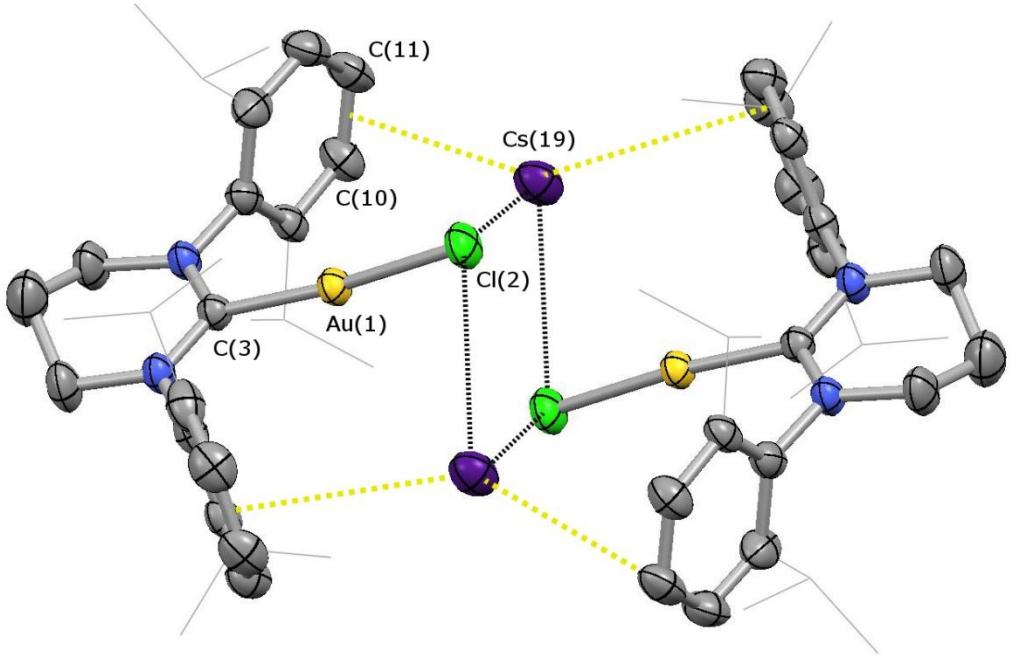

Fig 6.16: [(6-Dipp)Au{CsCl}][$HCB_{11}Me_{11}$] (**30**), with [$HCB_{11}Me_{11}$]$^-$ anion omitted, H atoms omitted and ^{i}Pr groups shown in wireframe for clarity; thermal ellipsoids set at 50% probability level. Key bond lengths (Å) and angles (°): Au(1)–Cl(2) 2.295(2), Au(1)–C(3) 2.000(7), Cs(19)$^{\cdots}$Cl(2) 3.470(1), centroid{C(10)–C(11)}–Cs(19) 3.630, C(3)–Au(1)–Cl(2) 173.2(2), Cl(2)–Cs(19)–Cl(2') 62.80(5).

There appears to be no statistical elongation of the Au–Cl distance in **30** over the parent (6-Dipp)AuCl,[30] suggesting the chloride is still strongly bound to gold. Yet the caesium ions approach the chloride to a distance of 3.470(1) Å, which is within the sum of their ionic radii (3.48 Å). Unfortunately, Cs^+ was not a sufficiently strong abstraction agent for this task due to the relatively low lattice enthalpy of CsCl compared to common, more charge dense abstraction agents, such as Na^+.

A third approach was attempted using another extremely weakly coordinating anion developed by Krossing, $[Al(OC(CF_3)_3)_4]^-$.[43] Krossing reports weak interaction of the fluorine atoms with electrophilic Ag^+ ions in the solid state, however, we hope that the 6-

Dipp ligand provides sufficient steric hindrance to reduce this interaction with the potential $[(6\text{-Dipp})Au]^+$ fragment. Halide abstraction was carried out in a range of polar, non-donor solvents, such as CH_2Cl_2, fluorobenzene and difluorobenzene. Analysis by ^1H and ^{19}F NMR was not conclusive evidence for the formation of a mono-valent gold species, and showed little variation from the spectra of the starting materials. A crystal was isolated from the fluorobenzene reaction by layering with hexane at 20 °C, suggesting a formally one-coordinate $[(6\text{-Dipp})Au]^+$ fragment stabilised by a molecule of fluorobezene (Fig 6.17).

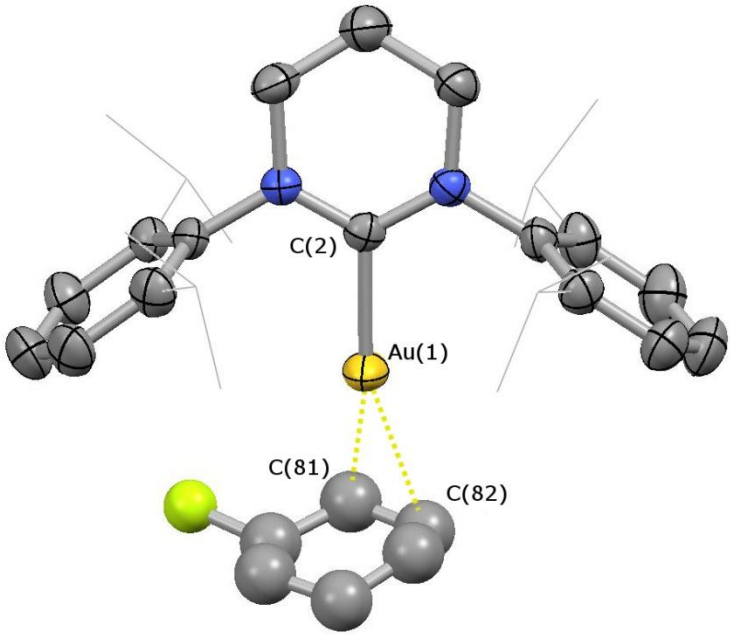

Figure 6.17: $[(6\text{-Dipp})Au\{C_6H_5F\}][Al(pftb)_4]$ (**31**), with $[Al(pftb)_4]^-$ anion omitted, H atoms omitted and ^{i}Pr groups shown in wireframe for clarity; thermal ellipsoids set at 50% probability level. Fluorobenzene displayed as ball and stick for clarity, because of large ellipsoids due to disordering over more than two positions. Key bond lengths (Å) and angles (°): Au(1)–C(2) 2.017(6), Au(1)···C(81) 2.57(2), Au(1)···C(82) 2.19(1), C(2)–Au(1)–C(82) 177.1(7).

The $Au–C_{NHC}$ distance [2.017(6) Å] is typical for 6-Dipp bound to gold. Due to the disordered nature of the fluorobenzene solvent, we have been unable to obtain accurate metrics for the interaction with the gold cation. A $Au–C_{solv}$ distance of 2.19(1) Å can be measured which is comparable with the gold-toluene separation in $[(IPr^{**})Au(toluene)][SbF_6]$ reported by Straub *et al*. [2.2252(8) Å].[15] Addition of the allyl-formamidine (**22**) to **31** leads to rapid ring closure (<5 min) to form, observed by ^{1}H NMR, $[(6\text{-Dipp})Au(6^a\text{-Dipp})][Al(pftb)_4]$, confirming the highly reactive nature of this species.

6.5 Gold Hydrides

The only structurally characterised monomeric gold hydrides are supported by NHCs.[27] Hence work was carried to synthesise a range of novel gold hydride species supported by expanded ring NHCs. Transformation of (6-Mes)AuCl to (6-Mes)AuH (**32**) using $K[HBEt_3]$ proceeded as expected via the reported literature method.[27] However, the ^{1}H NMR chemical shift of the hydride appears to be drastically different: δ_H 3.36 ppm in the case of **32**, compared to 5.11 ppm reported for (IPr)AuH. This implies a much more hydridic hydrogen, presumably due to the strong donation from the 6-Mes ligand.

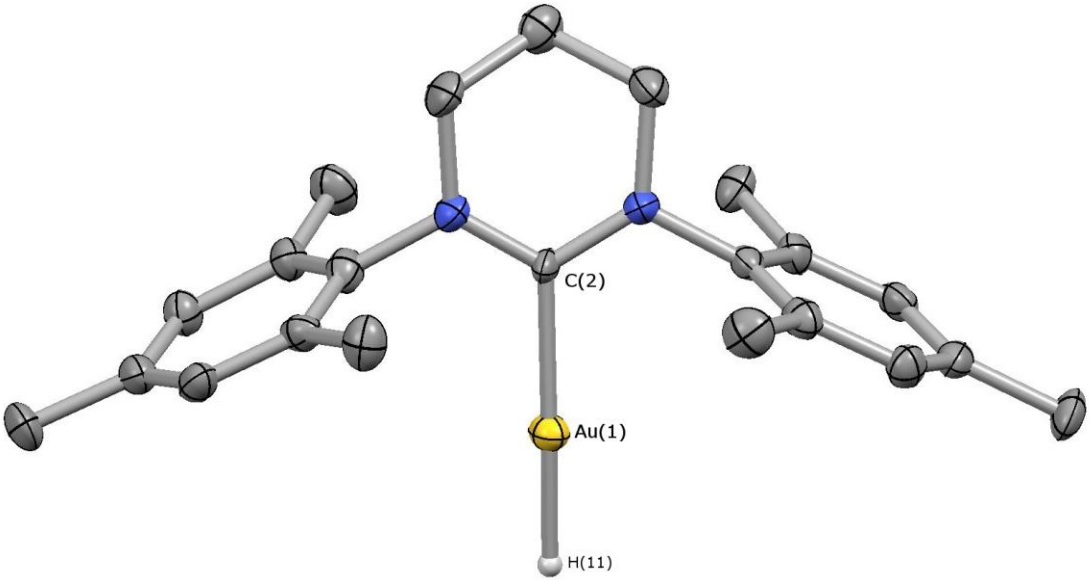

Figure 6.18: (6-Mes)AuH (**32**), with most H atoms omitted for clarity; thermal ellipsoids set at 50% probability level. Au–H located in the Fourier difference map and refined isotropically. Key bond lengths (Å) and angles (°): Au(1)–C(2) 2.066(7), Au(1)–H(11) 1.68, C(2)–Au(1)–H(11) 175.5.

Crystallographically, the metrics associated with this example of a monomeric gold hydride are as expected considering the previously reported (IPr)AuH by Sadighi *et al.*[26] The Au-C_{NHC} bond length in **32** [2.066(7) Å] is identical to (IPr)AuH [2.045(3) Å].

A hydride-bridged bimetallic gold system was reported to be formed when a LAuCl (L = xantphos-phosphole) species underwent halide abstraction in the presence of half an equivalent of silane.[29] In a similar fashion, [{(6-Xyl)Au}$_2$(μ-H)][BAr^f_4] (**32a**) was formed via the reaction of (6-Xyl)AuCl with Na[BAr^f_4] in the presence of $H_3B{\cdot}NHMe_2$. It should be noted that there was no reaction between the parent (6-Xyl)AuCl and $H_3B{\cdot}NHMe_2$ in the absence of a halide abstraction agent. An analogous system, [{(IPr)Au}$_2$(μ-H)][OTf], is reported to be formed from the reaction of (IPr)AuH with (IPr)AuOTf and via hydride abstraction from (IPr)AuH.[27] In the case of **32a**, the ^{1}H NMR spectrum in CD_2Cl_2 displays a hydride signal at δ_H -1.37 ppm which is upfield from [{(IPr)Au}$_2$(μ-H)][OTf] (δ_H 0.42

ppm) suggesting a significantly more hydridic species. Crystals were obtained from a layering of fluorobenzene with hexane at 20 °C and the structure reveals a cationic centre of $[Au_2H]^+$ supported by a 6-Xyl ligand coordinated to each gold centre. There is also no significant interaction from the $[BAr^f_4]^-$ counter-ion.

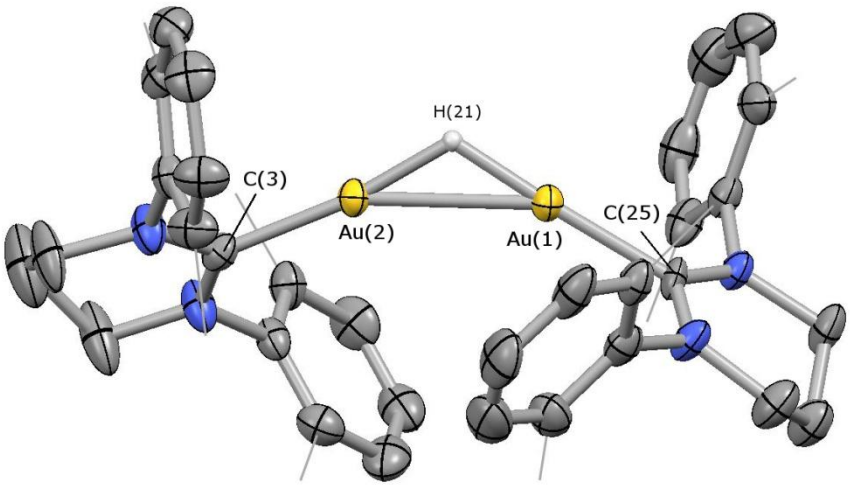

Figure 6.19: $[\{(6\text{-Xyl})Au\}_2(\mu\text{-H})][BAr^f_4]$ (**32a**), with $[BAr^f_4]^-$ anion omitted, most H atoms omitted and Me groups shown in wireframe for clarity; thermal ellipsoids set at 50% probability level. Au–H located in the Fourier difference map and refined isotropically. Key bond lengths (Å) and angles (°): Au(1)–Au(2) 2.7006(3), Au(1)–C(25) 2.044(8), Au(2)–C(3) 2.024(6), Au(1)–H(21) 1.57, Au(1)–H(21) 1.60, C(3)–Au(2)–Au(1) 156.5(2), Au(2)–Au(1)–C(25) 150.5(2).

The inter-Au distance in **32a** [2.7006(3) Å] is significantly shorter than that in previously reported $[(LAu)_2H]^+$ systems, $[\{(IPr)Au\}_2(\mu\text{-H})][OTf]$ (2.7099(4) Å)[27] and $[\{(Xantphos)Au\}_2(\mu\text{-H})][OTf]$ (2.7542(3) Å)[29], and short compared to other examples of Au(I)-dimers.[44, 45] **32a** could also be accessed by halide abstraction from (6-Xyl)AuCl in the presence of (6-Xyl)AuH, similar to the reaction of (IPr)AuH with (IPr)AuOTf reported

by Sadighi.[27] This synthesis supports the idea of the Au-H bond acting like a σ-donor, and that perhaps this could be considered as a σ-complex (Fig 6.20). This notion could be supported by the associated upfield shift of the hydride resonance (from δ_H 3.36 to -1.37 ppm for **32** to **32a**) in the ^{1}H NMR which is often characteristic of σ-complexation.

Figure 6.20: Model of bonding in **32a**, viewing the Au-H bond acting as a σ-donor.

In an attempt to hinder this formation of the binuclear complex to access the previously unreported H_3^+ analogue, $[(NHC)Au(H_2)]^+$, much more hindered AuH complexes bearing 6-Dipp and 7-Dipp were synthesised (Fig 6.21). It was hoped that increasing the bulk of the supporting ligands could separate the gold centres enough such that the hydride ligand might not bridge effectively.

(6-Dipp)AuH (**33a**) and (7-Dipp)AuH (**33b**) were synthesised by reaction of the corresponding gold chloride complex with K[HBEt$_3$] at -78 °C. The increased donor strength of 7-Dipp is exemplified in the more hydridic ^{1}H NMR resonance for **33b** (δ_H 3.15 ppm) compared with the 6-membered NHC systems (δ_H 3.57 for 6-Dipp; 3.36 for 6-Mes). Crystals obtained from concentrated diethyl ether solutions at -30 °C show the NHC coordinated to a gold centre bearing a *trans*-hydride ligand.

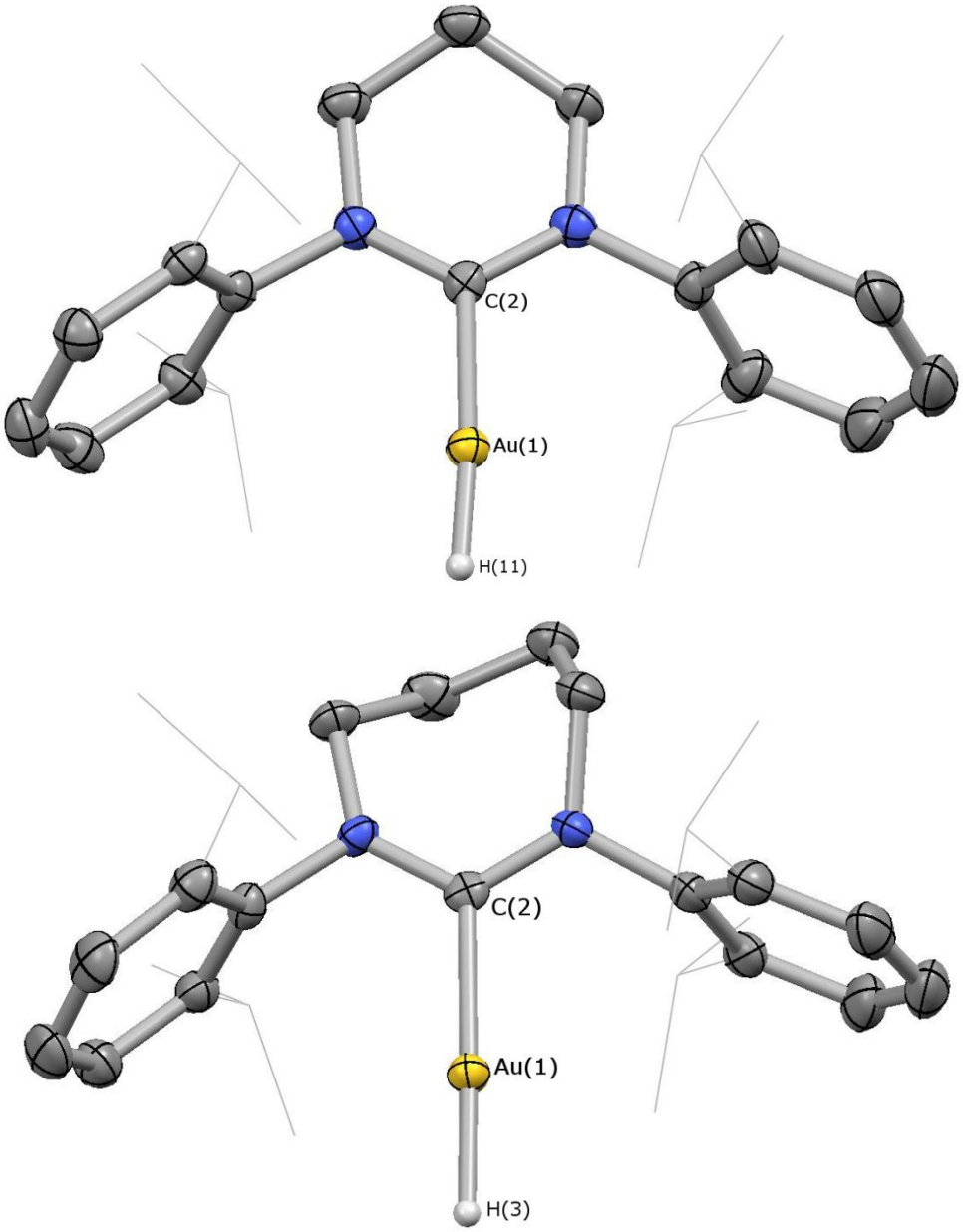

Figure 6.21: (6-Dipp)AuH (**33a**) (*top*), and (7-Dipp)AuH (**33b**) (*bottom*), with most H atoms omitted, ^{i}Pr groups shown in wireframe for clarity; thermal ellipsoids set at 50% probability level. Key bond lengths (Å) and angles (°): for **33a**, Au(1)–C(2) 2.006(5), Au(1)–H(11) 1.34; for **33b**, Au(1)–C(2) 2.071(3), Au(1)–H(3) 1.56(6).

33a has a significantly shorter Au–C_{NHC} bond [2.006(5) Å] than **33b** [2.071(3) Å] which is consistent with the increased donor strength of the 7-membered NHC.

33a and **33b** were subsequently subjected to addition of Brookhart's Acid at -80 °C in an attempt to protonate the hydride *in situ*. This was instantaneously accompanied by the appearance of a signal in the ^{1}H NMR spectra at δ_H -1.47 and -1.95 ppm (in CD_2Cl_2) for 6-Dipp and 7-Dipp respectively. Given the observation of a similar hydride signal for [{(6-Xyl)Au}$_2$(μ-H)][BAr$^f_4$] (**32a**) at δ_H -1.37 ppm, it appears the protonation of the hydride led to rapid loss of H_2 and replacement with (NHC)AuH to form a hydride-bridged binuclear complex, even at low temperature. Warming the sample to above 0 °C led to the decomposition of the product in CD_2Cl_2, hence subsequent handling was carried out in fluorobenzene and C_6D_5Br. X-ray structures were obtained for the 6-Dipp and 7-Dipp supported binuclear hydride complexes (Fig 6.22). Like **32a**, these show a $[Au_2H]^+$ core supported by 6-Dipp and 7-Dipp ligands; although due to the more sterically demanding NHCs, the NHC–Au–Au–NHC framework appears more linear.

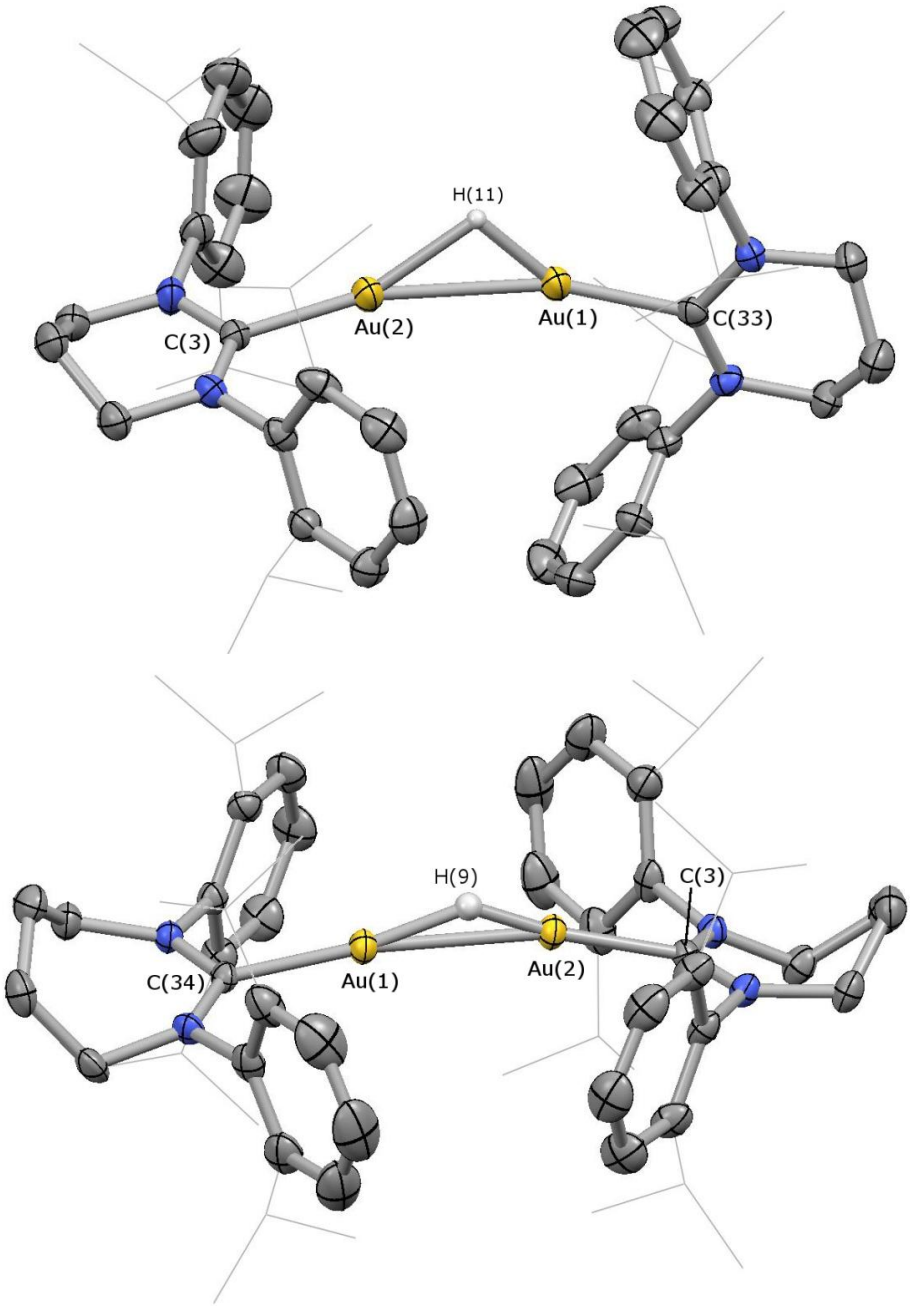

Figure 6.22: [{(6-Dipp)Au}$_2$(μ-H)][BAr$^f_4$] (**34a**) (*top*), and [{(7-Dipp)Au}$_2$(μ-H)][BAr$^f_4$] (**34b**) (*bottom*), with [BAr$^f_4$]$^-$ anion omitted, most H atoms omitted and ^{i}Pr groups shown in wireframe for clarity; thermal ellipsoids set at 50% probability level. Key bond lengths (Å) and angles (°): for **34a**, Au(1)–Au(2) 2.7571(3), Au(1)–C(33) 2.040(5), Au(2)–C(3) 2.049(5), Au(1)–Au(2)–C(3) 165.7(1), Au(2)–Au(1)–C(33) 164.6(1); for **34b**, Au(1)–Au(2) 2.7849(5), Au(1)–C(34) 2.048(4), Au(2)–C(3) 2.063(4), Au(1)–Au(2)–C(3) 164.8(1), Au(2)–Au(1)–C(34) 166.6(1).

The Au-Au distance for **34b** [2.7849(5) Å] is, as expected, significantly longer than that of **34a** [2.7571(3) Å] which in turn is much longer than [{(6-Xyl)Au}$_2$(μ-H)][BAr$^f_4$] **32a** [2.7006(3) Å] by 0.05 Å due to the increased steric demand from the Dipp groups. However, they are still in the range of a relatively short Au-Au contact. As a secondary effect of the increased steric profile, the C-Au-Au-C framework is much more linear for the Dipp-substituted complexes. The angles at the gold centres for **34a** and **34b** [165.7(1), 164.6(1)° and 164.8(1), 166.6(1)° respectively] are much larger than for **32a** [156.5(2), 150.5(2)°]. For **34b**, the hydride signal in the ^{1}H NMR spectrum occurs at δ_H -1.95 ppm which is significantly upfield of the 6-membered NHC complexes (**32a** and **34a**). The angles in this system and the hydridic nature of this hydrogen suggests an [(LAu)$_2$]$^{2+}$ moiety with a closely associated H$^-$ anion.

6.5.1 DFT Calculations

In order to rationalise the formation of **34a** resulting from the protonation of (6-Dipp)AuH, calculations were carried out by Dr Josh Bates using the model 6-Me ligand on the potential intermediate species created during this process. They indicate that the formation of the dihydrogen complex of [(6-Me)Au]$^+$ is potentially an isolable species, however the presence of an Au–H donor leads to the formation of an Au–H–Au unit as a thermodynamic sink (Table 6.23).

	Reaction	ΔG° (kcal/mol)
1	$H(OMe_2)^+ + L–AuH \rightarrow OMe_2 + [L–Au(H_2)]^+$	-41.41
2	$[L–Au(H_2)]^+ \rightarrow [L–Au]^+ + H_2$	9.50
3	$[L–Au]^+ + L–AuH \rightarrow [L–Au–H–Au–L]^+$	-51.01
4	$H(OMe_2)^+ + 2(L–AuH) \rightarrow OMe_2 + [L–Au–H–Au–L]^+$	-82.92

Table 6.23: Calculated free energies for the step-wise processes during the protonation of the gold hydride in the presence of free LAu–H (L = 6-Me).

It appears that the protonation of the gold-hydride with Brookhart's acid (reaction 1) has the potential to form a stable complex, perhaps under a hydrogen atmosphere. Loss of hydrogen from this complex is energetically unfavourable (reaction 2). However, the trapping of the subsequent gold cation with Au–H (reaction 3) is highly favourable.

6.5.2 Activation of the Hydride

Given that protonation of a gold-hydride bond results in rapid trapping by a second equivalent of LAuH to give the binuclear, hydride-bridged species, it was thought useful to probe the possibility for cleavage or weakening of the Au–H bond via other routes.

Tris(pentafluorophenyl)borane is well documented as a powerful Lewis acid,[46] and is capable of the abstraction of both hydride and alkyl moieties. As the $[LAu]^+$ fragment is also highly Lewis acidic, it was of interest to attempt to form an "activated" Au–H species. The competition of the $B(C_6F_5)_3$ and $[LAu]^+$ moieties for the hydride should lead to a complex with an elongation in the Au–H distance but not necessarily cleave the bond entirely. The reactions of various gold hydrides with $B(C_6F_5)_3$ were therefore performed at low temperature and monitored by ^1H, ^{11}B and ^{19}F NMR spectroscopy.

Monitoring the reaction of (6-Dipp)AuH with $B(C_6F_5)_3$ by *in situ* ^{11}B and ^{19}F NMR spectroscopy gives a strong indication of a significant interaction of the $B(C_6F_5)_3$ Lewis acid with the hydride. The ^{11}B resonance shifted from a broad signal at δ_B 60 ppm to a slightly sharper signal at δ_B -17.5 ppm indicating quaternisation of the boron centre. $[HB(C_6F_5)_3]^-$ is known to give rise to a ^{11}B NMR resonance at δ_B -24.4 ppm,[47] which would suggest incomplete hydride abstraction but a weaker, bridging type interaction. Further supporting data came from the ^{19}F NMR spectrum; pyramidalisation of the boron centre is associated with a reduction in the chemical shift difference between the signals for the *meta*- and *para*-fluorines ($\Delta\delta_{m,p}$). Free $B(C_6F_5)_3$ has $\Delta\delta_{m,p}$ = 17.5 ppm and $[HB(C_6F_5)_3]^-$ $\Delta\delta_{m,p}$ = 2.8 ppm.[48] Hence, a reduced gap between the *meta*- and *para*-fluorine signals serves as a good indicator of the strength of interaction of the boron centre with a Lewis base. We observe $\Delta\delta_{m,p}$ = 5.1 ppm which lies between these values for further $B(C_6F_5)_3$ and $[HB(C_6F_5)_3]^-$ thereby supporting the idea of a Au–H–B bridging interaction.

The gold containing product isolated from this reaction, however, does not contain any boron based on ^{11}B NMR spectroscopy. In addition, the signal in the ^{19}F NMR spectrum assigned to the *ortho*-CF has shifted downfield to δ_F -115.8 ppm (from δ_F -128.7 ppm). Thus, we assume the complex observed in the VT-NMR experiments has decomposed. Moreover, the crystal structure of the gold containing product was obtained from the reaction using (7-Dipp)AuH (Fig 6.24) and revealed a pentafluorophenyl fragment bound to gold.

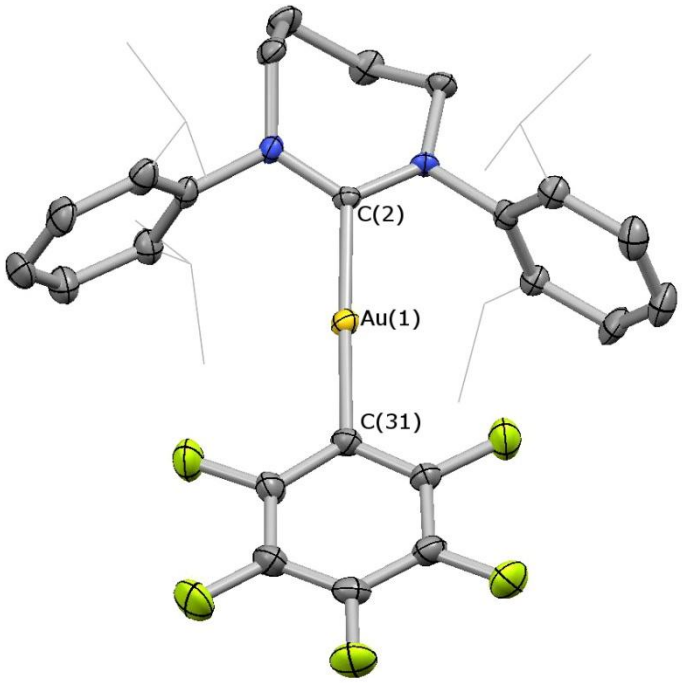

Figure 6.24: (7-Dipp)Au(C_6F_5) (**35b**), H atoms omitted and ^{i}Pr groups shown in wireframe for clarity; thermal ellipsoid set at 50% probability level. Key bond lengths (Å) and angles (°): Au(1)–C(2) 2.040(3), Au(1)–C(31) 2.043(4), C(2)–Au(1)–C(31) 175.2(1).

This complex is analogous to the species (IMes)Au(C_6F_5) reported by Limbach *et al.*[49] As expected, **35b** has a significantly longer Au-C_{NHC} distance than Limbach's complex [2.040(3) *cf.* 2.001(4) Å] due to the donor strength of 7-Dipp resulting in greater p-character of the carbene donor orbital. However, the bonds from Au–C_6F_5 are statistically identical for both complexes though [2.043(4) *cf.* 2.034(5) Å], suggesting minimal effect from the strong 7-Dipp ligand. The NMR data from the reaction of (6-Dipp)AuH with $B(C_6F_5)_3$ was then rationalised to identify the product as (6-Dipp)Au(C_6F_5) (**35a**).

It appears that the carbophilic nature of Au(I) results in the relatively facile abstraction of H^- and subsequently cleavage of the B–C bond. However, given **35b** is a monomeric structure, it implies that the abstraction of the hydride is either: (i) slow, such that there are no free (NHC)AuH in solution to trap the $[(NHC)Au]^+$ as $[\{(7\text{-Dipp})Au\}_2(\mu$-

H)][BAr^f_4] (**34b**); or (ii) incomplete, such that the [$HB(C_6F_5)_3$]$^-$ remains in close contact with the Au^+ resulting in a somewhat concerted reaction (Scheme 6.25).

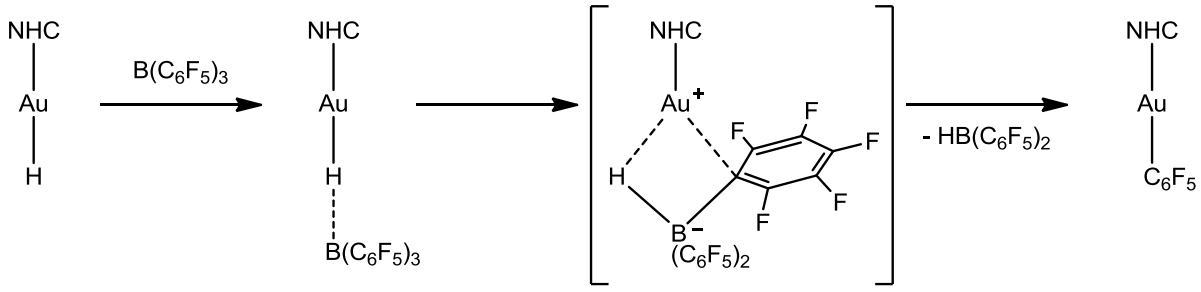

Scheme 6.25: Postulated mechanism involving a concerted intermediate leading to the monomeric product.

This metathesis process is supported by the identification of $HB(C_6F_5)_2$ (Piers' borane) in the ^{19}F NMR.[50] Formation of **35a** or **35b** is not observed in the ^{19}F NMR spectrum below 0 °C, however a signal typical of a tetra-coordinate boron centre appears in the ^{11}B NMR spectrum (δ_B -17.5 ppm) at -20 °C, which then disappears when standing at 20 °C for 1 d. This would suggest initial coordination of the hydride at boron as postulated in Scheme 6.25, but does not illuminate the exact nature of the abstraction process.

6.6 Conclusions

Due to a minimal increase in the steric protection, the chemistry of 6-Mes supported gold complexes appears to mirror that observed for previously report IPr systems. Hence, the increased donor strength has minimal impact on the stability of a putative one-coordinate gold cation. More sterically demanding ligands (such as 6-Dipp and 7-Dipp) result in the formation of binuclear complexes of the type [{(NHC)Au}$_2$(μ-X)]$^+$ (X = Cl, Ar^f) due to the inability to place two of these NHCs on a single metal atom. The target one-coordinate gold species will persist long enough to cleave bonds in the anion or exist with a

relatively electron poor arene solvent bound via the π-system. Ideal conditions for the formation of a solvent free system would involve alkane solvents, which could be possible if a sterically demanding NHC bearing a weakly coordinating anion were to be synthesised. Initial reactions of (THT)AuCl with K[(5-Dipp^{BArF})] have been promising but currently inconclusive.

The extreme steric demand of the 6-Dipp ligand was further probed by the attempted coordination of two 6-Dipp ligands to a single gold cation. This led to observations of coordination of one 6-Dipp ligand through activation of the heterocycle backbone. This is the first example of backbone-coordination behaviour in saturated NHCs, however it must be noted that this is not a carbene but an alkyl donor. Nevertheless, this new mode of reactivity has opened up a new avenue of coordination chemistry.

Expanded ring NHC complexes of AuH were synthesised and reported to exist as much more hydridic species than previously reported monomeric AuH complexes, due to the increased donor strength of the NHC. Attempted protonation or abstraction of the hydride led to the binuclear gold system containing a bridging hydride. Due to the bulk of the Dipp-based NHCs, the C–Au–Au–C framework was close to linear, and the hydride gave rise to a high field resonance in the ^{1}H NMR spectrum for gold complexes. Activation of the hydride with the boron-based Lewis acid, $B(C_6F_5)_3$, led to further reactivity consistent with previously observed B–C cleavage in borate anions.

6.7 References

1. A. S. K. Hashmi and G. J. Hutchings, *Angew. Chem. Int. Ed.*, 2006, **45**, 7896-7936.
2. A. S. K. Hashmi, *Chem. Rev.*, 2007, **107**, 3180-3211.
3. Z. G. Li, C. Brouwer and C. He, *Chem. Rev.*, 2008, **108**, 3239-3265.
4. N. Marion and S. P. Nolan, *Chem. Soc. Rev.*, 2008, **37**, 1776-1782.
5. J. Barluenga, R. Sigueiro, R. Vicente, A. Ballesteros, M. Tomas and M. A. Rodriguez, *Angew. Chem. Int. Ed.*, 2012, **51**, 10377-10381.

6. H. G. Raubenheimer and H. Schmidbaur, *Organometallics*, 2012, **31**, 2507-2522.
7. M. V. Baker, P. J. Barnard, S. K. Brayshaw, J. L. Hickey, B. W. Skelton and A. H. White, *Dalton Trans.*, 2005, 37-43.
8. D. S. Laitar, P. Muller, T. G. Gray and J. P. Sadighi, *Organometallics*, 2005, **24**, 4503-4505.
9. I. J. B. Lin and C. S. Vasam, *Can. J. Chem.- Rev. Can. Chim.*, 2005, **83**, 812-825.
10. P. de Fremont, R. Singh, E. D. Stevens, J. L. Petersen and S. P. Nolan, *Organometallics*, 2007, **26**, 1376-1385.
11. P. de Fremont, N. M. Scott, E. D. Stevens and S. P. Nolan, *Organometallics*, 2005, **24**, 2411-2418.
12. G. C. Fortman, A. Poater, J. W. Levell, S. Gaillard, A. M. Z. Slawin, I. D. W. Samuel, L. Cavallo and S. P. Nolan, *Dalton Trans.*, 2010, **39**, 10382-10390.
13. S. G. Weber, D. Zahner, F. Rominger and B. F. Straub, *Chem. Comm.*, 2012, **48**, 11325-11327.
14. V. Lavallo, G. D. Frey, S. Kousar, B. Donnadieu and G. Bertrand, *Proc. Nat. Acad. Sci. USA*, 2007, **104**, 13569-13573.
15. S. G. Weber, F. Rominger and B. F. Straub, *Eur. J. Inorg. Chem.*, 2012, 2863-2867.
16. H. Ito, K. Takagi, T. Miyahara and M. Sawamura, *Org. Lett.*, 2005, **7**, 3001-3004.
17. H. Ito, T. Saito, T. Miyahara, C. M. Zhong and M. Sawamura, *Organometallics*, 2009, **28**, 4829-4840.
18. P. Pyykko, *Angew. Chem. Int. Ed.*, 2004, **43**, 4412-4456.
19. H. T. Liu, Y. L. Wang, X. G. Xiong, P. D. Dau, Z. A. Piazza, D. L. Huang, C. Q. Xu, J. Li and L. S. Wang, *Chem. Sci.*, 2012, **3**, 3286-3295.
20. U. Ringstrom, *Nature*, 1963, **198**, 981.
21. X. F. Wang and L. Andrews, *Angew. Chem. Int. Ed.*, 2003, **42**, 5201-5206.
22. L. Andrews and X. F. Wang, *J. Am. Chem. Soc.*, 2003, **125**, 11751-11760.
23. H. Lehner, D. Matt, P. S. Pregosin, L. M. Venanzi and A. Albinati, *J. Am. Chem. Soc.*, 1982, **104**, 6825-6827.
24. B. D. Alexander, B. J. Johnson, S. M. Johnson, A. L. Casalnuovo and L. H. Pignolet, *J. Am. Chem. Soc.*, 1986, **108**, 4409-4417.
25. B. D. Alexander, M. P. Gomezsal, P. R. Gannon, C. A. Blaine, P. D. Boyle, A. M. Mueting and L. H. Pignolet, *Inorg. Chem.*, 1988, **27**, 3301-3308.
26. A. Albinati, S. Chaloupka, A. Currao, W. T. Klooster, T. F. Koetzle, R. Nesper and L. M. Venanzi, *Inorg. Chim. Acta*, 2000, **300**, 903-911.
27. E. Y. Tsui, P. Muller and J. R. Sadighi, *Angew. Chem. Int. Ed.*, 2008, **47**, 8937-8940.
28. H. B. Lv, J. H. Zhan, Y. B. Cai, Y. Yu, B. W. Wang and J. L. Zhang, *J. Am. Chem. Soc.*, 2012, **134**, 16216-16227.
29. A. Escalle, G. Mora, F. Gagosz, N. Mezailles, X. F. Le Goff, Y. Jean and P. Le Floch, *Inorg. Chem.*, 2009, **48**, 8415-8422.
30. J. J. Dunsford, K. J. Cavell and B. M. Kariuki, *Organometallics*, 2012, **31**, 4118-4121.
31. C. Hirtenlehner, C. Krims, J. Holbling, M. List, M. Zabel, M. Fleck, R. J. F. Berger, W. Schoefberger and U. Monkowius, *Dalton Trans.*, 2011, **40**, 9899-9910.

32. M. Baron, C. Tubaro, M. Basato, A. Biffis and C. Graiff, *J. Organomet. Chem.*, 2012, **714**.
33. T. J. Herrington, A. J. W. Thom, A. J. P. White and A. E. Ashley, *Dalton Trans.*, 2012, **41**, 9019-9022.
34. W. V. Konze, B. L. Scott and G. J. Kubas, *Chem. Comm.*, 1999, 1807-1808.
35. H. Salem, L. J. W. Shimon, G. Leitus, L. Weiner and D. Milstein, *Organometallics*, 2008, **27**, 2293-2299.
36. P. G. Jones, G. M. Sheldrick, R. Uson and A. Laguna, *Acta Cryst. B*, 1980, **36**, 1486-1488.
37. H. Schmidbaur, *Gold Bulletin*, 2000, **33**, 3-10.
38. A. S. K. Hashmi, M. Wieteck, I. Braun, M. Rudolph and F. Rominger, *Angew. Chem. Int. Ed.*, 2012, **51**, 10633-10637.
39. A. S. K. Hashmi, I. Braun, P. Nosel, J. Schadlich, M. Wieteck, M. Rudolph and F. Rominger, *Angew. Chem. Int. Ed.*, 2012, **51**, 4456-4460.
40. A. Gomez-Suarez, S. Dupuy, A. M. Z. Slawin and S. P. Nolan, *Angew. Chem. Int. Ed.*, 2013, **52**, 938-942.
41. V. J. Scott, J. A. Labinger and J. E. Bercaw, *Organometallics*, 2010, **29**, 4090-4096.
42. M. W. Johnson, S. L. Shevick, F. D. Toste and R. G. Bergman, *Chem. Sci.*, 2013, **4**, 1023-1027.
43. I. Krossing, *Chem. Eur. J.*, 2001, **7**, 490-502.
44. M. N. I. Khan, S. N. Wang and J. P. Fackler, *Inorg. Chem.*, 1989, **28**, 3579-3588.
45. L. J. Hao, R. J. Lachicotte, H. J. Gysling and R. Eisenberg, *Inorg. Chem.*, 1999, **38**, 4616-4617.
46. W. E. Piers and T. Chivers, *Chem. Soc. Rev.*, 1997, **26**, 345-354.
47. G. C. Welch and D. W. Stephan, *J. Am. Chem. Soc.*, 2007, **129**, 1880-1881.
48. J. M. Blackwell, E. R. Sonmor, T. Scoccitti and W. E. Piers, *Org. Lett.*, 2000, **2**, 3921-3923.
49. M. Pazicky, A. Loos, M. J. Ferreira, D. Serra, N. Vinokurov, F. Rominger, C. Jakel, A. S. K. Hashmi and M. Limbach, *Organometallics*, 2010, **29**, 4448-4458.
50. D. J. Parks, R. Spence and W. E. Piers, *Angew. Chem. Int. Ed.*, 1995, **34**, 809-811.

Appendix I

Publication List

- "Probing the limits of ligand steric bulk: C-H and C-N bond activation in the highly encumbered expanded ring N-heterocyclic carbene 6-Dipp", Phillips, N. *et al.*, Chemistry – A European Journal, **2014**, *20 (13), 3825-3830.*
- "Sterically Encumbered Iridium *Bis*(N-heterocyclic carbene) Complexes: Air Stable 14-electron Cations and Facile Degenerate C-H Activation", Phillips, N. *et al.*, Organometallics, **2012**, *31 (23)*, 8075-8078
- "Hydrogen shuttling: synthesis and reactivity of a 14-electron iridium complex featuring a bis(alkyl) tethered N-heterocyclic carbene ligand", Tang, C.Y., Phillips, N. *et al.*, Chemical Communications, **2012**, *48 (98)*, 11999-12001
- "Dimethylamine borane dehydrogenation chemistry: syntheses, X-ray and neutron diffraction studies of 18-electron aminoborane and 14-electron aminoboryl complexes", Tang, C.Y., Phillips, N. *et al.*, Chemical Communications, **2012**, *48 (65)*, 8096-8098
- "(Dimethylamino)borylene and Related Complexes of Electron-Rich Metal Fragments: Generation of Nucleophile-Resistant Cations by Spontaneous Halide Ejection", Addy, D.A., Phillips, N. *et al.*, Organometallics, **2012**, *31 (3)*, 1092-1102

- "Stable GaX_2, InX_2 and TlX_2 radicals", Protchenko, A.V. *et al.*, Nature Chemistry, **2014**, *6*, 315-319.
- "Formation of sub-valent carbenoid ligands by metal-mediated dehydrogenation chemistry: coordination and activation of $H_2Ga\{(NDippCMe)_2CH\}$", Turner, J. *et al.*, Chemical Science, **2013**, *4 (11)*, 4245-4250
- "Synthesis and Reactivity of Half-Sandwich Ruthenium k^2-Aminoborane Complexes", Addy, D.A. *et al.*, Australian Journal of Chemistry, **2013**, *66 (10)*, 1211-1218
- "Al-H sigma-bond coordination: expanded ring carbene adducts of AlH3 as neutral bi- and tri-functional donor ligands", Abdalla, J. *et al.*, Chemical Communications, **2013**, *49 (49)*, 5547-5549
- "Coordinative trapping of the boron beta-diketiminato system $[B(NMesCMe)_2CH]$ via metal-templated synthesis", Firinci, E. *et al.*, Chemical Communications, **2013**, *49 (15)*, 1509-1511

- "Salt metathesis for the synthesis of M-Al and M-H-Al bonds", Riddlestone, I. *et al.*, Dalton Transactions, **2013**, *42 (1),* 249-258
- "Borane to Boryl Hydride to Borylene Dihydride: Explicit Demonstration of Boron-to-Metal a-Hydride Migration in Aminoborane Activation", O'Neill, M. *et al.*, Journal of the American Chemical Society, **2011**, *133 (30),* 11500-11503
- "Modelling fundamental arene-borane contacts: spontaneous formation of a dibromoborenium cation driven by interaction between a borane Lewis acid and an arene p system", Mansaray, H. *et al.*, Chemical Communications, **2011**, *47 (45),* 12295-12297